

**Seismic Rehabilitation of Reinforced Concrete Columns  
Through Confinement By Steel Collars**

**Part 2**

**by**

**Munawar A. Hussain**

**and**

**Robert G. Driver**

**Structural Engineering Report No. 259**

**Department of Civil and Environmental Engineering  
University of Alberta  
Edmonton, Alberta, Canada**

**May 2005**

## 5. MODEL FOR CONCRETE CONFINED EXTERNALLY BY STEEL COLLARS

### 5.1 Introduction

Numerous experimental and analytical studies into the behaviour of concrete confined by conventional reinforcing steel ties have been reported (e.g., Richart *et al.* (1928, 1929), Chan (1955), Iyengar *et al.* (1970), Vallenias *et al.* (1977), Ahmad and Shah (1982, 1985), Sheikh and Uzumeri (1980, 1982), Park *et al.* (1982), Scott *et al.* (1982), Mander *et al.* (1988a, 1988b), Chung *et al.* (2002), Saatcioglu and Razvi (1992), Cusson and Paultre (1995), and L g ron and Paultre (2003)). Since the 1990s, a large number of researchers have focussed on the confinement of concrete by composite materials (e.g., Sadaatmanesh *et al.* (1994), Nanni and Bradford (1995), Mirmiran and Shahawy (1996, 1997), Seible *et al.* (1997), Samaan *et al.* (1998), and Fam and Rizkalla (2001)). In most of these studies, concrete material models have been proposed that account for the confinement of concrete based on the behaviour of the confining elements..

External confinement by simple bolted or welded collars made from steel hollow structural sections (HSS) has proved through experimental study at the University of Alberta to be an effective seismic rehabilitation scheme for square reinforced concrete columns. The experimental program consisted of two phases: in phase 1, the behaviour of externally confined columns under concentric axial loading was studied (Chapter 3); and in phase 2, the behaviour of externally confined columns under cyclic loading was studied (Chapter 4).

The existing confinement models for both conventional rebar confinement and for confinement of concrete by composite materials are unable to predict the behaviour of concrete columns confined externally by HSS collars under concentric monotonic axial loading because of either one or more of the following reasons:

- (1) The flexural stiffness of the confining elements affects the behaviour of confined concrete significantly, as has been demonstrated experimentally by Khaloo and Bozorgzadeh (2001) and through finite element analysis by Hussain and Driver (2001), and all of the aforementioned existing confinement models lack an explicit flexural stiffness parameter.
- (2) Most of the models for the confinement of concrete by conventional steel ties assume yielding of the confining steel at the peak stress of the confined concrete and hence, for

simplicity, assume constant confining pressure throughout the axial load history of the confined columns. However, because the steel collars are often either elastic or only partially yielded at this point, the variation of the confining pressure under the collars must be accounted for, as has been demonstrated by Hussain and Driver (2003) through finite element study.

- (3) Most of the models for conventional rebar confinement base their results on the yield strength of the confining steel without taking into consideration the shape of the stress vs. strain relationship which is known to be influential for collared columns (Hussain and Driver, 2003).

The modified Kent and Park model (Park *et al.*, 1982) and the models proposed by Sheikh and Uzumeri (1982), Mander *et al.* (1988b), and Saatcioglu and Razvi (1992) assume that complete yielding of the confining steel has taken place at the peak stress of the confined concrete and strain hardening is neglected. The models proposed by Ahmad and Shah (1982), Chung *et al.* (2002), Cusson and Paultre (1995), and Légeron and Paultre (2003) for the confinement of concrete by conventional ties do not assume yielding of the confining steel at the peak stress of the confined concrete and, hence, in these models confining pressure is not considered to remain constant. The models proposed by Ahmed and Shah (1982), Madas and Elnashai (1992), Cusson and Paultre (1995), and Légeron and Paultre (2003) take into consideration the complete stress vs. strain curve of the confining steel by making use of an incremental—iterative procedure to trace the stress vs. strain relationship of the confined concrete. All of these models lack an explicit flexural stiffness parameter. Generally, the confinement models are either based on or validated by the test results of columns confined by elements having small flexural stiffness. Therefore, the omission of this parameter from the confinement models has no adverse consequence on their performance if used for columns confined by confining elements with negligible flexural stiffness. However, their performance would be questionable if used for columns confined by elements with significant flexural stiffness in addition to axial stiffness. Moreover, none of the above mentioned confinement models have the ability to take into account the initial active confining pressure that may be present in the concrete confined with steel collars having bolted corner connections due to the pre-stressing of bolts.

## **5.2 Predictions by Existing Confinement Models**

In order to demonstrate that the existing confinement models are unable to predict the behaviour of concrete confined by HSS collars, the following models are chosen to predict the behaviour of column C06 (Chapter 3), which is considered typical: modified Kent and Park model (Park *et al.*,

1982); Sheikh and Uzumeri (1982); Mander *et al.* (1988b); Saatcioglu and Razvi (1992); and Légeron and Paultre (2003). The resulting confined stress vs. strain curves are depicted in Figure 5-1. The column is 300 x 300 mm in cross-section and is confined with collars made from steel hollow structural sections (HSS 51 x 51 x 6.35 mm) with welded corner connections. The centre-to-centre spacing of collars is 122 mm. The yield stress and modulus of elasticity of collars are 497 MPa and 203 400 MPa, respectively. The cylinder strength of concrete,  $f'_c$ , is 34.8 MPa. It is clear from Figure 5-1, that none of these confinement models are able to provide a good prediction of the behaviour of this collared column. Other column configurations lead to similar results. Therefore, in order to predict the behaviour of concrete columns confined by HSS collars, finite element methods were used in combination with a new confinement model, as described in the next sections.

### 5.3 Finite Element Analysis

Finite element analysis of the columns was carried out using the general purpose finite element program *ABAQUS* (HKS, 2004a, 2004b). Three dimensional finite element models were developed to predict the behaviour of externally confined columns under concentric loading. The formulation of the numerical model was based on small displacements and infinitesimal strains and material nonlinearities were taken into consideration. The analyses were conducted incrementally with equilibrium established in each increment.

#### 5.3.1 Geometric Modelling

Figure 5-2 shows a typical three-dimensional finite element model of a mid-height slice of an axially loaded concrete column confined externally with steel HSS collars having either bolted or welded corner connections. All of the columns were 300 x 300 mm in cross-section and uniform finite element meshes were used throughout the models. For mesh refinement studies, three meshes—12 x 12 x 13, 16 x 16 x 13, and 20 x 20 x 13—were tried and the same results were obtained. Hence, a mesh of 12 x 12 x 13 (as shown in Figure 5-2) was chosen for modelling all of the collared columns.

Eight node solid elements with reduced integration (C3D8R) were used to model the concrete. At each node, there were three translational degrees of freedom. The vertical reinforcement was modelled using two-node three-dimensional truss elements (T3D2) with three translational degrees of freedom per node. The truss elements of the vertical bars were connected to the nodes of the concrete elements (C3D8R) and hence no bond slip was assumed. HSS collars were modelled with two-node shear flexible three-dimensional beam elements (B33) with six

degrees of freedom per node (three translational and three rotational). The links between collar beam elements and concrete cube elements (outriggers) were also modelled using truss elements T3D2. The area of the cross-section of these links was chosen high enough to render them as axially rigid. As the collars are connected to the concrete with truss element links (T3D2) with no rotational degrees of freedom at the nodes, the collars were unstable in the vertical direction. Therefore, the vertical stability of the collars was obtained by constraining the vertical degrees of freedom of the four corner nodes of the collar to the central node of the concrete surface in the plane of the collar. By these constraints, the vertical displacements of the collars and those of the respective central nodes of the concrete remain equal.

In the present study, two types of collars made from hollow structural sections (HSS) were used, as described in Chapter 3. The collar beam elements were placed at the centreline of the collars. In the case of collars with rigid (welded) corner connections, the unsupported lengths of the elements at the collar corners affect the collar stiffness significantly. This problem was overcome by providing rigid diagonal elements in the corners of the collars, as shown in Figure 5-2. In the case of collars with bolted corner connections, the bolts were relatively flexible elements; therefore, the confining behaviour of the collars with bolted corner connections was highly dependent on the length of the corner bolts (threaded rods). In order to achieve the desired behaviour, measured bolt lengths between the undersides of the nuts were used in the models. The collars used in the experimental work were made from standard steel HSS. The HSS has round corners but in the finite element model, rectangular box sections with sharp corners were used to model the HSS. The thickness of the webs and flanges of the box sections were selected to provide the moment of inertia and area of cross-section equal to that of the actual HSS cross-section with round corners. As the HSS collars are 51 mm wide and they therefore cover a 51 mm depth on the concrete column surface, lumping the stiffness of collars in just one line was not considered appropriate. Therefore, each collar was modelled using two layers of beam elements (one at each of the two limits of contact with the concrete), as depicted in Figure 5-2.

### **5.3.2 Boundary Conditions and Loading**

Rigid surfaces were defined at the top and bottom ends of the model. All three degrees of freedom of the central node at the bottom surface of the model were fully restrained. The two horizontal degrees of freedom of the central node on the top surface were also fully restrained, leaving its third (vertical) degree of freedom unrestrained to apply axial load to the column using displacement control. The degrees of freedom of all the remaining nodes of the top and bottom surfaces were constrained to the central node of the respective surface.

The behaviour of the confined concrete columns is described in terms of load vs. axial strain relationships. The vertical load on the model is obtained from the vertical reaction of the central node at the bottom surface. The axial strain is determined from the relative displacements of two nodes on the vertical centreline of the model that are situated two layers away from the boundaries at either end. The reason for selecting nodes away from the boundaries is to exclude any effect of boundaries on the confining behaviour.

### **5.3.3 Solution Strategy**

Displacement control with a Newton-Raphson iterative scheme was used for solving the finite element models. In the full Newton-Raphson's method, the tangent stiffness matrix  $[K]$  is updated in all equilibrium iterations, making this nonlinear solution scheme expensive in terms of total solution time. In the modified Newton-Raphson's Method, the stiffness matrix is updated only at the beginning of every load or displacement increment, potentially resulting in a significant reduction of total solution time. *ABAQUS* automatically moves back and forth between Newton-Raphson's method and the modified Newton-Raphson's method based on the difficulties in updating  $[K]$  and the convergence rate (HKS, 2004a, 2004b).

### **5.3.4 Material Properties**

The finite element models consisted of concrete, reinforcing bars, steel HSS, and threaded rods. The collars with welded corner connections were grouted onto the columns using epoxy grout. However, the thickness of the grout layer was small (5 to 6 mm), so its effect on the behaviour of the confined columns was deemed negligible and it was not included in the finite element models (the inner faces of the collars were assumed to bear directly against the concrete). The material properties were taken from the experimental program. Properties that were not measured directly were estimated, as discussed below.

#### **5.3.4.1 Concrete**

For plain concrete, a constitutive model implemented in *ABAQUS* under the option of "concrete" was used. This material model encompasses tension as well as compression behaviour of concrete. For computational efficiency, several simplifications are included in the model. The response of concrete under compressive stresses is modelled with an elastic-plastic constitutive theory using a yield surface consisting of equivalent compressive stress and von Mises deviatoric stress (generally known as the Drucker-Prager yield surface). When the stress-state of the concrete reaches the yield surface, isotropic hardening and associated flow rules are used. The assumption of associated flow for concrete has not been justified by experiments. In addition, this

material model cannot take into account the inelastic response of concrete under high compressive stresses. This model works well for uniaxial and biaxial compression cases; however, due to the lack of third stress invariant in the failure surface and due to the inadequacy of plasticity hardening parameters, this material model cannot accurately predict the behaviour of concrete under tri-axial compression and tri-axial tension (HKS, 2004a).

In tension, cracking is assumed to occur in the concrete when the stress level reaches a failure surface called the “crack detection surface.” The model uses a smeared crack approach, which means that it does not track individual “macro cracks. ” In the smeared crack approach, the localized deformation of each crack is smeared over a characteristic length and the response in tension is described as a continuum in terms of stress vs. strain relationships. After the appearance of the cracks, the postfailure behaviour of the concrete is described by a damage elasticity model and a bilinear stress-crack opening relationship is used to define the tensile softening behaviour of the concrete (HKS, 2004a).

Some basic properties of concrete for phases 1 and 2 columns such as cylinder strength, modulus of elasticity, strain at peak stress, and Poisson’s ratio are reported in Chapters 3 and 4, respectively.

#### **5.3.4.2 Reinforcing Bars, Steel HSS, and Threaded Rods**

Tension tests were performed to determine the material properties of the rebars and threaded rods (bolts). Stub column tests were performed to find the material properties of the HSS. These material properties were reported in Chapters 3 and 4. The constitutive behaviour of the steel was defined by an elastic-plastic model with the von Mises yield criterion, associated flow rule, and isotropic strain hardening.

#### **5.3.5 Preliminary Finite Element Results and New Direction**

While conducting the finite element analyses, difficulties arose in tracing the descending branch of the confined concrete material curves and comparisons between the finite element and experimental results were not satisfactory due to the limitations of the program for modelling the concrete under tri-axial compression, as described above. Initially, attempts were made to overcome this problem by modifying the descending branch of the input concrete material curve as has been suggested by Johansson and Gylltoft (2002) and modelling explicitly the spalling of concrete between the collars by removing the cover elements during the axial loading history based on the observed behaviour in the experimental study (Chapter 3). The slope of the straight

line descending branch of the input material concrete material curve was decreased (*i.e.*, the descending branch was raised)—to obtain a good agreement with the test results—to compensate for the lack of the third stress invariant in the concrete material model available in ABAQUS and it seems logical to relate the modification of the descending branch to the magnitude of the confining pressure on the columns. In the experimental study reported in Chapter 3, columns with different levels of confining pressures were tested because of differences in the size, spacing, and corner connections of the collars. In addition, some of the collars with bolted corner connections were pre-stressed and had active confining pressure in addition to passive confining pressure, which is produced due to the expansion of the concrete during the axial load history of the columns. The question remains, however, of how much the descending branch of the input concrete material model should be modified to produce an accurate representation of the confined behaviour. In addition, it has been shown elsewhere (Hussain and Driver, 2003) and again it will be shown later in this chapter that the dilation rate of the concrete material model available in ABAQUS is quite different than that of an existing empirical concrete dilation model used in the present study (See Section 5.4.3).

Because of these reasons, it was decided not to use the ABAQUS concrete material model for predicting the confining behaviour of the collared columns. Therefore, a different approach was developed for this purpose, which requires as input the confining behaviour of the steel HSS collars in terms of confining pressure vs. lateral strain obtained through finite element analysis. The use of the confining pressure vs. lateral strain relationship from the finite element analysis reduces substantially the dependence of the results on the concrete material model because the results are related primarily to the collar behaviour itself.

### **5.3.6 Confining Pressure vs. Lateral Strain Relationships**

Although the finite element model described above is unable to predict the behaviour of concrete confined by steel HSS collars due to its various limitations, it is nevertheless useful to determine the behaviour of collars in terms of average confining pressure vs. average lateral strain. It seems reasonable to assume that this relationship, which is predominantly related to the restraining action of the collars themselves (*i.e.*, as a collar strains outward due to the laterally expanding concrete, the confining pressure increases by an amount that is a function of its stiffness), is largely independent of the concrete properties used as input. However, in order to assess the effect of the input concrete material curve on the confining behaviour of collars, different curves were used in the finite element analysis and it was confirmed that the resulting confining behaviour of collars is practically independent of the input concrete material curves. This is demonstrated by studying the dependency of the confining behaviour of the bolted collars of

column C01 and the welded collars of column C06 on the input concrete material curves. Five different input curves of normal strength concrete with modified (enhanced) curvilinear descending branches are shown in Figure 5-3. Using these input concrete material curves, the confining pressure versus lateral strain curves for column C01 (bolted collars) and C06 (welded collars) are determined through finite element analysis and are shown in Figures 5-4 and 5-5, respectively. The variations in the input concrete material curves have no effect on the confining behaviour of the bolted collars of column C01. This is because the bolts are relatively flexible components in the collars and most of the deformation takes place there. However, the confining behaviour of the welded collars of column C06 is slightly affected by the change in the input concrete material curve because welded collars tend to apply high confining pressure in the corners as compared to the mid-depth of the column.

The discrepancy for the welded collars can be solved by using an iterative procedure similar to the one used by Hussain and Driver (2003). In this method, the confining behaviour of collars is established with an input material curve similar to the ones shown in Figure 5-3, which is then used to determine the confined concrete material curve using the empirical model described later in this chapter. Using this confined material curve as a reference, the input concrete material curve for the finite element analysis is modified in such a way that the output confined concrete material curve obtained from FEM matches with the confined concrete material curve obtained by the empirical model. The level of accuracy can be improved by using the revised confining behaviour of collars in each iteration for the determination of confined concrete material curve by the proposed empirical model, which is used as the reference to compare the confined concrete material curve obtained from the finite element analysis. This procedure is repeated until the confined concrete material curve obtained by the finite element analysis is the same as that obtained by the proposed empirical model. Although this procedure is more accurate, it requires a large number of finite element runs just for one column and is therefore not considered to be practical for general use.

For simplicity and to make the procedure practical, it is assumed that the confining behaviour of welded collars is not affected by the change of the input concrete material. To assess the impact of this assumption, a sensitivity study is done on column C06. The selection of the particular curves given in Figure 5-3 was based on experimental experience (Chapter 3). Using the resulting confining pressure versus lateral strain curves 1 and 5 (Figure 5-5) of column C06, the confined concrete material curves of this column are determined using the empirical model. These curves are nearly identical, as shown in Figure 5-6. Using these confined concrete material curves, the column load versus axial strain curves of the column were obtained, which are also virtually identical (Figure 5-7). Hence, for normal strength concrete and for practical sizes of

collars, the assumption that the confining behaviour of collars is independent of the input concrete material curve is justified. For all subsequent studies presented in this chapter, as well as in Chapter 6, material curve No. 5 given in Figure 5-3 was used. It is expected that this curve will give very good results for typical concrete strengths and levels of collars confinement.

In some of the columns with bolted collars, an initial confining pressure was applied through pre-stressing. This pre-stressing force was generated in *ABAQUS* by applying a negative temperature change to the corner bolts of the collars. When the finite element model is loaded in the axial direction, the four sides of the confining collars are deformed laterally due to the dilation (*i.e.*, lateral strain) of concrete. In response, the confining collar applies confining pressure onto the concrete due to its restraining action. Although the confining pressure for columns with bolted collars is a combination of active and passive pressures, the pressure on the columns having collars with welded corner connections is purely passive. A behavioural curve of a typical steel HSS collar in terms of average confining pressure vs. average lateral strain is shown in Figure 5-8, where  $\sigma_{ct}$  is the average confining pressure and  $(\varepsilon_l)_{ct}$  is the average lateral strain corresponding to  $\sigma_{ct}$ .

The average confining pressure is obtained by dividing the total force in the outriggers located in a strip having a length equal to the column width and a depth equal to the centre-to-centre spacing,  $s$ , of collars, by the strip area. The average lateral strain is obtained by dividing the average horizontal displacements of the concrete surface nodes at which outriggers from the collars are connected, by half the width of the column. The finite element study showed that the collars remain in contact with the column during the great majority of the axial load history (see Chapter 6). Only at very high levels of axial strain may the collar and the concrete at mid-width of the column may break contact. For the practical range of axial strain, it is assumed that the contact between the concrete and the collars remains intact. This assumption has been justified by the testing of the columns in phase 1 of the project where no gap was observed in any of the tests (Chapter 3).

As noted previously, the confining pressure vs. lateral strain curve depends essentially on the behaviour of the steel HSS collar, although the influence of the profile in which the collars are pushed outward is also present in this curve. Moreover, because the curve is based on the finite element analysis, the effects of axial as well as flexural stiffness of the collars are present in these curves. The effect of flexural stiffness of the confining elements has largely been neglected in previous finite element models.

## 5.4 Proposed Model for Confinement of Concrete

A confinement model is proposed for the prediction of material curves for columns confined externally by HSS collars that takes into account active as well as passive confining pressures, variability of the confining pressure through the axial load history of the column, flexural stiffness of collars, axial stiffness of collars, spacing of collars, stress vs. strain behaviour of the collars, and properties of concrete such as strength, modulus of elasticity, Poisson's ratio, and strain at peak stress. The model uses certain features of existing confinement models. The proposed generalized stress vs. strain relationship of concrete confined externally by HSS collars is shown in Figure 5-9, where  $f'_{cc}$  is the peak stress of the confined concrete,  $\epsilon_{cc}$  is the strain at peak stress, and  $\epsilon_{cc85}$  is the strain corresponding to 85% of the peak stress in the post-peak region. The methods for constructing the various segments of this curve are described subsequently.

The confining pressure under the collars varies through the axial load history of the externally confined columns as is demonstrated subsequently. Similar to the models of Ahmad and Shah (1982), Madas and Elnashai (1992), Cusson and Paultre (1995), Fam and Rizkalla (2001), and Légeron and Paultre (2003), the proposed model also makes use of an incremental-iterative procedure to trace the stress vs. strain curve of confined concrete. During each increment, constant confining pressure is assumed. The confining pressure under the steel collars can be purely passive or it can have both active and passive components, and the passive confining pressures become dominant in the latter stages of the tests. It is assumed that active and passive confining pressures produce the same confined concrete material curve (Richart *et al.* 1928, 1929; Iyengar *et al.* 1970).

A typical reinforced concrete column with HSS collar confinement is shown in Figure 5-10(a). For simplicity, the discrete collars are not modelled individually but are assumed smeared over the height of the column equivalent to a continuous tube as shown in Figure 5-10(b). This assumption does not seem valid if the confining pressures under the collars and between the collars at the surface of the column are compared. However, this assumption becomes viable for relatively closely spaced collars if the confining pressure is considered a short distance away from the surface of the column. Similar assumptions have been made in the existing confinement models for columns with conventional transverse reinforcement (Sheikh and Uzumeri (1982); Mander *et al.* (1988b); Saatcioglu and Razvi (1992); and Légeron and Paultre (2003)).

The equivalent tube is assumed made of an orthotropic material having zero stiffness in the direction of column axis. The flexural stiffness of the tube in the direction normal to the longitudinal axis of the column should match the total flexural stiffness of all collars, over the height of the column, in the same direction. A similar argument applies to the axial stiffness of the equivalent tube and discrete collars. It is further assumed that the column with equivalent tube confinement expands uniformly over its height without bulging. Similar assumptions were made by Légeron and Paultre (2003) in the development of their confinement model for normal- and high-strength concrete, and by Caner and Bažant (2002) while applying their computational model with smeared confinement to columns confined by spiral reinforcement.

#### 5.4.1 Lateral Displacement Compatibility

Lateral displacement compatibility at the interface between the concrete prism and the confining tube is used to formulate the interaction between them. Consider the unconfined concrete column with square cross-section shown in Figure 5-10(c). When an axial strain,  $\varepsilon_c$ , is applied to the concrete column, it is assumed that free uniform lateral expansion of the concrete takes place over the height and width of the column. As the prism is free to expand laterally, the lateral displacement,  $u_{hco}$ , can be evaluated as:

$$[5.1] \quad u_{hco} = \frac{\nu_c h \varepsilon_c}{2}$$

where  $\nu_c$  is Poisson's ratio of the material; and  $h$  is the lateral dimension (width) of the square concrete prism.

When the expansion of the concrete takes place due to the Poisson's effect, the confining tube resists this expansion by developing confining pressure on the concrete column through its axial and flexural stiffness. For simplicity, it is assumed that the confining pressure under the tube is uniformly distributed along the height and width of the column. If the concrete prism is subjected to external bi-axial uniform confining pressure,  $\sigma_h$ , as shown in Figure 5-10(d) (the equivalent confining tube is not shown in the figure for clarity), the inward displacement,  $u_{hci}$ , at any face of the column is determined for elastic behaviour using the following constitutive relationship (Young 1989):

$$[5.2] \quad u_{hci} = \frac{1 - \nu_c}{2E_c} h \sigma_h$$

where  $E_c$  is the modulus of elasticity of the concrete.

Now consider the lateral expansion of the confining tube as shown in Figure 5-10(e). (There is no axial strain applied to the confining tube that is analogous to  $\varepsilon_c$  for the concrete due to the discontinuous nature of the collars in the real structure.) For equilibrium, the outward pressure from the concrete on the confining tube must be equal in magnitude to the inward pressure applied by the tube on the concrete, *i.e.*,  $\sigma_h$ . It is assumed that the outward pressure on the confining tube causes uniform expansion of the tube along the width and height of the column as shown in Figure 5-10(e). The outward displacement of any side of the confining tube caused by this pressure is denoted by  $u_{ht}$ . The compatibility condition requires that the equivalent confining tube and the column concrete surface remain in contact throughout the axial load history. Accordingly, the lateral displacement of the confining tube  $u_{ht}$  and the net resultant lateral displacement of the concrete ( $u_{hco} - u_{hci}$ ) are equal, *i.e.*:

$$[5.3] \quad u_{ht} = u_{hco} - u_{hci}$$

Due to the interaction between the concrete and the confining tube, Equation 5.3 does not result in a unique solution for  $u_{ht}$ . Equations 5.1 and 5.2 taken together (right hand side of Equation 5.3) provide an expression for the lateral displacement of the column under a certain confining pressure and axial strain that is based on the concrete behaviour alone. In order to develop an analogous expression for the lateral displacement based on the steel behaviour alone (left hand side of Equation 5.3), use is made of a confining pressure vs. lateral strain curve based on the tube behaviour, such as the typical one depicted in Figure 5-11. The behaviour of the confining tube may be determined by finite element analysis, as described above. This curve is nonlinear and it starts from the origin. In the case of collars with bolted corner connections, some initial confining pressure may exist due to the pre-stressing force in bolts. The initial active confining pressure is treated separately. The behavioural curve of the confining tube itself is considered independent of the concrete behaviour. However, the particular point on the curve where equilibrium is achieved under a certain axial column force depends on both the lateral expansion of the concrete under the Poisson effect due to the applied axial strain as well as the lateral contraction of the concrete due to the confining pressure applied by the tube. In the

present study, the general confining pressure from the curve based on the tube behaviour is denoted by  $\sigma_{ct}$ , whereas the equilibrium confining pressure for a particular axial strain, which includes the response of the concrete, is denoted by  $\sigma_h$ .

For a particular lateral displacement (or lateral strain) of the confining tube, a characteristic secant line can be constructed. From Figure 5-11, the slope of the  $i$ th secant line,  $(E_{ct})_i$ , is:

$$[5.4] \quad (E_{ct})_i = \frac{(\sigma_{ct})_i}{(\varepsilon_l)_i}$$

and the slope of a general secant line,  $E_{ct}$ , is:

$$[5.5] \quad E_{ct} = \frac{\sigma_{ct}}{\varepsilon_l}$$

where  $(\sigma_{ct})_i$  and  $(\varepsilon_l)_i$  are the confining pressure and lateral strain, respectively, corresponding to the point of intersection of the  $i$ th secant line with the confining pressure vs. lateral strain curve of the confining tube and  $\sigma_{ct}$  and  $\varepsilon_l$  are the confining pressure and lateral strain corresponding to the point of intersection of a general secant line with the confining pressure vs. lateral strain curve. It is to be noted that for a particular confining pressure or lateral strain,  $E_{ct}$  is a characteristic of the confining tube only.

It is assumed that a constant confining pressure,  $\sigma_h$ , develops at the interface between the concrete and the confining tube in a certain increment. By setting the confining pressure  $\sigma_{ct}$  equal to  $\sigma_h$ , the displacement of the confining tube can be derived from Equation 5.5 to give:

$$[5.6] \quad u_{ht} = \frac{\sigma_h h}{2E_{ct}}$$

By substituting the expressions for  $u_{hco}$ ,  $u_{hci}$ , and  $u_{ht}$  from Equations 5-1, 5-2, and 5-6, respectively, into Equation 5.3, the following expression for the unknown interfacial confining pressure,  $\sigma_h$ , is obtained:

$$[5.7] \quad \sigma_h = \frac{v_c \varepsilon_c}{\frac{1}{E_{ct}} + \frac{1-v_c}{E_c}}$$

Similar compatibility equations have been used by other researchers such as: Fam and Rizkalla (2001) for FRP confined circular columns; Cusson and Paultre (1995) for confinement of high-strength concrete columns of rectangular/square cross-section; and Légeron and Paultre (2003) for normal- and high-strength concrete columns of rectangular/square cross-section. The confining pressure vs. lateral strain relationship is linear for FRP confinement, whereas the confining pressure vs. lateral strain relationship for steel ties and steel collar confinement are nonlinear in nature (see Figure 5-11).

#### 5.4.2 Effect of Unconfined Concrete in the Core

In conventional columns, the core is generally defined as the region enclosed by the centreline of the ties. Figures 5-12(a) and 5-12(b) show the ineffectively confined regions between tie levels and at the ties that are approximately parabolic in shape, as described by, for example, Sheikh and Uzumeri (1982) and Mander *et al.* (1988b). In the confinement model by Sheikh and Uzumeri (1982), an expression for the strength enhancement factor was defined based on the core bounded by the centreline of the ties. It was assumed that the strength enhancement factor depends on the amount of transverse reinforcement, the stress in the transverse reinforcement at the peak stress of confined concrete, and the ratio of effectively confined concrete at the critical section to the core area bounded by the centreline of the ties, which in turn depends on the configuration and spacing of ties. Similarly, in the confinement model by Mander *et al.* (1988b), a confinement effectiveness coefficient was defined as the ratio of effectively confined concrete at the critical section to the concrete area in the core bounded by the centreline of the perimeter ties. The average confining pressure was calculated assuming yielding of the transverse reinforcement at the peak stress of the confined concrete. The average confining pressures on the sides of the column were then multiplied by the confinement effectiveness coefficients to obtain the equivalent confining pressure. The peak stress of the confined concrete was then determined under this equivalent confining pressure. Saatcioglu and Razvi (1992) also reported that the average confining pressure calculated by assuming yielding of the transverse reinforcement overestimates the confining pressure. A factor was therefore defined based on a

regression analysis of experimental data to convert the average confining pressure to an equivalent confining pressure. The model proposed by Chung *et al.* (2002) utilizes an effectively confined distance ratio, instead of area, to account for ineffectively confined regions in the core. The effectively confined distance ratio is defined as the ratio of the effectively confined width to the total width of the core concrete. This ratio takes the maximum value at the tie level and the minimum value at the critical section midway between two sets of ties. However, effectively and ineffectively confined regions were not dealt with separately. Instead, an expression for the strength enhancement factor was defined using regression in terms of the volumetric ratio of transverse steel, stress in the transverse steel at peak stress of the confined concrete, cylinder strength of the concrete, and effectively confined distance ratio.

In contrast to the approaches described above wherein the ineffectively confined concrete is accounted for by a reduction factor, the proposed model for externally confined columns separates explicitly the behaviour of the effectively and ineffectively confined regions in the core. The core of the externally confined columns is equal to the gross dimensions of the columns. The load vs. strain curves of the effectively and ineffectively confined concrete regions in the core are defined, and are then combined to get the overall load vs. strain curve of the concrete in the core. The load vs. strain curves can be converted to stress vs. strain curves by dividing the load by the core area. Figure 5-12(c) shows the effectively and ineffectively confined regions between the collars and Figure 5-12(d) shows that there are no ineffectively confined regions at the collar level because of the considerable flexural stiffness of the sides of the collars, in addition to their axial stiffness. This assumption has been verified by both experimental and finite element studies. To model the behaviour of the effectively confined regions in the core, the collars are assumed smeared over the height of the columns, as described before, with confining pressure uniformly distributed on the side of the columns. The ineffectively confined concrete acts simply as a filler to transfer the confining force to the effectively confined regions. First, the behaviour of the confined concrete in the core will be determined and then the behaviour of unconfined concrete in the core region will be studied.

### **5.4.3 Behaviour of Confined Concrete in Core**

Mander *et al.* (1988b) proposed a model for the stress vs. strain curve of concrete confined by conventional transverse steel reinforcement that assumes constant confining pressure through the axial load history. In this model, the stress vs. strain curve of confined concrete is represented by an equation proposed by Popovics (1973) for unconfined concrete. In addition, it utilizes the expression for strain at peak stress of the confined concrete proposed by Richart *et al.* (1928) based on the test results of cylinders under constant hydraulic confining pressure. In columns

confined externally by HSS collars, the confining pressure varies with the axial load history. Therefore, this model cannot be used directly to predict the stress vs. strain relationships of these columns. However, the model can still be utilized to predict the behaviour of these columns by applying only a small increment of axial strain over which confining pressure can be assumed constant. This leads to an incremental-iterative approach to predict the behaviour of externally confined columns similar to the approaches used by Ahmed and Shah (1982), Madas and Elnashai (1992), Cusson and Paultre (1995), and Légeron and Paultre (2003) for concrete confined by conventional rebar ties. Similarly, Fam and Rizkalla (2003) also used an incremental-iterative approach for concrete columns confined by FRP, a material that exhibits essentially elastic behaviour and results in varying confinement pressure as the column is loaded axially. During each increment, a different confined concrete material response forms with a different concrete secant modulus of elasticity,  $(E_c)_i$ , corresponding to a general point  $i$  on the confined concrete material curve at which the axial strain is  $(\varepsilon_c)_i$ .

Dilation properties of unconfined and confined concrete under active confining pressures have been well established by Chen (1982) and Pantazopoulou (1995). Madas and Elnashai (1992) used a relationship for Poisson's ratio in their model for conventional rebar confinement that was determined by performing a least square fit of a cubic polynomial on the test results of concrete under biaxial compression provided by Kupfer *et al.* (1969). Similarly, Fam and Rizkalla (2001) developed relationships for the dilation of concrete confined actively using hydrostatic pressure, based on the test results (triaxial compression tests) of Gardner (1969), for use with their model for FRP confinement. These relationships have been used in the proposed procedure for the confinement of concrete by steel collars.

Similar to the secant modulus of elasticity of concrete, the secant Poisson's ratio,  $\nu_c$ , also changes with the increase in the axial strain of the column. In addition, the secant Poisson's ratio,  $\nu_c$ , is also dependent on the magnitude of the confining pressure present in an increment of axial strain. The secant Poisson's ratio in the increment  $i$  can be represented by  $(\nu_c)_i$ . Gardner (1969) tested concrete cylinders and reported average lateral strain vs. axial strain curves at different levels of confining pressure. Using those results, Fam and Rizkalla (2001) developed the following relationship between the secant Poisson's ratio,  $\nu_c$ , and the axial strain of the confined concrete,  $\varepsilon_c$ , for different confining pressures:

$$[5.8] \quad \left( \frac{\nu_c}{\nu_{co}} \right) = C \left( \frac{\varepsilon_c}{\varepsilon_{cc}} \right) + 1$$

where  $\nu_{co}$  and  $\varepsilon_{cc}$  are the initial Poisson's ratio and strain at peak stress of confined concrete, respectively. It is clear from this equation that the Poisson's ratio increases with the increase of axial strain of the confined concrete. An upper limit of 0.5 is imposed on the secant Poisson's ratio in the present investigation as suggested by Madas and Elnashai (1992) because the Poisson's ratio of conventional engineering materials cannot exceed 0.5. The bulk modulus of concrete will become infinity at Poisson's ratio equal to 0.5. At the time of bursting of concrete, the Poisson's ratio may be taken equal to 0.5.

A linear expression for the constant  $C$  (it is considered constant within an increment) as a function of the confining pressure (again, assumed constant within an increment) was obtained by performing a regression analysis on the experimentally obtained values of  $C$  (Fam and Rizkalla 2001):

$$[5.9] \quad C = 1.914 \left( \frac{\sigma_h}{f'_{co}} \right) + 0.719$$

For increment  $i$ , Equations 5.8 and 5.9 can be written as:

$$[5.10] \quad \left( \frac{\nu_c}{\nu_{co}} \right)_i = (C)_i \left( \frac{\varepsilon_c}{\varepsilon_{cc}} \right)_i + 1$$

$$[5.11] \quad (C)_i = 1.914 \left[ \frac{(\sigma_h)_i}{f'_{co}} \right] + 0.719$$

The lateral strain  $(\varepsilon_l)_i$  in the increment can be calculated as:

$$[5.12] \quad (\varepsilon_l)_i = (\nu_c)_i (\varepsilon_c)_i$$

Knowing  $(\varepsilon_l)_i$ , the confining pressure,  $(\sigma_h)_i$ , can be found from the relationship between the confining pressure vs. lateral strain (similar to Figure 5-11) obtained from the finite element analysis by setting  $(\sigma_h)_i = (\sigma_{ct})_i$ . Then,  $(E_{ct})_i$  can be calculated as:

$$[5.13] \quad (E_{ct})_i = \frac{(\sigma_{ct})_i}{(\varepsilon_l)_i}$$

The confining pressure  $(\sigma_h)_i$  due to collar confinement in increment  $i$  can be calculated from the following equation, the derivation of which (Equation 5-7) has been given before:

$$[5.14] \quad (\sigma_h)_i = \frac{(v_c)_i}{\frac{1}{(E_{ct})_i} + \frac{1}{(E_c)_i}} (\varepsilon_c)_i$$

If there exists both active and passive confining pressures, as shown in Figure 5-13 (active confining pressure remains constant but the passive confining pressure varies through the axial load history), Equation 5.14 is applied only to the passive component of the confining pressure. The passive confining pressure is then added to the active component of the confining pressure to get the total confining pressure  $(\sigma_h)_i$  in that increment.

If  $(\sigma_h)_i$  is known in an increment  $i$ , various equations are available for calculating the peak stress of confined concrete  $(f'_{cc})_i$ . However, the present model makes use of the following equation for this purpose that assumes constant confining pressure (also used by Mander *et al.* (1988b)):

$$[5.15] \quad (f'_{cc})_i = f'_{co} \left[ 2.254 \sqrt{1 + \frac{7.94(\sigma_h)_i}{f'_{co}}} - 2 \frac{(\sigma_h)_i}{f'_{co}} - 1.254 \right]$$

This equation is based on the “five parameter” multiaxial failure surface of concrete under triaxial compression given by Willam and Warnke (1975) calibrated with test results of concrete under triaxial compression provided by Schickert and Winkler (1979).

Then, the strain at peak stress,  $(\varepsilon_{cc})_i$ , of the confined concrete material can be determined from the following equation (Richart *et al.* 1928):

$$[5.16] \quad (\varepsilon_{cc})_i = \varepsilon_{co} \left[ 1 + 5 \left( \frac{(f'_{cc})_i}{f'_{co}} - 1 \right) \right]$$

Then, according to the procedure of Mander *et al.* (1988b), the Popovics (1973) equation is utilized to determine the confined concrete stress,  $(f_{cc})_i$ , at axial strain  $(\varepsilon_c)_i$  as given below:

$$[5.17] \quad (f_{cc})_i = \frac{(f'_{cc})_i (x)_i (r)_i}{(r)_i - 1 + (x)_i^{(r)_i}}$$

where:

$$[5.18] \quad (r)_i = \left[ \frac{E_{co}}{E_{co} - (E_{sec})_i} \right]$$

$$[5.19] \quad (E_{sec})_i = \frac{(f'_{cc})_i}{(\varepsilon_{cc})_i}$$

$$[5.20] \quad (x)_i = \frac{(\varepsilon_c)_i}{(\varepsilon_{cc})_i}$$

Knowing the stress of confined concrete  $(f_{cc})_i$  at strain  $(\varepsilon_c)_i$ , the secant modulus of elasticity,  $(E_c)_i$ , of the confined material in increment  $i$  can be calculated as:

$$[5.21] \quad (E_c)_i = \frac{(f_{cc})_i}{(\varepsilon_c)_i}$$

The values for  $f'_{co}$ ,  $\varepsilon_{co}$ , and  $E_{co}$  in the foregoing equations are based on the unconfined column concrete response curve and can be estimated using well-established methods based on standard cylinder test data.

Using the procedure described above, twelve unknowns are encountered in a particular increment on the axial strain of the confined concrete. Specifically, for a particular level of axial strain in the  $i$ th increment,  $(\varepsilon_c)_i$ , the following parameters are all initially unknown: the resulting confining pressure,  $(\sigma_h)_i$ , the secant modulus of elasticity,  $(E_c)_i$ , the Poisson's ratio,  $(\nu_c)_i$ , the constant  $(C)_i$ , the strain at peak stress of confined concrete,  $(\varepsilon_{cc})_i$ , the secant slope of the behavioural curve of the confining tube,  $(E_{ct})_i$ , the lateral strain,  $(\varepsilon_l)_i$ , the peak stress of confined concrete,  $(f'_{cc})_i$ , the confined concrete stress,  $(f_{cc})_i$ , the confined concrete material curve parameters  $(x)_i$  and  $(r)_i$ , and the secant modulus of elasticity at the peak of the confined curve,  $(E_{sec})_i$ . Hence, the method of successive approximations is used on Equations 5.10 to 5.21 to converge to the solution within each increment. The values of the unknowns are assumed arbitrarily in the first iteration in an increment. In subsequent iterations in the same increment, the values from the immediately previous iteration are used. Iterations are performed until the values of these variables converge. Then, the next increment in axial strain of the confined is taken and the process is repeated. In this way, the stress vs. strain curve of externally confined concrete is traced until some failure criterion is met. This process of tracing the confined material curve is path-independent because we can find the confined concrete stress,  $(f_{cc})_i$ , at any level of axial strain,  $(\varepsilon_c)_i$ , in an increment  $i$  without knowing the trace of confined concrete material curves in the previous increments. A computer program C4P was written based on FORTRAN to perform these incremental-iterative calculations, the listing of which is given in Appendix L.

#### 5.4.4 Behaviour of Unconfined Concrete in Core

Some portion of the concrete in the core of the externally confined column is not effectively confined. The depth of this unconfined concrete into the core was determined based on tests of externally confined columns under concentric axial loading (Chapter 3). The average depth of parabolic concrete spalling between the collars at the peak load was found to be  $0.29 s'$ , which is higher than the depth of concrete spalling between ties equal to  $0.21 s'$  reported by Chung *et al.* (2002) based on analytical derivations, where  $s'$  is the clear spacing between the collars or ties. To simulate the behaviour of cover concrete, the following expression was proposed by Muto (1974) and is plotted in Figure 5-14:

$$[5.22] \quad f_c = 6.75 f'_c (e^{-0.812\xi} - e^{-1.218\xi})$$

where  $\xi = \varepsilon_c / \varepsilon_s$ ,  $f_c$  and  $\varepsilon_c$  are stress and strain of unconfined concrete, and  $\varepsilon_s$  is the strain at which spalling of the unconfined concrete starts. The same expression is adopted to represent the behaviour of the parabolic concrete region between the collars in externally confined columns. Muto (1974) took  $\varepsilon_s$  equal to the strain at peak stress of the unconfined concrete. For externally confined columns, the value can be determined more directly and it is recommended that  $\varepsilon_s$  be taken equal to the average of experimentally observed strains at which concrete spalling started based on the externally confined columns tested under concentric axial loading (Chapter 3). The average value of this strain was found to be 0.0039.

#### 5.4.5 The Descending Branch

The procedure for establishing the strain at peak stress,  $\varepsilon_{cc}$ , (i.e., at point A in Figure 5-9) and the slope of the descending branch (line A–C in Figure 5-9) of the confined concrete material curve is presented in this section. The descending branch is established after calculating the confined concrete stress,  $f'_{cc}$ , vs. axial strain,  $\varepsilon_c$ , relationship by the proposed model that does not in itself possess a failure criterion.

The slope of the descending branch of the confined concrete material curve can be established by knowing the values of  $f'_{cc}$ ,  $\varepsilon_{cc}$  and  $\varepsilon_{cc85}$  of the confined concrete material curve, where  $f'_{cc}$  is the peak stress of the confined concrete,  $\varepsilon_{cc}$  is the strain at peak stress of the confined concrete, and  $\varepsilon_{cc85}$  is the strain at 85% of  $f'_{cc}$  in the post-peak region. For these variables, the influencing parameters are established from the literature and models are proposed for  $\varepsilon_{cc}$  and  $\varepsilon_{cc85}$  for collared columns in terms of these parameters. The models are then calibrated using available experimental data. The value of  $f'_{cc}$  is determined from the confined concrete material curve, established by the model presented previously, at the strain corresponding to  $\varepsilon_{cc}$ .

In some of the confinement models established for conventional rebar confinement such as the modified Kent and Park (Park *et al.*, 1982), Sheikh and Uzumeri (1982), and Saatcioglu and Razvi (1992), the equations for determining the strain at peak stress and the slope of the descending branch of the confined concrete material curves were obtained empirically by

performing a regression analysis on the test results of concrete columns confined by conventional rebar ties.

In the modified Kent and Park model (Park *et al.*, 1982), the strain at peak stress of confined concrete depends on the following: (1) strain at peak stress of unconfined concrete; (2) volumetric ratio of the confining steel; (3) yield strength of the confining steel; and (4) cylinder strength of the concrete. The model assumes that with an increase in the cylinder strength of concrete, the strain at peak stress of the confined concrete will decrease. This model does not take into account the effect of tie spacing and the effect of distribution of longitudinal steel on the strain at peak stress of the confined concrete material curve. According to this model, the slope of the descending branch will increase (will become steeper) with an increase in cylinder strength of concrete, and will decrease (will become less steep or will tend to be flat) with an increase of the volumetric ratio and yield strength of the confining steel and by decreasing the ratio of tie spacing to the width of the column.

In the model proposed by Sheikh and Uzumeri (1982), the strain at peak stress depends on the following parameters: (1) volumetric ratio of the confining steel; (2) stress in the confining steel at peak stress of confined concrete; (3) cylinder strength of concrete; (4) strain at peak stress of unconfined concrete; (5) spacing of ties; and (6) distribution of the longitudinal bars of the column. According to this model, the strain at peak stress of the confined concrete will increase with an increase of the volumetric ratio and the stress of the confining steel at the peak stress of the confined concrete. The strain at peak stress of the confined concrete also increases with a decrease in spacing of transverse ties and with an increase of strain at the peak stress of unconfined concrete. Conversely, the strain at peak stress of confined concrete will decrease with an increase of centre-to-centre spacing of the longitudinal bars (this effect is related to both the distribution of longitudinal bars and the resulting tie configuration) and with an increase of cylinder strength of concrete. According to this model, the slope of the descending branch depends on the following two parameters: volumetric ratio of the confining steel and the ratio of tie spacing to the column width. In accordance with this model, the slope of the descending branch will decrease (will tend to become flat) with an increase of the volumetric ratio of the confining steel and with a decrease in spacing of transverse ties.

In the confinement model by Saatcioglu and Razvi (1992), the strain at peak stress of the confined concrete depends on the following parameters: (1) strain at peak stress of unconfined concrete; (2) equivalent confining pressure; and (3) unconfined concrete strength of the column. The equivalent confining pressure, in turn, takes into account the effect of the following parameters: (a) spacing of ties; (b) distance between the longitudinal bars of the column

(distribution of longitudinal bars of the columns); and (c) the sectional transverse steel ratio. In accordance with this model, the strain at peak stress of confined concrete increases with an increase of strain at peak stress of unconfined concrete and the equivalent confining pressure and it decreases with an increase of the strength of the column concrete. For determining the slope of the descending branch, no equation was defined in this model. However, an empirical expression for the strain at 85% of the peak stress of the confined concrete in the post-peak region was given, which indirectly establishes this slope. According to this model, this strain increases with an increase in the sectional transverse steel ratio, the strain at peak stress of confined concrete, and the strain at 85% of the peak stress of unconfined concrete in the post-peak region. The strain at peak stress of the confined concrete depends on the effective confining pressure, which in turn is related to the ratio of tie spacing to the column width. Hence, indirectly it can be established that in this model also, the slope of the descending branch depends on the ratio of tie spacing to the column width.

With this background from the literature, the proposed model for the confinement of concrete by HSS collars assumes that both the strain at peak stress and the slope of the descending branch of the confined concrete material curve depend on the following parameters:

- (1) the magnitude of the confining pressure at an axial strain of 0.10,  $\sigma_{h01}$ ;
- (2) the strain at peak stress of unconfined column concrete,  $\varepsilon_{co}$ ;
- (3) the strain at 85% of peak stress of unconfined column concrete in the post-peak region,  $\varepsilon_{co85}$ ;
- (4) the strength of unconfined column concrete,  $f'_{co}$ ;
- (5) the ratio of the clear spacing between the collars to the width of the confined concrete core (*i.e.*, the column width for collared columns),  $\frac{s'}{h_{column}}$ ; the clear spacing between the collars is calculated as  $s' = (s - t_{collar})$ , where  $s$  is the centre-to-centre spacing of the collars and  $t_{collar}$  is the width (parallel to the column axis) of the collar.

It is apparent that the confining pressure applied by the collar will affect the nature of the descending branch. This parameter includes the effects of the axial and flexural stiffnesses of the collar as well as the yield stress of the collar steel. In the confinement of concrete by steel collars, the confining pressure under the collars does not remain constant, as in the case of yielding rebar ties, but rather builds gradually with the increase of axial strain. A question arises, therefore, as to

what value of confining pressure should be used in developing equations for the strain at peak stress and the slope of the descending branch of the confined concrete material curve, although it must be at a level of strain within the descending branch of the confined material curve. The value of confining pressure at an axial strain of 0.10,  $\sigma_{h01}$ , is chosen because in the testing of some of the columns with welded collars (Chapter 3), an axial strain of 0.10 would likely have been achieved had the corner welds of the collars not fractured prematurely. The second justification for choosing a confining pressure at this large axial strain is the presence of active confining pressure in some of the columns with bolted collars. The effect of the presence of initial active confining pressure diminishes under increasing deformations and is considered negligible at this level of axial strain. The relationships between the confining pressure and axial strain determined by the proposed model (i.e., the model used for the ascending branch) are utilized to determine the value of  $\sigma_{h01}$ .

It is widely recognized that the character of the unconfined material curve is reflected in the confined material curve. Therefore,  $\varepsilon_{co}$ ,  $\varepsilon_{co85}$ , and  $f'_{co}$  are also included in the list of parameters that influence the descending branch. These parameters are consistent with those identified by other researchers, as described above.

It is also reasonable to assume that the descending branch depends on the ratio of the clear spacing between the collars to the width of the column,  $\frac{s'}{h_{column}}$ . The clear spacing has been observed experimentally (Chapters 3 and 4) to influence greatly the degree of spalling at large axial strains, which, in turn, has a fundamental effect on the effective material behaviour. The only parameter that was identified by the other research programs described previously as being influential for the descending branch of conventionally tied columns that has no equivalent in the list above is the spacing of the longitudinal reinforcing steel. This parameter has been neglected for collared columns because the efficiency of the collars in confining the column concrete tends to dominate the behaviour, making the spacing of the longitudinal bars less important.

As shown in Chapter 3, the descending branches of the confined concrete material curves of four of the collared columns, C01, C02, C03, and C04, were obtained experimentally. In order to develop the model for the descending branch, the confined concrete material curves of these columns were idealized.

To get an idealized counterpart of the confined concrete material curve, a straight-line equation was fit to the portion of the descending branch of each of these columns between 60% and 95% of the peak stress as shown in Figures 5-15 through 5-18. The selection of these limits was based on judgement, so that the idealized confined concrete material curves give the best representation of their corresponding experimental counterpart. The upper limit (95%) was chosen to exclude the local sharp curvature just beyond the peak that is not representative of the overall character of the descending branch. The lower limit (60%) was selected because data were available to this point for all the curves considered. The straight-line equations for these columns, obtained through regression, are shown in these figures.

Figures 5-19 through 5-22 show the experimental confined concrete material curves for columns C01 through C04, respectively, along with their idealized counterparts. The idealized curves were obtained by plotting horizontal lines at the peak stresses of the experimentally obtained confined concrete material curves and by plotting the equations for the descending branches obtained previously. The two lines intersect to define the beginning of the descending branch. The areas under the experimentally obtained confined concrete material curves were calculated up to 60% of the peak stress (in the descending branch) for each of these columns. The strains corresponding to this stress for columns C01, C02, C03, and C04 are 0.0672, 0.0721, 0.0521, and 0.0292, respectively. Vertical lines (called equal area lines) are also drawn in these figures to delineate this level of strain. Similarly, the areas under the idealized curves for these columns were also calculated up to this level of strain. The areas under the experimental curves and the corresponding idealized curves were slightly different. Therefore, the idealized descending branch lines were shifted towards the left until the areas under the experimental and idealized curves became equal. The idealized confined concrete curves shown in Figures 5-19 through 5-22 show the final location of inclined descending branches. (The second terms in the equations for the descending branches are very slightly different than those given in Figures 5-15 through 5-18.) From the idealized confined concrete material curves, the values of  $\epsilon_{cc}$  and  $\epsilon_{cc85}$  were determined. The strain at peak stress,  $\epsilon_{cc}$ , corresponds to the point of intersection of the horizontal line drawn at the peak stress of the experimentally obtained confined concrete material curve and the inclined descending branch after area equalization (point A in the figures). From the idealized curves, the strains corresponding to 85% of the peak stresses,  $\epsilon_{cc85}$ , (at point B) were also determined for these columns. The resulting values of  $\epsilon_{cc}$  and  $\epsilon_{cc85}$  are reported in Table 5.1, which are used to calibrate the proposed generalized model for the descending branch. The following equations are proposed for  $\epsilon_{cc}$  and  $\epsilon_{cc85}$  in terms of the confinement index,  $\omega$ , and the characteristics of the unconfined concrete material curves:

$$[5.23] \quad \varepsilon_{cc} = \varepsilon_{co} \left[ 1 + y_1 \left( \frac{\sigma_{h01} h_{column}}{s'f'_{co}} \right)^{y_2} \right]$$

$$[5.24] \quad \varepsilon_{cc85} = \varepsilon_{co85} \left[ 1 + y_3 \left( \frac{\sigma_{h01} h_{column}}{s'f'_{co}} \right)^{y_4} \right]$$

Substituting  $\omega = \frac{\sigma_{h01} h_{column}}{s'f'_{co}}$ ,  $\alpha = \frac{\varepsilon_{cc}}{\varepsilon_{co}}$ , and  $\beta = \frac{\varepsilon_{cc85}}{\varepsilon_{co85}}$  in the above equations, the following

equations are obtained that represent, respectively, the non-dimensional enhancement in the strain at peak stress and the strain at 85% of the peak stress in the descending branch due to collar confinement:

$$[5.25] \quad \alpha = 1 + y_1 \omega^{y_2}$$

$$[5.26] \quad \beta = 1 + y_3 \omega^{y_4}$$

The nature of Equations 5.23 through 5.26 is such that they will always remain dimensionally homogeneous and will not depend on the system of units for the constituent variables. The values of coefficients  $y_1$  through  $y_4$  were determined through regression based on the test results of columns C01, C02, C03, and C04; some key results are given in Table 5.1 and the remaining can be seen in Chapter 3. The strain at peak stress of the unconfined column concrete,  $\varepsilon_{co}$ , in the columns can be determined from the following common relationship that assumes a parabolic unconfined stress vs. strain response:

$$[5.27] \quad \varepsilon_{co} = \frac{2f'_{co}}{E_c}$$

where  $E_c = 3700\sqrt{f'_{co}}$  is the initial slope of the curve (with the coefficient determined from concrete cylinders). The computed values of this strain,  $\varepsilon_{co}$ , for the column concrete are given in Table 5.1. A comparison of the values of  $\varepsilon_{co}$  with the values of  $\varepsilon_o$ , determined experimentally for

the associated concrete cylinder tests (Table 3.2; Chapter 3), provides further support for the use of Equation 5.27.

No direct measurements were made for the strain at 85% of the peak stress in the post-peak region,  $\varepsilon_{co85}$ , of the unconfined concrete material curve. Based on the available evidence in the literature, the strains  $\varepsilon_{co85}$  were conservatively assumed to be 1.75 times the strain  $\varepsilon_{co}$ . Saatcioglu and Razvi (1992) suggested that in the case of an absence of experimental data, the strain at peak stress of unconfined concrete,  $\varepsilon_{co}$ , can be assumed to be 0.002. They also suggested that the strains  $\varepsilon_{co85}$  can be assumed to be 0.0038. According to these suggestions, the ratio of  $\varepsilon_{co85}$  to  $\varepsilon_{co}$  is 1.9, which is higher than 1.75 assumed in the present research. The computed values of  $\varepsilon_{co85}$  are also given in Table 5.1. The strength of unconfined concrete in the column,  $f'_{co}$ , in Equations 5.23 through 5.26, is taken equal to 85% of the cylinder strength of concrete,  $f'_c$ .

The values of  $\alpha$  are plotted with respect to the values of  $\omega$  for columns C01, C02, C03, and C04 in Figure 5-23. Through regression, the following expression is obtained for  $\alpha$  :

$$[5.28] \quad \alpha = 1 + 3.0\omega^{2.5}$$

Similarly, the values of  $\beta$  are plotted with respect to  $\omega$  for columns C01, C02, C03, and C04 depicted in Figure 5-24. Through regression, the following expression was obtained for the values of  $\beta$  :

$$[5.29] \quad \beta = 1 + 3.0\omega^{1.8}$$

It is to be noted that Equations 5.28 and 5.29 were calibrated for the values of confinement index,  $\omega$ , ranging from 0.76 to 1.79 (Table 5.1). These equations may not produce good results outside of this range. More experimental testing is recommended to increase the range of these equations.

Knowing the values of  $\alpha$  and  $\beta$  for a column, the slope of the descending branch of the confined concrete in the core can be determined by the following equation:

$$[5.30] \quad z = \frac{0.15}{(\varepsilon_{cc85} - \varepsilon_{cc})}$$

Then the descending branch is traced as follows:

$$[5.31] \quad f_{cc} = f'_{cc} [1 - z(\varepsilon_c - \varepsilon_{cc})]$$

The descending branch A–C extends to the horizontal sustaining branch of the confined concrete material curve at a stress level of  $0.3f'_{cc}$  (Figure 5-9). This constant stress level of the sustaining branch has been assumed similar to the confinement models proposed by Vallenias *et al.* (1977), Sheikh and Uzumeri (1982), and Chung *et al.* (2002). However, more experimental data are required to justify this stress level.

#### 5.4.6 Application of the Proposed Model

The proposed model was applied to determine the confined concrete material curves for collared columns (C01 to C09) tested in phase 1 of the project as well as collared columns (CL1 TO CL8) tested in phase 2. The phase 1 columns were tested under concentric axial loading and the phase 2 columns were tested under lateral cyclic loading, either with or without axial load. The details of the phase 1 columns are described in Chapter 3 and those of the phase 2 columns are given in Chapter 4.

Confining pressure vs. lateral strain relationships for the collared columns were obtained through finite element analyses to establish the confining behaviour of the collars. Figures 5-25 and 5-26 show the confining pressure vs. lateral strain relationships for the phase 1 (C01 to C09) columns. The curves for columns C02, C03, C04, and C05 are composite curves in that they consist of a combination of active and passive confining pressures. The initial active confining pressure was generated in the finite element models by inducing a negative temperature change in the bolts. Figure 5-27 shows the confining pressure vs. lateral strain relationships for the phase 2 (CL1 to CL9) columns with welded corner connections. The confining pressure vs. lateral strain curves are used to obtain the confined concrete material curves.

It is interesting to compare the confining behaviour determined from the proposed procedure with that obtained directly from the finite element analyses to demonstrate the need for the proposed procedure. The proposed procedure can also convert the confining pressure vs. lateral strain relationships to confining pressure vs. axial strain relationships for the externally confined

columns. Figures 5-28 through 5-36 show the relationship between the confining pressure vs. axial strain for the phase 1 columns (C01 to C09). For comparison, the confining pressure vs. axial strain relationships for these columns obtained directly from the finite element analyses using *ABAQUS* are also shown in these figures. It is clear that at a particular level of axial strain, the finite element curves show higher confining pressure, which is a direct indicator of the higher dilation rate of the concrete material model embedded in *ABAQUS* as compared to the dilation behaviour in the proposed model.

The proposed model was used to determine the confined concrete material curves for the reduced cores (*i.e.*, reduced area due to spalling between the collars) of the phase 1 and phase 2 columns (using the program C4P in the Appendix L) and these are depicted in Figures 5-37 through 5-39. These curves represent the stresses attained at the smallest cross-section accounting for the presence of spalling. The behaviour of the spalling concrete has been modelled by the equation proposed by Muto (1974). Figure 5-14 shows the behaviour of the spalling concrete during the axial load history of a typical column C01 (phase 1). The behaviour of the reduced cores and the spalling concrete in the columns were then combined to obtain the confined concrete material curves of the collared columns for phase 1 and phase 2 (Figure 5-40 and 5-41).

The abscissa of the confined concrete materials curves of the columns, confined concrete material curves of the reduced cores, and the material curves of the spalling concrete are identical. Therefore, the following equation can be used to calculate the ordinates of the confined concrete material curves:

$$[5.34] \quad f_{cc} = \frac{f_{cer}(A_{rcc} - A_{st}) + f_c A_{spc}}{(A_g - A_{st})}$$

where:

- $A_g$  = gross cross-sectional area of column;
- $A_{rcc}$  = cross-sectional area of the reduced core;
- $A_{spc}$  = cross-sectional area of the spalling concrete;
- $A_{st}$  = total cross-sectional area of longitudinal steel bars in column;
- $f_c$  = stress of unconfined concrete in the core;

$f_{cc}$  = stress of confined concrete in core;

$f_{ccr}$  = stress of confined concrete in the reduced core;

After determining the confined concrete material curves, the descending branches of these curves were established by the method proposed in Section 5.4.5.

The values of the confinement indices,  $\omega$ , for all the collared columns tested in phase 1 are given in Table 5.2. The values of the confinement index for columns C01, C02, C03, C04, and C09 fall in the range of confinement index over which the Equations 5.28 and 5.29 were developed. Hence, the descending branches can be established accurately only for these columns. Therefore, for the remaining columns, C05, C06, C07, and C08, the descending branches were not established, although the values of  $\varepsilon_{cc}$  and  $\varepsilon_{cc85}$  that result from this method are also reported in Table 5.2.

Similarly, the values of confinement indices,  $\omega$ , for collared columns tested in phase 2 are much higher than the range over which the Equations 5.28 and 5.29 were calibrated (Table 5.3). Therefore, the descending branches for these columns are not established. The values of  $\varepsilon_{cc}$  and  $\varepsilon_{cc85}$  for these columns are reported in Table 5.3, although they may not be accurate.

Figures 5-42 and 5-43 show the material curves of the longitudinal reinforcing bars of the phase 1 and phase 2 columns. Using the confined concrete material curves, the load vs. strain curves of the columns can be obtained. The ordinates of the load vs. strain curves of the columns can be obtained by the following equation:

$$[5.35] \quad P = f_{cc}(A_g - A_{st}) + f_s A_{st}$$

The load versus strain curves for the phase 1 collared columns (C01 through C09) predicted by the proposed model and those obtained experimentally are shown in Figures 5-44 to 5-52. The predicted results show good agreement with the experimental results except for columns C07 and C08. The reason for this discrepancy is attributed to the considerably higher strength of concrete of these columns and the fact the column C07 was tested in two steps.

Similarly, Figures 5-53 through 5-60 show the predicted load vs. strain curves for the phase 2 columns (CL1 to CL8). No experimental load vs. strain curves are available for these columns for comparison.

The descending branches of the confined concrete material curves of columns C01, C02, C03, C04, and C09 show reasonably good agreement with that of the experimental curves.

## 5.5 Summary and Conclusions

It has been demonstrated experimentally in Chapter 3 that both the strength and ductility of concrete improve significantly through confinement by steel HSS collars. Previously existing confinement models are unable to predict the stress vs. strain behaviour of the concrete columns confined externally by steel collars because of one or more of the following reasons: (1) lack of an explicit flexural stiffness parameter of the confining elements; (2) inability to account for variability of the confining pressure through the axial load history of the columns; (3) results based on the yield stress of the confining steel without taking into account the complete stress vs. strain curve of the confining steel; and (4) inability to accommodate a combination of active and passive confining pressures. A general purpose finite element program, *ABAQUS*, was also used to predict the behaviour of externally confined columns but no satisfactory results were obtained because of various limitations in the concrete material model available in the software package.

Columns of 300 x 300 mm were tested in phase 1 of the project (Chapter 3). Various parameters control the behaviour of the externally confined columns by steel HSS collars. Hence, there was a need to propose a confinement model that is able to predict the stress vs. strain behaviour of collared columns of different dimensions, collar spacing, and material properties. The proposed model makes use of an incremental-iterative procedure for which a computer program is required. The key component of the proposed confinement model is that the confining behaviour of the collars is expressed in terms of average confining pressure vs. average lateral strain. The confining pressure vs. lateral strain relationships of the collars are also important because the axial and flexural stiffness of the confining devices is incorporated into the proposed model through these relationships. Because the confining pressure was variable through the axial load history of the columns, the analysis was performed in increments and in each increment a constant confining pressure was assumed and the model of Mander *et al.* (1988b) was applied in that increment. For the dilation of the confined concrete, the relationships developed by Fam and Rizkalla (2001) based on the test results of Gardner (1969) were used. In each increment, there were initially several unknowns. They were set to arbitrary values and an iterative process was performed until the variables converged to unique values and then the next increment was taken and the process was repeated. In this way, the entire stress vs. strain curve of the confined concrete was traced.

The proposed model was validated by applying it to columns confined externally by steel HSS collars with bolted and welded corner connections tested in phase 1 of the project (Chapter 3). Some columns with bolted collars had initial active confining pressure due to the pre-stressing of the bolts. The results predicted by the model show good agreement with the experimental results. Equations for establishing the descending branches of the confined concrete material curves have also been proposed that show good results but they need more experimental data for calibration outside of the range of the confinement index considered.

Table 5.1: Measured and assumed properties of confined concrete columns for developing models for strain at peak stress and slope of descending branch

Column	$s'$ (mm)	$f'_{co}$ (MPa)	$\sigma_{h01}$ (MPa)	$\omega$	$\varepsilon_{co}$	$\varepsilon_{co85}$	$\varepsilon_{cc}$	$\varepsilon_{cc85}$	$\alpha$	$\beta$
C01	71	32.22	12.66	1.66	0.0031	0.0054	0.0377	0.0494	12.28	9.20
C02	71	32.90	13.60	1.75	0.0031	0.0054	0.0414	0.0524	13.51	9.77
C03	71	32.13	13.63	1.79	0.0031	0.0054	0.0397	0.0443	12.96	8.26
C04	119	32.13	9.74	0.76	0.0031	0.0054	0.0078	0.0154	2.54	2.86

Table 5.2: Relevant data and computed values of  $\varepsilon_{cc}$  and  $\varepsilon_{cc85}$  for phase 1 columns

Column	$s'$ (mm)	$f'_{co}$ (MPa)	$\sigma_{h01}$ (MPa)	$\omega$	$\alpha$	$\beta$	$\varepsilon_{co}$	$\varepsilon_{co85}$	$\varepsilon_{cc}$	$\varepsilon_{cc85}$
C01	71	32.22	12.66	1.66	11.65	8.47	0.0031	0.0054	0.0361	0.0460
C02	71	32.89	13.60	1.75	13.11	9.19	0.0031	0.0054	0.0406	0.0499
C03	71	32.13	13.60	1.79	13.83	9.54	0.0031	0.0054	0.0429	0.0518
C04	119	32.13	9.74	0.76	2.53	2.85	0.0031	0.0054	0.0078	0.0155
C05*	44	30.94	17.10	3.77	83.70	33.67	0.0031	0.0054	0.2595	0.1827
C06*	71	29.58	20.25	2.89	43.69	21.30	0.0029	0.0051	0.1267	0.1081
C07*	71	39.95	28.26	2.99	47.34	22.53	0.0034	0.0060	0.1609	0.1341
C08*	71	44.88	36.20	3.41	65.33	28.27	0.0036	0.0063	0.2352	0.1781
C09	119	30.85	16.99	1.39	7.81	6.42	0.0030	0.0053	0.0234	0.0337

Note: The confinement indices for the starred columns exceed the limit of calibration of the model for the descending branch

Table 5.3: Relevant data and computed values of  $\varepsilon_{cc}$  and  $\varepsilon_{cc85}$  for phase 2 columns

Column	$s'$ mm	$f'_{co}$ MPa	$\sigma_{h01}$ MPa	$\omega$	$\alpha$	$\beta$	$\varepsilon_{co}$	$\varepsilon_{co85}$	$\varepsilon_{cc}$	$\varepsilon_{cc85}$
CL1	50	10.45	23.03	13.22	1909.0	314.05	0.0017	0.0031	3.3358	0.9603
CL2	100	13.52	19.24	4.27	113.96	41.90	0.0020	0.0035	0.2265	0.1457
CL3	50	13.09	23.31	10.68	1119.9	214.18	0.0020	0.0034	2.1903	0.7330
CL4	50	27.79	23.21	5.01	169.62	55.57	0.0028	0.0050	0.4833	0.2771
CL5	50	22.35	28.58	7.67	490.17	118.49	0.0026	0.0045	1.2526	0.5299
CL6	100	27.71	23.42	2.54	31.71	17.01	0.0028	0.0050	0.0902	0.0847
CL7	50	30.09	30.50	6.08	274.47	78.30	0.0030	0.0052	0.8138	0.4063
CL8	50	30.00	23.56	4.71	145.59	49.85	0.0030	0.0052	0.4310	0.2583

Note: The confinement indices for all the columns exceed the limit of the calibration of the model for the descending branch

- (1) Experimental
- (2) Modified Kent and Park (Park *et al.*, 1982)
- (3) Sheikh and Uzumeri (1982)
- (4) Mander *et al.* (1988b)
- (5) Saatcioglu and Razvi (1992)
- (6) Hoshikuma *et al.* (1997)
- (7) L g ron and Paultre (2003)

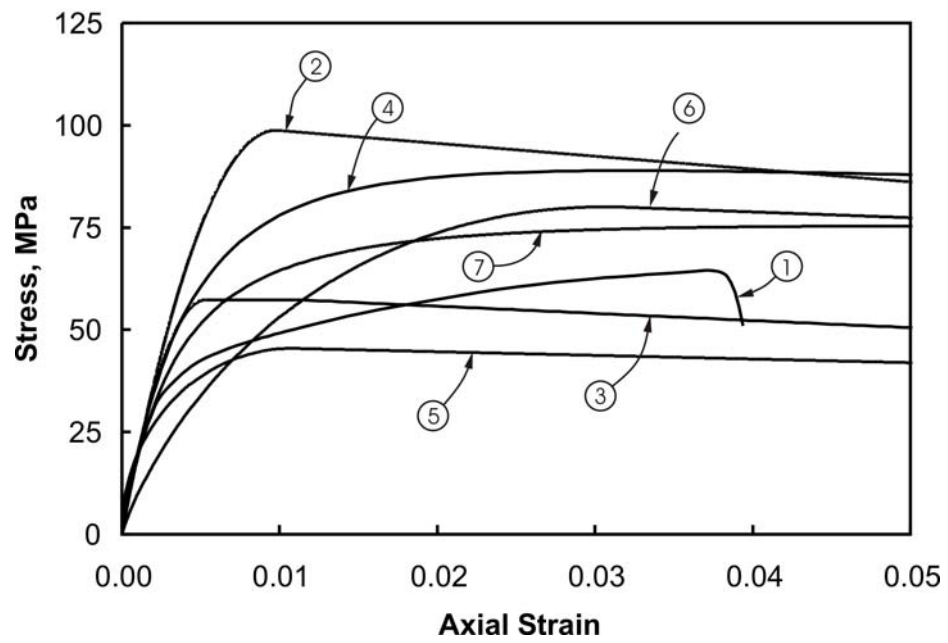


Figure 5-1: Prediction of confined concrete material curve for column C06 by existing confinement models

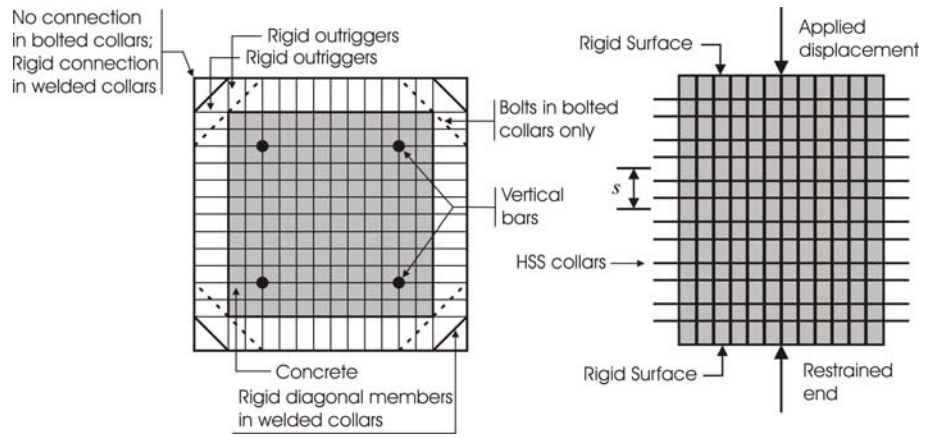


Figure 5-2: Plan and elevation of a typical finite element model for an externally confined column

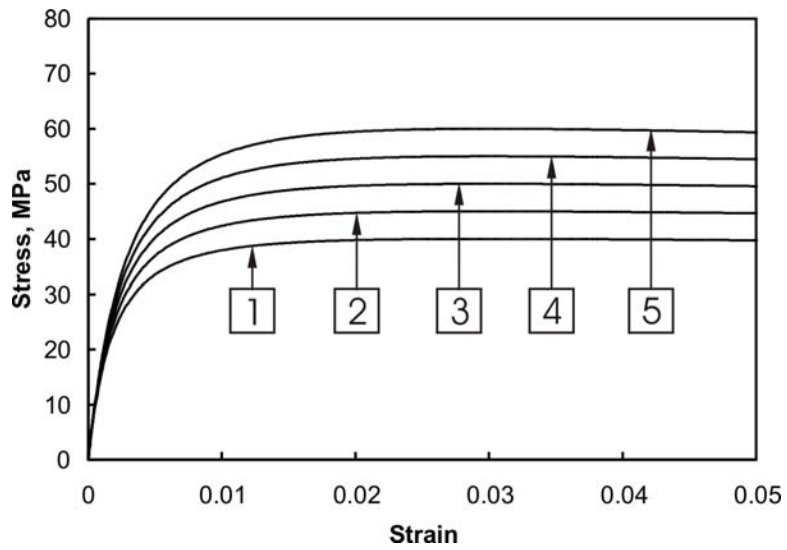


Figure 5-3: Concrete material curves with modified descending branches

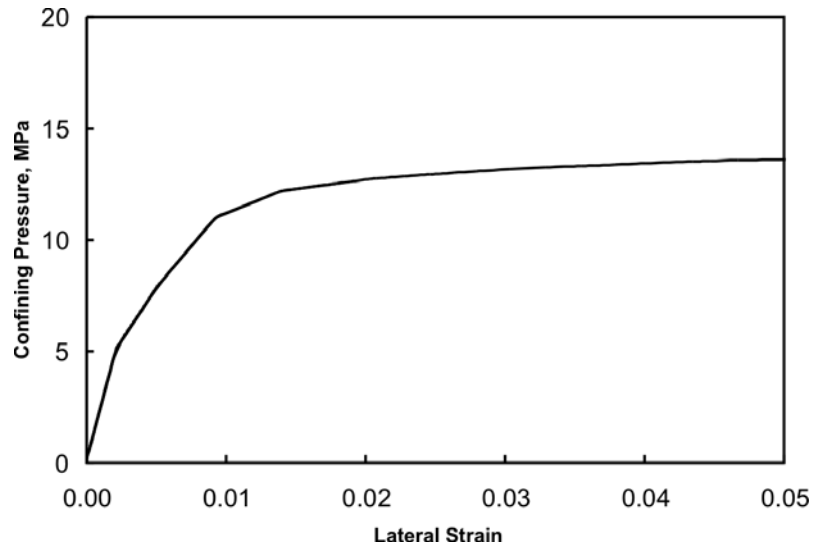


Figure 5-4: Effect of concrete material curve on the confining pressure versus lateral strain curve of collars of column C01

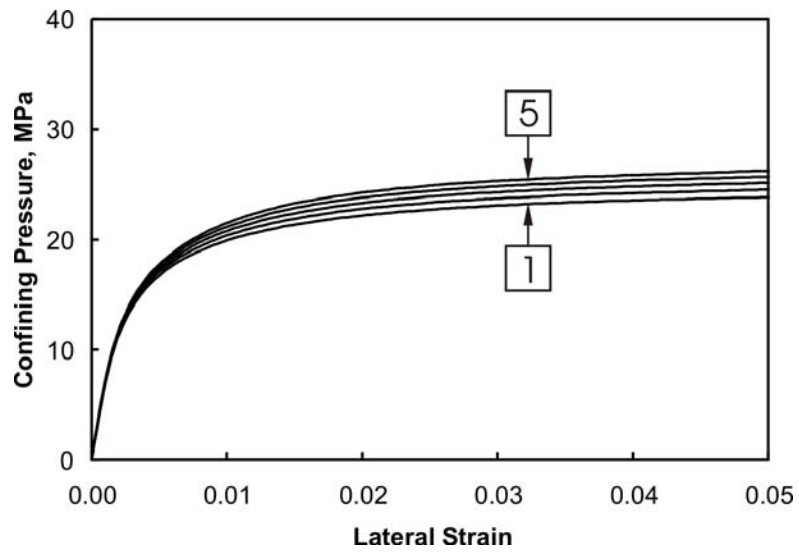


Figure 5-5: Effect of concrete material curve on the confining pressure versus lateral strain curve of collars of column C06

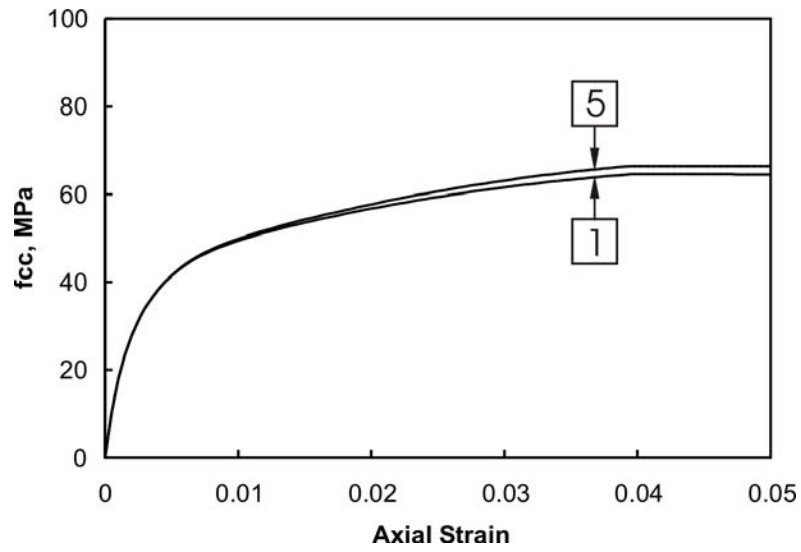


Figure 5-6: Confined concrete material curves for column C06

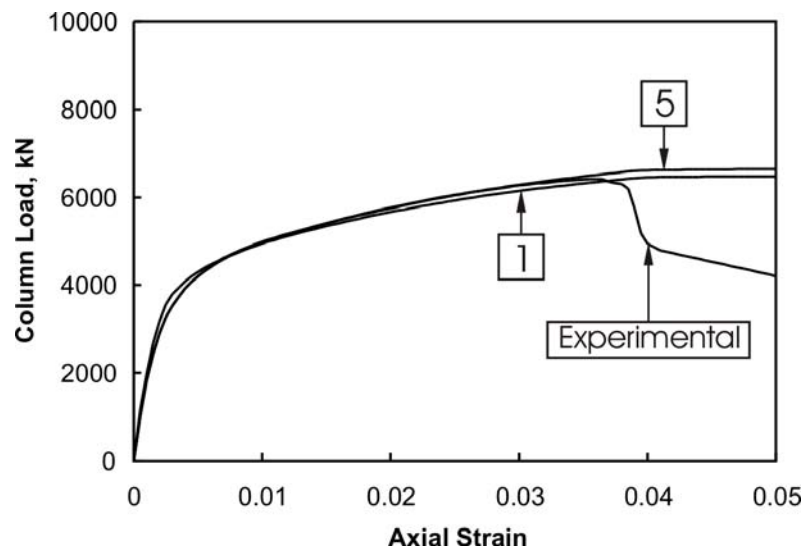


Figure 5-7: Column load versus axial strain for column C06

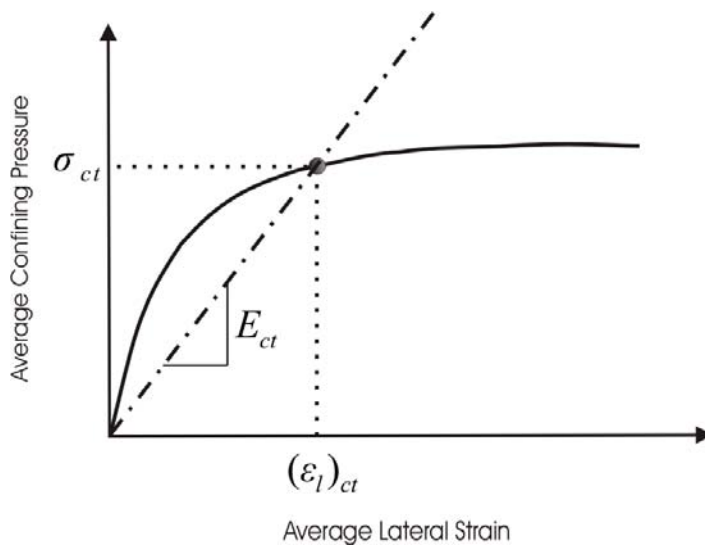


Figure 5-8: A typical behavioural curve of steel collars

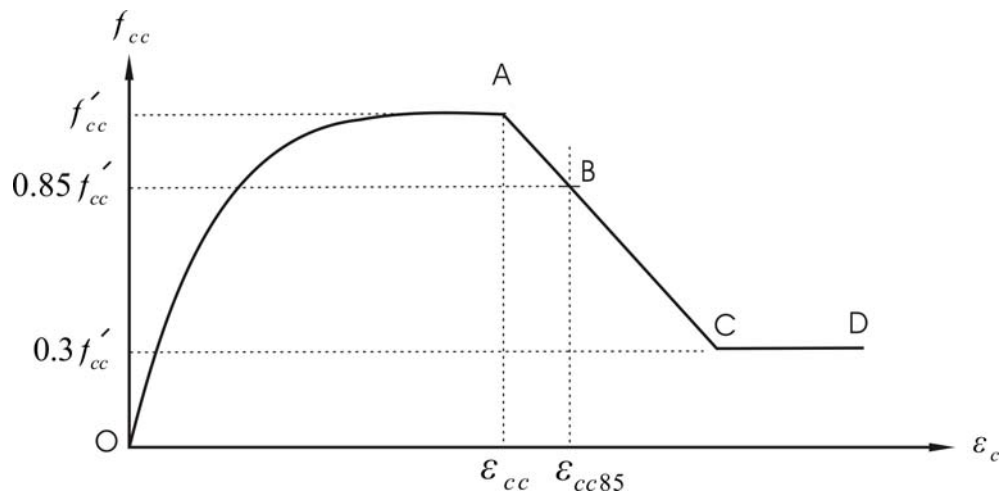


Figure 5-9: Proposed material curve for concrete confined externally by steel collars

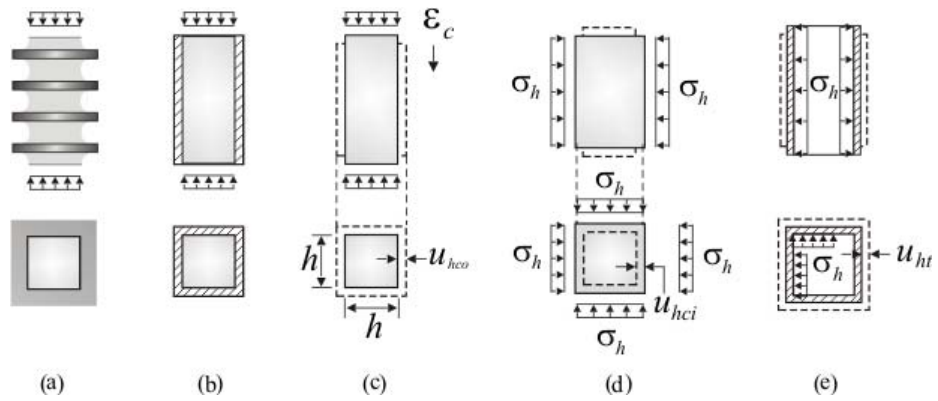


Figure 5-10: Discrete and smeared collars on a concrete prism under different stresses

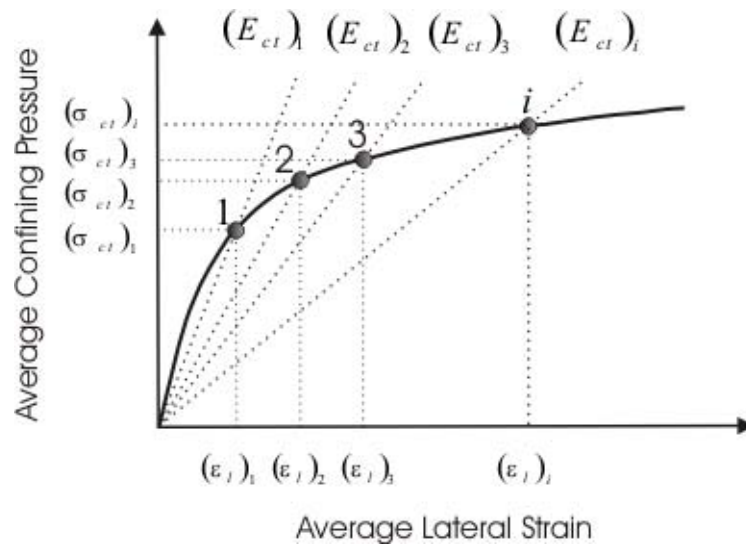


Figure 5-11: A typical confining pressure vs. lateral strain curve

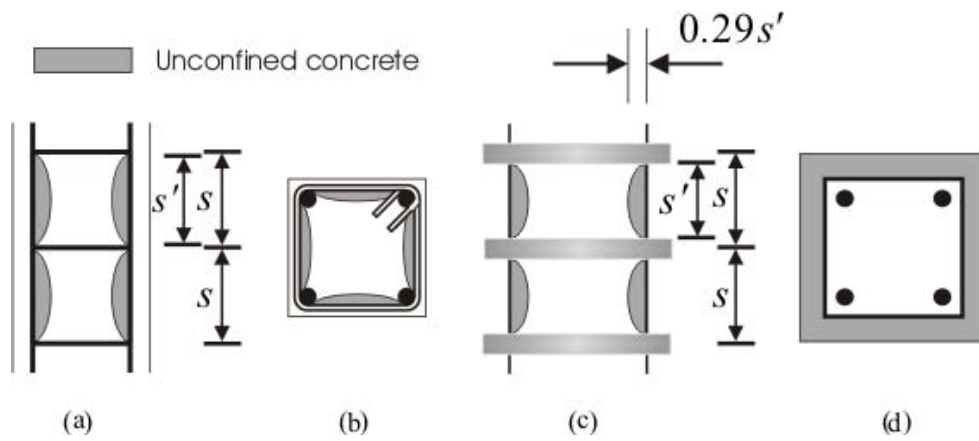


Figure 5-12: Unconfined concrete: (a) between tie levels; (b) at tie level; (c) between HSS collars; and (d) at HSS collar level (fully confined)

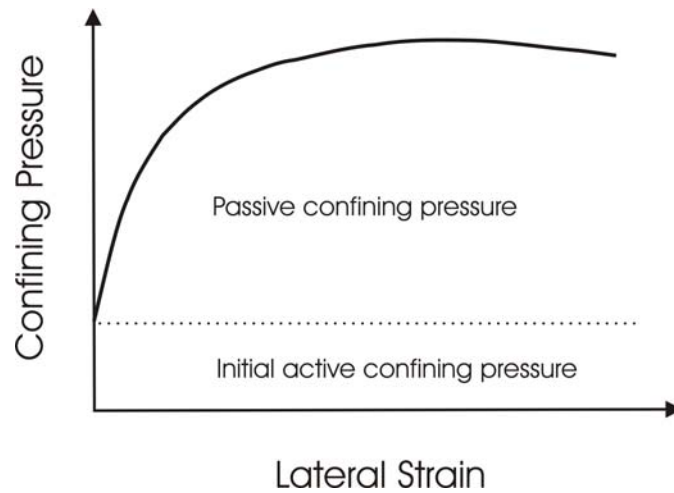


Figure 5-13: A typical relationship between confining pressure vs. lateral strain with confining pressure consisting of active and passive components

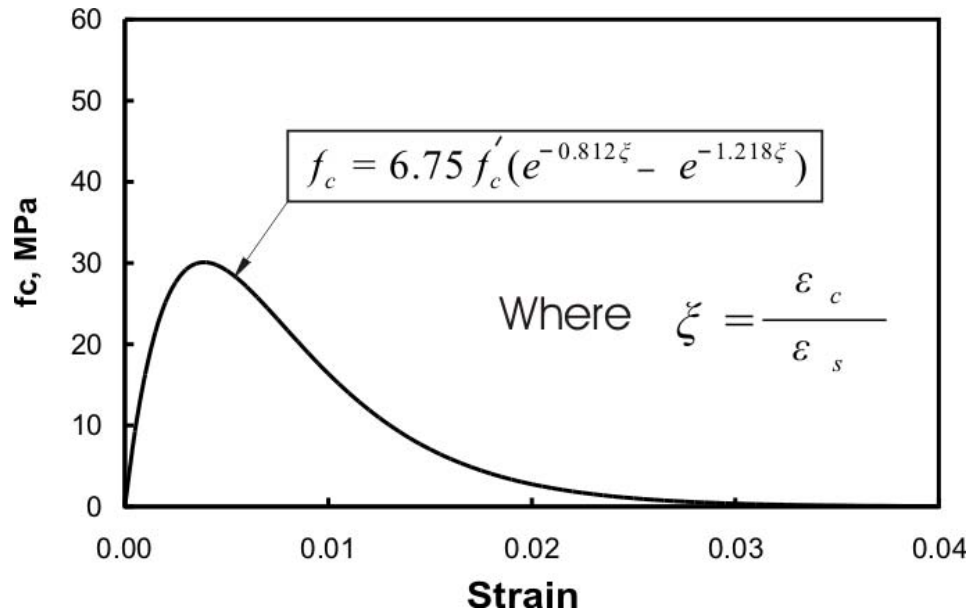


Figure 5-14: Behaviour of spalling concrete in column C01

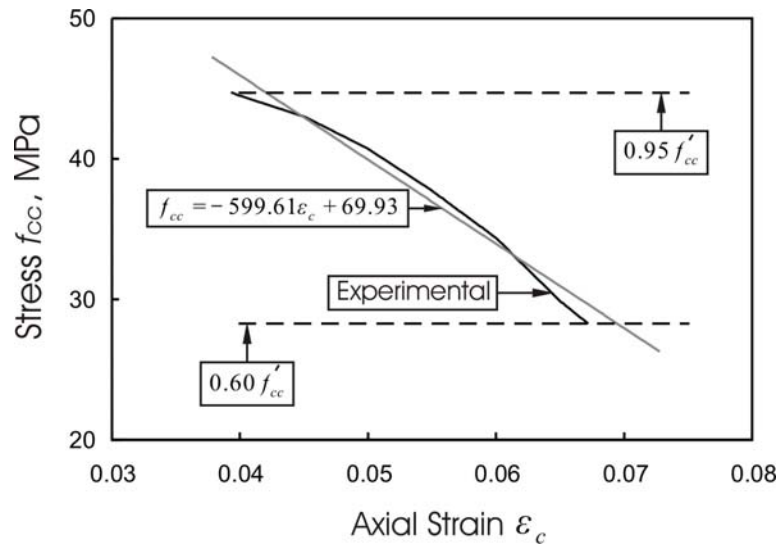


Figure 5-15: Slope of descending branch of column C01

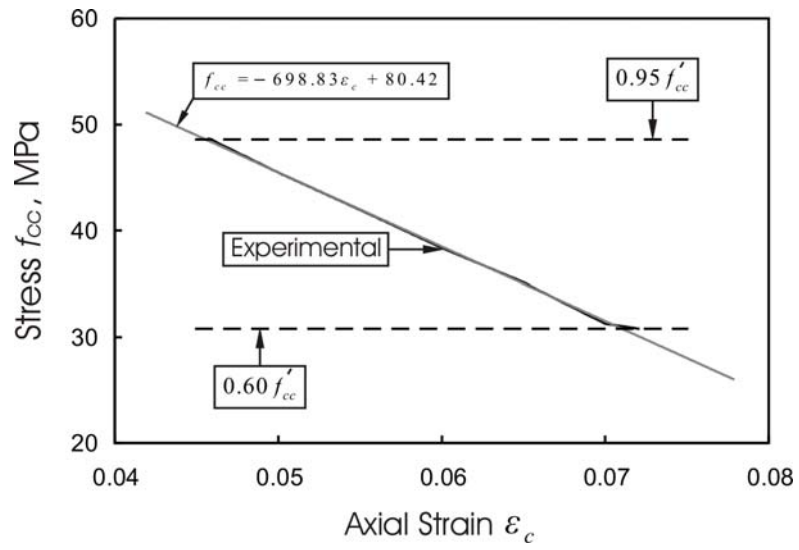


Figure 5-16: Slope of descending branch of column C02

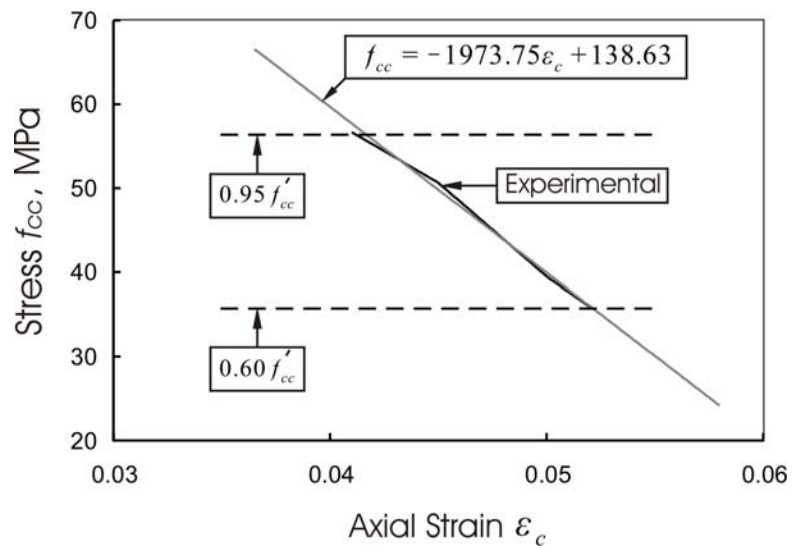


Figure 5-17: Slope of descending branch of column C03

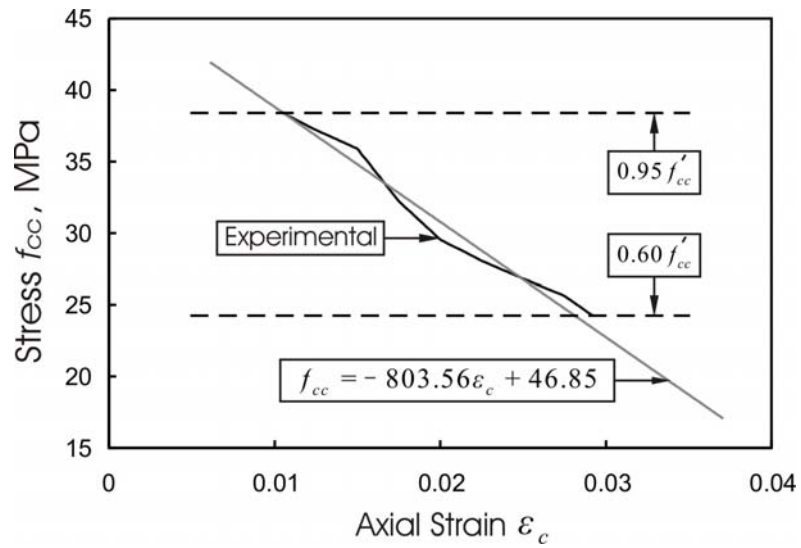


Figure 5-18: Slope of descending branch of column C04

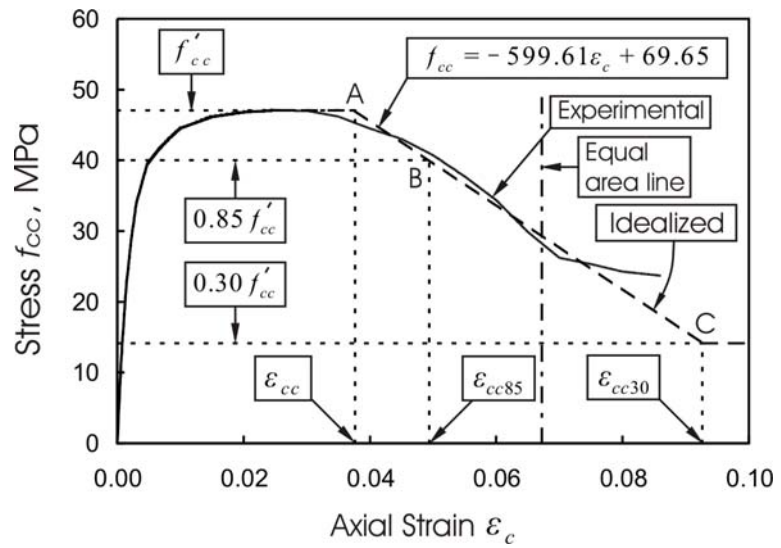


Figure 5-19: Idealized stress vs. strain curve for column C01

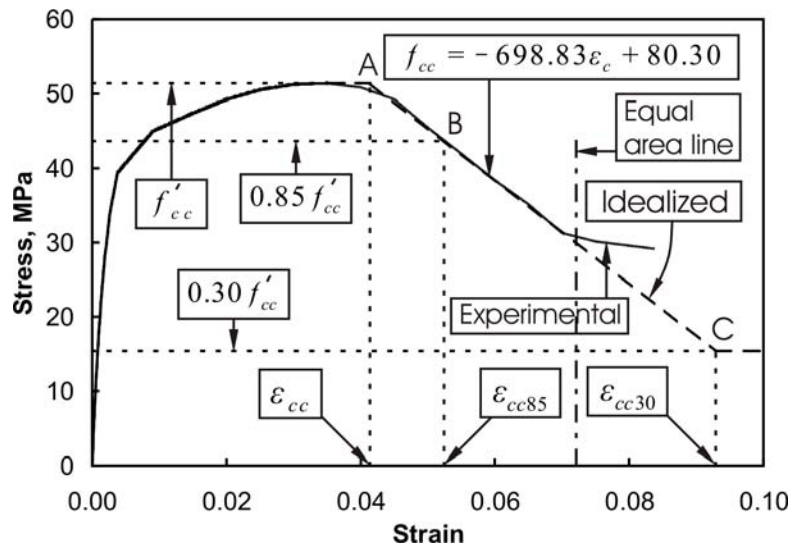


Figure 5-20: Idealized stress vs. strain curve for column C02

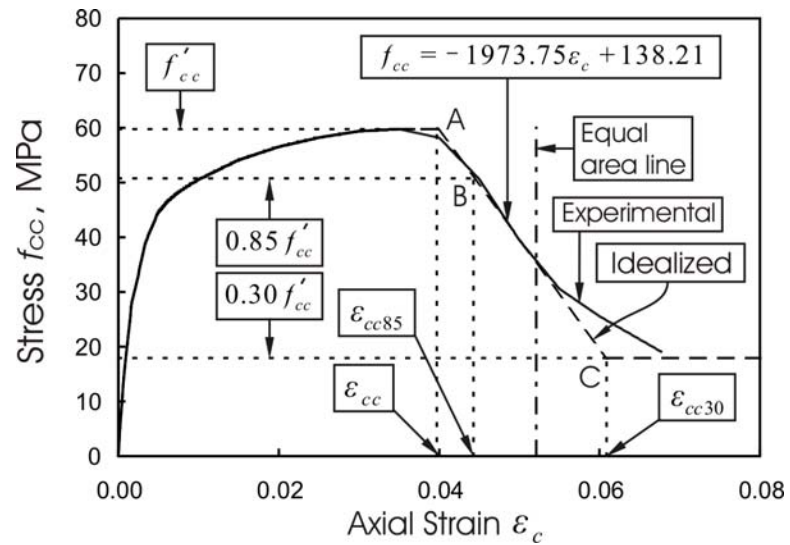


Figure 5-21: Idealized stress vs. strain curve for column C03

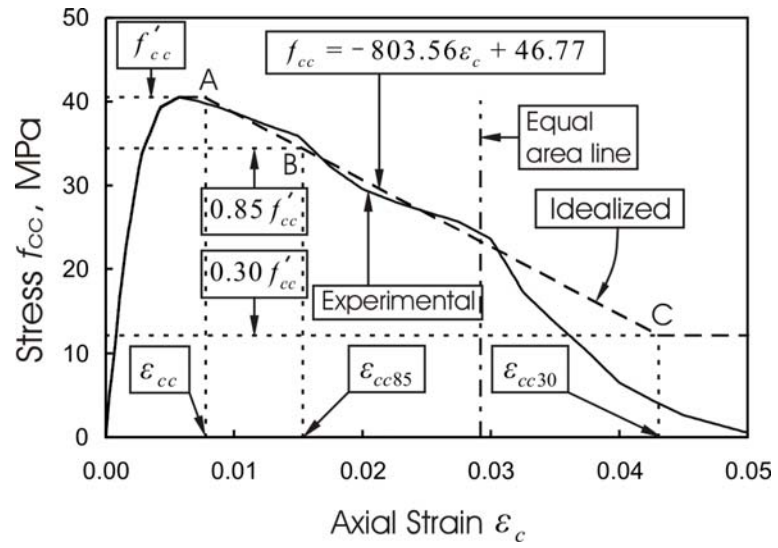


Figure 5-22: Idealized stress vs. strain curve for column C04

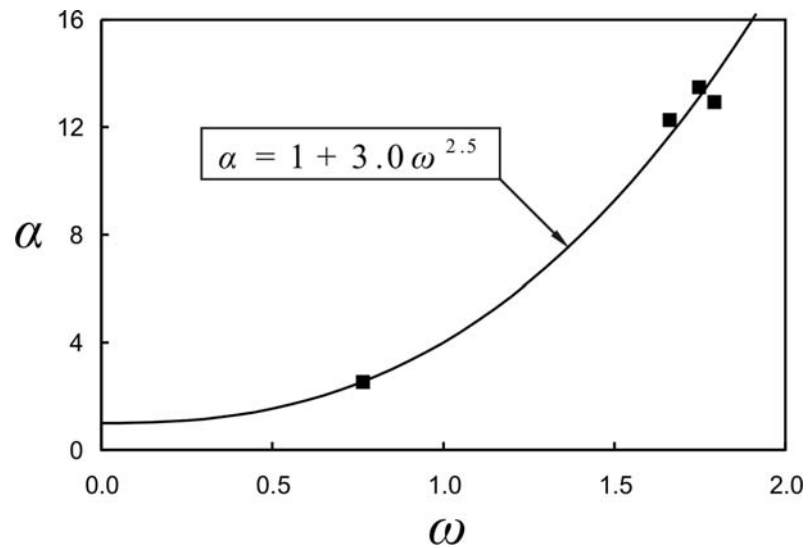


Figure 5-23: Relationship between  $\alpha$  and  $\omega$

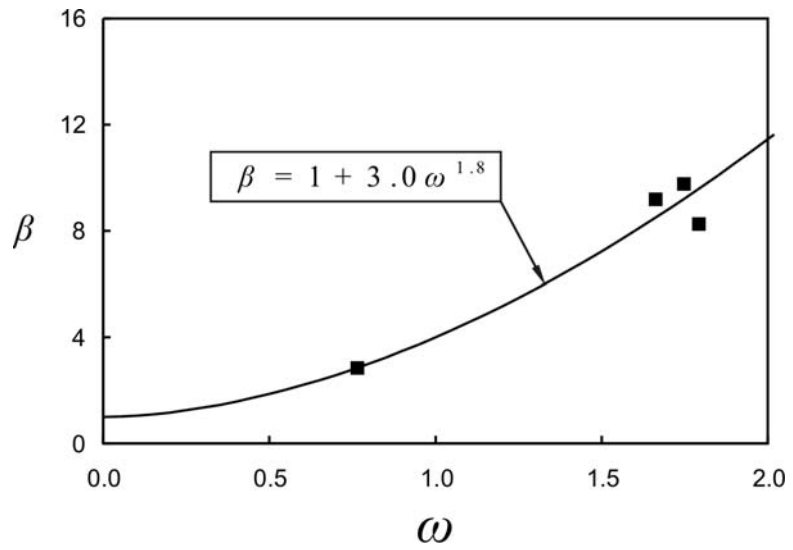


Figure 5-24: Relationship between  $\beta$  and  $\omega$

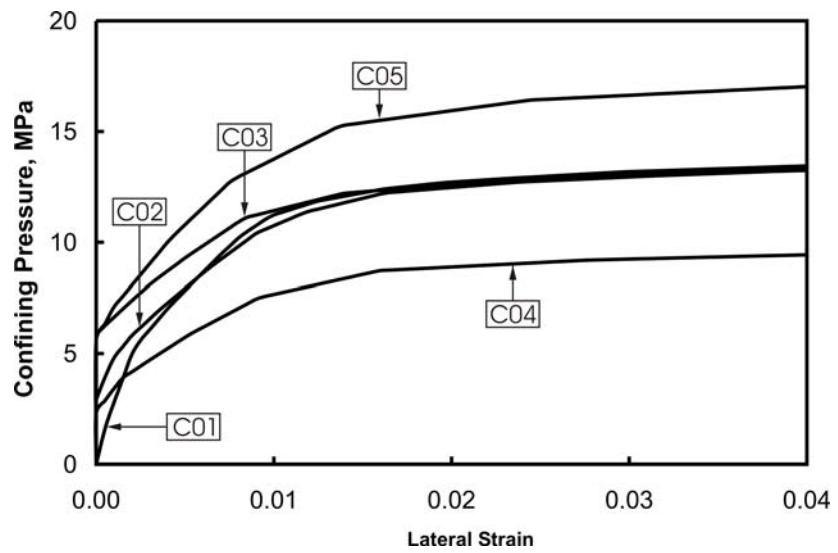


Figure 5-25: Confining pressure vs. lateral strain curves for collars with bolted corner connections (phase 1)

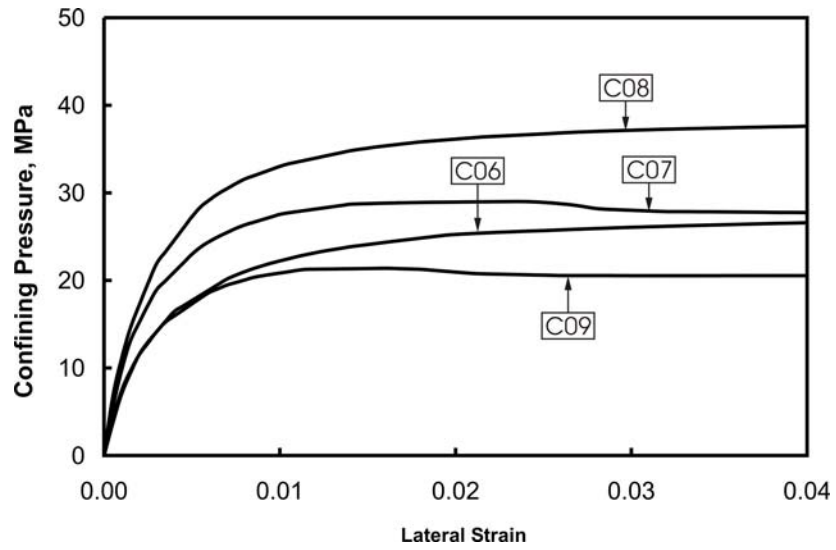


Figure 5-26: Confining pressure vs lateral strain curves for collars with welded corner connection (phase 1)

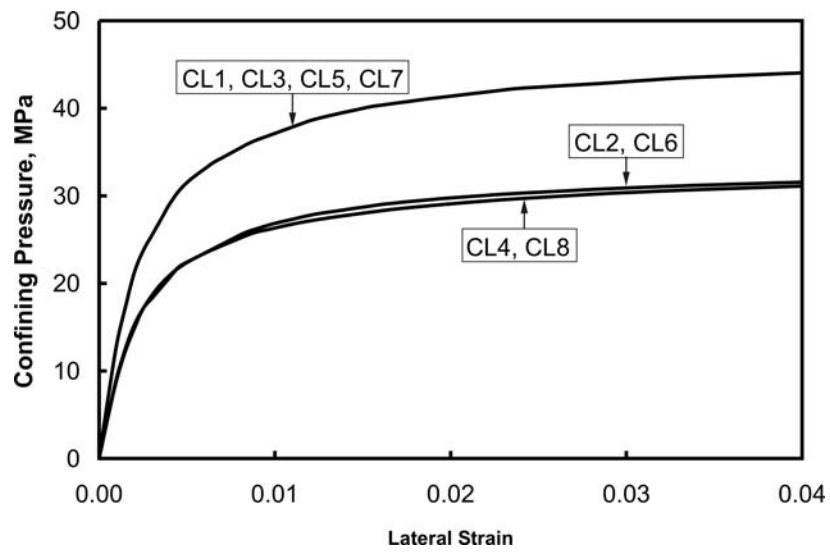


Figure 5-27: Confining pressure vs. lateral strain curves for columns CL1 to CL8 (phase 2)

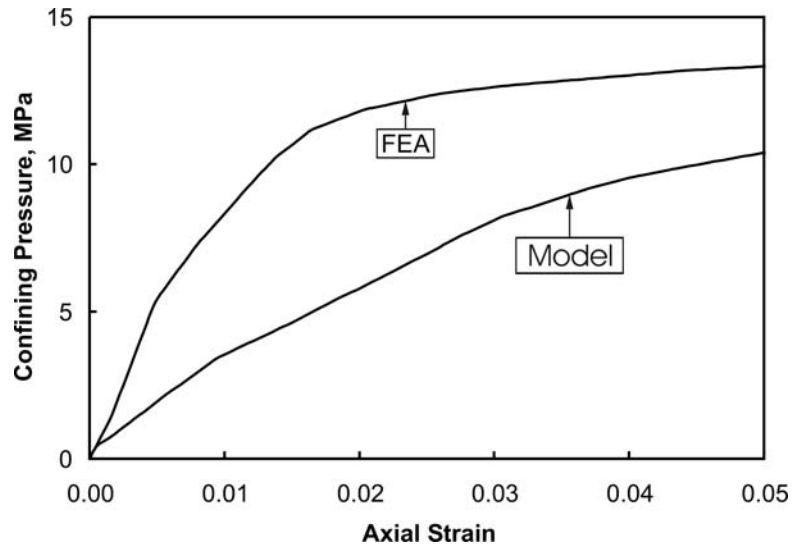


Figure 5-28: Confining pressure vs. axial strain for column C01

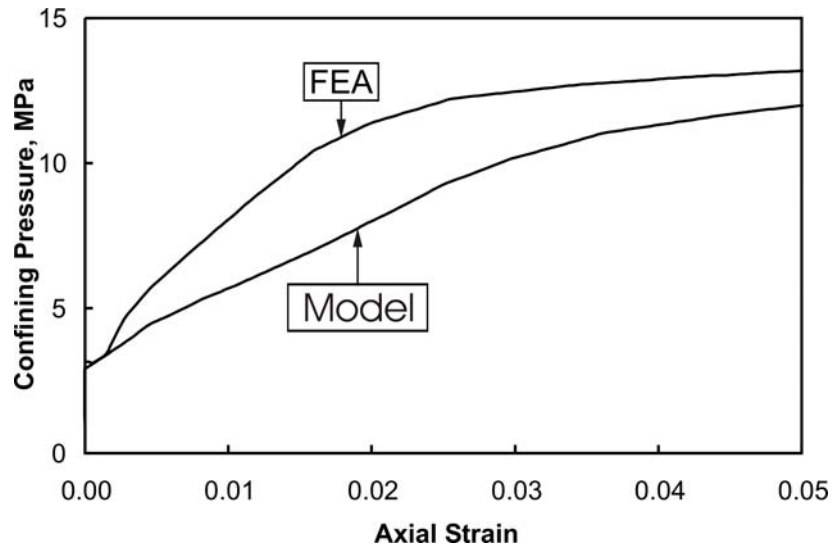


Figure 5-29: Confining pressure vs. axial strain for column C02

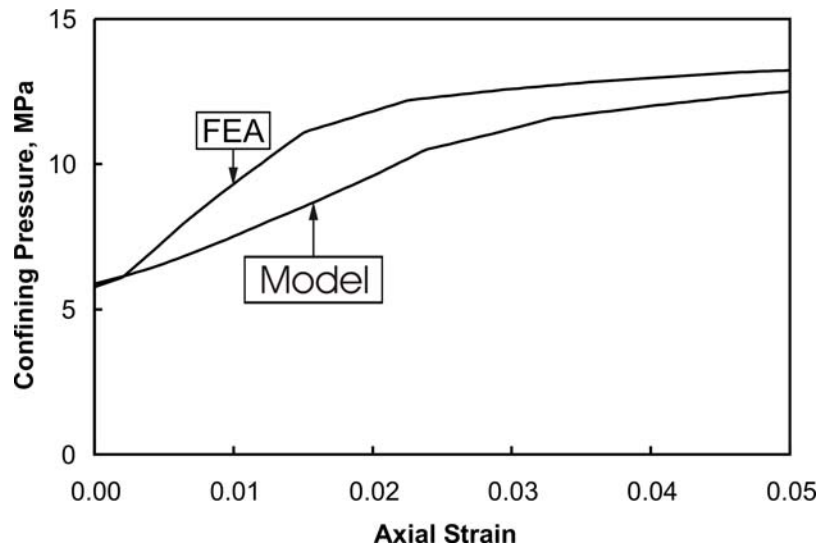


Figure 5-30: Confining pressure vs. axial strain for column C03

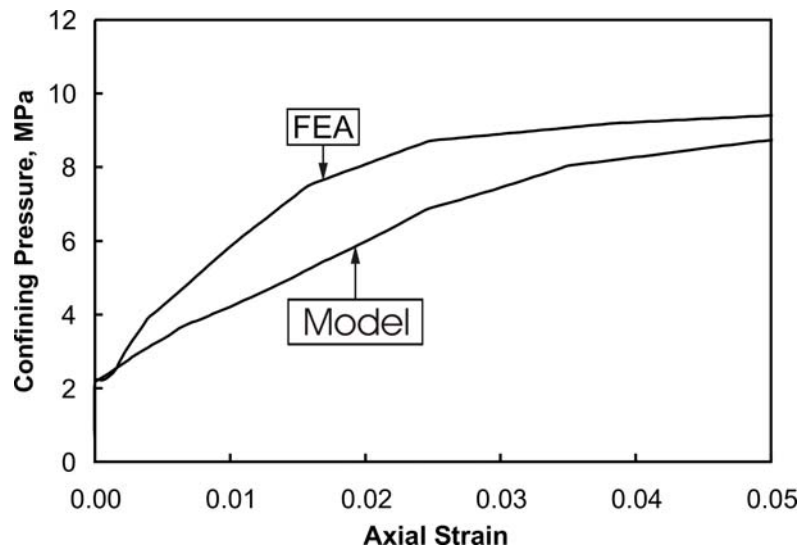


Figure 5-31: Confining pressure vs. axial strain for column C04

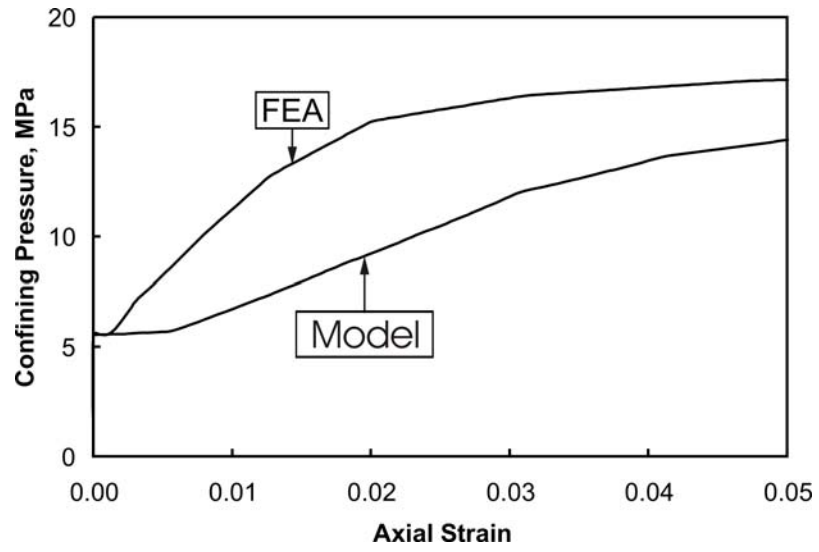


Figure 5-32: Confining pressure vs. axial strain for column C05

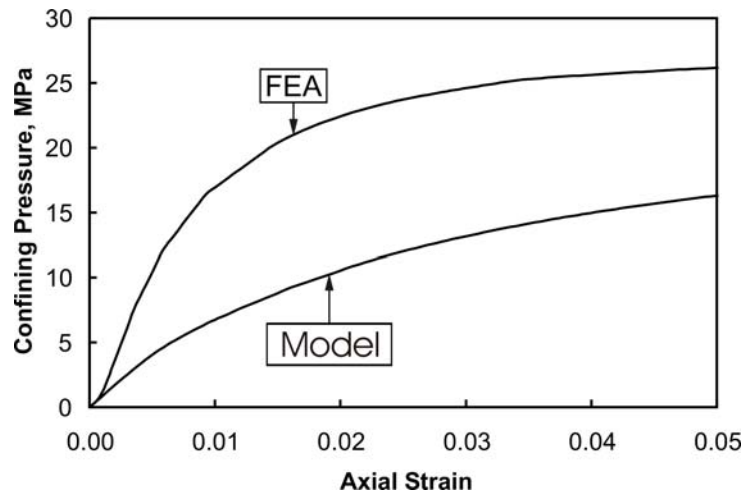


Figure 5-33: Confining pressure vs. axial strain for column C06

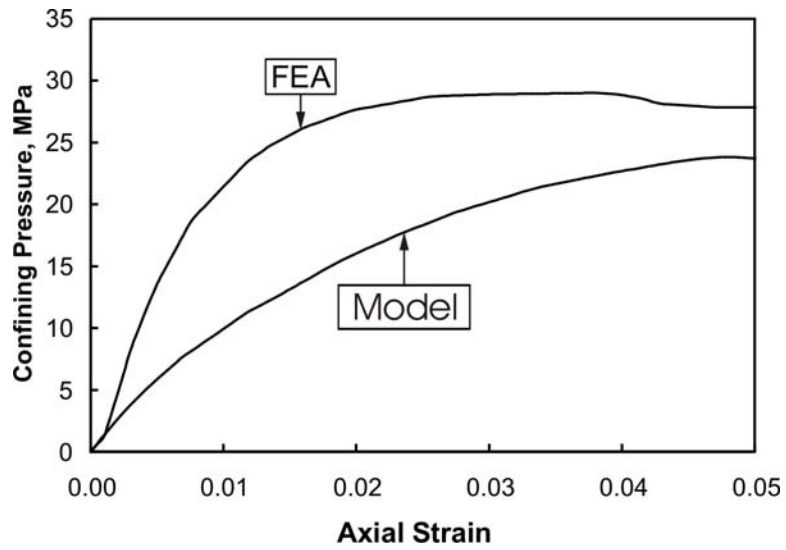


Figure 5-34: Confining pressure vs. axial strain for column C07

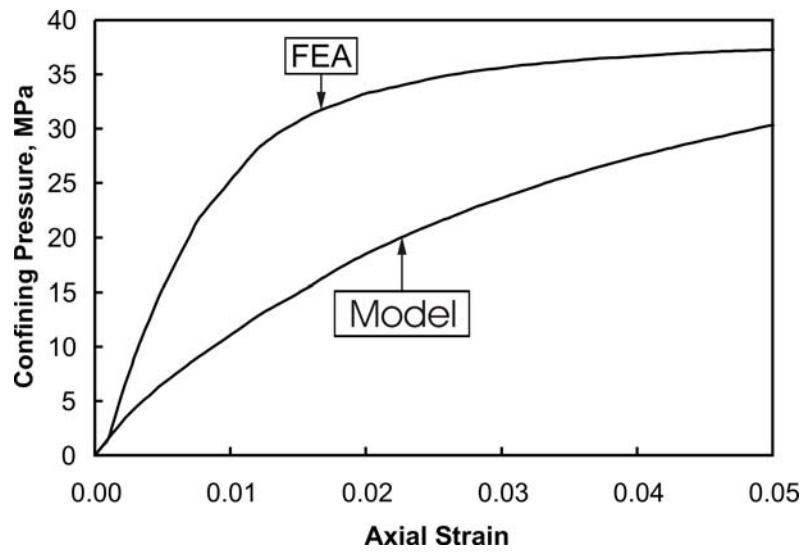


Figure 5-35: Confining pressure vs. axial strain for column C08

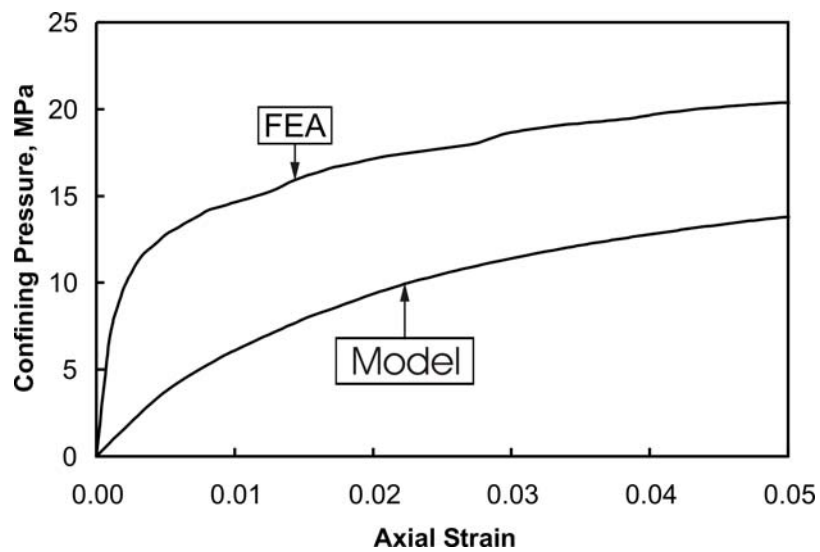


Figure 5-36: Confining pressure vs. axial strain for column C09

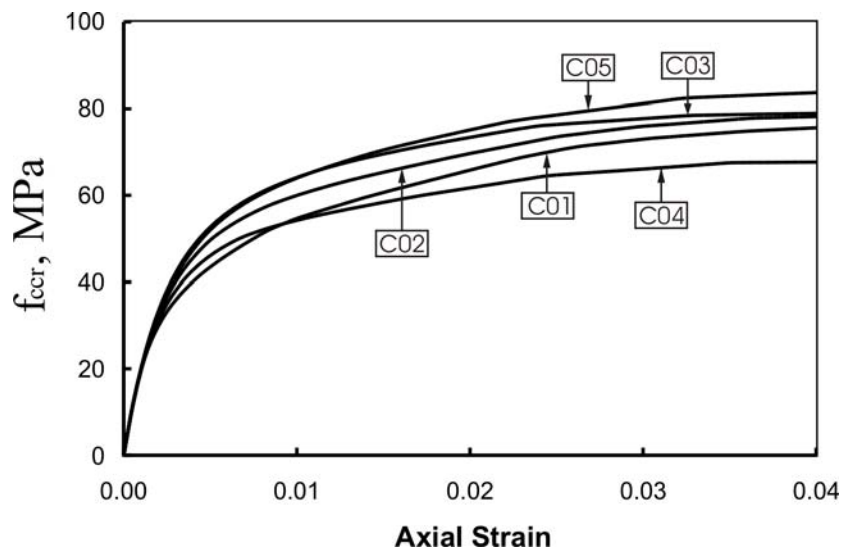


Figure 5-37: Confined concrete material curve for reduced cores in the phase 1 columns with bolted collars

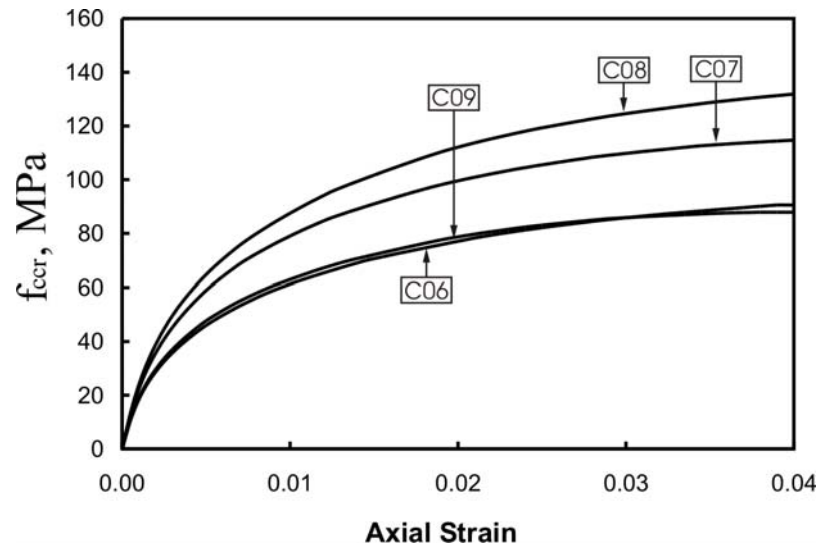


Figure 5-38: Confined concrete material curve for reduced cores in the phase 1 columns with welded collars

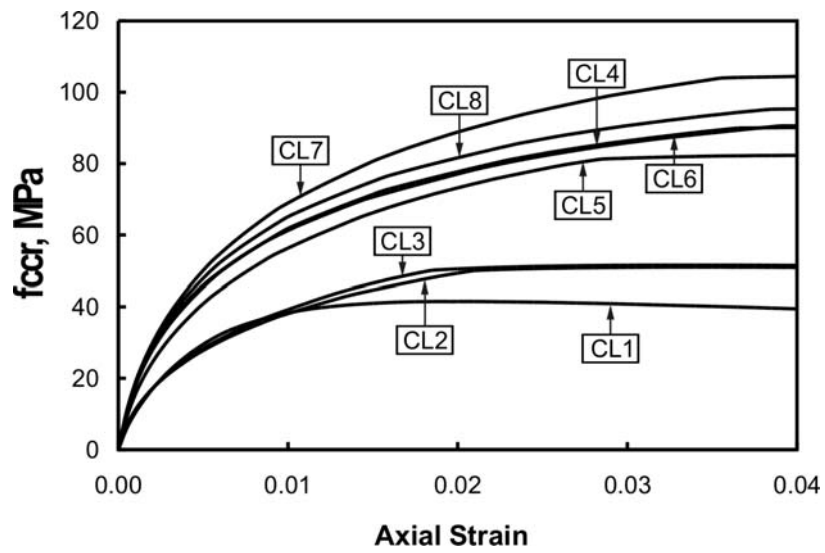


Figure 5-39: Confined concrete material curve for reduced cores in the phase 2 columns CL1 to CL8

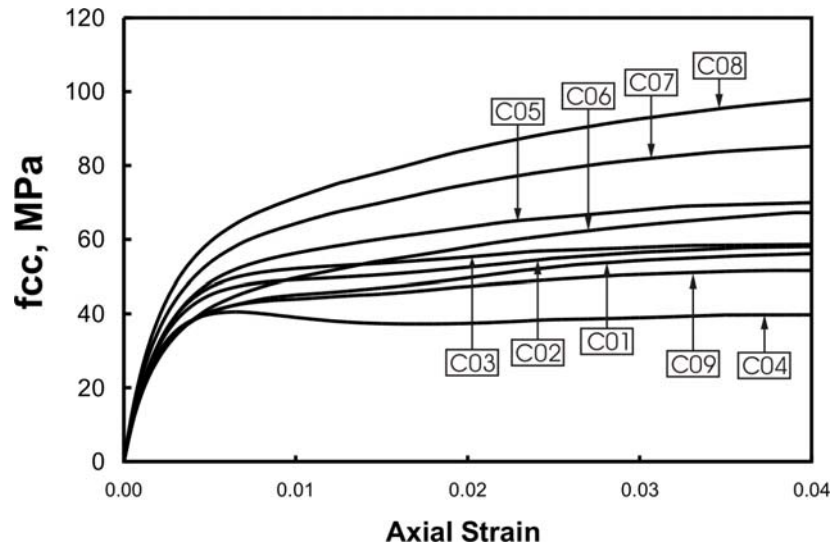


Figure 5-40: Confined concrete material curves of columns C01 to C09.

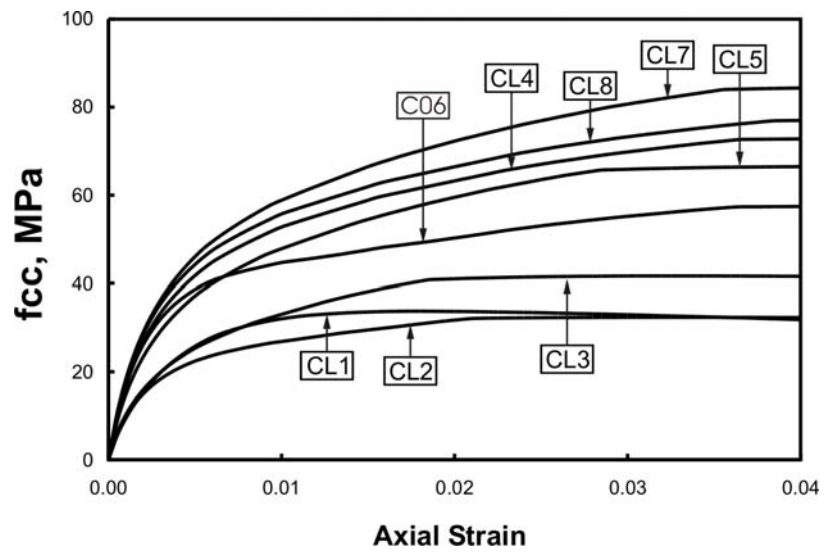


Figure 5-41: Confined concrete material curves of columns CL1 to CL8

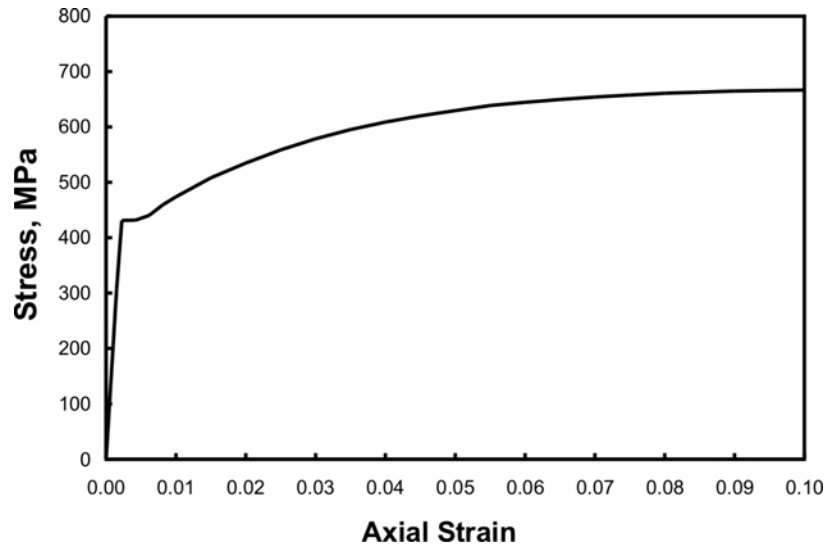


Figure 5-42: Stress vs. strain curve for 20 mm dia. vertical bars of phase 1 columns

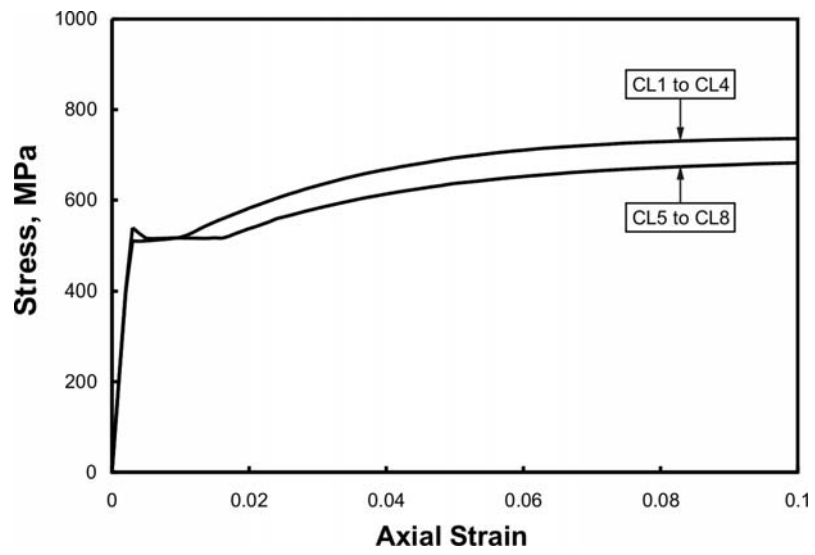


Figure 5-43: Stress vs. strain curves for vertical bars of phase 2 columns

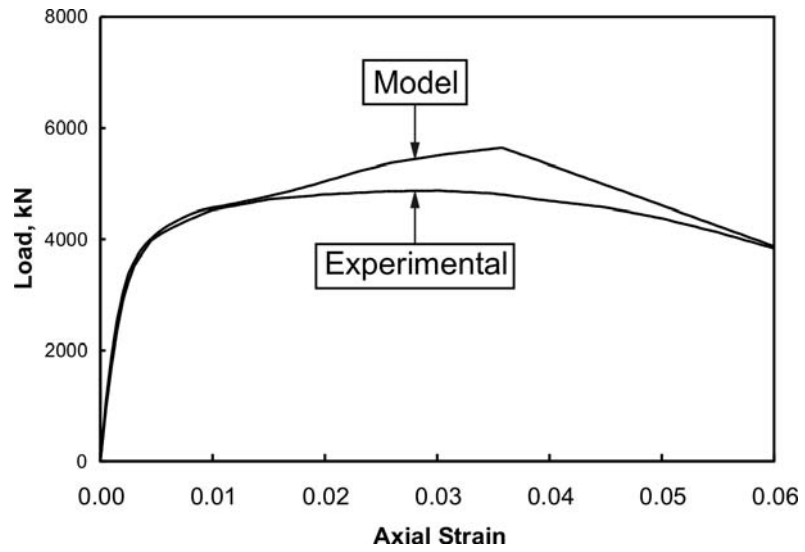


Figure 5-44: Load vs strain curves for column C01

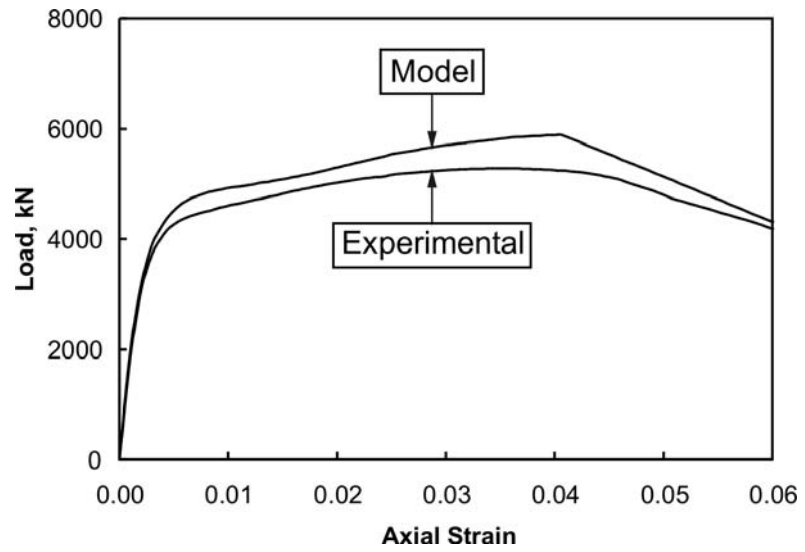


Figure 5-45: Load vs. strain curves for column C02

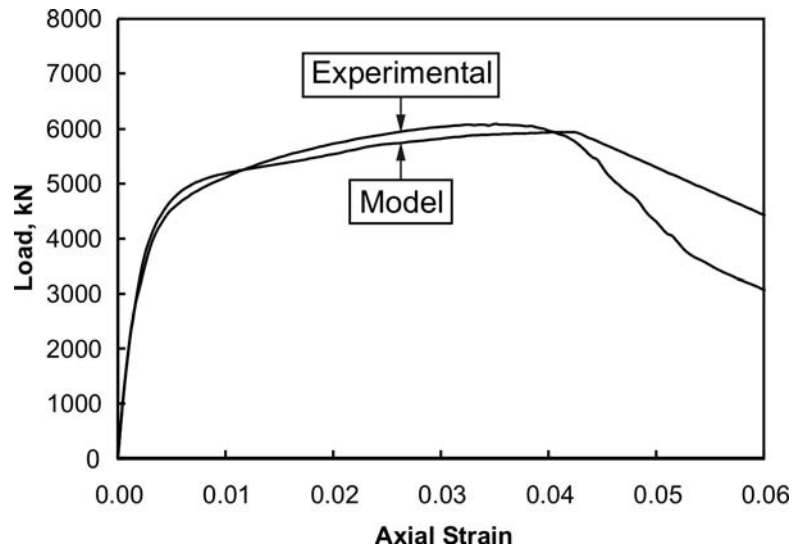


Figure 5-46: Load vs. strain curves for column C03

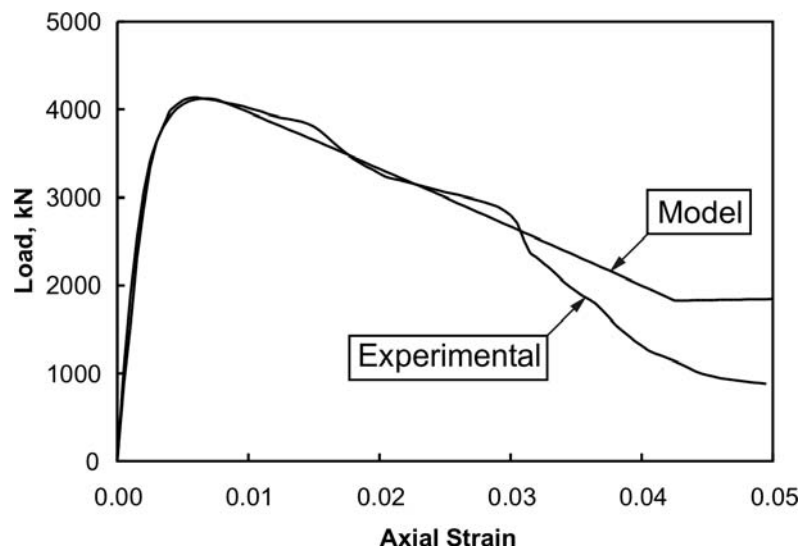


Figure 5-47: Load vs. axial strain curve of column C04

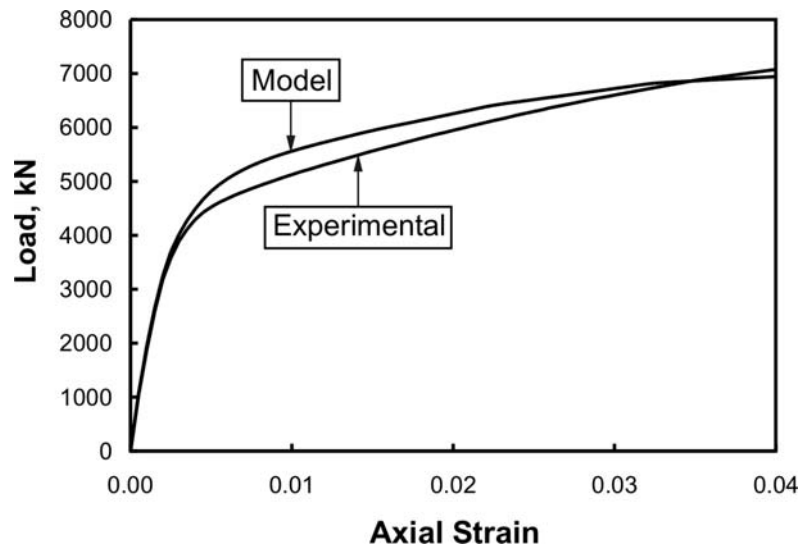


Figure 5-48: Load vs. axial strain curve of column C05

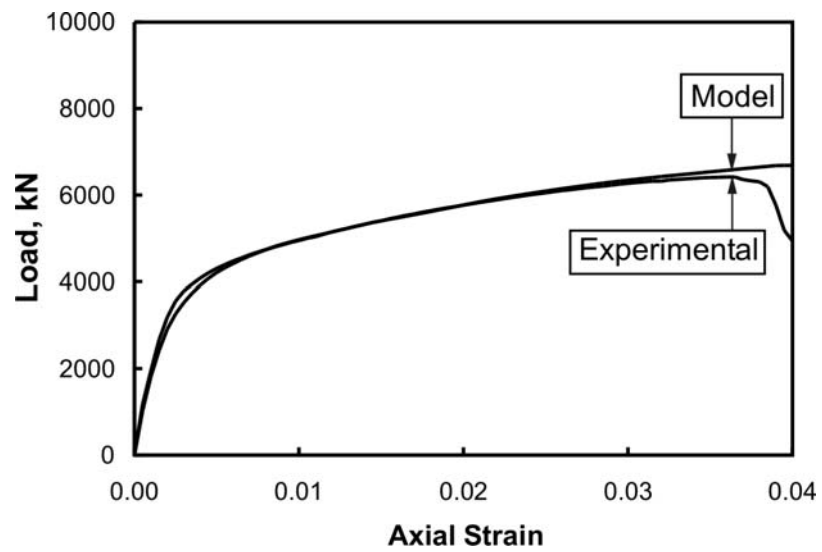


Figure 5-49: Load vs. axial strain curve of column C06

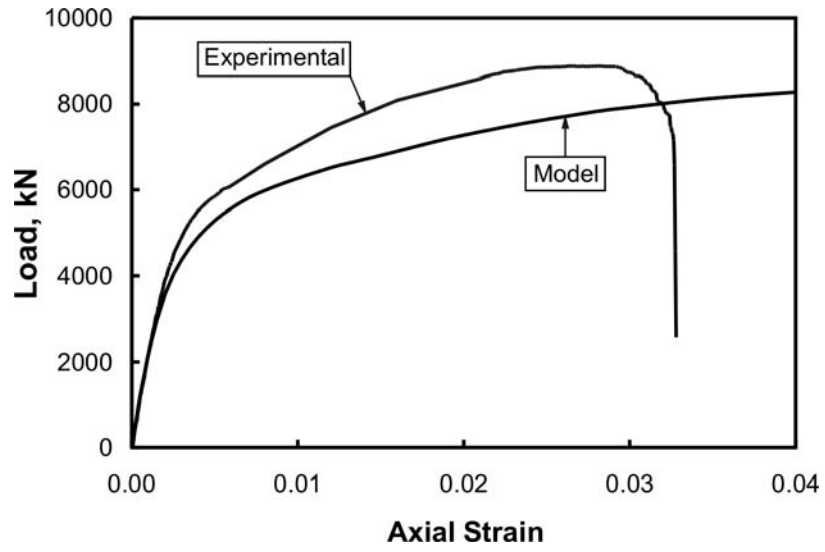


Figure 5-50: Load vs. axial strain curve of column C07

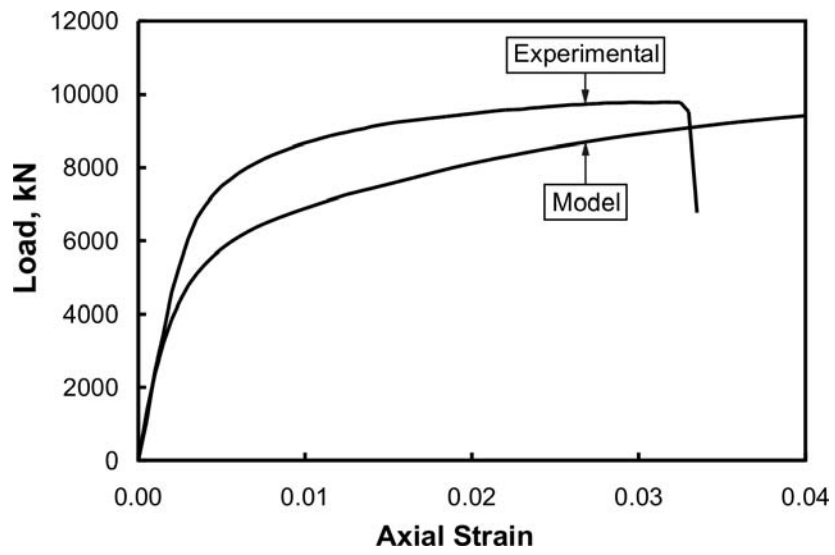


Figure 5-51 Load vs. axial strain curve of column C08

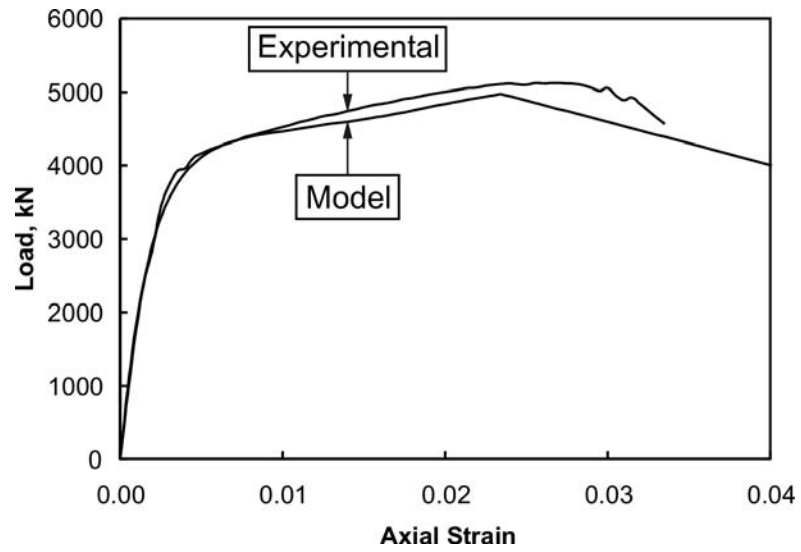


Figure 5-52: Load vs. axial strain curve of column C09

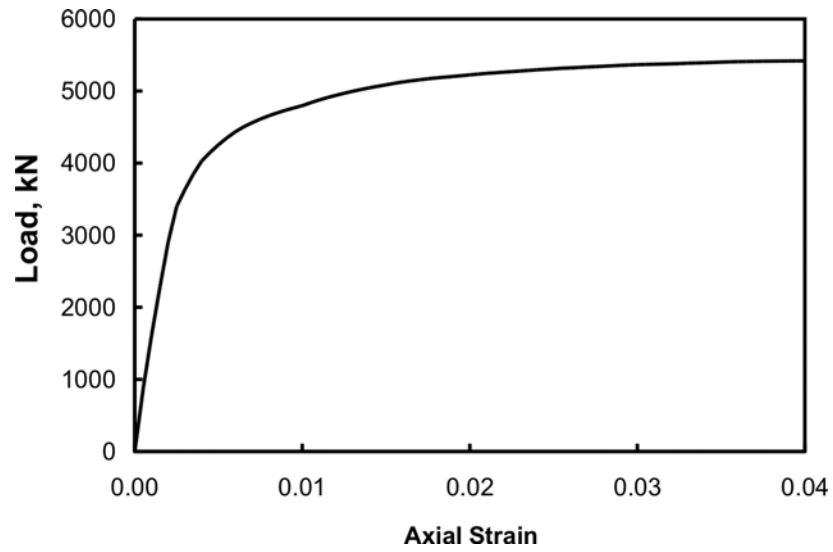


Figure 5-53 Load vs. axial strain curve of column CL1

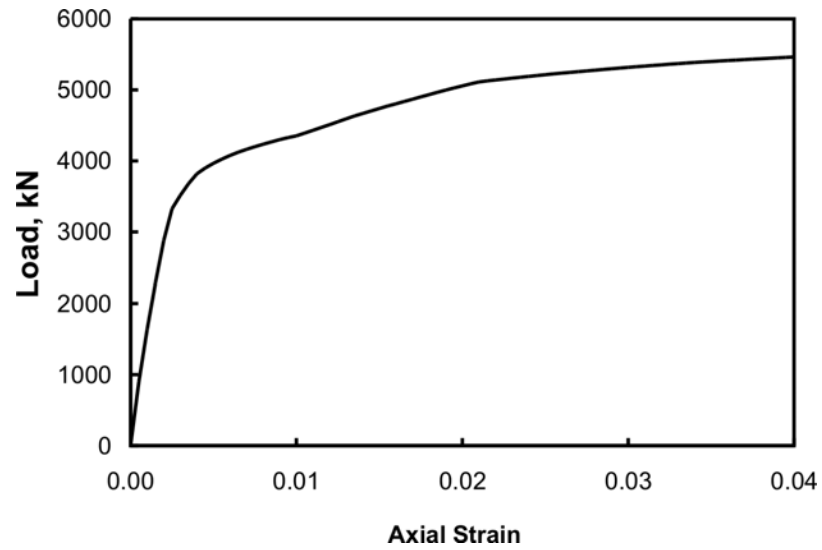


Figure 5-54: Load vs. axial strain curve of column CL2

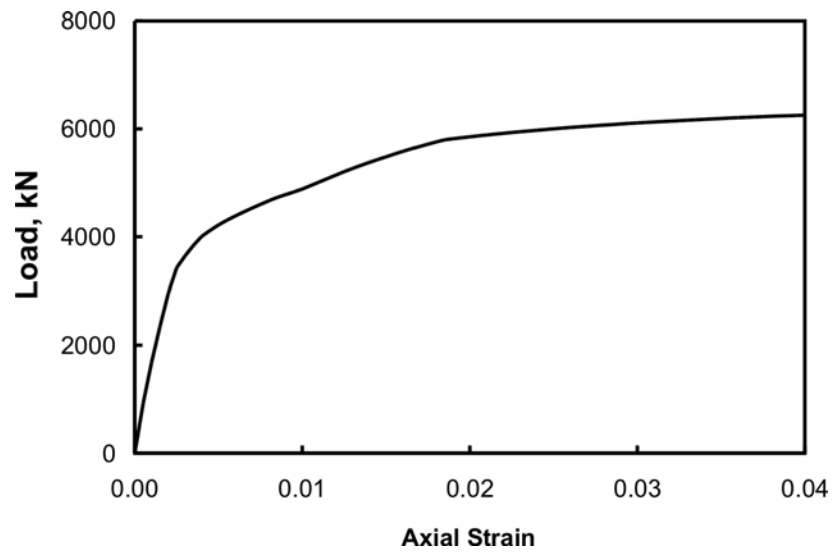


Figure 5-55: Load vs. axial strain curve of column CL3

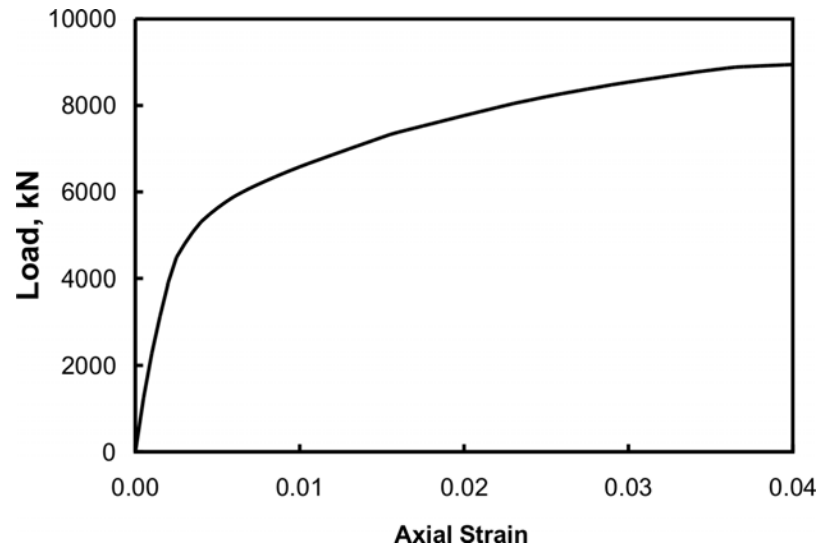


Figure 5-56 Load vs. axial strain curve of column CL4

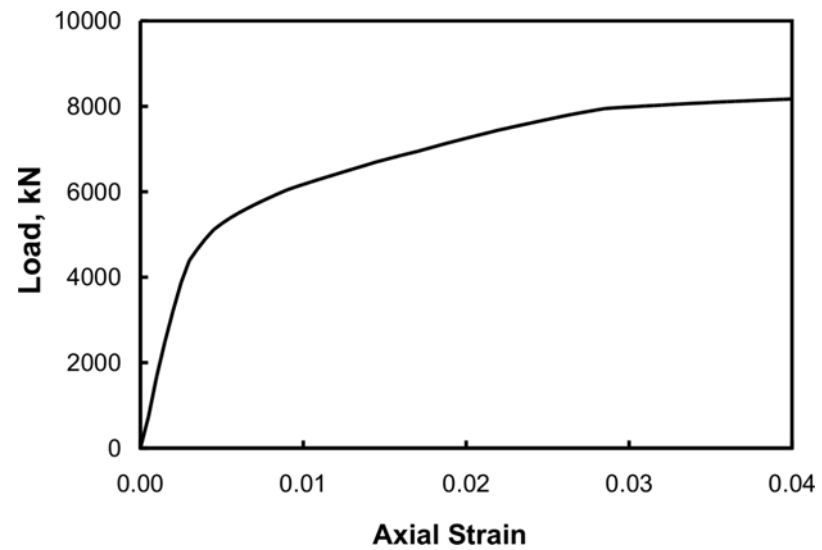


Figure 5-57: Load vs. axial strain curve of column CL5

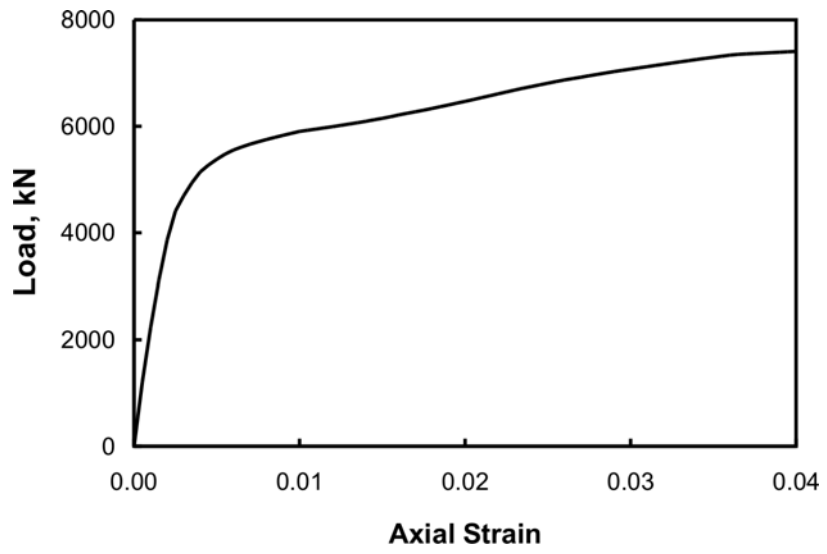


Figure 5-58: Load vs. axial strain curve of column CL6

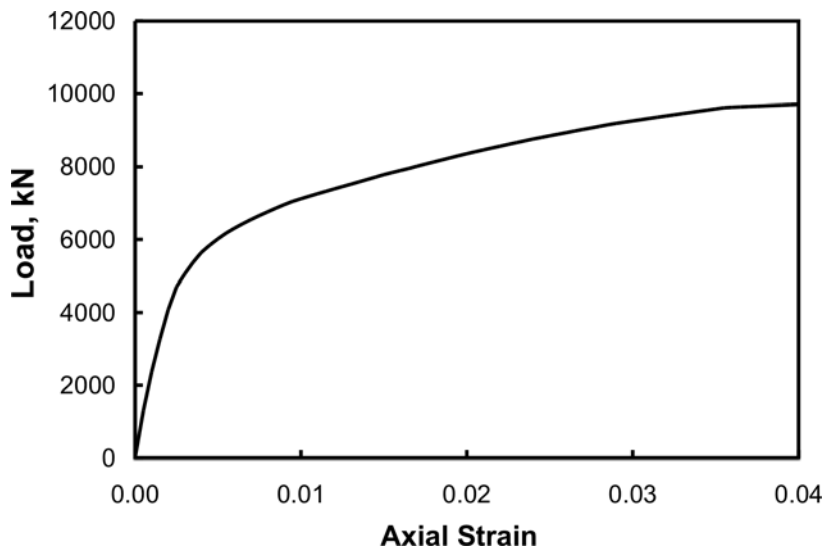


Figure 5-59: Load vs. axial strain curve of column CL7

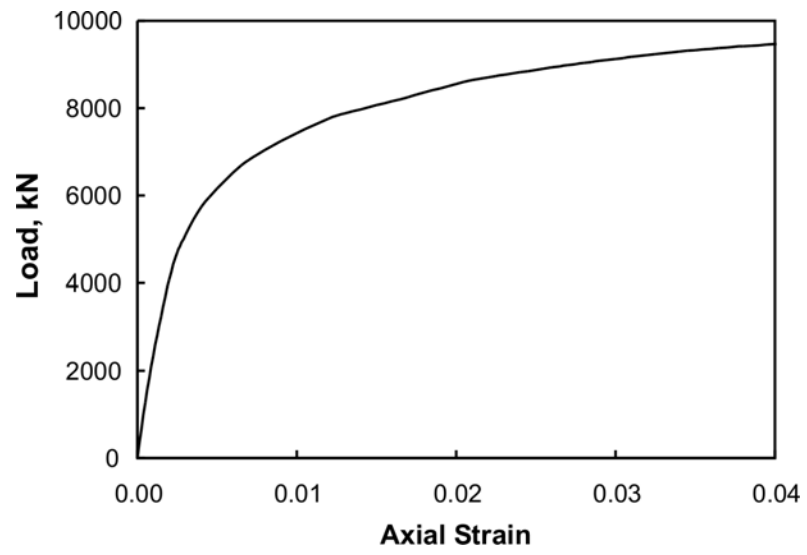


Figure 5-60 Load vs. axial strain curve of column CL8

## 5.6 REFERENCES

- Ahmad, S.H. and Shah, S.P. 1982. Stress-strain curves of concrete confined by spiral reinforcement. *ACI Journal*, November-December, pp. 484-490.
- Ahmad, S.H. and Shah, S.P. 1985. Behaviour of hoop confined concrete under high strain rates. *ACI Journal*, September-October, pp. 634-647.
- Caner, F.C. and Bažant, Z.P. 2002. Lateral confinement needed to suppress softening of concrete in compression. *ASCE, Journal of Engineering Mechanics*, V. 128, No. 12, December 1, pp. 1304-1313.
- Chan, W.W.L. 1955. The ultimate strength and deformation of plastic hinges in reinforced concrete frameworks. *Magazine of Concrete Research*, Vol. 7, No. 21, November, pp. 121-132.
- Chen, W.F. 1982. *Plasticity in reinforced concrete*. McGraw-Hill, New York.
- Chung, H., Yang, K., Lee, Y., and Eun, H. 2002. Stress-strain curve of laterally confined concrete. *Engineering Structures*. Vol. 24, pp. 1153-1163.
- Cusson, D. and Paultre, P. 1995. Stress-strain model for confined high-strength concrete. *Journal of Structural Engineering*, ASCE, Vol. 121, No. 3, pp. 468-477.
- Fam, A. and Rizkalla, S.H. 2001. Confinement model for axially loaded concrete confined by circular fiber-reinforced polymer tubes. *ACI Structural Journal*, Vol. 98, No. 4, pp. 451-461.
- Gardner, N.J. 1969. Triaxial behaviour of concrete. *ACI Journal*, Vol. 114, No. 8, pp. 136-146.
- Hussain, M.A., and Driver, R.G. 2001. Finite element study on the strength and ductility of externally confined rectangular and square concrete columns. 29th Annual Conference of the Canadian Society for Civil Engineering, Victoria, B.C., Canada, May 30-June 2, 2001.

- Hussain, M.A., and Driver, R.G. 2003. Finite element analysis of reinforced concrete columns seismically upgraded by external collar confinement. 1st Conference on Response of Structures to Extreme Loading, Elsevier, Toronto, August 3-6.
- Hibbitt, Karlsson & Sorensen, Inc. 2004a. ABAQUS/Standard Version 6.2 User's Manual, Pawtucket, R.I.
- Hibbitt, Karlsson & Sorensen, Inc. 2004b. ABAQUS/Standard Version 6.2 Theory Manual, Pawtucket, R.I.
- Iyengar, K.T.S.R; Desayi, P.; and Reddy, K.N. 1970. Stress-strain characteristics of concrete confined in steel binders. Magazine of Concrete Research, Vol. 22, No.72, pp. 173-184.
- Johansson, M., and Gylltoft, K. 2002. Mechanical behaviour of circular steel-concrete composite stub columns. ASCE, Journal of Structural Engineering, Vol. 128, No. 8, pp. 1073-1081.
- Khaloo, A.R., Bozorgzadeh, A. 2001. Influence of confining hoop flexural stiffness on the behaviour of high-strength lightweight concrete columns. ACI Structural Journal, Vol. 98, No. 5, September-October, pp.657-664.
- Kupfer, H., Hilsdorf, H.K. and Rüsç, H. 1969. Behaviour of concrete under biaxial stresses. Journal of American Concrete Institute, Vol. 66, pp 656-666.
- Légeron, F. and Paultre, P. 2003. Uniaxial confinement model for normal- and high-strength concrete columns. ASCE, Journal of Structural Engineering, Vol. 129, No. 2, pp. 241-252.
- Madas, P. and Elnashai, A.S. 1992. A new passive confinement model for the analysis of concrete structures subjected to cyclic and transient dynamic loading. Earthquake Engineering and Structural Dynamics, Vol. 21, pp. 409-431.
- Mander, J.B., Priestley, M.J.N., and Park, R. 1988a. Observed stress-strain behaviour of confined concrete. ASCE, Journal of Structural Engineering, Vol. 114, No. 8, pp. 1827-1849.
- Mander, J.B., Priestley, M.J.N., and Park, R. 1988b. Theoretical stress-strain model for confined concrete. ASCE, Journal of Structural Engineering, Vol. 114, No. 8, pp. 1804-1826.
- Mirmiran, A. and Shahawy, M. 1996. A new concrete-filled hollow FRP composite column. composites, Part B, 27B(3-4), pp. 263-268.

- Mirmiran, A. and Shahawy, M. 1997. Behaviour of concrete columns confined by fiber composites. ASCE, Journal of Structural Engineering, Vol. 123, No. 5, pp. 583-590.
- Muto, C. 1974. Seismic Design Series—The plastic design of reinforced concrete structures (in Japanese).
- Nanni, A. and Bradford, N.M. 1995. FRP jacketed concrete under uniaxial compression. Construction and Building Materials, Vol. 9, No. 2, pp. 115-124.
- Pantazopoulou, S.J. 1995. Role of expansion on mechanical behaviour of concrete. ASCE, Journal of Structural Engineering, Vol. 121, No. 12, pp. 1795-1805.
- Park, R., Priestley, M.J.N., and Gill, W.D. 1982. Ductility of squared-confined concrete columns. ASCE, Journal of the Structural Division, Vol. 108, No. ST4, pp. 929-950.
- Popovics, S.A. 1973. A numerical approach to the complete stress-strain curve of concrete. Cement and Concrete Research, Pergamon Press, Inc., No. 3, pp. 583-599.
- Richart, F.E., Brandtzaeg, A., and Brown, R.L. 1928. A study of the failure of concrete under combined compressive stresses. University of Illinois Engineering Experimental Station, Bulletin No. 185, 104pp.
- Richart, F.E., Brandtzaeg, A., and Brown, R.L. 1929. The failure of plain and spirally reinforced concrete in compression. University of Illinois Engineering Experimental Station, Bulletin No. 190, 74pp.
- Saatcioglu, M. and Razvi, S.R. 1992. Strength and ductility of confined concrete. ASCE, Journal of Structural Engineering, Vol. 118, No. 6, pp. 1590-1607.
- Sadatmanesh, H. and Ehsani, M.R., and Li, M.W. 1994. Strength and ductility of concrete columns externally reinforced with fiber composite straps. ACI Structural Journal, Vol. 91, No. 4, pp. 434-447.
- Samaan, M., Mirmiran, A., and Shahawy, M. 1998. Model of concrete confined by fiber composites. ASCE, Journal of Structural Engineering, Vol. 124, No. 9, pp. 1025-1031.
- Schickert, G., and Winkler, H. 1979. Results of tests concerning strength and strain of concrete subjected to multiaxial compressive stresses. Deutscher Ausschuss für Stahlbeton, Heft 277, Berlin, West Germany.
- Scott, B.D., Park, R., and Priestley, M.J.N. 1982. Stress-strain behavior of concrete confined by overlapping hoops at low and high strain rates. ACI Journal, January-February, pp. 13-27.

- Seible, F, Priestley, N., Hegemier, G.A., and Innamorato, D. 1997. Seismic retrofit of RC columns with continuous carbon fiber jackets. *Journal of Composites for Construction*, Vol. 1, No. 2, pp. 52-62.
- Sheikh, S.A. and Uzumeri, S.M. 1980. Strength and ductility of tied concrete columns. *ASCE, Journal of the Structural Division*, Vol. 106, No. ST5, pp. 1079-1102.
- Sheikh, S.A. and Uzumeri, S.M. 1982. Analytical model for concrete confinement in tied columns. *ASCE, Journal of the Structural Division*, Vol. 108, No. ST12, pp. 2703-2722.
- Vallenas, J., Bertero, V.V., and Popov, E.P. 1977. Concrete confined by rectangular hoops subjected to axial loads. Report 77/13. Earthquake Engineering Research Centre, University of California, Berkeley, CA.
- Willam, K.J., and Warnke, E.P. 1975. Constitutive model for the triaxial behaviour of concrete of concrete. *Proceeding, International Association Bridge Structural Engineer*, 19, pp. 1-30.
- Young, W.C. 1989. *Roark's formulas for stress and strain*. Sixth Edition, McGraw-Hill, Inc., 832 pp.

## 6. NON-DIMENSIONAL MODEL FOR COLUMN CONFINING BEHAVIOUR OF HSS AND SOLID COLLARS WITH RIGID CORNER CONNECTIONS

### 6.1 Introduction

Many concrete confinement models exist for columns with conventional reinforcing steel including those proposed by Kent and Park (1971), Sheikh and Uzumeri (1982), Mander *et al.* (1988), Saatcioglu and Razvi (1992), Légeron and Paultre (2003), and Chung *et al.* (2002). Other models for confinement by composite materials have been proposed by Samaan *et al.* (1998) and Fam and Rizkalla (2001). However, none are able to predict the behaviour of columns confined externally by steel collars with significant flexural stiffness because of the lack of an explicit flexural stiffness parameter of the confining elements in these models. Hussain and Driver (2001) demonstrated through finite element study that both axial and flexural stiffness of the confining elements play significant roles and therefore need to be included in a comprehensive confinement model. This chapter presents a numerical investigation into the confining behaviour of steel HSS and solid collars with rigid corner connections on square concrete columns in terms of non-dimensional parameters. A parametric study and multi-dimensional regression was performed on the data generated using the finite element model described in Chapter 5 to develop equations that are capable of predicting confining behaviour in terms of average confining stress vs. average lateral strain.

A typical reinforced concrete column with collar confinement is shown in Figure 6-1(a). For simplicity, the discrete collars can be assumed smeared over the height of the column to form an equivalent continuous tube, as shown in Figure 6-1(b), provided the effect of smearing on the confining behaviour is taken into consideration. The tube is assumed to be made of an orthotropic material having zero stiffness in the direction of column axis. The flexural stiffness of the tube in the direction normal to the longitudinal axis of the column is the total flexural stiffness of all collars, over the height of the column, in the same direction. A similar argument applies to the axial stiffness of the equivalent tube as compared to the discrete collars. It is further assumed that the column with equivalent tube confinement expands uniformly over its height without bulging. Similar assumptions have been made by Légeron and Paultre (2003) in the development of their confinement model for conventionally reinforced normal- and high-strength concrete columns, and by Caner and Bažant (2002) while applying their computational model with smeared confinement to columns confined by spiral reinforcement. The equivalent confining tube is not shown for clarity in Figure 6-1(c), which depicts the lateral expansion of the concrete,  $u_{hco}$ , under axial compressive stress.

Figure 6-2(a) shows a general relationship between the average confining stress and average lateral strain for a confining tube. These confining stress vs. lateral strain curves, generated for many cases using the finite element model described in Chapter 5, are used to determine a representative non-dimensional curve, as depicted in Figure 6-2(b). The variables shown in the figure that are used to define this curve are described subsequently.

## 6.2 Confining Stress vs. Lateral Strain Relationship

In conventional columns, the core is generally defined as the region enclosed by the centreline of the ties. Figures 6-3(a) and 6-3(b) show the ineffectively confined regions within the core between tie levels and at the ties, respectively, that are approximately parabolic in shape, as described by, for example, Sheikh and Uzumeri (1982) and Mander *et al.* (1988). In the confinement model by Sheikh and Uzumeri (1982), an expression for the strength enhancement factor was defined based on the core bounded by the centreline of the ties. It was assumed that the strength enhancement factor depends on the amount of transverse reinforcement, the stress in the transverse reinforcement at the peak strength of confined concrete, and the ratio of the effectively confined concrete area at the critical section to the core area, which in turn depends on the configuration and spacing of the ties. Similarly, in the confinement model by Mander *et al.* (1988), a confinement effectiveness coefficient was defined as the ratio of the effectively confined concrete area at the critical section to the concrete core area bounded by the centreline of the perimeter ties. The average confining stress was calculated assuming that yielding of the transverse reinforcement occurs at the peak stress of the confined concrete. The average confining stresses on the sides of the column were then multiplied by the confinement effectiveness coefficients to get the equivalent confining stress. The peak stress of the confined concrete was then determined under this equivalent confining stress. Saatcioglu and Razvi (1992) also reported that the average confining stress calculated by assuming yielding of the transverse reinforcement overestimates the effective confining stress by a significant margin. A factor was therefore defined, based on a regression analysis of experimental data, to convert the average confining stress to an equivalent confining stress. The model proposed by Chung *et al.* (2002) utilizes an effectively confined distance ratio instead of area ratio to account for ineffectively confined regions within the core. The effectively confined distance ratio is defined as the ratio of the effectively confined width to the total width of the core concrete. This ratio takes the maximum value at the tie level and the minimum value at the critical section midway between two sets of ties. However, effectively and ineffectively confined regions were not dealt with separately. Instead, an expression for the strength enhancement factor was defined using regression in terms of the volumetric ratio of transverse steel, stress in the transverse steel at

peak stress of the confined concrete, cylinder strength of the concrete, and the effectively confined distance ratio.

The core of externally confined columns is equal to the gross dimensions of the columns. In contrast to the approaches described above wherein the ineffectively confined concrete is accounted for indirectly by a reduction factor applied to the behaviour of the entire core, the proposed model for externally confined columns separates explicitly the behaviour of the effectively and ineffectively confined regions in the core. The load vs. strain curves of the effectively and ineffectively confined concrete regions in the core are defined, and are then combined to get the overall load vs. strain curve. The load vs. strain curves can be converted to average stress vs. strain curves by dividing the load by the core area. Figure 6-3(c) shows the effectively and ineffectively confined regions between the collars and Figure 6-3(d) shows that there are no ineffectively confined regions at the collar level because of the considerable flexural stiffness of the sides of the collars, in addition to their axial stiffness. This assumption has been verified experimentally in this research program and its numerical verification will be given subsequently. To model the behaviour of the effectively confined regions in the core, the collars are assumed smeared over the height of the columns, as described before, with confining stress uniformly distributed on the sides of the columns. The ineffectively confined concrete acts simply as a filler to transfer the confining force to the effectively confined regions.

### **6.3. Finite Element Model**

The general-purpose finite element program *ABAQUS* (HKS 2004a; 2004b) was used to obtain the average confining stress vs. average lateral strain curves for the confining tube. Figure 6-4 shows the plan and elevation of a typical finite element model of a column segment with collars having rigid corner connections. The collars are represented by beam elements located a distance of one-half the collar depth from the concrete surface and are connected to the concrete by axially rigid outriggers. The complete description of the finite element model has been given in Chapter 5.

When the finite element model is loaded in the axial direction, the confining tube is strained laterally due to the dilation of concrete. In response, the confining tube applies confinement stress onto the concrete due to its restraining action. The pressure on the columns is purely passive. It can be observed from the elevation of the model that an individual collar has been divided into a number of layers within the actual center-to-centre spacing,  $s$ , to represent the equivalent confining tube described above. Any reasonable number of layers could be selected, provided the effect of collar smearing (described later) is taken into consideration. Smearing is used in order to keep the ranges of the non-dimensional parameters relatively small to improve

the accuracy of the resulting equation, while still accounting for all realistic collar configurations. The average confining stress is obtained by dividing the total force in the outriggers located in a strip having a length equal to the column width and a depth equal to the centre-to-centre spacing  $s$  of collars, by the strip area. The average lateral strain is obtained by dividing the average horizontal displacements of the concrete surface nodes at which outriggers from the smeared collars are connected, by half the width of the column.

### 6.3.1 Concrete Material Curve

The confining behaviour of the collars deduced from the finite element model is expressed as the average confining stress vs. average lateral strain. It has been demonstrated in Chapter 5 that the confining behaviour of collars with rigid corner connections is affected slightly by making a significant change in the input concrete material curve. However, this marginal effect on the confining behaviour of collars has been neglected in the parametric study presented in this chapter. The concrete material curve No. 5 shown in Figure 6-5 is used in the present chapter. Additional discussion of the curves in this figure is presented in Chapter 5.

### 6.3.2 Steel Material Curve

The confining behaviour of the collars depends on material properties of the confining steel such as yield stress and modulus of elasticity, and the shape of the material curve. Stub column tests were performed to determine material properties of the HSS collars used in phase 1 (Chapter 3) and phase 2 (Chapter 4) of the project. The material curves of all the HSS were round-shaped because of the presence of residual stresses. In all of these curves, the 0.2% offset method was used to determine the yield stress. As the parametric study on confining behaviour covers HSS collars as well as solid collars, in which the behaviour of the confining steel plays a pivotal role, it was considered that the range of parameters should be selected in such a way that they cover most commonly occurring cases. For this purpose, reference values of yield stress and modulus of elasticity were required. The reference values need not be exactly central over the range of interest. In the present study, the reference values of yield stress and modulus of elasticity were obtained by averaging the results of yield stresses and moduli of elasticity obtained from the stub column tests given in Chapters 3 and 4. The average values of yield stress and modulus of elasticity were found to be 465 MPa and 203 250 MPa, respectively. The reference value of yield stress is denoted by  $f_{yref}$  and that of modulus of elasticity is denoted by  $E_{sref}$ .

Figure 6-6(a) shows the stress vs. strain curve for a typical HSS 76x51x6.35 obtained from a stub column test (phase 2). There are different conventions to define the yield stress of this type

of steel material curve. Among them, the most commonly used conventions are: (a) 0.2% offset method; and (b) the stress at a particular level of axial strain,  $\varepsilon_{py}$ . The 0.2% offset method, widely used for civil engineering materials with round-shaped material curves, was used in the present study to determine the yield stresses of HSS. In this method, a line is drawn parallel to the initial slope of the curve beginning at a strain of 0.002. The stress at the point of intersection of this line with the curve represents the yield stress,  $f_y$ , of the material. The yield stress and modulus of elasticity of steel material shown in Figure 6-6(a) are  $f_y = 512$  MPa and  $E_s = 206\,660$  MPa.

The Ramberg-Osgood model can be calibrated to match the round-shaped steel material curves (Chen and Han 1988). The equation of the Ramberg-Osgood model using conventional notation is:

$$[6.1] \quad \varepsilon_{true} = \frac{f_{true}}{E_s} + a \left( \frac{f_{true}}{f_y} \right)^n$$

The shape of the material curve is controlled by four parameters:  $a$ ,  $n$ ,  $E_s$ , and  $f_y$ . These parameters can be selected by a trial-and-error procedure to produce a material curve that closely matches the experimentally obtained curve. However, if it is required that all of the generated curves have a yield stress,  $f_y$ , at 0.2% strain, then the parameter  $a$  must be set equal to 0.002. The generated steel material curve using the Ramberg-Osgood model shown in Figure 6-6(a) was obtained for the parameters set at the following values:  $a = 0.002$ ,  $n = 11$ ,  $E_s = 206\,660$  MPa, and  $f_y = 512$  MPa.

The confining steel material curves can therefore be generated for a constant value of  $a = 0.002$  (0.2% offset method) by varying the three other parameters:  $n$ ,  $E_s$ , and  $f_y$ .

### 6.3.3 Generation of Steel Material Curves for Parametric Study

Using the three parameters required to define a steel material curve ( $n$ ,  $E_s$ , and  $f_y$ ), four groups of curves for confining steel can be generated:

- (1) Figure 6-6(b) shows curves with different values of  $n$ , keeping  $f_y$  and  $E_s$  constant at their reference values, i.e.,  $f_y = f_{yref}$  and  $E_s = E_{sref}$ . In these curves,  $n$  was varied from 10 to 20 using the following values:  $n = 10, 11, 12, 14, 16, 18,$  and  $20$ . The initial slope of these curves are identical due to the invariance of  $E_s$ . The rounded parts of these curves approaching the yield stress are affected only slightly by the variations in the value of  $n$ , which has been ignored in the present study for simplicity. Conversely, the second parts of these curves (beyond the yield stress) vary considerably with  $n$ .
- (2) Figure 6-6(c) shows the generated material curves with different values of  $f_y$  and  $E_s$  for a constant value of  $n$ . The value of  $n$  can be set equal to its reference value, the choice of which is arbitrary as long as it is in the range over which it varies in the problem under consideration. For these curves, the reference value of  $n$  was taken equal to 11. The variation of  $f_y$  and  $E_s$  is done in such a way that their ratio ( $f_y / E_s$ ) remains constant. This approach leads to variation over the full extent of the curves, as seen in Figure 6-6(c). It will be noted in the subsequent parametric study that  $f_y$  and  $E_s$  influence the behavioural curves of the collars in a distinct way. However, it was considered difficult to capture the effect of simultaneous variation of both  $f_y$  and  $E_s$  on the confining behaviour of collars. Moreover, the value of  $E_s$  would be expected to vary little for structural steel, while  $f_y$  can vary considerably. Therefore, the influence of the variation of  $f_y$  and  $E_s$  on the behavioural curves of collars are studied separately, which required the generation of two more sets of steel material curves described in (3) and (4) below.
- (3) Figure 6-7(a) shows curves with different values of  $f_y$ , keeping  $n$  and  $E_s$  constant at their reference values. In this case, only the latter part of the material curve is affected significantly.

- (4) Figure 6-7(b) shows curves with different values of  $E_s$ , keeping  $n$  and  $f_y$  constant at their reference values. It is evident that varying the properties in this way has the greatest effect on the initial slope and the “knee” of the curve.

## 6.4 Contact of Collars with the Concrete Column

A total of nine collared columns were tested in phase 1 (see Chapter 3) of the project under concentric axial loading to very large strains. Although the collars deformed considerably during the axial load history, no gap was observed between the collars and the concrete of the column. Therefore, it is reasonable to assume that the pressures developed by the collars in the finite element model will always be compressive and gap elements are not required, nor is it necessary to distinguish between cases of collars installed with and without epoxy grout. This assumption was validated numerically using model 2 of group 1 given in Table 6.1. The average confining pressures on the respective elements at the surface of the column across its width are plotted in Figure 6-8(a) with respect to the average lateral strain of the column. There are 12 concrete elements across the width of the column; element 1 is in the corner and element 6 is adjacent to the centreline of the column. The confining pressure at element 1 is high and it diminishes towards the column centerline. As shown in Figure 6-8(b), the pressure in the corner of the column increases with an increase of average lateral strain. No tension force was observed in the outriggers in the practical range of lateral strain, validating the assumption that no gap develops between the concrete and steel collars.

## 6.5 Model for HSS Collars for Square Concrete Columns

A model for the confining behaviour of HSS collars for square concrete columns has been developed in terms of non-dimensional parameters. The output parameters of the parametric analyses, related to the confinement stress and lateral strain, represent the characteristic confinement curves. There are several equations that can be calibrated to approximate these curves. Of those considered, it was found that the Popovics equation (Popovics 1973) gave the best fit to the finite element results and was therefore used in the present study.

### 6.5.1. Non-Dimensional Parameters

The objective of the study is to develop equations to predict the confining behaviour of HSS collars. Based on the experimental work and finite element studies, it is assumed that this behaviour for square concrete columns depends on the following ten primary variables:

- (1) area of cross-section of a side of a collar,  $A_{collar}$  ;
- (2) moment of inertia of a side of a collar about an axis parallel to the axis of the column,  $I_{collar}$  ;
- (3) width of the column (inside length of a collar side),  $h_{column}$  ;
- (4) depth of the collar (perpendicular to column axis),  $h_{collar}$  ;
- (5) centre-to-centre spacing  $s$  ;
- (6) yield stress of the confining steel,  $f_y$  ;
- (7) modulus of elasticity of the confining steel,  $E_s$  ;
- (8) value of  $n$  in the Ramberg-Osgood confining steel material model
- (9) average lateral strain,  $\varepsilon_l$  ; and
- (10) average confinement stress,  $\sigma_{ct}$  .

It is to be noted that variables (6) to (8) ( $f_y$ ,  $E_s$ , and  $n$ ) are related to the material curve of the confining steel. It should also be noted that since the depth, width, and wall thickness (horizontal and vertical wall thicknesses were varied independently to enhance the generality of the study) of the hollow steel tubes can all be varied, variables (1), (2), and (4) ( $A_{collar}$ ,  $I_{collar}$ , and  $h_{collar}$ ) ,are independent. (The corner rounds have been neglected for simplicity.) Conversely, since only square concrete columns are being considered,  $h_{column}$ ,  $A_{column}$ , and  $I_{column}$  represent only a single independent quantity symbolized by variable (3) ( $h_{column}$ ). The confining behaviour of collars is represented by variables (9) and (10) ( $\varepsilon_l$  and  $\sigma_{ct}$ ). These two variables are dependent and the rest are independent parameters.

In order to perform a parametric study on ten parameters, a large number of analyses are required to study the effect of each individually on the confining behaviour of collars. The details of dimensional analysis are not presented here (see, for example, Taylor (1974)), however, in general the procedure is to relate groups of two or more primary variables to produce a reduced number of new non-dimensional variables (parameters) that reflect the effect of the variables combined. By dealing with combined non-dimensional parameters, the number of analyses required for the parametric study are considerably reduced and the scale effects can be eliminated. The dimensional analysis approach is suitable for this application because it leads to the development of simplified equations for the confining behaviour of collars with a reduced

number of independent parameters, but still takes into account the effects of all the primary variables.

The confining behaviour of the HSS collars depends on the ten primary variables. Two of these are already dimensionless: lateral strain  $\varepsilon_l$ ; and the value of  $n$  in the Ramberg-Osgood model. Hence, remaining are eight variables to be combined to form dimensionless parameters.

According to Taylor (1974), if the behaviour of a physical problem is represented by a set of  $m$  variables,  $A_1, A_2, A_3, \dots, A_m$ , the relationship between these variables can be expressed in terms of a homogeneous function:

$$[6.2] \quad F(A_1, A_2, A_3, \dots, A_m) = 0$$

There are a variety of ways to reduce the primary variables and to develop a proper set of non-dimensional parameters to characterize the behaviour of a physical problem. Among them, the most commonly used method is the Buckingham Pi theorem (Langhaar, 1951) which is stated below:

*If an equation is dimensionally homogeneous, it can be reduced to a relationship among a complete set of dimensionless products.*

Langhaar (1951) demonstrated that the number of non-dimensional parameters needed to correlate the variables in a given physical problem is equal to  $n-r$ , where  $r$  is the rank of the dimensional matrix of the variables  $A_1, A_2, A_3, \dots, A_m$ . The rank of a matrix is the largest order of any square sub-matrix that has a non-zero determinant. After developing the non-dimensional parameters ( $\beta_1, \beta_2, \beta_3, \dots, \beta_{m-r}$ ) using the Buckingham Pi theorem, the homogeneous function [6.2] can be rewritten as follows:

$$[6.3] \quad F(\beta_1, \beta_2, \beta_3, \dots, \beta_{m-r}) = 0$$

The dimensional matrix of eight primary variables (after taking out the two dimensionless parameters) in terms of fundamental units of mass,  $M$ , length,  $L$ , and time,  $T$ , can be written in the following form:

	$A_{collar}$	$I_{collar}$	$h_{collar}$	$h_{column}$	$s$	$f_y$	$E_s$	$\sigma_{ct}$
M	0	0	0	0	0	1	1	1
L	2	4	1	1	1	-1	-1	-1
T	0	0	0	0	0	-2	-2	-2

The rank of this dimensional matrix is two, therefore, six non-dimensional parameters are required (in addition to the two dimensionless parameters mentioned above) to describe this physical behaviour, *i.e.*, the confining behaviour of the collars. For concrete columns confined by HSS collars, the following eight trial non-dimensional parameters were chosen (including the two that were already dimensionless):

- $\beta_1 = \frac{A_{collar}}{A_{column}}$
- $\beta_2 = \frac{I_{collar}}{I_{column}}$
- $\beta_3 = \frac{s}{h_{column}}$
- $\beta_4 = \frac{h_{collar}}{h_{column}}$
- $\beta_5 = \frac{f_y}{E_s}$
- $\beta_6 = n$
- $\beta_7 = \varepsilon_l$
- $\beta_8 = \frac{\sigma_{ct}}{E_s}$

It is to be noted that  $\beta_7$  and  $\beta_8$  are output parameters and  $\beta_1$  to  $\beta_6$  are input parameters. The parameter  $\beta_5$  is the ratio of yield stress,  $f_y$ , to modulus of elasticity,  $E_s$ , of the confining steel. The variation in  $\beta_5$  can be obtained by varying yield stress,  $f_y$ , and/or the modulus of elasticity,

$E_s$ . However, their effects on the relationship between the output parameters,  $\beta_7$  and  $\beta_8$ , are different. In order to differentiate their effects, the notation  $\beta_5$  will be used when varying  $f_y$ , while keeping  $E_s$  and  $n$  constant. The constant value of  $E_s$  can be set equal to  $E_{sref}$  and the definition of the parameter becomes:

- $$\beta_5 = \frac{f_y}{E_{sref}}$$

Figure 6.7(a) shows the resulting input steel material curves with different values of  $f_y$  for constant values of  $E_s$  and  $n$ :  $E_s = E_{sref}$  and  $n = 11$ . Because these curves have a constant modulus of elasticity,  $E_s$ , the initial parts of the curves coincide. However, the second parts of the curves differ significantly. The curves with higher values of  $f_y$  are higher and vice versa.

The notation  $\beta'_5$  is used when varying  $E_s$ , while keeping,  $f_y$  and  $n$  constant. The constant value of  $f_y$  and  $n$  are set equal to  $f_{yref}$  and 11, respectively; and the definition of  $\beta'_5$  becomes:

- $$\beta'_5 = \frac{f_{yref}}{E_s}$$

Figure 6-7(b) shows a group of curves with different values of  $E_s$ , while keeping  $f_y$  constant. The initial slopes of these curves differ, however, beyond the knee of the curves they converge. This means that a change in modulus of elasticity,  $E_s$ , should not have a significant effect on the peak of the output curves generated by  $\beta_7$  and  $\beta_8$ . In order to remove the dependence of the output parameter  $\beta_8$  on  $E_s$ , the value of  $E_s$  in the denominator of  $\beta_8$  is held constant at a value of  $E_{sref}$ , the reference modulus of elasticity. Therefore, the definition of  $\beta_8$  is adjusted as follows:

- $$\beta_8 = \frac{\sigma_{ct}}{E_{sref}}$$

## 6.5.2 Ranges of Parameters and Reference Model

The reference model is an arbitrarily selected model for which the input parameters fall within the ranges over which the parametric study is performed. The ranges considered accommodate the

practical cases of columns and confining collars likely to be encountered. Attempts to capture the behavioural trends over wider ranges tend to lead to very complicated functions to achieve a good fit to the data points. In order to simplify the functions by reducing the ranges over which the parametric study is performed and regression equations are developed, collars of a practical size can be smeared into a series of smaller collars.

The geometry of the columns confined by HSS collars is controlled by the following four parameters:  $\beta_1$ ;  $\beta_2$ ;  $\beta_3$ ; and  $\beta_4$ . The ranges of these parameters that have been used in the parametric study are:

- $\beta_1 = 0.00262$  to  $0.00527$
- $\beta_2 = 2.48 \times 10^{-4}$  to  $5.56 \times 10^{-4}$
- $\beta_3 = 0.00625$  to  $0.2125$
- $\beta_4 = 0.20$  to  $0.31$

Small deviations from these ranges are acceptable while using the prediction equations (yet to be developed). However, large deviations might jeopardize the accuracy of predicted results. The nature of the prediction equation for a particular parameter gives insight into how much deviation from its range might be acceptable, while still maintaining the accuracy of predicted results.

The other parameters are related to the material curve of the confining steel. The parameter  $a$  was set at  $0.002$ . The effect of parameters  $\beta_5$ ,  $\beta'_5$ , and  $\beta_6$  on the confining behaviour of collars was studied over the following ranges:

- $\beta_5 = 0.001968$  to  $0.002952$
- $\beta'_5 = 0.00177$  to  $0.00266$
- $\beta_6 = 10.00$  to  $20.00$

This covers all the practical material curves for the confining steel.

Model 6 in Table 6.2 is the reference model for the parametric study of HSS collars. This model recurs for the study of each individual variable. The values of the input parameters for this model, along with the ranges of parameters over which the parametric studies were performed, are given below:

- $\beta_1 = 0.00365$  (Range:  $0.00262$  to  $0.00527$ )

- $\beta_2 = 0.0003634$  (Range: 0.00024876 to 0.00055588)
- $\beta_3 = 0.075$  (Range: 0.00625 to 0.2125)
- $\beta_4 = 0.25$  (Range: 0.20 to 0.31)
- $\beta_5 = 0.002287$  (Range: 0.001968 to 0.00295)
- $\beta'_5 = 0.002287$  (Range: 0.00177 to 0.00266)
- $\beta_6 = 11.00$  (Range: 10.00 to 20.00)

The values of input parameters for the reference model do not necessarily fall in the middle of the ranges of the parameters for HSS collars.

### 6.5.3 Scale Effect

In order to verify that the non-dimensional parameters are independent of any scale effect, ten analyses were performed in two groups, the details of which are given in Table 6.1. The objective is to vary the constituent (primary) variables of the non-dimensional parameters, while keeping the non-dimensional parameters themselves constant. If the input parameters selected truly and fully represent the behaviour defined by the output parameters, the output curves will be identical over the full range of interest. It is to be noted that in order to keep  $\beta_1$  through  $\beta_4$  constant, the constituent variables of each non-dimensional parameter cannot be varied individually. This is because once the cross-sectional column dimension,  $h_{column}$ , has been selected, the associated area,  $A_{column}$ , and moment of inertia,  $I_{column}$ , are also set. The numerators of the respective non-dimensional input parameters are therefore also unique in order to achieve specific values of  $\beta_1$  through  $\beta_4$ . Conversely, the constituent (primary) variables of  $\beta_5$  and  $\beta'_5$  can be varied individually. In this scale effect study only the constituents of  $\beta_1$  through  $\beta_4$  are varied. The analogous effects of  $\beta_5$  and  $\beta'_5$  are studied separately and presented subsequently.

The two groups of models for assessing the scale effect are shown in Table 6.1. Group 1 consists of six models and group 2 consists of four models. Although the primary variables are different for the various models in each of these groups, the values of the non-dimensional input parameters are the same within a group. The values of the input parameters for the models in group 1 are:

- $\beta_1 = 3.65 \times 10^{-3}$

- $\beta_2 = 3.634 \times 10^{-4}$
- $\beta_3 = 0.075$
- $\beta_4 = 0.25$
- $\beta_5 = 2.288 \times 10^{-3}$
- $\beta'_5 = 2.288 \times 10^{-3}$
- $\beta_6 = 11.00$

The values of the input parameters in group 2 are:

- $\beta_1 = 7.979 \times 10^{-3}$
- $\beta_2 = 7.495 \times 10^{-4}$
- $\beta_3 = 0.20$
- $\beta_4 = 0.25$
- $\beta_5 = 2.288 \times 10^{-3}$
- $\beta'_5 = 2.288 \times 10^{-3}$
- $\beta_6 = 11.00$

The relationships between  $\beta_7$  and  $\beta_8$  for the analyses of models in groups 1 and 2 are depicted in Figure 6-9. The curves for the different models in each group overlap each other, confirming that the parameters are independent of scale effects. However, the two groups have different output curves because of the difference in the values of the non-dimensional input parameters.

#### 6.5.4. Parametric Study and Prediction Equation

In order to capture trends in the confining behaviour of welded hollow collars, use of a generalized equation proposed by Popovics (1973), for unconfined concrete, has been made. This equation was selected because it tends to provide a better fit to the output curves than other common methods due primarily to the ability to control the curvature of the ascending branch. Moreover, the Popovics equation can be controlled by two simple variables, as described below. The relationship between  $\beta_7$  and  $\beta_8$  can therefore be expressed as:

$$[6.4] \quad \beta_8 = \frac{(\beta_8)_{\max} x^r}{r - 1 + x^r}$$

where  $x = \frac{\beta_7}{(\beta_7)_{\max}}$ ,  $r = \frac{\gamma_o}{\gamma_o - \gamma_{\text{sec}}}$ , and  $\gamma_{\text{sec}} = \frac{(\beta_8)_{\max}}{(\beta_7)_{\max}}$

A typical relationship between  $\beta_7$  and  $\beta_8$  is presented in Figure 6-2(b) to define the variables  $\gamma_o$ ,  $\gamma_{\text{sec}}$ ,  $(\beta_7)_{\max}$ , and  $(\beta_8)_{\max}$ , where  $\gamma_o$  is the initial slope of the curve;  $\gamma_{\text{sec}}$  is the secant slope of the curve to the point defined as the “peak;” and  $(\beta_8)_{\max}$  is the value of  $\beta_8$  at  $\beta_7 = (\beta_7)_{\max}$ . The shape of the curve obtained by Equation 6.4 can be controlled by three variables:  $\gamma_o$ ,  $(\beta_8)_{\max}$ , and  $(\beta_7)_{\max}$ . The variable  $(\beta_7)_{\max}$  has been set equal to 1.0 to be used for obtaining the best fit to the finite element results. (It is to be noted that this point is arbitrary and the curve fitting exercise takes place only over the range of reasonable lateral strains (i.e., values of  $\beta_7$ )). Hence, there are only two variables ( $\gamma_o$  and  $(\beta_8)_{\max}$ ) remaining to fully control the shape of the curve. The following relationships are hypothesised for  $(\beta_8)_{\max}$  and  $\gamma_o$ :

[6.5]

$$(\beta_8)_{\max}(\beta_1, \beta_2, \beta_3, \beta_4, \beta_5, \beta_5', \beta_6) = \lambda_1(\beta_1) \times \lambda_2(\beta_2) \times \lambda_3(\beta_3) \times \lambda_4(\beta_4) \times \lambda_5(\beta_5) \times \lambda_5'(\beta_5') \times \lambda_6(\beta_6)$$

[6.6]

$$\gamma_o(\beta_1, \beta_2, \beta_3, \beta_4, \beta_5, \beta_5', \beta_6) = \gamma_1(\beta_1) \times \gamma_2(\beta_2) \times \gamma_3(\beta_3) \times \gamma_4(\beta_4) \times \gamma_5(\beta_5) \times \gamma_5'(\beta_5') \times \gamma_6(\beta_6)$$

The functions  $\lambda_1(\beta_1)$ ,  $\lambda_2(\beta_2)$ ,  $\lambda_3(\beta_3)$ ,  $\lambda_4(\beta_4)$ ,  $\lambda_5(\beta_5)$ ,  $\lambda_5'(\beta_5')$ ,  $\lambda_6(\beta_6)$ ,  $\gamma_1(\beta_1)$ ,  $\gamma_2(\beta_2)$ ,  $\gamma_3(\beta_3)$ ,  $\gamma_4(\beta_4)$ ,  $\gamma_5(\beta_5)$ ,  $\gamma_5'(\beta_5')$ , and  $\gamma_6(\beta_6)$  are determined by performing regression analyses on the data generated through parametric study using finite element models, the details of which is given in the following sections. Once these functions are established, the non-dimensional output curve can be generated easily with Equation 6.4 for any values of the non-dimensional input variables that are consistent with the parametric study.

#### 6.5.4.1 Overview of Regression Analysis

The objective of a regression analysis is to determine the values of parameters for a function that cause the function to provide a best fit to a given set of data generated either numerically or experimentally. In the present study, it was found that power series could generally be selected

to provided a good fit to the data without becoming unduly complex. There are several procedures to check the quality of fitness of a function to the given numerical data; some of them are listed below:

- Final Sum of Squared Deviations
- Average and Maximum Deviations
- Coefficient of Multiple Determination
- Adjusted Coefficient of Multiple Determination

In the present study, the “coefficient of multiple determination” method was used to check the quality of fitness by using the following deviation parameter:

$$[6.7] \quad R^2 = 1 - \frac{V_p}{V_m}$$

where  $V_p$  is the variance using the predicted values, and  $V_m$  is the variance using the mean value. The variance using the mean value,  $V_m$ , is defined as the sum of the squared differences between the mean value and the values of the dependent variable at all data points. The variance using the predicted value,  $V_p$ , is defined as the sum of the squared differences between the values of the dependent variable predicted by the function and the actual values at all data points.

The goodness of fit of a function to a set of numerical data is determined from the value of  $R^2$ , as defined in Equation 6.7. If the function fits the data perfectly, the value of  $R^2$  is equal to 1.00. In the worst case, the value of  $R^2$  can become equal to zero, which means that the function is no better than simply using the mean of the observed values.

#### **6.5.4.2 Effect of Parameter $\beta_1$ on the Confining Behaviour of HSS Collars**

Table 6.2 shows the details of the analyses to study the effect of variation of  $\beta_1$  on the confining behaviour. It is to be noted that the model 6 in this table is the reference model. The collar dimensions are modified in such a way that only  $\beta_1$  varies and the other input parameters ( $\beta_2, \beta_3, \beta_4, \beta_5, \beta'_5$  and  $\beta_6$ ) remain constant. Figure 6-10 shows the relationship between  $\beta_7$

and  $\beta_8$  for all the analyses for  $\beta_1$  varying from 0.00262 to 0.00527. The values of the other parameters were set at the following values:

- $\beta_2 = 0.003634$
- $\beta_3 = 0.075000$
- $\beta_4 = 0.250000$
- $\beta_5 = 0.002288$
- $\beta'_5 = 0.002288$
- $\beta_6 = 11.00$

The curves shown in this figure have essentially two parts, the first part (steep) and the second part (nearly horizontal), which are joined by a curve. The slope of the initial part of the curve is represented by  $\gamma_o$ . The parameter  $(\beta_8)_{\max}$  is the value of  $\beta_8$  at  $(\beta_7)_{\max}$ . Although the location of  $(\beta_8)_{\max}$  is not on the graph of Figure 6-10, it can be concluded from the shape of these curves that both  $\gamma_o$  and  $(\beta_8)_{\max}$  increase with an increase of  $\beta_1$ . In order to capture the trends of these curves, Equation 6.4 was made to provide a best fit up to a practical value of lateral strain,  $\beta_7$ , and the resulting values of  $\gamma_o$  and  $(\beta_8)_{\max}$  are given in Table 6.2. A total of 11 models were used (see Table 6.2). By inspection, curve fitting to case 11 appeared to be worse as compared to the other 10 cases. The following values of  $R^2$  were calculated for this case up to different levels of lateral strains to quantify the level of curve fitting that could be achieved by this process:

$R^2 = 0.9905$  up to a lateral strain of 0.06

$R^2 = 0.9924$  up to a lateral strain of 0.05

$R^2 = 0.9920$  up to a lateral strain of 0.04

$R^2 = 0.9901$  up to a lateral strain of 0.03

These values of  $R^2$  indicate very good curve fitting even for the worst case. Similarly, in other cases in the parametric study, approximately the same level of curving fitting was maintained. It was decided to use 0.03 as the limit of lateral strain for curve fitting procedures.

The values of  $(\beta_8)_{\max}$  and  $\gamma_o$  listed in Table 6.2 are equivalent to  $\lambda_1$  and  $\gamma_1$ , respectively, and they account directly for the effect of  $\beta_1$  in Equation 6.4. The effects of the other input

parameters must therefore be formulated to account only for the required adjustments to these base values. Figure 6-11(a) shows the relationship between  $\lambda_1$  and  $\beta_1$ . Using a power series function, the following equation was obtained for  $\lambda_1(\beta_1)$ :

$$[6.8] \quad \lambda_1(\beta_1) = 0.0238\beta_1^{0.842}$$

Similarly, Figure 6-11(b) shows the relationships between  $\gamma_1$  and  $\beta_1$  and the following best fit equation was obtained for  $\gamma_1(\beta_1)$ :

$$[6.9] \quad \gamma_1(\beta_1) = 1.243\beta_1^{0.547}$$

#### 6.5.4.3 Effect of Parameter $\beta_2$ on the Confining Behaviour of HSS Collars

Table 6.3 shows the details of the models used to study the effect of variation of  $\beta_2$  on the confining behaviour. Model 6 is the reference model. The collar dimensions are modified in such a way that only  $\beta_2$  varies from  $2.4876 \times 10^{-4}$  to  $5.5588 \times 10^{-4}$  and the other input parameters ( $\beta_1, \beta_3, \beta_4, \beta_5, \beta_5'$  and  $\beta_6$ ) remain constant at the following values:

- $\beta_1 = 0.00365$
- $\beta_3 = 0.07500$
- $\beta_4 = 0.25000$
- $\beta_5' = 0.002288$
- $\beta_5 = 0.002288$
- $\beta_6 = 11.00$

The resulting output curves relating  $\beta_7$  and  $\beta_8$  are shown in Figure 6-12 up to  $\beta_7 = 0.05$ . It is clear from these curves that the variation of  $\beta_2$  affects the first part (initial slope) of the curves. Although the curves seem to be converging, the small variation in the so-called peak values (i.e., at  $\beta_7 = 1.0$ ) has also been captured by fitting an equation. Equation 6.4 was fit to the finite

element curves relating  $\beta_7$  to  $\beta_8$  (Figure 6-12) up to  $\beta_7$  equal to 0.03, and the respective values of  $\gamma_o$  and  $(\beta_8)_{\max}$  are given in Table 6.3. Table 6.4 also lists the values of  $\gamma_o$  and  $(\beta_8)_{\max}$  for all the models, in addition to the ratio of  $(\beta_8)_{\max}$  of all the models to the value of  $(\beta_8)_{\max}$  of model 6 (reference model). These ratios are denoted by  $\lambda_2$ . It is to be noted that the value of  $\lambda_2$  for the reference model necessarily becomes equal to 1.0. Figure 6-13(a) shows the plot of values of  $\lambda_2$  vs.  $\beta_2$ . A power series function was fit to these data points and the following expression is obtained for  $\lambda_2(\beta_2)$ :

$$[6.10] \quad \lambda_2(\beta_2) = 0.7331(\beta_2)^{-0.0396}$$

Table 6.4 also shows the ratio of  $\gamma_o$  for all the models to  $\gamma_o$  of reference model. These ratios are denoted by  $\gamma_2$ . The value of  $\gamma_2$  for the reference model becomes equal to 1.0. Figure 6-13(b) shows the plot of  $\gamma_2$  vs.  $\beta_2$ . A power series function was fit to these data points and the following expression is obtained for  $\gamma_2(\beta_2)$ :

$$[6.11] \quad \gamma_2(\beta_2) = 12.5\beta_2^{0.32}$$

#### 6.5.4.4 Effect of Parameter $\beta_3$ on the Confining Behaviour of HSS Collars

Table 6.5 shows the detail of finite element models to study the effect of variation of  $\beta_3$  on the confining behaviour. Model 10 in this table is the reference model. The collar spacing was varied to get variation in  $\beta_3$  (from 0.00625 to 0.2125), while keeping the other input parameters ( $\beta_1, \beta_2, \beta_4, \beta_5, \beta'_5$  and  $\beta_6$ ) at the following constant values:

- $\beta_1 = 0.003650$
- $\beta_2 = 0.036340$
- $\beta_4 = 0.250000$
- $\beta_5 = 0.002288$
- $\beta'_5 = 0.002288$

- $\beta_6 = 11.00$

The curves between  $\beta_7$  and  $\beta_8$  for all the models given in Table 6.5 were plotted to study the effect of change of  $\beta_3$  on the confining behaviour. The curves for models 1, 2, 4, 5, 7, 9, 11, and 16 are depicted in Figure 6-14. The study of these curves showed that the change in  $\beta_3$  has a large effect on both  $\gamma_o$  and  $(\beta_8)_{\max}$ . Equation 6.4 was made fit to all these curves, and the respective values of  $\gamma_o$  and  $(\beta_8)_{\max}$  are reported in Table 6.6. The values of  $\gamma_o$  and  $(\beta_8)_{\max}$  thus obtained were normalized with respect to the respective values of  $\gamma_o$  and  $(\beta_8)_{\max}$  of the curve of model 10 and the resulting normalized values of  $\gamma_o$  and  $(\beta_8)_{\max}$ , referred to as  $\gamma_3$  and  $\lambda_3$ , respectively, are also given in Table 6.6. The values of  $\lambda_3$  were plotted with respect to  $\beta_3$  and the resulting curve is shown in Figure 6-15(a). A power series function was fit to this curve and the following expression for  $\lambda_3(\beta_3)$  was obtained:

$$[6.12] \quad \lambda_3(\beta_3) = 0.1152\beta_3^{-0.850}$$

Similarly, the values of  $\gamma_3$  were plotted with respect to  $\beta_3$  and the resulting curve is shown in Figure 6-15(b). A power series function was fit to this curve and the following expression for  $\gamma_3(\beta_3)$  was obtained:

$$[6.13] \quad \gamma_3(\beta_3) = 0.0931\beta_3^{-0.939}$$

#### 6.5.4.5 Effect of Parameter $\beta_4$ on the Confining Behaviour of HSS Collars

Table 6.7 shows the detail of models to study the effect of variation of  $\beta_4$  on the confining behaviour. In this case, model 5 is the reference model. The collar depth  $h_{collar}$  was varied to get variation in  $\beta_4$  (0.20 to 0.31), while keeping the other input parameters ( $\beta_1, \beta_2, \beta_3, \beta_5, \beta_5'$  and  $\beta_6$ ) at the following constant values:

- $\beta_1 = 0.003650$
- $\beta_2 = 0.036340$

- $\beta_3 = 0.075000$
- $\beta_5 = 0.002288$
- $\beta'_5 = 0.002288$
- $\beta_6 = 11.00$

The curves relating  $\beta_7$  and  $\beta_8$  for these models are shown in Figure 6-16. From these curves, it is clear that the variation in  $\beta_4$  only affects  $(\beta_8)_{\max}$ , without affecting  $\gamma_o$ . With the increase of  $\beta_4$ , the value of  $(\beta_8)_{\max}$  increases. Equation 6.4 was fit to these curves and the resulting values of  $\gamma_o$  and  $(\beta_8)_{\max}$  for each case is given in Table 6.8. The values of  $\gamma_o$  and  $(\beta_8)_{\max}$  were normalized with respect to the values of  $\gamma_o$  and  $(\beta_8)_{\max}$ , respectively, of the curve of the reference model (model 5 in Table 6.8). The normalized values of  $\gamma_o$  and  $(\beta_8)_{\max}$ , denoted by  $\gamma_4$  and  $\lambda_4$  are also given in the Table 6.8. The values of  $\lambda_4$  were plotted with respect to the values of  $\beta_4$  and the resulting curve is shown in Figure 6-17. A power series function was fit to the data and the following expression was obtained for  $\lambda_4(\beta_4)$ :

$$[6.14] \lambda_4(\beta_4) = 1.3506\beta_4^{0.213}$$

It is clear from Table 6.8 that the values of  $\gamma_4$  are constant at 1.0 and therefore have no dependence on  $\beta_4$ , which leads to the following expression for  $\gamma_4(\beta_4)$ :

$$[6.15] \gamma_4(\beta_4) = 1.00$$

#### 6.5.4.6 Effect of Parameter $\beta_5$ on the Confining Behaviour of HSS Collars

The parameter  $\beta_5$  represents the ratio of yield stress,  $f_y$ , to modulus of elasticity,  $E_s$ , of the confining steel. The effect of this parameter on the confining behaviour of HSS collars is studied in two ways: (a) variation in both yield stress,  $f_y$ , and modulus of elasticity,  $E_s$ , in such a way that  $\beta_5$  remains constant; and (b) variation in yield stress,  $f_y$ , or modulus of elasticity,  $E_s$ , or both such that  $\beta_5$  does not remain constant. The effect of variation of both  $f_y$  and  $E_s$ , such that

parameter  $\beta_5$  remains constant, on the relationship between  $\beta_7$  and  $\beta_8$  is presented initially. This is analogous to the studies of  $\beta_1$  through  $\beta_4$  in the section on scale effect. Table 6.9 shows the detail of the finite element models used for this study with the following values of input parameters:

- $\beta_1 = 0.003650$
- $\beta_2 = 0.036340$
- $\beta_3 = 0.075000$
- $\beta_4 = 0.250000$
- $\beta_5 = 0.002288$

Based on the analyses of these models, the curves relating parameters  $\beta_7$  and  $\beta_8$  are shown in Figure 6-18. Although  $\beta_5$  is constant for these curves, they do not coincide. This casts doubt on the validity of  $\beta_5$  as a characteristic non-dimensional parameter. This discrepancy can be explained with the help of Figure 6.7, which shows material curves for HSS generated by the calibrated Ramberg-Osgood model: (a) with different values of  $f_y$  and a constant value of  $E_s$  (Figure 6-7(a)); and (b) with different values of  $E_s$  and a constant value of  $f_y$  (Figure 6-7(b)). The initial parts of the curves shown in Figure 6-7(a) essentially overlap because these curves were generated for a constant value of  $E_s$ . The variation in the values of  $f_y$  is reflected in the second parts of these curves. Similarly, Figure 6-7(b) shows material curves of confining steel with different values of  $E_s$  and a constant value of  $f_y$ . The change in  $E_s$  is reflected in the initial parts of these curves but they tend to converge past the knee. Because of the distinct effect  $f_y$  and  $E_s$  show in the different curve regions, it seems preferable to vary these variables separately and this can be done by normalizing each with the reference values  $E_{sref}$  and  $f_{yref}$ , respectively, as discussed previously.

Table 6.10 shows the details of the finite element models to study the effect of variation of  $f_y$  (i.e., variation of  $\beta_5$ ) on the confining behaviour of the collars with  $E_s$  set equal to the reference

value. Model 3 in this table is the reference model. The parameter  $\beta_5$  was varied from 0.001968 to 0.002952; the other input parameters ( $\beta_1, \beta_2, \beta_3, \beta_4, \beta'_5$ , and  $\beta_6$ ) were set at the following constant values:

- $\beta_1 = 0.003650$
- $\beta_2 = 0.036340$
- $\beta_3 = 0.075000$
- $\beta_4 = 0.250000$
- $\beta'_5 = 0.002288$
- $\beta_6 = 0.250000$

The resulting curves between  $\beta_7$  and  $\beta_8$  for these analyses are shown in Figure 6-19. The initial parts of these curves overlap each other but the second parts, or the so-called peak values of these curves, are affected significantly by changing  $f_y$ . The Equation 6.4 was fit to all these curves and the resulting values of  $\gamma_o$  and  $(\beta_8)_{\max}$  are given in Table 6.11. These values of  $\gamma_o$  and  $(\beta_8)_{\max}$  were normalized with respect to the values of  $\gamma_o$  and  $(\beta_8)_{\max}$  of the reference model. The normalized values of  $\gamma_o$  and  $(\beta_8)_{\max}$ , denoted by  $\gamma_5$  and  $\lambda_5$ , respectively, are also given in Table 6.11.

The values of  $\lambda_5$  are plotted with respect to the respect to  $\beta_5$  and the resulting curve is shown in Figure 6-20. In this case, a power function was not required to obtain good accuracy and a linear function was fit to this curve by setting the y-intercept equal to zero, resulting in the following expression for  $\lambda_5(\beta_5)$ :

$$[6.16] \lambda_5(\beta_5) = 435\beta_5$$

The values of  $\gamma_o$  remains essentially unaffected by changing  $\beta_5$ . Therefore, the values of  $\gamma_5$  becomes 1.00 for all these curves, resulting in the following expression for  $\gamma_5(\beta_5)$ :

$$[6.17] \gamma_5(\beta_5) = 1.00$$

#### 6.5.4.7 Effect of Parameter $\beta_5'$ on the Confining Behaviour of HSS Collars

Table 6.12 summaries the details of the models used to study the effect of variation of  $E_s$  (i.e., variation in  $\beta_5'$ ) on the confining behaviour of collars with  $f_y$  set equal to the reference value. Model 3 in this table is the reference model. The parameter  $\beta_5'$  was varied from 0.00177 to 0.00266, keeping the other input parameters ( $\beta_1, \beta_2, \beta_3, \beta_4, \beta_5$ , and  $\beta_6$ ) at the following constant values:

- $\beta_1 = 0.003650$
- $\beta_2 = 0.036340$
- $\beta_3 = 0.075000$
- $\beta_4 = 0.250000$
- $\beta_5 = 0.002288$
- $\beta_6 = 11.00$

Figure 6-21 shows the relationship between  $\beta_7$  and  $\beta_8$  for different values of  $\beta_5'$ . The study of these curves shows that the variation in  $E_s$  essentially affects the initial slope,  $\gamma_o$ , of the curves, without affecting the second parts of the curves. The Equation 6.4 was fit to these curves and the resulting values of  $(\beta_8)_{\max}$  and  $\gamma_o$  are listed in Table 6.13. These values of  $(\beta_8)_{\max}$  and  $\gamma_o$  were normalized with respect to the values of  $(\beta_8)_{\max}$  and  $\gamma_o$ , respectively, of the reference model (model 3). The normalized values of  $(\beta_8)_{\max}$  and  $\gamma_o$ , denoted by  $\lambda_5'$  and  $\gamma_5'$ , respectively, are also listed in this table. Although  $\lambda_5'$  is affected by a change in  $\beta_5'$ , the effect is considered small enough to neglect. Therefore, the values of  $\lambda_5'$  for all these curves become equal to 1.00, resulting in the following expression for  $\lambda_5'(\beta_5)$ :

$$[6.18] \quad \lambda_5'(\beta_5) = 1$$

The values of  $\gamma'_5$  are plotted with respect to the values of  $\beta'_5$  in Figure 6-22. A power series function was fit to this curve and the following expression was obtained for  $\gamma'_5(\beta'_5)$ :

$$[6.19] \quad \gamma'_5(\beta'_5) = 0.0077\beta'^{-0.80}$$

#### 6.5.4.8 Effect of Parameter $\beta_6$ on the Confining Behaviour of HSS Collars

The confining behaviour of HSS collars also depends on the shape of the material curves of the confining steel, which in turn depends on the value of  $n$  in addition to  $a$ ,  $f_y$  and  $E_s$  (Equation 6.1). The effect of a change in the value of  $n$  on the confining behaviour of collars is now considered. Table 6.14 gives the details of the finite element models used for this study. The Model 2 in this table is the reference. In these models, the value of  $\beta_6$  is varied from 10 to 20 and the other parameters were set at the following at the following constant values:

- $\beta_1 = 0.003650$
- $\beta_2 = 0.036340$
- $\beta_3 = 0.075000$
- $\beta_4 = 0.250000$
- $\beta_5 = 0.002288$
- $\beta'_5 = 0.002288$

Figure 6-23 shows the relationship between  $\beta_7$  and  $\beta_8$  for different values of  $\beta_6$ . The study of these curves shows that the variation of  $\beta_6$  affects essentially the second parts of the curves without affecting the initial slope,  $\gamma_o$ . The Equation 6.4 was fit to all these curves and the resulting values of  $\gamma_o$  and  $(\beta_8)_{\max}$  are given in Table 6.15. These values of  $\gamma_o$  and  $(\beta_8)_{\max}$  were normalized with respect to the values of  $\gamma_o$  and  $(\beta_8)_{\max}$  of the reference model. The normalized values of  $\gamma_o$  and  $(\beta_8)_{\max}$ , denoted by  $\gamma_6$  and  $\lambda_6$  respectively, are also given in Table 6.15. Figure 6-24 shows the plot relating  $\lambda_6$  and  $\beta_6$ . A power series function was fit to this curve with the help of regression, resulting in the following expression for  $\lambda_6(\beta_6)$ :

$$[6.20] \lambda_6(\beta_6) = 1.50\beta_6^{-0.17}$$

The values of  $\gamma_6$  are constant with respect to  $\beta_6$ , which leads to the following expression for  $\gamma_6(\beta_6)$ :

$$[6.21] \gamma_6(\beta_6) = 1.00$$

#### 6.5.4.9 Effect of Collar Smearing on the Confining Behaviour of HSS Collars

Table 6.16 shows the detail of finite element models to study the effect of collar smearing on the confining behaviour. It is to be noted that model 4 in this table is the reference model. All of these models are equivalent in that although different degrees of smearing are present, the total axial and flexural stiffnesses of the collars are identical. Hence, all the model should give the same result in terms of the relationship between the output parameters  $\beta_7$  and  $\beta_8$  if there is no smearing effect. The models in Table 6.16 show variation of  $\beta_3$  from 0.01875 to 0.30, accompanied by concomitant variations in parameter  $\beta_1$  from  $9.125 \times 10^{-4}$  to  $1.46 \times 10^{-2}$  and parameter  $\beta_2$  from  $9.0841 \times 10^{-5}$  to  $1.4535 \times 10^{-3}$  such that the models remain equivalent to each other. The other input parameters of these models were kept at the following constant values (*i.e.*, the reference values):

- $\beta_4 = 0.250000$
- $\beta_5 = 0.002288$
- $\beta'_5 = 0.002288$
- $\beta_6 = 11.00$

Only for Models 3, 4, and 5 do all of the parameters  $\beta_1$ ,  $\beta_2$ , and  $\beta_3$  fall within the ranges considered in the parametric study. It is important to note that it is the models with the higher numbers that have values for collar area, stiffness, and spacing that are closer to those that would be expected for real columns (*i.e.*, “unsmeared”). Figure 6-25 shows that although the initial slope is unaffected by smearing, an effect on the peak of the curve is observed, primarily for Models 1 and 2. It is significant that smearing by a small amount has a relatively small effect

and only for the severe smearing of Models 1 and 2 is the effect highly pronounced. This effect over the range of Models 3, 4, and 5 is considered negligible, so smearing to any degree that falls within the ranges of the non-dimensional input parameters considered in the parametric study can be taken as equivalent.

The effect of smearing can be related to any one of the three input parameters  $\beta_1$ ,  $\beta_2$ , and  $\beta_3$  because of the equivalency in their variations. In the present study, the effect of smearing on the output behavioural curves of the collars is related to  $\beta_3$ . Equation 6.4 was fit to the curves in Figure 6-25 and the corresponding values of  $\gamma_o$  and  $(\beta_8)_{\max}$  are given in Table 6.17. These values are then normalized with respect to the respective values of  $\gamma_o$  and  $(\beta_8)_{\max}$  of reference model (model 4). The normalized values of  $(\beta_8)_{\max}$  and  $\gamma_o$ , denoted by  $\lambda_s$  and  $\gamma_s$ , have also been given in Table 6.17. The values of  $\lambda_s$  are plotted with respect to  $\beta_3$  and the resulting curve is shown in Figure 6-26. A power series function was fit to this curve, resulting in the following expression for  $\lambda_s(\beta_3)$ :

$$[6.22] \quad \lambda_s(\beta_3) = 1.1418\beta_3^{0.0525}$$

The values of  $\gamma_s$  for all the models are 1.00 in Table 6.17, which leads to the following relation for  $\gamma_s(\beta_3)$ :

$$[6.23] \quad \gamma_s(\beta_3) = 1.00$$

The correction for smearing can be applied to the so-called peak values of the behavioural curves of the collars. If the  $\beta_3$  parameters for the actual and smeared models are denoted by  $\beta'_3$  and  $\beta_3$ , respectively, a factor  $a_s$  is defined to account for the effect of smearing on the peak value of the confining behaviour (using Equation 6.22):

$$[6.24] \quad a_s = \left(\frac{\beta'_3}{\beta_3}\right)^{0.0524}$$

The value of this factor will be greater than 1 if the spacing of the collars in the actual model is bigger than that of the smeared model, which will always be true for practical cases.

#### 6.5.4.10 Expressions for $(\beta_8)_{\max}$ and $\gamma_o$ for HSS Collars

The expression for  $(\beta_8)_{\max}$  can be obtained by substituting the values of  $\lambda_1(\beta_1)$ ,  $\lambda_2(\beta_2)$ ,  $\lambda_3(\beta_3)$ ,  $\gamma_4(\beta_4)$ ,  $\lambda_5(\beta_5)$ ,  $\lambda'_5(\beta'_5)$ , and  $\lambda_6(\beta_6)$  into Equation 6.5, and adding the smearing correction factor,  $a_s$ . The resulting expression is:

$$[6.25] \quad (\beta_8)_{\max} = \frac{1.77133\beta_1^{0.842}\beta_4^{0.213}\beta_5 a_s}{\beta_2^{0.0396}\beta_3^{0.85}\beta_6^{0.17}}$$

Similarly, the expression for  $\gamma_o$  can be obtained by substituting the expressions for  $\gamma_1(\beta_1)$ ,  $\gamma_2(\beta_2)$ ,  $\gamma_3(\beta_3)$ ,  $\gamma_4(\beta_4)$ ,  $\gamma_5(\beta_5)$ ,  $\gamma'_5(\beta'_5)$ , and  $\gamma_6(\beta_6)$  into Equation 6.6. The resulting expression is:

$$[6.26] \quad \gamma_o = \frac{0.0111384\beta_1^{0.547}\beta_2^{0.32}}{\beta_3^{0.939}\beta'_5^{0.80}}$$

Equation 6.26 could be simplified somewhat without impacting the accuracy of the results significantly by treating the modulus of elasticity as a constant, as is often done for structural steel. Moreover, both Equations 6.25 and 6.26 could be simplified by eliminating the factors that have a very small effect on the output curves within the prescribed ranges, such as  $\lambda_2(\beta_2)$ . Further simplification could be achieved by selecting linear functions that closely match some of the near-linear power functions selected, such as  $\lambda_1(\beta_1)$ . Nevertheless, Equations 6.25 and 6.26 are not onerous to evaluate and the following verification study is performed on these equations as presented.

#### 6.5.4.11 Verification of the Proposed Model for HSS Collars

The proposed empirical confinement model has been verified using 14 case studies. It is to be noted that for verification purposes, collared columns of 300x300 mm in cross-section have been used, whilst the equations of the proposed model were developed based on the results of collared columns of 400x400 mm in cross-section. Table 6.18 shows the details of all the finite element models used for this purpose. These are not intended to represent real columns, however, they were developed in such a way that their non-dimensional parameters are close to those of real columns (i.e., they have not been smeared, as is required for the empirical

equation). The results of these models in terms of confinement stress vs. lateral strain are depicted in Figures 6-27 through 6-40.

While using the proposed model to determine the confining behaviour of collars, it is possible to violate slightly the ranges used in the parametric study at the cost of accuracy of the predicted results. Through applying the proposed model to the 14 cases given in Table 6.18, it has been observed that the predicted results are more sensitive to the range of parameter  $\beta_1$  (0.00262 to 0.00527) than any other parameter. Therefore, while applying the proposed model, it is recommended that the parameter  $\beta_1$  remain within its prescribed range, while other parameters can violate their ranges slightly without affecting the accuracy of predicted results drastically. In order to keep the parameter  $\beta_1$  within its range, the real collars are smeared over the column at a relatively small spacing, although excessive smearing is not recommended. Only need-based smearing is recommended in order to bring the parameter  $\beta_1$  within its range. Table 6.19 shows the details of models, equivalent to those given in Table 6.18, obtained through need-based smearing of the collars. The proposed empirical model was applied to these cases to determine their respective confining behaviour in terms of confinement stress vs. lateral strain, also depicted in Figures 6-27 through 6-40 for comparison with the respective finite element results. The curves are shown up to lateral strain of 0.06, which is a very high level of lateral strain. The coefficient of multiple determination,  $R^2$ , was used to measure the accuracy of the predictions for each curve up to four levels of lateral strains, *i.e.*, 0.06, 0.05, 0.04, and 0.03. The corresponding values of  $R^2$  are given in Table 6.20 for each of the 14 cases. A study of the values of  $R^2$  shows that very good agreement exists between the finite element results and those of the proposed model. In order to demonstrate the procedures used in the verification exercise, the details of one of the cases (Case 8) is given below.

The finite element analyses for Case 8 were performed on a 300x300 mm column with steel HSS collars of 25.5x51 mm (web 3.175 mm and flange 6.35 mm thick) spaced at 61.00 mm on centres. These are hypothetical steel HSS sections without round corners and with varying wall thickness. The yield stress,  $f_y$ , and modulus of elasticity,  $E_s$ , of the confining steel are 470 MPa and 210 000 MPa, respectively. The values of the non-dimensional parameters for this model are (note that the prime symbol is included on  $\beta_3$  to signify the actual, rather than smeared, condition for consistency with Equation 6.24 that accounts for the smearing effect):

- $\beta_1 = 0.006306$
- $\beta_2 = 0.000285$

- $\beta'_3 = 0.203333$
- $\beta_4 = 0.170000$
- $\beta_5 = 0.002312$
- $\beta'_5 = 0.002214$
- $\beta_6 = 11.00000$

As the value of parameter  $\beta_1$  exceeds its specified range, in order to apply the proposed model the collars need to be smeared. (Although  $\beta_4$  also falls outside of its prescribed range, the method is much less sensitive to this parameter.) After smearing, the collar size becomes 12.75 x 51.00 mm (web 1.5875 mm and flange 6.35 mm thick) and the centre-to-centre spacing becomes 30.50 mm. The non-dimensional parameters of the equivalent model (Case 8 in Table 6.19) with smeared collars becomes:

- $\beta_1 = 0.0031500$
- $\beta_2 = 0.0001424$
- $\beta_3 = 0.1016600$
- $\beta_4 = 0.170000$
- $\beta_5 = 0.002312$
- $\beta'_5 = 0.002214$
- $\beta_6 = 11.00000$

Now the value of the non-dimensional parameter  $\beta_1$  falls within the range over which the parametric study was performed. Using Equation 6.24 that accounts for the smearing effect, the value of  $a_s$  is calculated to be:

- $a_s = 1.037$

Applying Equation 6.25, the value of  $(\beta_8)_{\max}$  can be calculated:

- $(\beta_8)_{\max} = 0.0001517$

Applying Equation 6.26, the value of  $\gamma_o$  is calculated:

- $\gamma_o = 0.03027$

Substituting the values of  $(\beta_8)_{\max}$  and  $\gamma_o$  into Equation 6.4, the relationship between  $\beta_7$  and  $\beta_8$  can be established. This curve is then converted to confinement stress,  $\sigma_{ct}$ , vs. lateral strain by multiplying the values of  $\beta_8$  by the constant  $E_{sref} = 203\,250$  MPa. It is to be noted that the parameter  $\beta_7$  represents the lateral strain of the collar directly. The relationships between confinement stress and lateral strain determined with both the finite element analysis and the empirical model using need-based smearing are shown in Figure 6.34. The curves can be compared with the help of the values of  $R^2$  in Table 6.20. The values of  $R^2$  for this curve up to lateral strains of 0.06, 0.05, 0.04, and 0.03 are 0.9971, 0.9968, 0.9965, 0.9961, respectively.

#### 6.5.4.12 Application of the Proposed Model to Real Cases

In this section, the proposed model is applied to columns C06 and C09 tested under concentric axial loading in phase 1 of the project (Chapter 3).

##### 6.5.4 12.1 Column C06

Column C06 is 300x300 mm in cross-section confined with collars of HSS 51x51x6.35 mm with welded corner connections, spaced at 122 mm on centres. The area of the cross-section of this HSS is 1085 mm<sup>2</sup> and the moment of inertia of the collar about its major axis is 0.319x10<sup>6</sup> mm<sup>2</sup>. The material curve for the HSS was obtained from a stub column test and is shown in Figure 6-41. The Ramberg-Osgood model was calibrated to this curve and the best fit was obtained at the following values of material parameters:

- $f_y = 497$  MPa
- $E_s = 203\,400$  MPa
- $a = 0.002$  MPa

- $n = 12.80 \text{ MPa}$

For establishing the confining behaviour of the collars of this column using finite element analysis, it is reasonable to approximate the actual condition by splitting each collar into two equivalent collars. This is necessary because the actual collars apply confining pressure across a 51 mm deep strip and in the model, pressure is applied along a line at the collar centreline. Hence, the collars of this column can be assumed to consist of HSS 25.5x51 mm (web 3.175 mm and flange 6.35 mm thick) spaced at 61 mm on centers, with cross-sectional area of  $542.5 \text{ mm}^2$  and moment of inertia of  $0.1595 \times 10^6 \text{ mm}^4$  taking into account the effect of round corners.

With this information, the non-dimensional parameters of this column were calculated to be:

- $\beta_1 = 0.0060277$
- $\beta_2 = 0.0002363$
- $\beta'_3 = 0.2033333$
- $\beta_4 = 0.170000$
- $\beta_5 = 0.002445$
- $\beta'_5 = 0.002286$
- $\beta_6 = 12.80000$

The value of parameter  $\beta_1$  exceeds the range (0.00262 to 0.00527) over which the parametric study was performed. In order to get the best results from the proposed model, it is required that the collars be smeared over the height of the column under consideration. For this purpose, each collar of the original column (i.e., with center-to-center spacing of collars of 122 mm) is divided into four smaller collars, resulting in the following values of the non-dimensional parameters:

- $\beta_1 = 0.0030139$
- $\beta_2 = 0.0001182$
- $\beta_3 = 0.1016667$
- $\beta_4 = 0.170000$
- $\beta_5 = 0.002445$

- $\beta'_5 = 0.002286$
- $\beta_6 = 12.80000$

Substituting the values of the non-dimensional parameters into Equations 6.25 and 6.26, and applying  $a_s$ , the following values of  $(\beta_8)_{\max}$  and  $\gamma_o$  are found:

- $(\beta_8)_{\max} = 0.00015145$
- $\gamma_o = 0.02861$

Using these values in Equation 6.4, the relationship between  $\beta_7$  and  $\beta_8$  can be obtained and transformed to a confinement stress vs. lateral strain curve, which is shown in Figure 6.42, by multiplying  $\beta_8$  by  $E_{sref}$ . This figure also shows the relationship between the confinement stress and lateral strain obtained directly from the finite element analysis. The coefficient of multiple determination was used to compare these two curves. The following values of  $R^2$  were found:

- $R^2 = 0.9726$  up to lateral strain of 0.06
- $R^2 = 0.9780$  up to lateral strain of 0.05
- $R^2 = 0.9828$  up to lateral strain of 0.04
- $R^2 = 0.9852$  up to lateral strain of 0.03.

These values of  $R^2$  show that the two curves compare well with each other. The confinement stress vs. lateral strain curve obtained by the proposed model was used to determine the confined concrete material curve for the core concrete according to the procedure given in Chapter 5. The behaviour of spalling concrete and the longitudinal reinforcing bars was modelled separately. Combining the contributions of core concrete, cover concrete, and the longitudinal reinforcing bars, the axial load vs. axial strain curve for the column was obtained and is shown in Figure 6-43. The experimentally obtained load vs. strain curve of the column is also given in this figure for comparison. Very good agreement exists between the two curves, validating the proposed model.

#### 6.5.4.12.2 Column C09

Column C09 is 300x300 mm in cross-section confined with collars of HSS 76x51x6.35 mm with welded corner connections, spaced at 170 mm on centres. The area of cross-section of this HSS

is  $1375 \text{ mm}^2$  and the moment of inertia of the collar about its major axis is  $0.919 \times 10^6 \text{ mm}^2$ . The material curve of the HSS for this column, obtained from the stub column test, is shown in Figure 6-44. The Ramberg-Osgood model was calibrated to this curve and the best fit was obtained at the following values of material parameters:

- $f_y = 445 \text{ MPa}$
- $E_s = 202\,700 \text{ MPa}$
- $a = 0.002 \text{ MPa}$
- $n = 20.00 \text{ MPa}$

For the confining behaviour of the collars of this column using finite element analysis, it is reasonable to split each collar of this column into two equivalent collars because the actual collars apply confining pressure on about a 51 mm width. Hence, the collars of this column can be assumed to consist of HSS 25.5x76 mm (web 3.175 mm and flange 6.35 mm thick) spaced at 85 mm on centres, with a cross-sectional area of  $687.50 \text{ mm}^2$  and moment of inertia of  $0.4595 \times 10^6 \text{ mm}^4$ .

With this information, the non-dimensional parameters for this column can be calculated as:

- $\beta_1 = 0.007639$
- $\beta_2 = 0.000681$
- $\beta'_3 = 0.283333$
- $\beta_4 = 0.253333$
- $\beta_5 = 0.002189$
- $\beta'_5 = 0.002294$
- $\beta_6 = 20.00000$

The value of parameter  $\beta_1$  exceeds the range (0.00262 to 0.00527) over which parametric study was performed, so the collars must be smeared. For this purpose, each collar of the original column (spacing equal to 170 mm) is divided into four smaller collars, resulting in the following values of the non-dimensional parameters:

- $\beta_1 = 0.0038195$
- $\beta_2 = 0.0003405$
- $\beta_3 = 0.1416666$
- $\beta_4 = 0.2533333$
- $\beta_5 = 0.002189$
- $\beta'_5 = 0.002294$
- $\beta_6 = 20.00$

Substituting the values of the non-dimensional parameters into Equations 6.25 and 6.26, and applying  $a_s$ , the following values of  $(\beta_8)_{\max}$  and  $\gamma_o$  are found:

- $(\beta_8)_{\max} = 0.0001203$
- $\gamma_o = 0.03336$

Using these values in Equation 6.4, the relationship between  $\beta_7$  and  $\beta_8$  can be obtained and then transformed to confinement stress vs. lateral strain, shown in Figure 6-45. This figure also shows the relationship between the confinement stress and lateral strain obtained directly from the finite element analysis. The coefficient of multiple determination was used to compare the two curves. The following values of  $R^2$  were found:

- $R^2 = 0.9800$  up to lateral strain of 0.06
- $R^2 = 0.9785$  up to lateral strain of 0.05
- $R^2 = 0.9762$  up to lateral strain of 0.04
- $R^2 = 0.9725$  up to lateral strain of 0.03.

The values of  $R^2$  shows that the two curves compare well. The confinement stress vs. lateral strain curve obtained by the proposed model was used to determine the confined concrete material curve for the core concrete according to the procedure given in Chapter 5. Adding the contributions of core concrete, cover concretes and the longitudinal reinforcing bars, the load vs. axial strain curve for the column was obtained, as shown in Figure 6-46. The experimentally obtained load vs. strain curve of the column is also given in this figure for comparison. Very good agreement exists between the two curves, again validating the proposed model.

## 6.6 Model for Solid Collars

In a manner similar to the procedure used for HSS (hollow) collars, a model for the confining behaviour of solid collars with rigid corner connections has been developed in terms of non-dimensional parameters. The derivation of the model is provided in the following sections.

### 6.6.1. Non-Dimensional Parameters for Solid Collars

Based on the experimental work and finite element studies, it is assumed that the confining behaviour of the solid collars for square concrete columns depends on the following nine primary variables:

- (1) area of cross-section of a side of a collar,  $A_{collar}$
- (2) moment of inertia of the side of the collar,  $I_{collar}$
- (3) width of the column (inside length of a collar side),  $h_{column}$
- (4) centre-to-centre spacing,  $s$  ;
- (5) yield stress of the confining steel,  $f_y$
- (6) modulus of elasticity of the confining steel,  $E_s$
- (7) value of  $n$  in the Ramberg-Osgood model
- (8) average lateral strain,  $\varepsilon_l$
- (9) average confinement stress,  $\sigma_{ct}$

It is to be noted that, the three ( $f_y$ ,  $E_s$ , and  $n$ ) of above nine variables are related to the material curve of the confining steel. In case of solid collars, the quantities  $A_{collar}$  and  $I_{collar}$  can be varied independently. Conversely, since only square concrete columns are being considered,  $h_{column}$ ,  $A_{column}$ , and  $I_{column}$  represent only a single independent quantity,  $h_{column}$ .

The dimensional matrix of seven primary variables (after taking out the two dimensionless parameters) in terms of fundamental units of mass,  $M$ , length,  $L$ , and time,  $T$ , can be written in the following form:

	$A_{collar}$	$I_{collar}$	$h_{column}$	$s$	$f_y$	$E_s$	$\sigma_{ct}$
M	0	0	0	0	1	1	1
L	2	4	1	1	-1	-1	-1
T	0	0	0	0	-2	-2	-2

The rank of this dimensional matrix is two; therefore, five non-dimensional parameters are required (in addition to the two dimensionless primary variables) to describe this physical behaviour, *i.e.*, the confining behaviour of solid collars. The following seven trial non-dimensional parameters were chosen:

- $\beta_1 = \frac{A_{collar}}{A_{column}}$
- $\beta_2 = \frac{I_{collar}}{I_{column}}$
- $\beta_3 = \frac{s}{h_{column}}$
- $\beta_5 = \frac{f_y}{E_s}$
- $\beta_6 = n$
- $\beta_7 = \varepsilon_l$
- $\beta_8 = \frac{\sigma_{ct}}{E_s}$

For consistency, the same nomenclature has been used for the parameters for solid collars as was used for hollow collars. It is to be noted that parameter  $\beta_4$  does not exist for solid collars. Again,  $\beta_7$  and  $\beta_8$  are output parameters and  $\beta_1$ ,  $\beta_2$ ,  $\beta_3$ ,  $\beta_5$ , and  $\beta_6$  are input parameters. The parameter  $\beta_5$  is the ratio of yield stress,  $f_y$ , to modulus of elasticity,  $E_s$ , of the confining

steel. As was done for hollow collars and for the same reasons, this parameter is split into two parameters:

- $\beta_5 = \frac{f_y}{E_{sref}}$
- $\beta'_5 = \frac{f_{yref}}{E_s}$

The definition of  $\beta_8$  is again revised to:

- $\beta_8 = \frac{\sigma_{ct}}{E_{sref}}$

### 6.6.2 Ranges of Parameters and Reference Model for Solid Collars

The geometry of the columns confined by solid collars is controlled by three parameters:  $\beta_1$ ;  $\beta_2$ ; and  $\beta_3$ . The ranges of these parameters used in the parametric study are:

- $\beta_1 = 0.004$  to  $0.056$
- $\beta_2 = 0.000096$  to  $0.0192$
- $\beta_3 = 0.020$  to  $0.30$

These ranges cover most practical cases. The reference model is an arbitrarily selected model whose parameters fall in the ranges over which the parametric studies were performed. Model 5 in Table 6.21 is the reference model for the parametric study of solid collars. The values of input parameters (including material and geometric parameters) for this model along with their ranges over which the parametric studies were performed are given below:

- $\beta_1 = 0.02083$  (Range:  $0.004$  to  $0.056$ )
- $\beta_2 = 0.001302$  (Range:  $0.000096$  to  $0.0192$ )
- $\beta_3 = 0.16667$  (Range:  $0.020$  to  $0.30$ )
- $\beta_5 = 0.002288$  (Range:  $0.001476$  to  $0.00344$ )
- $\beta'_5 = 0.002288$  (Range:  $0.00177$  to  $0.00266$ )

- $\beta_6 = 11.00$  (Range: 10.00 to 20.00)

These ranges are sufficiently wide to accommodate practical sizes of solid collars without requiring collar smearing. However, the effect of collar smearing on the confining behaviour of solid collars was also studied; if required, it can be used to predict the behaviour of relatively larger solid collars.

### 6.6.3 Scale Effect for Solid Collars

In order to verify that the non-dimensional parameters are independent of any scale effect, eleven analyses were performed, the details of which are given in Table 6.21. The values of input parameters for all the models in this table are:

- $\beta_1 = 0.0208333$
- $\beta_2 = 0.001302$
- $\beta_3 = 0.16667$
- $\beta_5 = 0.002288$
- $\beta'_5 = 0.002288$
- $\beta_6 = 11.00$

The relationships between  $\beta_7$  and  $\beta_8$  for the analyses of these models are depicted in Figure 6-47. The curves generated by the different models coincide exactly, confirming that the parameters are independent of scale effect.

### 6.6.4 Parametric Study and Prediction Equation for Solid Collars

In order to capture trends in the confining behaviour of solid collars, Equation 6.4 is again used. From the finite element study it was deduced that the variables  $(\beta_8)_{\max}$  and  $\gamma_o$  in this equation depend on the non-dimensional parameters  $\beta_1$ ,  $\beta_2$ ,  $\beta_3$ ,  $\beta_5$ ,  $\beta'_5$ , and  $\beta_6$ . Hence, the following relationships are hypothesised for  $(\beta_8)_{\max}$  and  $\gamma_o$ :

[6.27]

$$(\beta_8)_{\max}(\beta_1, \beta_2, \beta_3, \beta_5, \beta'_5, \beta_6) = \lambda_1(\beta_1) \times \lambda_2(\beta_2) \times \lambda_3(\beta_3) \times \lambda_5(\beta_5) \times \lambda'_5(\beta'_5) \times \lambda_6(\beta_6)$$

$$[6.28] \gamma_o(\beta_1, \beta_2, \beta_3, \beta_5, \beta'_5, \beta_6) = \gamma_1(\beta_1) \times \gamma_2(\beta_2) \times \gamma_3(\beta_3) \times \gamma_5(\beta_5) \times \gamma'_5(\beta'_5) \times \gamma_6(\beta_6)$$

The functions  $\lambda_1(\beta_1)$ ,  $\lambda_2(\beta_2)$ ,  $\lambda_3(\beta_3)$ ,  $\lambda_5(\beta_5)$ ,  $\lambda'_5(\beta'_5)$ ,  $\lambda_6(\beta_6)$ ,  $\gamma_1(\beta_1)$ ,  $\gamma_2(\beta_2)$ ,  $\gamma_3(\beta_3)$ ,  $\gamma_5(\beta_5)$ ,  $\gamma'_5(\beta'_5)$ , and  $\gamma_6(\beta_6)$  are determined by performing regression analyses on the data generated through parametric study using finite element models, the details of which is given in the following sections.

#### 6.6.4.1 Effect of Parameter $\beta_1$ on the Confining Behaviour of Solid Collars

Table 6.22 shows the details of the 15 models used to study the effect of variation of  $\beta_1$  on the confining behaviour. Model 6 in this table is the reference model. Figure 6-48 shows the relationship between  $\beta_7$  and  $\beta_8$  for all the analyses for  $\beta_1$  varying from 0.004 to 0.056. The values of other parameters were set at the following values, which are same as those for the reference model:

- $\beta_2 = 0.001302$
- $\beta_3 = 0.166666$
- $\beta_5 = 0.002288$
- $\beta'_5 = 0.002288$
- $\beta_6 = 11.00$

The quantities  $\gamma_o$  and  $(\beta_8)_{\max}$  shown in Table 6.22 are equivalent to  $\lambda_1$  and  $\gamma_1$ , respectively (without modification because the normalizing factor is 1.00). By inspection, curve fitting to case 4 appeared to be the least precise as compared to the other 14 cases. The following values of  $R^2$  (coefficient of multiple determination) were calculated for this case up to different levels of lateral strains in order to quantify the level of curve fitting:

- $R^2 = 0.9935$  up to a lateral strain of 0.06
- $R^2 = 0.9936$  up to a lateral strain of 0.05
- $R^2 = 0.9947$  up to a lateral strain of 0.04
- $R^2 = 0.9938$  up to a lateral strain of 0.03

These values of  $R^2$  indicate very good curve fitting even for the worst case. (In all the subsequent cases, a similar quality of curve fitting was maintained.) Figures 6-49(a) and 6-49(b) show the relationships between  $\lambda_1$  and  $\beta_1$  for two  $\beta_1$  ranges: (a) 0.004 to 0.024; and (b) 0.024 to 0.056; respectively. Several trials were made to get a single expression for the complete range of  $\beta_1$  (0.004 to 0.056), but a satisfactory function could not be obtained. Therefore, it was decided to split the  $\beta_1$  range into two parts and for each range, separate functions were obtained through curve fitting:

$$[6.29] \quad \lambda_1(\beta_1) = 0.00769\beta_1^{0.731} \text{ for } \beta_1 = 0.004 \text{ to } 0.024$$

$$[6.30] \quad \lambda_1(\beta_1) = 0.0049\beta_1^{0.619} \text{ for } \beta_1 = 0.024 \text{ to } 0.056$$

Figures 6-50(a) and 6-50(b) show the relationships between  $\gamma_1$  and  $\beta_1$  for the same two ranges that lead to the following functions:

$$[6.31] \quad \gamma_1(\beta_1) = 1.45\beta_1^{0.642} \text{ for } \beta_1 = 0.004 \text{ to } 0.024$$

$$[6.32] \quad \gamma_1(\beta_1) = 0.5301\beta_1^{0.368} \text{ for } \beta_1 = 0.024 \text{ to } 0.056$$

#### 6.6.4.2 Effect of Parameter $\beta_2$ on the Confining Behaviour of Solid Collars

Table 6.23 shows the details of models to study the effect of variation of  $\beta_2$  on the confining behaviour. Model 6 in this table is the reference model. The collar dimensions are modified in such a way that only  $\beta_2$  varies from 0.000096 to 0.0192 and the other input parameters ( $\beta_1$ ,  $\beta_3$ ,  $\beta_5$ ,  $\beta'_5$  and  $\beta_6$ ) remain constant at the following values, which are same as those for the reference model:

:

- $\beta_1 = 0.020833$
- $\beta_3 = 0.16667$
- $\beta'_5 = 0.002288$
- $\beta_5 = 0.002288$
- $\beta_6 = 11.00$

The resulting output curves between  $\beta_7$  and  $\beta_8$  are shown in Figure 6-51 up to  $\beta_7 = 0.05$ . It is clear from these curves that the variation of  $\beta_2$  affects both the first part (initial slope) and the second part (so-called peaks) of the curves. Equation 6.4 was fit to these curves up to a strain of 0.03 and the respective values of  $\gamma_o$  and  $(\beta_8)_{\max}$  are given in Table 6.23. The same quality of fitness was maintained as was in the previous section. The values of  $\gamma_o$  and  $(\beta_8)_{\max}$  for all the models were normalized with respect to the respective values of  $\gamma_o$  and  $(\beta_8)_{\max}$  of the reference model. These normalized values of  $\gamma_o$  and  $(\beta_8)_{\max}$  are denoted by  $\lambda_2$  and  $\gamma_2$ , respectively, and are given in Table 6.24. The values of  $\lambda_2$  were plotted with respect to  $\beta_2$  and several trials were made to get a single expression through regression, which gives best fit to the complete range of  $\beta_2$  (0.000096 to 0.0192) but a satisfactory function could not be obtained. Therefore, it was decided to split the  $\beta_2$  range into two parts and for each part a separate expression of  $\lambda_2(\beta_2)$  was obtained. Figures 6-52(a) and 6-52(b) show the plot of  $\lambda_2$  with respect to  $\beta_2$  for  $\beta_2$  ranges: (a) 0.000096 to 0.00288; and (b) 0.00288 to 0.0192; respectively. A power series function was fit to the data points in each of these ranges and the following expressions for  $\lambda_2(\beta_2)$  were obtained:

$$[6.33] \quad \lambda_2(\beta_2) = 3.434\beta_2^{0.1855} \text{ for } \beta_2 = 0.000096 \text{ to } 0.00288$$

$$[6.34] \quad \lambda_2(\beta_2) = 2.7429\beta_2^{0.1433} \text{ for } \beta_2 = 0.00288 \text{ to } 0.0192$$

Similarly, Figures 6-53(a) and 6-53(b) show the plots of  $\gamma_2$  with respect to  $\beta_2$  for  $\beta_2$  the same ranges. Power series functions were fit to the data points in these ranges and the following expressions for  $\gamma_2(\beta_2)$  were obtained:

$$[6.35] \quad \gamma_2(\beta_2) = 12.7145\beta_2^{0.385} \text{ for } \beta_2 = 0.000096 \text{ to } 0.00288$$

$$[6.36] \quad \gamma_2(\beta_2) = 4.3655\beta_2^{0.2003} \text{ for } \beta_2 = 0.00288 \text{ to } 0.0192$$

#### 6.6.4.3 Effect of Parameter $\beta_3$ on the Confining Behaviour of Solid Collars

Table 6.25 shows the details of the finite element models to study the effect of variation of  $\beta_3$  on the confining behaviour. Model 9 in this table is the reference model. The collar spacing was varied to get a variation in  $\beta_3$  (from 0.020 to 0.30), while keeping the other input parameters ( $\beta_1$ ,  $\beta_2$ ,  $\beta_5$ ,  $\beta'_5$  and  $\beta_6$ ) at the following constant values, which are same as those for the reference model:

- $\beta_1 = 0.020833$
- $\beta_2 = 0.001302$
- $\beta_5 = 0.002288$
- $\beta'_5 = 0.002288$
- $\beta_6 = 11.00$

The curves relating  $\beta_7$  and  $\beta_8$  for all the models in this table were plotted. However, only a few of these curves are depicted in Figure 6-54 for clarity. A study of these curves shows that the change in  $\beta_3$  has a large effect on both  $\gamma_o$  and  $(\beta_8)_{\max}$ . Equation 6.4 was fit to all the curves, and the respective values of  $\gamma_o$  and  $(\beta_8)_{\max}$  are reported in Table 6.25. The values of  $\gamma_o$  and  $(\beta_8)_{\max}$  thus obtained were normalized with respect to the respective values of  $\gamma_o$  and  $(\beta_8)_{\max}$  of model 9 (reference model) and the resulting normalized values of  $\gamma_o$  and  $(\beta_8)_{\max}$ , denoted by  $\lambda_3$  and  $\gamma_3$  respectively, are also given in Table 6.26. Figure 6-55(a) show a plot of  $\lambda_3$  with respect to  $\beta_3$ . A power series function was fit to this curve and the following expression for  $\lambda_3(\beta_3)$  was obtained:

$$[6.37] \quad \lambda_3(\beta_3) = 0.209\beta_3^{-0.886} \text{ for } \beta_3 = 0.02 \text{ to } 0.30$$

Similarly, Figure 6-55(b) shows the plot of  $\gamma_3$  with respect to  $\beta_3$ . A power series function was fit to this curve and the following expression for  $\gamma_3(\beta_3)$  was obtained:

$$[6.38] \quad \gamma_3(\beta_3) = 0.178\beta_3^{-0.967} \text{ for } \beta_3 = 0.02 \text{ to } 0.30$$

#### 6.6.4.4 Effect of Parameter $\beta_5$ on the Confining Behaviour of Solid Collars

Table 6.27 shows the details of the finite element models to study the effect of variation of  $\beta_5$  (Range: 0.001476 to 0.00344) (due to varying  $f_y$ ) on the confining behaviour of solid collars while keeping the other input parameters at the following constant values, which are same as those for the reference model:

- $\beta_1 = 0.020833$
- $\beta_2 = 0.001302$
- $\beta_3 = 0.166667$
- $\beta'_5 = 0.002288$

Based on the analyses of these models, the curves relating parameters  $\beta_7$  and  $\beta_8$  are shown in Figure 6-56. A study of these curves shows that the initial parts of these curves overlap each other but the second parts are affected by the change of  $f_y$ . Equation 6-4 was fit to all these curves and the resulting values of  $\gamma_o$  and  $(\beta_8)_{\max}$  are given in Table 6.28. These values of  $\gamma_o$  and  $(\beta_8)_{\max}$  were then normalized with respect to the values of  $\gamma_o$  and  $(\beta_8)_{\max}$  of the reference model. The normalized values of  $\gamma_o$  and  $(\beta_8)_{\max}$ , denoted by  $\gamma_5$  and  $\lambda_5$  respectively, are also given in Table 6.28.

The values of  $\lambda_5$  are plotted with respect to  $\beta_5$  and the resulting curve is shown in Figure 6-57. A linear function was fit to this curve by setting the y-intercept equal to zero, resulting in the following expression for  $\lambda_5(\beta_5)$ :

$$[6.39] \quad \lambda_5(\beta_5) = 435\beta_5 \text{ for } \beta_5 = 0.001476 \text{ to } 0.003444$$

The values of  $\gamma_o$  remain essentially unaffected by changing  $\beta_5$ ; therefore, the values of  $\gamma_5$  become 1.00 for all these curves, resulting in the following expression for  $\gamma_5(\beta_5)$ :

$$[6.40] \gamma_5(\beta_5) = 1.00$$

#### 6.6.4.5 Effect of Parameter $\beta_5'$ on the Confining Behaviour of Solid Collars

Table 6.29 summaries the details of the models used to study the effect of variation of  $E_s$  (i.e., variation in  $\beta_5'$ ) on the confining behaviour of collars. Model 3 in this table is the reference model. The parameter  $\beta_5'$  was varied from 0.00177 to 0.00266, keeping the other input parameters ( $\beta_1$ ,  $\beta_2$ ,  $\beta_3$ ,  $\beta_5$ , and  $\beta_6$ ) at the following constant values, which are same as those for the reference model:

- $\beta_1 = 0.020833$
- $\beta_2 = 0.001302$
- $\beta_3 = 0.166666$
- $\beta_5 = 0.002288$
- $\beta_6 = 11.00$

Figure 6-58 shows the relationship between  $\beta_7$  and  $\beta_8$  for different values of  $\beta_5'$ . A study of these curves shows that the variation in  $E_s$  affects essentially the initial slope,  $\gamma_o$ , of these curves, without affecting the second parts of the curves. Equation 6-4 was fit to these curves and the resulting values of  $(\beta_8)_{\max}$  and  $\gamma_o$  are listed in Table 6.30. These values of  $(\beta_8)_{\max}$  and  $\gamma_o$  were normalized with respect to the values of  $(\beta_8)_{\max}$  and  $\gamma_o$ , respectively, of the reference model (model 3). The normalized values of  $(\beta_8)_{\max}$  and  $\gamma_o$ , denoted by  $\lambda_5'$  and  $\gamma_5'$  respectively, are also listed in this table. As the so-called peaks of these curves are not affected significantly by a change in  $\beta_5'$ , the values of  $\lambda_5'$  for all these curves can be set to 1.00, resulting in the following expression for  $\lambda_5'(\beta_5)$ :

$$[6.41] \quad \lambda'_5(\beta'_5) = 1.0$$

The values of  $\gamma'_5$  are plotted with respect to  $\beta'_5$  in Figure 6-59. A power series function was fit to this curve and the following expression was obtained for  $\gamma'_5(\beta'_5)$ :

$$[6.42] \quad \gamma'_5(\beta'_5) = 0.0077 \beta'^{-0.80}_5 \text{ for } \beta'_5 = 0.00177 \text{ to } 0.00266$$

#### 6.6.4.6 Effect of Parameter $\beta_6$ on the Confining Behaviour of Solid Collars

Table 6.31 gives the details of the finite element models used to study the effect of a change in the value of  $n$  from the function representing the material curve on the confining behaviour of collars.. Model 2 in this table is the reference. In these models, the value of  $\beta_6$  is varied from 10 to 20 and the other parameters are set at the following at the following constant values, which are same as those for the reference model:

- $\beta_1 = 0.020833$
- $\beta_2 = 0.001302$
- $\beta_3 = 0.166667$
- $\beta_5 = 0.002288$
- $\beta'_5 = 0.002288$

Figure 6-60 shows the relationship between  $\beta_7$  and  $\beta_8$  for different values of  $\beta_6$ . The variation of  $\beta_6$  affects essentially the second parts of the curves, without affecting the initial slope,  $\gamma_o$ , of the curve. Equation 6-4 was fit to all these curves and the resulting values of  $\gamma_o$  and  $(\beta_8)_{\max}$  are given in Table 6-32. These values of  $\gamma_o$  and  $(\beta_8)_{\max}$  were normalized with respect to the values of  $\gamma_o$  and  $(\beta_8)_{\max}$  of the reference model. The normalized values of  $\gamma_o$  and  $(\beta_8)_{\max}$ , denoted by  $\gamma_6$  and  $\lambda_6$  respectively, are also given in Table 6-32. Figure 6-61 shows the plot of  $\lambda_6$  versus  $\beta_6$ . A power series function was fit to this curve with the help of regression, resulting in the following expression for  $\lambda_6(\beta_6)$ :

$$[6.43] \quad \lambda_6(\beta_6) = 1.50\beta_6^{-0.17} \text{ for } \beta_6 = 10.00 \text{ to } 20.00$$

The values of  $\gamma_6$  are constant with respect to  $\beta_6$  which leads to the following expression for  $\gamma_6(\beta_6)$ :

$$[6.44] \quad \gamma_6(\beta_6) = 1.00$$

#### 6.6.4.7 Effect of Collar Smearing on the Confining Behaviour of Solid Collars

Table 6-33 shows the details of finite element models used to study the effect of collar smearing on the confining behaviour. Model 4 in this table is the reference model. All of these models are equivalent and should give the same relationship between output parameters  $\beta_7$  and  $\beta_8$ . But in the present study, a slight reduction in confining pressure has been observed due to collars smearing. The models in Table 6-33 show a variation in  $\beta_3$  from 0.0208 to 0.250, accompanied by concomitant variations in parameter  $\beta_1$  from  $2.5417 \times 10^{-3}$  to  $3.125 \times 10^{-2}$  and parameter  $\beta_2$  from  $1.5885 \times 10^{-4}$  to  $1.9531 \times 10^{-3}$  such that the models remain equivalent. The other input parameters of these models were kept at the following constant values, which are same as those for the reference model:

- $\beta_5 = 0.002288$
- $\beta'_5 = 0.002288$
- $\beta_6 = 11.00$

The relationships between  $\beta_7$  and  $\beta_8$  for all these models are given in Figure 6-62. Collar smearing only affects the so-called peak values of these curves, without affecting their initial slopes significantly. The effect of smearing can be related to any one of the three input parameters such as  $\beta_1$ ,  $\beta_2$ , and  $\beta_3$  because of equivalency in their variations. In the present study, the effect of smearing on the output behavioural curves of the collars is related to  $\beta_3$ . Equation 6.4 was fit to these curves and the corresponding values of  $\gamma_o$  and  $(\beta_8)_{\max}$  are given in Table 6.34. These values of  $\gamma_o$  and  $(\beta_8)_{\max}$  are normalized with respect to the respective to values of  $\gamma_o$  and  $(\beta_8)_{\max}$  of reference model (model 4). The normalized values of  $(\beta_8)_{\max}$  and

$\gamma_o$ , denoted by  $\lambda_s$  and  $\gamma_s$ , have also been given in Table 6.34. The values of  $\lambda_s$  are plotted with respect to  $\beta_3$  and the resulting curve is shown in Figure 6-63. A power series function was fit to this curve, resulting in the following expression for  $\lambda_s(\beta_3)$ :

$$[6.45] \quad \lambda_s(\beta_3) = 1.097\beta_3^{0.0525} \text{ for } \beta_3 = 0.020833 \text{ to } 0.25$$

Table 6.34 shows that the values of  $\gamma_s$  for all the models are 1.00, which leads to the following relation for  $\gamma_s(\beta_3)$ :

$$[6.46] \quad \gamma_s(\beta_3) = 1.00$$

The correction for smearing can be applied to the so-called peak values of the behavioural curves of the collars. If the  $\beta_3$  parameters for the actual and smeared models are denoted by  $\beta'_3$  and  $\beta_3$ , respectively, a factor  $a_s$  is defined to account for the effect of smearing on the peak value of the confining behaviour (using Equation 6.45):

$$[6.47] \quad a_s = \left(\frac{\beta'_3}{\beta_3}\right)^{0.0525}$$

The value of this factor will be greater than 1 if the spacing of the collars in the actual column is bigger than that of the smeared model, or vice versa. This factor may not be used very often for solid collars, because the prediction equations for solid collars were developed over a range that covers almost all the practically occurring solid collars.

#### 6.6.4.8 Expressions for $(\beta_8)_{\max}$ and $\gamma_o$ for Solid Collars

The expression for  $(\beta_8)_{\max}$  can be obtained by substituting the values of  $\lambda_1(\beta_1)$ ,  $\lambda_2(\beta_2)$ ,  $\lambda_3(\beta_3)$ ,  $\lambda_5(\beta_5)$ ,  $\lambda'_5(\beta'_5)$ , and  $\lambda_6(\beta_6)$  into Equation 6-27, and adding the smearing correction factor,  $a_s$ . As discussed previously, the ranges of  $\beta_1$  and  $\beta_2$  were so wide that single and satisfactory expressions could not be obtained for these ranges. Therefore, both of these ranges were split into smaller ranges and separate functions were fit to the curves over each short

range. Hence, four expressions for  $(\beta_8)_{\max}$  are required to cover the full ranges of  $\beta_1$  and  $\beta_2$ .

The resulting expressions are given below:

For  $\beta_1 = 0.004$  to  $0.024$  and  $\beta_2 = 0.000096$  to  $0.00288$

$$[6.48a] \quad (\beta_8)_{\max} = \frac{3.60125 \beta_1^{0.731} \beta_2^{0.1855} \beta_5 a_s}{\beta_3^{0.886} \beta_6^{0.17}}$$

For  $\beta_1 = 0.024$  to  $0.056$  and  $\beta_2 = 0.00288$  to  $0.0192$

$$[6.48b] \quad (\beta_8)_{\max} = \frac{1.8329 \beta_1^{0.619} \beta_2^{0.1433} \beta_5 a_s}{\beta_3^{0.886} \beta_6^{0.17}}$$

For  $\beta_1 = 0.004$  to  $0.024$  and  $\beta_2 = 0.00288$  to  $0.0192$

$$[6.48c] \quad (\beta_8)_{\max} = \frac{2.8765 \beta_1^{0.731} \beta_2^{0.1433} \beta_5 a_s}{\beta_3^{0.886} \beta_6^{0.17}}$$

For  $\beta_1 = 0.024$  to  $0.056$  and  $\beta_2 = 0.000096$  to  $0.00288$

$$[6.48d] \quad (\beta_8)_{\max} = \frac{2.2947 \beta_1^{0.619} \beta_2^{0.1855} \beta_5 a_s}{\beta_3^{0.886} \beta_6^{0.17}}$$

Similarly, the expression for  $\gamma_o$  can be obtained by substituting the expressions for  $\gamma_1(\beta_1)$ ,  $\gamma_2(\beta_2)$ ,  $\gamma_3(\beta_3)$ ,  $\gamma_5(\beta_5)$ ,  $\gamma'_5(\beta'_5)$ , and  $\gamma_6(\beta_6)$  into Equation 6.28. The ranges of  $\beta_1$  and  $\beta_2$  were split into two short ranges and the following four expressions are obtained to predict the values of  $\gamma_o$ :

For  $\beta_1 = 0.004$  to  $0.024$  and  $\beta_2 = 0.000096$  to  $0.00288$

$$[6.49a] \quad \gamma_o = \frac{0.025268 \beta_1^{0.642} \beta_2^{0.385}}{\beta_3^{0.967} \beta'_5^{0.80}}$$

For  $\beta_1 = 0.024$  to  $0.056$  and  $\beta_2 = 0.00288$  to  $0.0192$

$$[6.49b] \quad \gamma_o = \frac{0.003172\beta_1^{0.368}\beta_2^{0.20}}{\beta_3^{0.967}\beta_5^{0.80}}$$

For  $\beta_1 = 0.004$  to  $0.024$  and  $\beta_2 = 0.00288$  to  $0.0192$

$$[6.49c] \quad \gamma_o = \frac{0.008675\beta_1^{0.642}\beta_2^{0.20}}{\beta_3^{0.967}\beta_5^{0.80}}$$

For  $\beta_1 = 0.024$  to  $0.056$  and  $\beta_2 = 0.000096$  to  $0.00288$

$$[6.49d] \quad \gamma_o = \frac{0.009238\beta_1^{0.368}\beta_2^{0.385}}{\beta_3^{0.967}\beta_5^{0.80}}$$

As discussed for hollow collars, simplifications of Equations 6.48 and 6.49 are possible. However, these equations are not difficult to evaluate and the verification study presented in the next section utilizes these equations as presented.

#### 6.6.4.9 Verification of the Proposed Model for Solid Collars

In this section, the proposed empirical confinement model is verified with the help of 10 case studies. For verification purposes, columns with various cross-sectional dimensions have been used, whilst the equations of the proposed model were developed based on the results of collared columns of 500x500 mm in cross-section. Table 6.35 shows the details of all the finite element models used for this purpose. The results of these models in terms of confinement stress vs. lateral strain, as well as the associated curves using the proposed model, are depicted in Figures 6-64 through 6-73. The corresponding values of  $R^2$  are given in Table 6.36, showing that very good agreement exists between the finite element results and those of the proposed model. The details of one of the case studies (Case 5) is given below.

The column in Case 5 is 400x400 mm in cross-section and confined by solid steel collars of 50 mm width (parallel to column axis) and 85 mm depth, spaced at 100 mm on centres. The yield

stress,  $f_y$ , and modulus of elasticity,  $E_s$ , of the confining steel are 520 MPa and 202 000 MPa, respectively. The values of non-dimensional parameters for this model are calculated to be:

- $\beta_1 = 0.0265625$
- $\beta_2 = 0.0011995$
- $\beta_3 = 0.250$
- $\beta_5 = 0.0025584$
- $\beta'_5 = 0.0023019$
- $\beta_6 = 12.00000$

Equation 6.48(d) was used to calculate the value of  $(\beta_8)_{\max}$  and Equation 6.49(d) was used to calculate the value of  $\gamma_o$ :

- $(\beta_8)_{\max} = 0.0003994$
- $\gamma_o = 0.08981$

These values of  $(\beta_8)_{\max}$  and  $\gamma_o$  can be substituted in Equation 6.4 to determine the relationship between  $\beta_8$  and  $\beta_7$ , which can be converted to confinement stress vs. lateral strain by multiplying the values of  $\beta_8$  by  $E_{sref}$ , where  $E_{sref} = 203\,250$  MPa.

The resulting curve is shown in Figure 6-68, along with the curve generated directly using finite element analysis. These curves are compared using the coefficient of multiple determination,  $R^2$ , given in Table 6.36. The values of  $R^2$  for this curve up to lateral strains of 0.06, 0.05, 0.04, and 0.03 are 0.9960; 0.9974; 0.9975; and 0.9970; respectively. From these values of  $R^2$ , one can conclude that the two curves show very good agreement, validating the proposed model for the confining behaviour of solid collars.

## 6.7 Comparison of Equations for HSS and Solid Collars

It is of interest to compare the equations for predicting the behaviour of HSS and solid collars. As one might expect, the equations related to the geometry of the collared columns are different for

HSS and solid collars. However, the equations for the behaviour of both HSS and solid collars based on the material properties of the confining steel are the same. For example, Equation 6.16 is the same as Equation 6.39; Equation 6.19 is the same as Equation 6.42; and Equation 6.20 is the same as Equation 6.43. Moreover, the remaining equations based on material properties (Equations 6.17, 6.18, 6.21, 6.40, 6.41, and 6.44) show no dependence on the respective non-dimensional parameters.

To explain the apparent lack of dependence on the cross-sectional shape of the various material-based parameters for predicting the confining pressure vs. lateral strain behaviour of the collars, it is helpful to consider each case separately. Consider the case of varying  $E_s$  only. The initial slope of the confining pressure vs. lateral strain curve is dependent only on the elastic collar stiffness. Furthermore, both the axial and flexural stiffnesses of the collars are linearly related to  $E_s$  (i.e., proportional to  $E_s A$  or  $E_s I$ , respectively). Therefore, increasing  $E_s$  by a specific amount will increase the initial slope of the confining pressure vs. lateral strain curve by an amount that does not depend on the shape of the cross-section. As a result, the expression for  $\gamma'_s(\beta'_s)$  does not depend on cross-sectional shape.

It is interesting to note also that an increase in  $E_s$  does not result in an equal increase (proportionally) in the initial slope of the confining pressure vs. lateral strain curve because only the average values are used in establishing this curve. This phenomenon occurs because the stress distribution on the collar sides actually depends on the flexural stiffness of the collars themselves, which is clearly affected by a change in  $E_s$ . Consequently, the deflected shapes of two collars with different flexural stiffnesses are different at the same average lateral strain, which affects the resulting average pressure. However, this effect is relatively small since the axial stresses are dominant in the initial part of the curve.

Consider now the case of varying  $f_y$  only. In assessing the effect on the "peak" of the confining pressure vs. lateral strain curve, it can be assumed that yielding in the collar is extensive under a combination of axial force and bending moment. The confining pressure arises due to the axial force, developed in the collar through "membrane" action, and the bending moment, developed through "bulging" between the column corners. The near-fully plastic stress distribution at the peak can be resolved into an axial force and bending moment combination. Neglecting the small elastic zone, by increasing the yield stress the axial force and bending moments both increase by the same amount (proportionally), regardless of the cross-sectional shape. Therefore, the

expression for  $\lambda_5(\beta_5)$  does not depend on cross-sectional shape. Similar arguments can be made for the case of the material parameter  $n$ .

## 6.8 Summary and Conclusions

A confinement model for use with concrete columns confined with collars having significant flexural stiffness has been proposed in Chapter 5. The proposed model requires as input the confining pressure vs. lateral strain curve, which is primarily a function of the behaviour of the collar alone. One method of obtaining these curves is to conduct finite element analyses of detailed models. However, to eliminate the need for finite element modelling, empirical models have been developed in terms of non-dimensional parameters for predicting the confining behaviour of collars fabricated from steel hollow structural sections (HSS) and solid steel sections for square concrete columns. In both cases, the corner connections of the collars are assumed rigid.

In order to eliminate the scale effect, non-dimensional parameters for the confining behaviour of HSS collars and solid collars were identified and validated. Then, a comprehensive parametric study was performed in terms of these parameters using finite element models. Based on the analytical results, non-dimensional empirical equations were developed through nonlinear regression for predicting the confining behaviour of collars in terms of the non-dimensional parameters.

The proposed empirical models for the confining behaviour of HSS and solid collars were verified with the help of several case studies, including physical tests conducted as part of this research program. The results predicted by the proposed empirical models were found to correlate very well with the finite element and test results. Therefore, the empirical models represent a viable alternate to the more onerous finite element analyses for predicting confining pressure vs. lateral strain curves.

Table 6.1: Detail of finite element models to study the effect of scale on the confining behaviour of HSS collars

Group	No.	$h_{column}$ (mm)	$A_{column}$ (mm <sup>2</sup> )	$I_{column}$ (mm <sup>4</sup> )	$A_{collar}$ (mm <sup>2</sup> )	$I_{collar}$ (mm <sup>4</sup> )	$h_{collar}$ (mm)	$s$ (mm)	$f_y$ (MPa)	$E_s$ (MPa)
1	1	300	90 000	0.675x10 <sup>9</sup>	0.3285x10 <sup>3</sup>	0.2453x10 <sup>6</sup>	75	22.5	465	203 250
	2	400	160 000	2.133x10 <sup>9</sup>	0.5840x10 <sup>3</sup>	0.7752x10 <sup>6</sup>	100	30.0	465	203 250
	3	500	250 000	5.208x10 <sup>9</sup>	0.9125x10 <sup>3</sup>	1.8930x10 <sup>6</sup>	125	37.5	465	203 250
	4	600	360 000	10.80x10 <sup>9</sup>	1.314x10 <sup>3</sup>	3.9240x10 <sup>6</sup>	150	45.0	465	203 250
	5	700	490 000	20.00x10 <sup>9</sup>	1.789x10 <sup>3</sup>	7.2700x10 <sup>6</sup>	175	52.5	465	203 250
	6	800	640 000	34.13x10 <sup>9</sup>	2.336x10 <sup>3</sup>	12.400x10 <sup>6</sup>	200	60.0	465	203 250
2	1	300	90 000	0.675x10 <sup>9</sup>	0.7181x10 <sup>3</sup>	0.5059x10 <sup>6</sup>	75	60.0	465	203 250
	2	400	160 000	2.133x10 <sup>9</sup>	1.276x10 <sup>3</sup>	1.5990x10 <sup>6</sup>	100	80.0	465	203 250
	3	500	250 000	5.208x10 <sup>9</sup>	1.994x10 <sup>3</sup>	3.9040x10 <sup>6</sup>	125	100.0	465	203 250
	4	600	360 000	10.80x10 <sup>9</sup>	2.872x10 <sup>3</sup>	8.0950x10 <sup>6</sup>	150	120.0	465	203 250

Table 6.2: Detail of finite element models to study the effect of variation of  $\beta_1$  on the confining behaviour of HSS collars

No.	$h_{column}$ (mm)	$A_{column}$ (mm <sup>2</sup> )	$I_{column}$ (mm <sup>4</sup> )	$A_{collar}$ (mm <sup>2</sup> )	$I_{collar}$ (mm <sup>4</sup> )	$h_{collar}$ (mm)	$s$ (mm)	$\beta_1$	$\gamma_0$	$(\beta_8)_{max}$
1	400	160 000	2.133x10 <sup>9</sup>	419.1	775.2	100	30	2.6196x10 <sup>-3</sup>	0.0465	0.0001605
2	400	160 000	2.133x10 <sup>9</sup>	456.9	775.2	100	30	2.8557x10 <sup>-3</sup>	0.0500	0.0001719
3	400	160 000	2.133x10 <sup>9</sup>	488.5	775.2	100	30	3.0532x10 <sup>-3</sup>	0.0530	0.0001809
4	400	160 000	2.133x10 <sup>9</sup>	520.2	775.2	100	30	3.2515x10 <sup>-3</sup>	0.0550	0.0001907
5	400	160 000	2.133x10 <sup>9</sup>	552.0	775.2	100	30	3.4504x10 <sup>-3</sup>	0.0571	0.0001999
6	400	160 000	2.133x10 <sup>9</sup>	584.0	775.2	100	30	3.6500x10 <sup>-3</sup>	0.0587	0.0002105
7	400	160 000	2.133x10 <sup>9</sup>	616.1	775.2	100	30	3.8504x10 <sup>-3</sup>	0.0601	0.0002220
8	400	160 000	2.133x10 <sup>9</sup>	648.2	775.2	100	30	4.0515x10 <sup>-3</sup>	0.0615	0.0002330
9	400	160 000	2.133x10 <sup>9</sup>	680.5	775.2	100	30	4.2534x10 <sup>-3</sup>	0.0630	0.0002440
10	400	160 000	2.133x10 <sup>9</sup>	778.1	775.2	100	30	4.8634x10 <sup>-3</sup>	0.0665	0.0002700
11	400	160 000	2.133x10 <sup>9</sup>	843.8	775.2	100	30	5.2742x10 <sup>-3</sup>	0.0694	0.000284

Note: Model No. 6 is the reference model

Table 6.3: Detail of finite element models to study the effect of variation of  $\beta_2$  on the confining behaviour of HSS collars

No.	$h_{column}$ (mm)	$A_{column}$ (mm <sup>2</sup> )	$I_{column}$ (mm <sup>4</sup> )	$A_{collar}$ (mm <sup>2</sup> )	$I_{collar}$ (mm <sup>4</sup> )	$h_{collar}$ (mm)	$s$ (mm)	$\beta_2$	$\gamma_0$	$(\beta_8)_{max}$
1	400	160 000	2.133x10 <sup>9</sup>	584	530.69x10 <sup>3</sup>	100	30	248.76x10 <sup>-6</sup>	0.0497	213.0x10 <sup>-6</sup>
2	400	160 000	2.133x10 <sup>9</sup>	584	581.73x10 <sup>3</sup>	100	30	272.69x10 <sup>-6</sup>	0.0521	212.8x10 <sup>-6</sup>
3	400	160 000	2.133x10 <sup>9</sup>	584	632.40x10 <sup>3</sup>	100	30	296.44x10 <sup>-6</sup>	0.0539	212.7x10 <sup>-6</sup>
4	400	160 000	2.133x10 <sup>9</sup>	584	682.70x10 <sup>3</sup>	100	30	320.02x10 <sup>-6</sup>	0.0554	212.5x10 <sup>-6</sup>
5	400	160 000	2.133x10 <sup>9</sup>	584	732.66x10 <sup>3</sup>	100	30	343.43x10 <sup>-6</sup>	0.0565	212.6x10 <sup>-6</sup>
6	400	160 000	2.133x10 <sup>9</sup>	584	775.18x10 <sup>3</sup>	100	30	363.37x10 <sup>-6</sup>	0.0587	210.0x10 <sup>-6</sup>
7	400	160 000	2.133x10 <sup>9</sup>	584	859.44x10 <sup>3</sup>	100	30	402.86x10 <sup>-6</sup>	0.0595	210.0x10 <sup>-6</sup>
8	400	160 000	2.133x10 <sup>9</sup>	584	942.64x10 <sup>3</sup>	100	30	441.86x10 <sup>-6</sup>	0.0616	208.0x10 <sup>-6</sup>
9	400	160 000	2.133x10 <sup>9</sup>	584	1024.8x10 <sup>3</sup>	100	30	480.36x10 <sup>-6</sup>	0.0650	207.8x10 <sup>-6</sup>
10	400	160 000	2.133x10 <sup>9</sup>	584	1105.9x10 <sup>3</sup>	100	30	518.37x10 <sup>-6</sup>	0.0660	207.6x10 <sup>-6</sup>
11	400	160 000	2.133x10 <sup>9</sup>	584	1185.9x10 <sup>3</sup>	100	30	555.88x10 <sup>-6</sup>	0.0675	2.077x10 <sup>-6</sup>

Note: Model No. 6 is the reference model

Table 6.4: Relationship between: (a)  $\gamma_2$  and  $\beta_2$ ; and (b)  $\lambda_2$  and  $\beta_2$  for HSS collars

No.	$\beta_2$	$\gamma_o$	$(\beta_8)_{\max}$	$\gamma_2$	$\lambda_2$
1	$248.76 \times 10^{-6}$	0.0497	$213.0 \times 10^{-6}$	0.8467	1.0143
2	$272.69 \times 10^{-6}$	0.0521	$212.8 \times 10^{-6}$	0.8876	1.0133
3	$296.44 \times 10^{-6}$	0.0539	$212.7 \times 10^{-6}$	0.9182	1.0130
4	$320.02 \times 10^{-6}$	0.0554	$212.5 \times 10^{-6}$	0.9438	1.0119
5	$343.43 \times 10^{-6}$	0.0565	$212.6 \times 10^{-6}$	0.9625	1.0124
6	$363.37 \times 10^{-6}$	0.0587	$210.0 \times 10^{-6}$	1.0000	1.0000
7	$402.86 \times 10^{-6}$	0.0595	$210.0 \times 10^{-6}$	1.0136	1.0000
8	$441.86 \times 10^{-6}$	0.0616	$208.0 \times 10^{-6}$	1.0494	0.9905
9	$480.36 \times 10^{-6}$	0.0650	$207.8 \times 10^{-6}$	1.1073	0.9895
10	$518.37 \times 10^{-6}$	0.0660	$207.6 \times 10^{-6}$	1.1244	0.9886
11	$555.88 \times 10^{-6}$	0.0675	$207.7 \times 10^{-6}$	1.1499	0.9890

Note: Model No. 6 is the reference model

Table 6.5: Detail of finite element models to study the effect of variation of  $\beta_3$  on the confining behaviour of HSS collars

No.	$h_{column}$ (mm)	$A_{column}$ (mm <sup>2</sup> )	$I_{column}$ (mm <sup>4</sup> )	$A_{collar}$ (mm <sup>2</sup> )	$I_{collar}$ (mm <sup>4</sup> )	$h_{collar}$ (mm)	$s$ (mm)	$\beta_3$	$\gamma_o$	$(\beta_8)_{max}$
1	400	160 000	2.133x10 <sup>9</sup>	584	775 180	100	2.5	0.00625	0.7300	2070.0x10 <sup>-6</sup>
2	400	160 000	2.133x10 <sup>9</sup>	584	775 180	100	5.0	0.0125	0.3550	1037.0x10 <sup>-6</sup>
3	400	160 000	2.133x10 <sup>9</sup>	584	775 180	100	7.5	0.0188	0.2300	702.0x10 <sup>-6</sup>
4	400	160 000	2.133x10 <sup>9</sup>	584	775 180	100	10.0	0.0250	0.1730	533.9x10 <sup>-6</sup>
5	400	160 000	2.133x10 <sup>9</sup>	584	775 180	100	12.5	0.0313	0.1350	437.5x10 <sup>-6</sup>
6	400	160 000	2.133x10 <sup>9</sup>	584	775 180	100	15.0	0.0375	0.1130	373.0x10 <sup>-6</sup>
7	400	160 000	2.133x10 <sup>9</sup>	584	775 180	100	17.5	0.0438	0.0970	327.5x10 <sup>-6</sup>
8	400	160 000	2.133x10 <sup>9</sup>	584	775 180	100	20.0	0.0500	0.0850	292.0x10 <sup>-6</sup>
9	400	160 000	2.133x10 <sup>9</sup>	584	775 180	100	25.0	0.0625	0.0675	244.0x10 <sup>-6</sup>
10	400	160 000	2.133x10 <sup>9</sup>	584	775 180	100	30.0	0.0750	0.0587	210.0x10 <sup>-6</sup>
11	400	160 000	2.133x10 <sup>9</sup>	584	775 180	100	35.0	0.0875	0.0517	185.0x10 <sup>-6</sup>
12	400	160 000	2.133x10 <sup>9</sup>	584	775 180	100	40.0	0.1000	0.0450	167.5x10 <sup>-6</sup>
13	400	160 000	2.133x10 <sup>9</sup>	584	775 180	100	45.0	0.1125	0.0414	153.0x10 <sup>-6</sup>
14	400	160 000	2.133x10 <sup>9</sup>	584	775 180	100	50.0	0.1250	0.0385	141.7x10 <sup>-6</sup>
15	400	160 000	2.133x10 <sup>9</sup>	584	775 180	100	55.0	0.1375	0.0358	132.0x10 <sup>-6</sup>
16	400	160 000	2.133x10 <sup>9</sup>	584	775 180	100	60.0	0.1500	0.0334	123.5x10 <sup>-6</sup>
17	400	160 000	2.133x10 <sup>9</sup>	584	775 180	100	65.0	0.1625	0.0319	118.0x10 <sup>-6</sup>
18	400	160 000	2.133x10 <sup>9</sup>	584	775 180	100	70.0	0.1750	0.0289	110.5x10 <sup>-6</sup>
19	400	160 000	2.133x10 <sup>9</sup>	584	775 180	100	75.0	0.1875	0.0275	105.0x10 <sup>-6</sup>
20	400	160 000	2.133x10 <sup>9</sup>	584	775 180	100	80.0	0.2000	0.0260	99.00x10 <sup>-6</sup>
21	400	160 000	2.133x10 <sup>9</sup>	584	775 180	100	85.0	0.2125	0.0260	95.00x10 <sup>-6</sup>

Note: Model No. 10 is the reference model

Table 6.6: Relationship between: (a)  $\lambda_3$  and  $\beta_3$ ; and (b)  $\gamma_3$  and  $\beta_3$  for solid collars

No.	$\beta_3$	$\gamma_o$	$(\beta_8)_{\max}$	$\gamma_3$	$\lambda_3$
1	0.00625	0.7300	$2070.0 \times 10^{-6}$	12.4361	9.8571
2	0.0125	0.3550	$1037.0 \times 10^{-6}$	6.04770	4.9381
3	0.0188	0.2300	$702.0 \times 10^{-6}$	3.9182	3.3428
4	0.0250	0.1730	$533.9 \times 10^{-6}$	2.9472	2.5424
5	0.0313	0.1350	$437.5 \times 10^{-6}$	2.2998	2.0833
6	0.0375	0.1130	$373.0 \times 10^{-6}$	1.9250	1.7762
7	0.0438	0.0970	$327.5 \times 10^{-6}$	1.6525	1.5595
8	0.0500	0.0850	$292.0 \times 10^{-6}$	1.4480	1.3905
9	0.0625	0.0675	$244.0 \times 10^{-6}$	1.1499	1.1619
10	0.0750	0.0587	$210.0 \times 10^{-6}$	1.0000	1.0000
11	0.0875	0.0517	$185.0 \times 10^{-6}$	0.8807	0.8809
12	0.1000	0.0450	$167.5 \times 10^{-6}$	0.7666	0.7976
13	0.1125	0.0414	$153.0 \times 10^{-6}$	0.7053	0.7286
14	0.1250	0.0385	$141.7 \times 10^{-6}$	0.6559	0.6747
15	0.1375	0.0358	$132.0 \times 10^{-6}$	0.6099	0.6286
16	0.1500	0.0334	$123.5 \times 10^{-6}$	0.5690	0.5881
17	0.1625	0.0319	$118.0 \times 10^{-6}$	0.5431	0.5619
18	0.1750	0.0289	$110.5 \times 10^{-6}$	0.4923	0.5262
19	0.1875	0.0275	$105.0 \times 10^{-6}$	0.4685	0.50000
20	0.2000	0.0260	$99.00 \times 10^{-6}$	0.4429	0.4714
21	0.2125	0.0260	$95.00 \times 10^{-6}$	0.4429	0.4524

Note: Model No. 10 is the reference model

Table 6.7: Detail of finite element models to study the effect of variation of  $\beta_4$  on the confining behaviour of HSS collars

No.	$h_{column}$ (mm)	$A_{column}$ (mm <sup>2</sup> )	$I_{column}$ (mm <sup>4</sup> )	$A_{collar}$ (mm <sup>2</sup> )	$I_{collar}$ (mm <sup>4</sup> )	$h_{collar}$ (mm)	$s$ (mm)	$\beta_4$	$\gamma_o$	$(\beta_8)_{max}$
1	400	160 000	2.133x10 <sup>9</sup>	584	775 180	80	30	0.200	0.0587	202.0x10 <sup>-6</sup>
2	400	160 000	2.133x10 <sup>9</sup>	584	775 180	85	30	0.213	0.0587	204.0x10 <sup>-6</sup>
3	400	160 000	2.133x10 <sup>9</sup>	584	775 180	90	30	0.225	0.0587	206.0x10 <sup>-6</sup>
4	400	160 000	2.133x10 <sup>9</sup>	584	775 180	95	30	0.238	0.0587	208.0x10 <sup>-6</sup>
5	400	160 000	2.133x10 <sup>9</sup>	584	775 180	100	30	0.250	0.0587	212.0x10 <sup>-6</sup>
6	400	160 000	2.133x10 <sup>9</sup>	584	775 180	105	30	0.263	0.0587	214.2x10 <sup>-6</sup>
7	400	160 000	2.133x10 <sup>9</sup>	584	775 180	110	30	0.275	0.0587	216.0x10 <sup>-6</sup>

Note: Model No. 5 is the reference model

Table 6.8: Relationship between: (a)  $\gamma_4$  and  $\beta_4$ ; and (b)  $\lambda_4$  and  $\beta_4$  for HSS collars

No.	$\beta_4$	$\gamma_o$	$(\beta_8)_{\max}$	$\gamma_4$	$\lambda_4$
1	0.200	0.0587	$202.0 \times 10^{-6}$	1	0.9619
2	0.213	0.0587	$204.0 \times 10^{-6}$	1	0.9714
3	0.225	0.0587	$206.0 \times 10^{-6}$	1	0.9810
4	0.238	0.0587	$208.0 \times 10^{-6}$	1	0.9905
5	0.250	0.0587	$212.0 \times 10^{-6}$	1	1.0000
6	0.263	0.0587	$214.2 \times 10^{-6}$	1	1.0200
7	0.275	0.0587	$216.0 \times 10^{-6}$	1	1.0286

Note: Model No. 5 is the reference model

Table 6.9: Detail of finite element models to study the effect of variation of  $f_y$  and  $E_s$  keeping  $\beta_5$  constant on the confining behaviour of HSS collars

No.	$h_{column}$ (mm)	$A_{column}$ (mm <sup>2</sup> )	$I_{column}$ (mm <sup>4</sup> )	$A_{collar}$ (mm <sup>2</sup> )	$I_{collar}$ (mm <sup>4</sup> )	$h_{column}$ (mm)	$s$ (mm)	$f_y$ (MPa)	$E_s$ (MPa)	$\beta_5$
1	400	160 000	2.133x10 <sup>9</sup>	584	775 180	100	30	400	174 838	2.2878x10 <sup>-3</sup>
2	400	160 000	2.133x10 <sup>9</sup>	584	775 180	100	30	450	196 693	2.2878x10 <sup>-3</sup>
3	400	160 000	2.133x10 <sup>9</sup>	584	775 180	100	30	465	203 250	2.2878x10 <sup>-3</sup>
4	400	160 000	2.133x10 <sup>9</sup>	584	775 180	100	30	500	218 548	2.2878x10 <sup>-3</sup>
5	400	160 000	2.133x10 <sup>9</sup>	584	775 180	100	30	550	240 403	2.2878x10 <sup>-3</sup>
6	400	160 000	2.133x10 <sup>9</sup>	584	775 180	100	30	600	262 258	2.2878x10 <sup>-3</sup>

Note: Model No. 3 is the reference model

Table 6.10: Detail of finite element models to study the effect of variation of  $f_y$ , keeping  $E_s$  and  $n$  constant on the confining behaviour of HSS collars

No.	$h_{column}$ (mm)	$A_{column}$ (mm <sup>2</sup> )	$I_{column}$ (mm <sup>4</sup> )	$A_{collar}$ (mm <sup>2</sup> )	$I_{collar}$ (mm <sup>4</sup> )	$h_{column}$ (mm)	$s$ (mm)	$f_y$ (MPa)	$E_s$ (MPa)	$\beta_5$
1	400	160 000	2.133x10 <sup>9</sup>	584	775 180	100	30	400	203 250	1.968x10 <sup>-3</sup>
2	400	160 000	2.133x10 <sup>9</sup>	584	775 180	100	30	450	203 250	2.214x10 <sup>-3</sup>
3	400	160 000	2.133x10 <sup>9</sup>	584	775 180	100	30	465	203 250	2.288x10 <sup>-3</sup>
4	400	160 000	2.133x10 <sup>9</sup>	584	775 180	100	30	500	203 250	2.460x10 <sup>-3</sup>
5	400	160 000	2.133x10 <sup>9</sup>	584	775 180	100	30	550	203 250	2.706x10 <sup>-3</sup>
6	400	160 000	2.133x10 <sup>9</sup>	584	775 180	100	30	600	203 250	2.952x10 <sup>-3</sup>

Note: Model No. 3 is the reference model

Table 6.11: Relationship between: (a)  $\gamma_5$  and  $\beta_5$ ; and (b)  $\lambda_5$  and  $\beta_5$  for HSS collars

No.	$\beta_5$	$\gamma_o$	$(\beta_8)_{\max}$	$\gamma_5$	$\lambda_5$
1	$1.9680 \times 10^{-3}$	0.0587	$183.0 \times 10^{-6}$	0.8714	1
2	$2.2140 \times 10^{-3}$	0.0587	$202.5 \times 10^{-6}$	0.9643	1
3	$2.2878 \times 10^{-3}$	0.0587	$210.0 \times 10^{-6}$	1.0000	1
4	$2.4600 \times 10^{-3}$	0.0587	$225.5 \times 10^{-6}$	1.0738	1
5	$2.7060 \times 10^{-3}$	0.0587	$246.0 \times 10^{-6}$	1.1714	1
6	$2.9520 \times 10^{-3}$	0.0587	$267.0 \times 10^{-6}$	1.2714	1

Note: Model No. 3 is the reference model

Table 6.12: Detail of finite element models to study the effect of variation of  $E_s$ , keeping  $f_y$  and  $n$  constant on the confining behaviour of HSS collars

No.	$h_{column}$ (mm)	$A_{column}$ (mm <sup>2</sup> )	$I_{column}$ (mm <sup>4</sup> )	$A_{collar}$ (mm <sup>2</sup> )	$I_{collar}$ (mm <sup>4</sup> )	$h_{column}$ (mm)	$s$ (mm)	$f_y$ (MPa)	$E_s$ (MPa)	$\beta'_5$
1	400	160 000	2.133x10 <sup>9</sup>	584	775 180	100	30	465	174 838	2.6596x10 <sup>-3</sup>
2	400	160 000	2.133x10 <sup>9</sup>	584	775 180	100	30	465	196 693	2.3641x10 <sup>-3</sup>
3	400	160 000	2.133x10 <sup>9</sup>	584	775 180	100	30	465	203 250	2.2878x10 <sup>-3</sup>
4	400	160 000	2.133x10 <sup>9</sup>	584	775 180	100	30	465	218 548	2.1277x10 <sup>-3</sup>
5	400	160 000	2.133x10 <sup>9</sup>	584	775 180	100	30	465	240 403	1.9343x10 <sup>-3</sup>
6	400	160 000	2.133x10 <sup>9</sup>	584	775 180	100	30	465	262 258	1.7731x10 <sup>-3</sup>

Note: Model No. 3 is the reference model

Table 6.13: Relationship between: (a)  $\gamma'_5$  and  $\beta'_5$ ; and (b)  $\lambda'_5$  and  $\beta'_5$  for HSS collars

No.	$\beta'_5$	$\gamma_o$	$(\beta_8)_{\max}$	$\gamma'_5$	$\lambda'_5$
1	$2.6596 \times 10^{-3}$	0.0514	$213.0 \times 10^{-6}$	0.8756	1.0143
2	$2.3641 \times 10^{-3}$	0.0565	$211.5 \times 10^{-6}$	0.9625	1.0071
3	$2.2878 \times 10^{-3}$	0.0587	$210.0 \times 10^{-6}$	1.0000	1.0000
4	$2.1277 \times 10^{-3}$	0.0617	$208.0 \times 10^{-6}$	1.0511	0.9904
5	$1.9343 \times 10^{-3}$	0.0669	$207.0 \times 10^{-6}$	1.1397	0.9857
6	$1.7731 \times 10^{-3}$	0.0720	$206.0 \times 10^{-6}$	1.2266	0.9809

Note: Model No. 3 is the reference model

Table 6.14: Detail of finite element models to study the effect of variation of  $\beta_6$  on the confining behaviour of HSS collars

No.	$h_{column}$ (mm)	$A_{column}$ (mm <sup>2</sup> )	$I_{column}$ (mm <sup>4</sup> )	$A_{collar}$ (mm <sup>2</sup> )	$I_{collar}$ (mm <sup>4</sup> )	$h_{column}$ (mm)	$s$ (mm)	$f_y$ (MPa)	$E_s$ (MPa)	$\beta_6$
1	400	160 000	2.133x10 <sup>9</sup>	584	775 180	100	30	465	203 250	10
2	400	160 000	2.133x10 <sup>9</sup>	584	775 180	100	30	465	203 250	11
3	400	160 000	2.133x10 <sup>9</sup>	584	775 180	100	30	465	203 250	12
4	400	160 000	2.133x10 <sup>9</sup>	584	775 180	100	30	465	203 250	14
5	400	160 000	2.133x10 <sup>9</sup>	584	775 180	100	30	465	203 250	16
6	400	160 000	2.133x10 <sup>9</sup>	584	775 180	100	30	465	203 250	18
7	400	160 000	2.133x10 <sup>9</sup>	584	775 180	100	30	465	203 250	20

Note: Model No. 2 is the reference model

Table 6.15: Relationship between: (a)  $\gamma_6$  and  $\beta_6$ ; and (b)  $\lambda_6$  and  $\beta_6$  for HSS collars

No.	$\beta_6$	$\gamma_o$	$(\beta_s)_{\max}$	$\gamma_6$	$\lambda_6$
1	10	0.0587	$215.0 \times 10^{-6}$	1	1.0238
2	11	0.0587	$210.0 \times 10^{-6}$	1	1.0000
3	12	0.0587	$206.0 \times 10^{-6}$	1	0.9810
4	14	0.0587	$200.0 \times 10^{-6}$	1	0.9524
5	16	0.0587	$194.5 \times 10^{-6}$	1	0.9262
6	18	0.0587	$192.5 \times 10^{-6}$	1	0.9167
7	20	0.0587	$189.0 \times 10^{-6}$	1	0.9000

Note: Model No. 2 is the reference model

Table 6.16: Detail of finite element models to study the effect of smearing on the confining behaviour of HSS collars

No.	$h_{column}$ (mm)	$A_{column}$ (mm <sup>2</sup> )	$I_{column}$ (mm <sup>4</sup> )	$A_{collar}$ (mm <sup>2</sup> )	$I_{collar}$ (mm <sup>4</sup> )	$s$ (mm)	$\beta_1$	$\beta_2$	$\beta_3$
1	400	160 000	2.133x10 <sup>9</sup>	146	193.79x10 <sup>3</sup>	7.5	0.9125x10 <sup>-3</sup>	90.841x10 <sup>-6</sup>	18.750x10 <sup>-3</sup>
2	400	160 000	2.133x10 <sup>9</sup>	292	387.59x10 <sup>3</sup>	15.0	1.825x10 <sup>-3</sup>	181.68x10 <sup>-6</sup>	37.500x10 <sup>-3</sup>
3	400	160 000	2.133x10 <sup>9</sup>	438	581.38x10 <sup>3</sup>	22.5	2.738x10 <sup>-3</sup>	272.52x10 <sup>-6</sup>	56.250x10 <sup>-3</sup>
4	400	160 000	2.133x10 <sup>9</sup>	584	775.18x10 <sup>3</sup>	30.0	3.650x10 <sup>-3</sup>	363.37x10 <sup>-6</sup>	75.000x10 <sup>-3</sup>
5	400	160 000	2.133x10 <sup>9</sup>	730	968.97x10 <sup>3</sup>	37.5	4.563x10 <sup>-3</sup>	454.21x10 <sup>-6</sup>	93.750x10 <sup>-3</sup>
6	400	160 000	2.133x10 <sup>9</sup>	876	1162.8x10 <sup>3</sup>	45.0	5.475x10 <sup>-3</sup>	545.05x10 <sup>-6</sup>	112.50x10 <sup>-3</sup>
7	400	160 000	2.133x10 <sup>9</sup>	1022	1356.6x10 <sup>3</sup>	52.5	6.388x10 <sup>-3</sup>	635.89x10 <sup>-6</sup>	131.25x10 <sup>-3</sup>
8	400	160 000	2.133x10 <sup>9</sup>	1168	1550.4x10 <sup>3</sup>	60.0	7.300x10 <sup>-3</sup>	726.73x10 <sup>-6</sup>	150.00x10 <sup>-3</sup>
9	400	160 000	2.133x10 <sup>9</sup>	1460	1937.9x10 <sup>3</sup>	75.0	9.125x10 <sup>-3</sup>	908.41x10 <sup>-6</sup>	187.50x10 <sup>-3</sup>
10	400	160 000	2.133x10 <sup>9</sup>	1752	2325.5x10 <sup>3</sup>	90.0	1.095x10 <sup>-3</sup>	1090.1x10 <sup>-6</sup>	225.00x10 <sup>-3</sup>
11	400	160 000	2.133x10 <sup>9</sup>	2336	3100.7x10 <sup>3</sup>	120.0	14.60x10 <sup>-3</sup>	1453.5x10 <sup>-6</sup>	300.00x10 <sup>-3</sup>

Note: Model No. 4 is the reference model

Table 6.17: Relationship between: (a)  $\gamma_s$  and  $\beta_3$ ; and (b)  $\lambda_s$  and  $\beta_3$  for HSS collars

No.	$\beta_3$	$\gamma_o$	$(\beta_8)_{\max}$	$\gamma_s$	$\lambda_s$
1	0.01875	0.0587	$188.0 \times 10^{-6}$	1	0.8952
2	0.03750	0.0587	$200.0 \times 10^{-6}$	1	0.9524
3	0.05625	0.0587	$207.0 \times 10^{-6}$	1	0.9857
4	0.07500	0.0587	$210.0 \times 10^{-6}$	1	1.0000
5	0.09375	0.0587	$213.0 \times 10^{-6}$	1	1.0143
6	0.11250	0.0587	$214.5 \times 10^{-6}$	1	1.0214
7	0.13125	0.0587	$216.0 \times 10^{-6}$	1	1.0286
8	0.15000	0.0587	$217.0 \times 10^{-6}$	1	1.0333
9	0.18750	0.0587	$219.0 \times 10^{-6}$	1	1.0429
10	0.22500	0.0587	$220.5 \times 10^{-6}$	1	1.0500
11	0.30000	0.0587	$221.1 \times 10^{-6}$	1	1.0529

Note: Model No. 4 is the reference model

Table 6.18: Detail of finite element models to check the proposed equations

Case	$h_{column}$ (mm)	$b_{collar}$ (mm)	$h_{collar}$ (mm)	$T_w$ (mm)	$T_f$ (mm)	$s$ (mm)	$f_y$ (MPa)	$E_s$ (MPa)	$n$
1	300	25.5	51	3.175	6.35	61.00	465	203 250	11
2	300	25.5	51	3.175	6.35	61.00	500	203 250	11
3	300	17.0	51	2.117	6.35	40.67	465	203 250	11
4	300	17.0	51	2.117	6.35	40.67	500	203 250	11
5	300	25.5	51	3.175	6.35	61.00	465	196 693	11
6	300	17.0	51	2.117	6.35	40.67	465	196 693	11
7	300	25.5	51	3.175	6.35	61.00	400	200 000	11
8	300	25.5	51	3.175	6.35	61.00	470	210 000	11
9	300	25.5	76	3.175	6.35	61.00	465	203 250	11
10	300	25.5	76	3.175	6.35	61.00	500	203 250	11
11	300	8.5	76	1.058	6.35	20.33	465	203 250	11
12	300	25.5	102	3.175	6.35	61.00	465	203 250	11
13	300	25.5	102	3.175	6.35	61.00	500	203 250	11
14	300	6.375	102	0.794	6.35	15.25	465	203 250	11

Table 6.19: Detail of equivalent models obtained after collar smearing in order to apply proposed equations for the confining of HSS collars

Case	$h_{column}$ (mm)	$b_{collar}$ (mm)	$h_{collar}$ (mm)	$T_w$ (mm)	$T_f$ (mm)	$s$ (mm)	$f_y$ (MPa)	$E_s$ (MPa)	$n$
1	300	12.75	51	1.5875	6.35	30.50	465	203 250	11
2	300	17.00	51	2.1167	6.35	40.66	500	203 250	11
3	300	17.00	51	2.1167	6.35	40.66	465	203 250	11
4	300	17.00	51	2.1167	6.35	40.66	500	203 250	11
5	300	12.75	51	1.5875	6.35	30.50	465	196 693	11
6	300	12.75	51	1.5875	6.35	30.50	465	196 693	11
7	300	12.75	51	1.5875	6.35	30.50	400	200 000	11
8	300	12.75	51	1.5875	6.35	30.50	470	210 000	11
9	300	12.75	76	1.5875	6.35	30.50	465	203 250	11
10	300	12.75	76	1.5875	6.35	30.50	500	203 250	11
11	300	12.75	76	1.5875	6.35	30.50	465	203 250	11
12	300	12.75	102	1.5875	6.35	30.50	465	203 250	11
13	300	12.75	102	1.5875	6.35	30.50	500	203 250	11
14	300	12.75	102	1.5875	6.35	30.50	465	203 250	11

Table 6.20: Coefficients of multiple determinations  $R^2$  up to various level of lateral strains for columns confined by HSS collars

Cases	$R^2$			
	$\beta_7 = 0.06$	$\beta_7 = 0.05$	$\beta_7 = 0.04$	$\beta_7 = 0.03$
1	0.9967	0.9953	0.9958	0.9949
2	0.9885	0.9883	0.9873	0.9854
3	0.9742	0.9765	0.9774	0.9767
4	0.9879	0.9878	0.9869	0.9850
5	0.9962	0.9958	0.9952	0.9941
6	0.9960	0.9957	0.9950	0.9939
7	0.9741	0.9780	0.9803	0.9806
8	0.9971	0.9968	0.9965	0.9961
9	0.9813	0.9810	0.9820	0.9851
10	0.9710	0.9721	0.9751	0.9809
11	0.9819	0.9804	0.9798	0.9812
12	0.9857	0.9842	0.9832	0.9832
13	0.9833	0.9821	0.9818	0.9832
14	0.9915	0.9911	0.9898	0.9891

Table 6.21: Detail of finite element models to study the effect of scale on the confining behaviour of solid collars

No.	$h_{column}$ (mm)	$A_{column}$ (mm <sup>2</sup> )	$I_{column}$ (mm <sup>4</sup> )	$A_{collar}$ (mm <sup>2</sup> )	$I_{collar}$ (mm <sup>4</sup> )	$s$ (mm)	$f_y$ (MPa)	$E_s$ (MPa)
1	300	90.00x10 <sup>3</sup>	0.675x10 <sup>9</sup>	1875	0.879x10 <sup>6</sup>	50.00	465	203 250
2	350	122.5x10 <sup>3</sup>	1.251x10 <sup>9</sup>	2552	1.628x10 <sup>6</sup>	58.33	465	203 250
3	400	160.0x10 <sup>3</sup>	2.133x10 <sup>9</sup>	3333	2.778x10 <sup>6</sup>	66.67	465	203 250
4	450	202.5x10 <sup>3</sup>	3.417x10 <sup>9</sup>	4219	4.449x10 <sup>6</sup>	75.00	465	203 250
5	500	250.0x10 <sup>3</sup>	5.208x10 <sup>9</sup>	5208	6.782x10 <sup>6</sup>	83.33	465	203 250
6	550	302.5x10 <sup>3</sup>	7.626x10 <sup>9</sup>	6302	9.929x10 <sup>6</sup>	91.66	465	203 250
7	600	360.0x10 <sup>3</sup>	10.80x10 <sup>9</sup>	7500	14.06x10 <sup>6</sup>	100.00	465	203 250
8	650	422.5x10 <sup>3</sup>	14.88x10 <sup>9</sup>	8802	19.37x10 <sup>6</sup>	108.33	465	203 250
9	700	490.0x10 <sup>3</sup>	20.01x10 <sup>9</sup>	10210	26.05x10 <sup>6</sup>	116.66	465	203 250
10	750	562.5x10 <sup>3</sup>	26.37x10 <sup>9</sup>	11720	34.33x10 <sup>6</sup>	125.00	465	203 250
11	800	640.0x10 <sup>3</sup>	34.13x10 <sup>9</sup>	13330	44.44x10 <sup>6</sup>	133.33	465	203 250

Note: Model No. 5 is the reference model

Table 6.22: Detail of finite element models to study the effect of variation of  $\beta_1$  on the confining behaviour of solid collars

No.	$h_{column}$ (mm)	$A_{column}$ (mm <sup>2</sup> )	$I_{column}$ (mm <sup>4</sup> )	$A_{collar}$ (mm <sup>2</sup> )	$I_{collar}$ (mm <sup>4</sup> )	$s$ (mm)	$\beta_1$	$\gamma_0$	$(\beta_8)_{max}$
1	500	250 000	5.208x10 <sup>9</sup>	1000	6.782x10 <sup>6</sup>	83.33	0.004	0.042	130x10 <sup>-6</sup>
2	500	250 000	5.208x10 <sup>9</sup>	2000	6.782x10 <sup>6</sup>	83.33	0.008	0.064	235x10 <sup>-6</sup>
3	500	250 000	5.208x10 <sup>9</sup>	3000	6.782x10 <sup>6</sup>	83.33	0.012	0.085	315x10 <sup>-6</sup>
4	500	250 000	5.208x10 <sup>9</sup>	4000	6.782x10 <sup>6</sup>	83.33	0.016	0.103	378x10 <sup>-6</sup>
5	500	250 000	5.208x10 <sup>9</sup>	5000	6.782x10 <sup>6</sup>	83.33	0.020	0.117	439x10 <sup>-6</sup>
6	500	250 000	5.208x10 <sup>9</sup>	5208	6.782x10 <sup>6</sup>	83.33	0.02083	0.120	448x10 <sup>-6</sup>
7	500	250 000	5.208x10 <sup>9</sup>	6000	6.782x10 <sup>6</sup>	83.33	0.024	0.132	485x10 <sup>-6</sup>
8	500	250 000	5.208x10 <sup>9</sup>	7000	6.782x10 <sup>6</sup>	83.33	0.028	0.142	540x10 <sup>-6</sup>
9	500	250 000	5.208x10 <sup>9</sup>	8000	6.782x10 <sup>6</sup>	83.33	0.032	0.150	579x10 <sup>-6</sup>
10	500	250 000	5.208x10 <sup>9</sup>	9000	6.782x10 <sup>6</sup>	83.33	0.036	0.158	630x10 <sup>-6</sup>
11	500	250 000	5.208x10 <sup>9</sup>	10000	6.782x10 <sup>6</sup>	83.33	0.040	0.164	665x10 <sup>-6</sup>
12	500	250 000	5.208x10 <sup>9</sup>	11000	6.782x10 <sup>6</sup>	83.33	0.044	0.170	710x10 <sup>-6</sup>
13	500	250 000	5.208x10 <sup>9</sup>	12000	6.782x10 <sup>6</sup>	83.33	0.048	0.174	750x10 <sup>-6</sup>
14	500	250 000	5.208x10 <sup>9</sup>	13000	6.782x10 <sup>6</sup>	83.33	0.052	0.177	790x10 <sup>-6</sup>
15	500	250 000	5.208x10 <sup>9</sup>	14000	6.782x10 <sup>6</sup>	83.33	0.056	0.180	818x10 <sup>-6</sup>

Note: Model No. 6 is the reference model

Table 6.23: Detail of finite element models to study the effect of variation of  $\beta_2$  on the confining behaviour of solid collars

No.	$h_{column}$ (mm)	$A_{column}$ (mm <sup>2</sup> )	$I_{column}$ (mm <sup>4</sup> )	$A_{collar}$ (mm <sup>2</sup> )	$I_{collar}$ (mm <sup>4</sup> )	$s$ (mm)	$\beta_2$	$\gamma_o$	$(\beta_8)_{max}$
1	500	250 000	5.208x10 <sup>9</sup>	5208	0.50x10 <sup>6</sup>	83.33	0.096x10 <sup>-3</sup>	0.045	275.3x10 <sup>-6</sup>
2	500	250 000	5.208x10 <sup>9</sup>	5208	1.00x10 <sup>6</sup>	83.33	0.192x10 <sup>-3</sup>	0.054	317.0x10 <sup>-6</sup>
3	500	250 000	5.208x10 <sup>9</sup>	5208	2.50x10 <sup>6</sup>	83.33	0.480x10 <sup>-3</sup>	0.079	373.3x10 <sup>-6</sup>
4	500	250 000	5.208x10 <sup>9</sup>	5208	4.00x10 <sup>6</sup>	83.33	0.768x10 <sup>-3</sup>	0.097	405.3x10 <sup>-6</sup>
5	500	250 000	5.208x10 <sup>9</sup>	5208	5.00x10 <sup>6</sup>	83.33	0.960x10 <sup>-3</sup>	0.106	422.6x10 <sup>-6</sup>
6	500	250 000	5.208x10 <sup>9</sup>	5208	6.782x10 <sup>6</sup>	83.33	1.302x10 <sup>-3</sup>	0.120	448.0x10 <sup>-6</sup>
7	500	250 000	5.208x10 <sup>9</sup>	5208	15.00x10 <sup>6</sup>	83.33	2.880x10 <sup>-3</sup>	0.160	521.1x10 <sup>-6</sup>
8	500	250 000	5.208x10 <sup>9</sup>	5208	30.00x10 <sup>6</sup>	83.33	5.760x10 <sup>-3</sup>	0.188	594.3x10 <sup>-6</sup>
9	500	250 000	5.208x10 <sup>9</sup>	5208	40.00x10 <sup>6</sup>	83.33	7.680x10 <sup>-3</sup>	0.199	619.7x10 <sup>-6</sup>
10	500	250 000	5.208x10 <sup>9</sup>	5208	50.00x10 <sup>6</sup>	83.33	9.600x10 <sup>-3</sup>	0.208	638.0x10 <sup>-6</sup>
11	500	250 000	5.208x10 <sup>9</sup>	5208	60.00x10 <sup>6</sup>	83.33	11.520x10 <sup>-3</sup>	0.216	650.2x10 <sup>-6</sup>
12	500	250 000	5.208x10 <sup>9</sup>	5208	70.00x10 <sup>6</sup>	83.33	13.440x10 <sup>-3</sup>	0.222	665.4x10 <sup>-6</sup>
13	500	250 000	5.208x10 <sup>9</sup>	5208	80.00x10 <sup>6</sup>	83.33	15.360x10 <sup>-3</sup>	0.226	674.6x10 <sup>-6</sup>
14	500	250 000	5.208x10 <sup>9</sup>	5208	90.00x10 <sup>6</sup>	83.33	17.280x10 <sup>-3</sup>	0.230	682.7x10 <sup>-6</sup>
15	500	250 000	5.208x10 <sup>9</sup>	5208	100.00x10 <sup>6</sup>	83.33	19.200x10 <sup>-3</sup>	0.235	685.7x10 <sup>-6</sup>

Note: Model No. 6 is the reference model

Table 6.24: Relationship between: (a)  $\gamma_2$  and  $\beta_2$ ; and (b)  $\lambda_2$  and  $\beta_2$  for solid collars

No.	$\beta_2$	$\gamma_o$	$(\beta_8)_{\max}$	$\gamma_2$	$\lambda_2$
1	$0.096 \times 10^{-3}$	0.045	$275.3 \times 10^{-6}$	0.3750	0.6145
2	$0.192 \times 10^{-3}$	0.054	$317.0 \times 10^{-6}$	0.4500	0.7075
3	$0.480 \times 10^{-3}$	0.079	$373.3 \times 10^{-6}$	0.6542	0.8333
4	$0.768 \times 10^{-3}$	0.097	$405.3 \times 10^{-6}$	0.8083	0.9048
5	$0.960 \times 10^{-3}$	0.106	$422.6 \times 10^{-6}$	0.8833	0.9433
6	$1.302 \times 10^{-3}$	0.120	$448.0 \times 10^{-6}$	1.0000	1.0000
7	$2.880 \times 10^{-3}$	0.160	$521.1 \times 10^{-6}$	1.3333	1.1632
8	$5.760 \times 10^{-3}$	0.188	$594.3 \times 10^{-6}$	1.5667	1.3265
9	$7.680 \times 10^{-3}$	0.199	$619.7 \times 10^{-6}$	1.6583	1.3832
10	$9.600 \times 10^{-3}$	0.208	$638.0 \times 10^{-6}$	1.7333	1.4240
11	$11.520 \times 10^{-3}$	0.216	$650.2 \times 10^{-6}$	1.8017	1.4512
12	$13.440 \times 10^{-3}$	0.222	$665.4 \times 10^{-6}$	1.8517	1.4853
13	$15.360 \times 10^{-3}$	0.226	$674.6 \times 10^{-6}$	1.8833	1.5057
14	$17.280 \times 10^{-3}$	0.230	$682.7 \times 10^{-6}$	1.9167	1.5238
15	$19.200 \times 10^{-3}$	0.235	$685.7 \times 10^{-6}$	1.9583	1.5306

Note: Model No. 6 is the reference model

Table 6.25: Detail of finite element models to study the effect of variation of  $\beta_3$  on the confining behaviour of solid collars

No.	$h_{column}$ (mm)	$A_{column}$ (mm <sup>2</sup> )	$I_{column}$ (mm <sup>4</sup> )	$A_{collar}$ (mm <sup>2</sup> )	$I_{collar}$ (mm <sup>4</sup> )	$s$ (mm)	$\beta_3$	$\gamma_o$	$(\beta_8)_{max}$
1	500	250 000	5.208x10 <sup>9</sup>	5208	6.782x10 <sup>6</sup>	10.00	0.0200	0.950	3180x10 <sup>-6</sup>
2	500	250 000	5.208x10 <sup>9</sup>	5208	6.782x10 <sup>6</sup>	15.00	0.0300	0.630	2133x10 <sup>-6</sup>
3	500	250 000	5.208x10 <sup>9</sup>	5208	6.782x10 <sup>6</sup>	20.00	0.0400	0.480	1625x10 <sup>-6</sup>
4	500	250 000	5.208x10 <sup>9</sup>	5208	6.782x10 <sup>6</sup>	30.00	0.0600	0.320	1117x10 <sup>-6</sup>
5	500	250 000	5.208x10 <sup>9</sup>	5208	6.782x10 <sup>6</sup>	40.00	0.0800	0.240	848.3x10 <sup>-6</sup>
6	500	250 000	5.208x10 <sup>9</sup>	5208	6.782x10 <sup>6</sup>	50.00	0.1000	0.195	690.8x10 <sup>-6</sup>
7	500	250 000	5.208x10 <sup>9</sup>	5208	6.782x10 <sup>6</sup>	60.00	0.1200	0.169	584.1x10 <sup>-6</sup>
8	500	250 000	5.208x10 <sup>9</sup>	5208	6.782x10 <sup>6</sup>	70.00	0.1400	0.145	513.0x10 <sup>-6</sup>
9	500	250 000	5.208x10 <sup>9</sup>	5208	6.782x10 <sup>6</sup>	83.33	0.1667	0.120	448.0x10 <sup>-6</sup>
10	500	250 000	5.208x10 <sup>9</sup>	5208	6.782x10 <sup>6</sup>	90.00	0.1800	0.110	421.6x10 <sup>-6</sup>
11	500	250 000	5.208x10 <sup>9</sup>	5208	6.782x10 <sup>6</sup>	100.00	0.2000	0.099	391.1x10 <sup>-6</sup>
12	500	250 000	5.208x10 <sup>9</sup>	5208	6.782x10 <sup>6</sup>	110.00	0.2200	0.092	360.6x10 <sup>-6</sup>
13	500	250 000	5.208x10 <sup>9</sup>	5208	6.782x10 <sup>6</sup>	120.00	0.2400	0.086	338.3x10 <sup>-6</sup>
14	500	250 000	5.208x10 <sup>9</sup>	5208	6.782x10 <sup>6</sup>	130.00	0.2600	0.078	320.0x10 <sup>-6</sup>
15	500	250 000	5.208x10 <sup>9</sup>	5208	6.782x10 <sup>6</sup>	140.00	0.2800	0.075	300.7x10 <sup>-6</sup>
16	500	250 000	5.208x10 <sup>9</sup>	5208	6.782x10 <sup>6</sup>	150.00	0.3000	0.068	286.5x10 <sup>-6</sup>

Note: Model No. 9 is the reference model

Table 6.26: Relationship between: (a)  $\gamma_3$  and  $\beta_3$ ; and (b)  $\lambda_3$  and  $\beta_3$  for solid collars

No.	$\beta_3$	$\gamma_o$	$(\beta_8)_{\max}$	$\gamma_3$	$\lambda_3$
1	0.0200	0.950	$3180 \times 10^{-6}$	7.9167	7.0975
2	0.0300	0.630	$2133 \times 10^{-6}$	5.2500	4.7619
3	0.0400	0.480	$1625 \times 10^{-6}$	4.0000	3.6281
4	0.0600	0.320	$1117 \times 10^{-6}$	2.6667	2.4943
5	0.0800	0.240	$848.3 \times 10^{-6}$	2.0000	1.8934
6	0.1000	0.195	$690.8 \times 10^{-6}$	1.6250	1.5419
7	0.1200	0.169	$584.1 \times 10^{-6}$	1.4083	1.3039
8	0.1400	0.145	$513.0 \times 10^{-6}$	1.2083	1.1451
9	0.1667	0.120	$448.0 \times 10^{-6}$	1.0000	1.0000
10	0.1800	0.110	$421.6 \times 10^{-6}$	0.9167	0.9410
11	0.2000	0.099	$391.1 \times 10^{-6}$	0.8250	0.8730
12	0.2200	0.092	$360.6 \times 10^{-6}$	0.7667	0.8050
13	0.2400	0.086	$338.3 \times 10^{-6}$	0.7167	0.7551
14	0.2600	0.078	$320.0 \times 10^{-6}$	0.6500	0.7143
15	0.2800	0.075	$300.7 \times 10^{-6}$	0.6250	0.6712
16	0.3000	0.068	$286.5 \times 10^{-6}$	0.5658	0.6395

Note: Model No. 9 is the reference model

Table 6.27: Detail of finite element models to study the effect of variation of  $f_y$ , keeping  $E_s$  and  $n$  constant on the confining behaviour of solid collars

No.	$h_{column}$ (mm)	$A_{column}$ (mm <sup>2</sup> )	$I_{column}$ (mm <sup>4</sup> )	$A_{collar}$ (mm <sup>2</sup> )	$I_{collar}$ (mm <sup>4</sup> )	$s$ (mm)	$f_y$ MPa	$E_s$ MPa	$\beta_5$
1	500	250 000	5.208x10 <sup>9</sup>	5208	6.782x10 <sup>6</sup>	83.33	300	203 250	1.476x10 <sup>-3</sup>
2	500	250 000	5.208x10 <sup>9</sup>	5208	6.782x10 <sup>6</sup>	83.33	350	203 250	1.722x10 <sup>-3</sup>
3	500	250 000	5.208x10 <sup>9</sup>	5208	6.782x10 <sup>6</sup>	83.33	400	203 250	1.968x10 <sup>-3</sup>
4	500	250 000	5.208x10 <sup>9</sup>	5208	6.782x10 <sup>6</sup>	83.33	450	203 250	2.214x10 <sup>-3</sup>
5	500	250 000	5.208x10 <sup>9</sup>	5208	6.782x10 <sup>6</sup>	83.33	465	203 250	2.288x10 <sup>-3</sup>
6	500	250 000	5.208x10 <sup>9</sup>	5208	6.782x10 <sup>6</sup>	83.33	500	203 250	2.460x10 <sup>-3</sup>
7	500	250 000	5.208x10 <sup>9</sup>	5208	6.782x10 <sup>6</sup>	83.33	550	203 250	2.706x10 <sup>-3</sup>
8	500	250 000	5.208x10 <sup>9</sup>	5208	6.782x10 <sup>6</sup>	83.33	600	203 250	2.952x10 <sup>-3</sup>
9	500	250 000	5.208x10 <sup>9</sup>	5208	6.782x10 <sup>6</sup>	83.33	650	203 250	3.198x10 <sup>-3</sup>
10	500	250 000	5.208x10 <sup>9</sup>	5208	6.782x10 <sup>6</sup>	83.33	700	203 250	3.444x10 <sup>-3</sup>

Note: Model No. 5 is the reference model

Table 6.28: Relationship between: (a)  $\gamma_5$  and  $\beta_5$ ; and (b)  $\lambda_5$  and  $\beta_5$  for solid collars

No.	$\beta_5$	$\gamma_o$	$(\beta_8)_{\max}$	$\gamma_5$	$\lambda_5$
1	$1.476 \times 10^{-3}$	0.12	$298.7 \times 10^{-6}$	1	0.6667
2	$1.722 \times 10^{-3}$	0.12	$344.4 \times 10^{-6}$	1	0.7687
3	$1.968 \times 10^{-3}$	0.12	$388.8 \times 10^{-6}$	1	0.8679
4	$2.214 \times 10^{-3}$	0.12	$433.8 \times 10^{-6}$	1	0.9683
5	$2.288 \times 10^{-3}$	0.12	$448.0 \times 10^{-6}$	1	1.0000
6	$2.460 \times 10^{-3}$	0.12	$482.5 \times 10^{-6}$	1	1.0771
7	$2.706 \times 10^{-3}$	0.12	$523.2 \times 10^{-6}$	1	1.1678
8	$2.952 \times 10^{-3}$	0.12	$571.9 \times 10^{-6}$	1	1.2766
9	$3.198 \times 10^{-3}$	0.12	$619.7 \times 10^{-6}$	1	1.3832
10	$3.444 \times 10^{-3}$	0.12	$665.4 \times 10^{-6}$	1	1.4853

Note: Model No. 5 is the reference model

Table 6.29: Detail of finite element models to study the effect of variation of  $E_s$  keeping  $f_y$  and  $n$  constant on the confining behaviour of solid collars

No.	$h_{column}$ (mm)	$A_{column}$ (mm <sup>2</sup> )	$I_{column}$ (mm <sup>4</sup> )	$A_{collar}$ (mm <sup>2</sup> )	$I_{collar}$ (mm <sup>4</sup> )	$s$ (mm)	$f_y$ (MPa)	$E_s$ (MPa)	$\beta'_5$
1	500	250 000	5.208x10 <sup>9</sup>	5208	6.782x10 <sup>6</sup>	83.33	465	174 838	2.6596x10 <sup>-3</sup>
2	500	250 000	5.208x10 <sup>9</sup>	5208	6.782x10 <sup>6</sup>	83.33	465	196 693	2.3641x10 <sup>-3</sup>
3	500	250 000	5.208x10 <sup>9</sup>	5208	6.782x10 <sup>6</sup>	83.33	465	203 250	2.2878x10 <sup>-3</sup>
4	500	250 000	5.208x10 <sup>9</sup>	5208	6.782x10 <sup>6</sup>	83.33	465	218 548	2.1277x10 <sup>-3</sup>
5	500	250 000	5.208x10 <sup>9</sup>	5208	6.782x10 <sup>6</sup>	83.33	465	240 403	1.9343x10 <sup>-3</sup>
6	500	250 000	5.208x10 <sup>9</sup>	5208	6.782x10 <sup>6</sup>	83.33	465	262 258	1.7731x10 <sup>-3</sup>

Note: Model No. 3 is the reference model

Table 6.30: Relationship between: (a)  $\gamma'_5$  and  $\beta'_5$ ; and (b)  $\lambda'_5$  and  $\beta'_5$  for solid collars

No.	$\beta'_5$	$\gamma_o$	$(\beta_8)_{\max}$	$\gamma'_5$	$\lambda'_5$
1	$2.6596 \times 10^{-3}$	0.1073	$451.0 \times 10^{-6}$	0.8942	1.0068
2	$2.3641 \times 10^{-3}$	0.1173	$448.5 \times 10^{-6}$	0.9775	1.0011
3	$2.2878 \times 10^{-3}$	0.1200	$448.0 \times 10^{-6}$	1.0000	1.0000
4	$2.1277 \times 10^{-3}$	0.1269	$447.4 \times 10^{-6}$	1.0575	0.9987
5	$1.9343 \times 10^{-3}$	0.1375	$441.9 \times 10^{-6}$	1.1458	0.9864
6	$1.7731 \times 10^{-3}$	0.1480	$438.9 \times 10^{-6}$	1.2333	0.9796

Note: Model No. 3 is the reference model

Table 6.31: Detail of finite element models to study the effect of variation of  $n$  on the confining behaviour of solid collars

No.	$h_{column}$ (mm)	$A_{column}$ (mm <sup>2</sup> )	$I_{column}$ (mm <sup>4</sup> )	$A_{collar}$ (mm <sup>2</sup> )	$I_{collar}$ (mm <sup>4</sup> )	$s$ (mm)	$f_y$ (MPa)	$E_s$ (MPa)	$n$	$\beta_6$
1	500	250 000	5.208x10 <sup>9</sup>	5208	6.782x10 <sup>6</sup>	83.33	465	203 250	10	10
2	500	250 000	5.208x10 <sup>9</sup>	5208	6.782x10 <sup>6</sup>	83.33	465	203 250	11	11
3	500	250 000	5.208x10 <sup>9</sup>	5208	6.782x10 <sup>6</sup>	83.33	465	203 250	12	12
4	500	250 000	5.208x10 <sup>9</sup>	5208	6.782x10 <sup>6</sup>	83.33	465	203 250	14	14
5	500	250 000	5.208x10 <sup>9</sup>	5208	6.782x10 <sup>6</sup>	83.33	465	203 250	16	16
6	500	250 000	5.208x10 <sup>9</sup>	5208	6.782x10 <sup>6</sup>	83.33	465	203 250	18	18
7	500	250 000	5.208x10 <sup>9</sup>	5208	6.782x10 <sup>6</sup>	83.33	465	203 250	20	20

Note: Model No. 2 is the reference model

Table 6.32: Relationship between: (a)  $\gamma_6$  and  $\beta_6$ ; and (b)  $\lambda_6$  and  $\beta_6$  for solid collars

No.	$\beta_6$	$\gamma_o$	$(\beta_8)_{\max}$	$\gamma_6$	$\lambda_6$
1	10	0.12	$294 \times 10^{-6}$	1	1.0181
2	11	0.12	$339 \times 10^{-6}$	1	1.0000
3	12	0.12	$382 \times 10^{-6}$	1	0.9841
4	14	0.12	$427 \times 10^{-6}$	1	0.9569
5	16	0.12	$441 \times 10^{-6}$	1	0.9388
6	18	0.12	$475 \times 10^{-6}$	1	0.9184
7	20	0.12	$515 \times 10^{-6}$	1	0.9048

Note: Model No. 2 is the reference model

Table 6.33: Detail of finite element models to study the effect of collar smearing on the confining behaviour of solid collars

No.	$h_{column}$ (mm)	$A_{column}$ (mm <sup>2</sup> )	$I_{column}$ (mm <sup>4</sup> )	$A_{collar}$ (mm <sup>2</sup> )	$I_{collar}$ (mm <sup>4</sup> )	$s$ (mm)	$\beta_1$	$\beta_2$	$\beta_3$
1	500	250 000	5.208x10 <sup>9</sup>	635.4	8.274x10 <sup>5</sup>	10.42	2.5417x10 <sup>-3</sup>	0.1588x10 <sup>-3</sup>	20.833x10 <sup>-3</sup>
2	500	250 000	5.208x10 <sup>9</sup>	1271	1.655x10 <sup>6</sup>	20.83	5.0833x10 <sup>-3</sup>	0.3177x10 <sup>-3</sup>	41.667x10 <sup>-3</sup>
3	500	250 000	5.208x10 <sup>9</sup>	2604	3.391x10 <sup>6</sup>	41.67	10.417x10 <sup>-3</sup>	0.6510x10 <sup>-3</sup>	83.333x10 <sup>-3</sup>
4	500	250 000	5.208x10 <sup>9</sup>	5208	6.782x10 <sup>6</sup>	83.33	20.833x10 <sup>-3</sup>	1.3021x10 <sup>-3</sup>	166.67x10 <sup>-3</sup>
5	500	250 000	5.208x10 <sup>9</sup>	6510	8.477x10 <sup>6</sup>	104.17	26.042x10 <sup>-3</sup>	1.6276x10 <sup>-3</sup>	208.33x10 <sup>-3</sup>
6	500	250 000	5.208x10 <sup>9</sup>	7813	10.17x10 <sup>6</sup>	125.00	31.250x10 <sup>-3</sup>	1.9531x10 <sup>-3</sup>	250.00x10 <sup>-3</sup>

Note: Model No. 4 is the reference model

Table 6.34: Relationship between: (a)  $\gamma_s$  and  $\beta_3$ ; and (b)  $\lambda_s$  and  $\beta_3$  for solid collars

No.	$\beta_3$	$\gamma_o$	$(\beta_8)_{\max}$	$\gamma_s$	$\lambda_s$
1	$20.83 \times 10^{-3}$	0.12	$398.22 \times 10^{-6}$	1	0.8889
2	$41.67 \times 10^{-3}$	0.12	$418.03 \times 10^{-6}$	1	0.9331
3	$83.33 \times 10^{-3}$	0.12	$434.79 \times 10^{-6}$	1	0.9705
4	$166.67 \times 10^{-3}$	0.12	$448.00 \times 10^{-6}$	1	1.0000
5	$208.33 \times 10^{-3}$	0.12	$452.67 \times 10^{-6}$	1	1.0104
6	$250.00 \times 10^{-3}$	0.12	$453.89 \times 10^{-6}$	1	1.0131

Note: Model No. 4 is the reference model

Table 6.35: Detail of finite element models to test the proposed equations for the confining behaviour of solid collars

No.	$h_{column}$ (mm)	$b_{collar}$ (mm)	$h_{collar}$ (mm)	$s$ (mm)	$f_y$ (MPa)	$E_s$ (MPa)	$n$
1	250	25	75	45	430	203 250	11
2	325	25	75	45	430	203 250	11
3	350	25	80	60	500	202 000	12
4	350	25	80	65	500	203 250	12
5	400	50	85	100	520	202 000	12
6	400	50	85	100	520	202 000	12
7	450	50	85	100	520	202 000	12
8	500	50	85	100	520	202 000	12
9	600	50	85	100	520	202 000	12
10	700	50	85	100	520	202 000	12

Table 6.36: Coefficients of multiple determinations  $R^2$  up to various level of lateral strains for column confined by solid collars

Cases	$R^2$			
	$\beta_7 = 0.06$	$\beta_7 = 0.05$	$\beta_7 = 0.04$	$\beta_7 = 0.03$
1	0.9834	0.9911	0.9950	0.9960
2	0.9879	0.9917	0.9924	0.9910
3	0.9959	0.9955	0.9948	0.9949
4	0.9919	0.9909	0.9905	0.9917
5	0.9960	0.9974	0.9975	0.9970
6	0.9728	0.9724	0.9743	0.9798
7	0.9977	0.9983	0.9982	0.9979
8	0.9978	0.9984	0.9984	0.9981
9	0.9941	0.9963	0.9977	0.9982
10	0.9798	0.9851	0.9892	0.9921

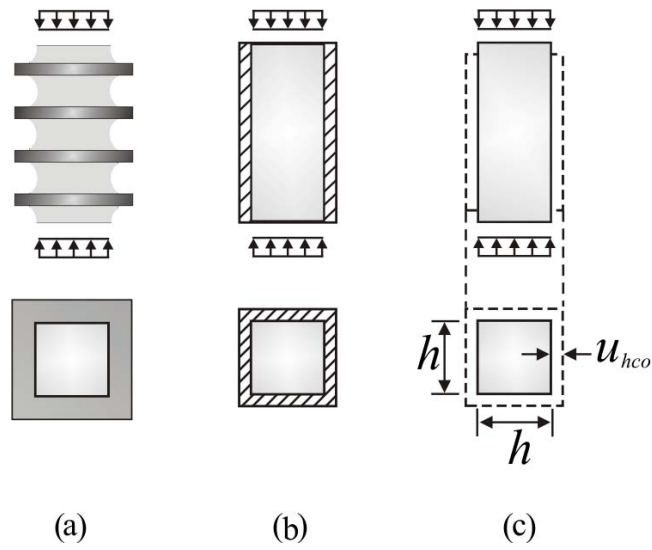


Figure 6-1: Confinement mechanism

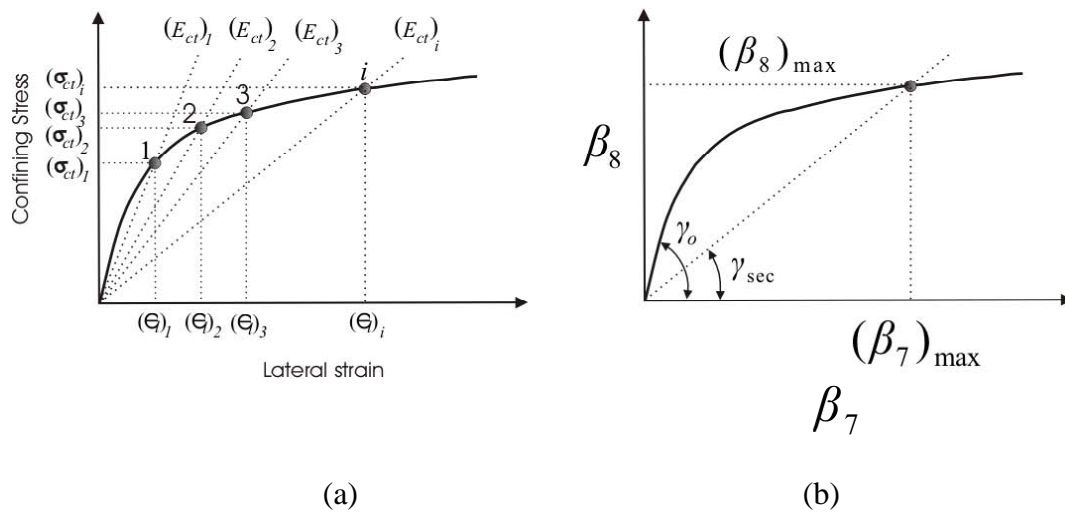


Figure 6-2: (a) Typical confining stress vs lateral strain curves; (b) relationship between  $\beta_7$  and  $\beta_8$

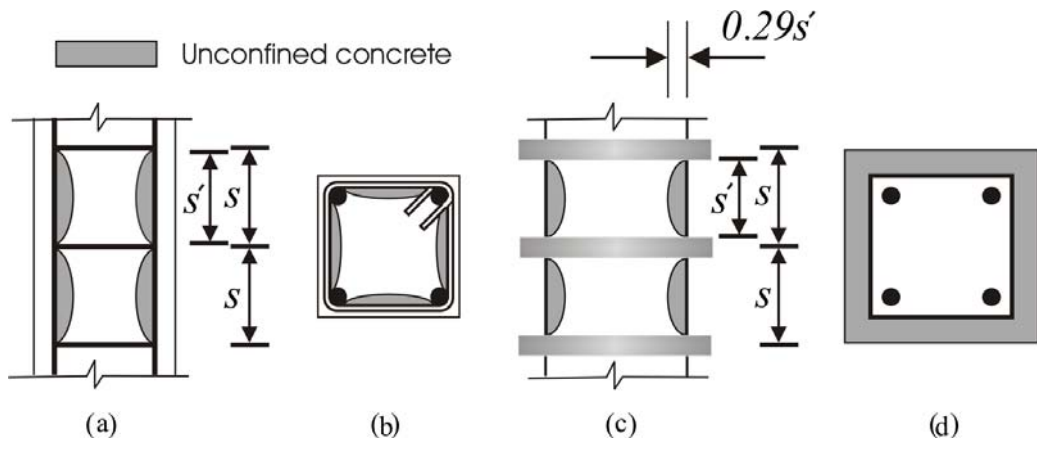


Figure 6-3: Unconfined concrete: (a) between tie levels; (b) at tie level; (c) between collars; and (d) at collar level (fully confined)

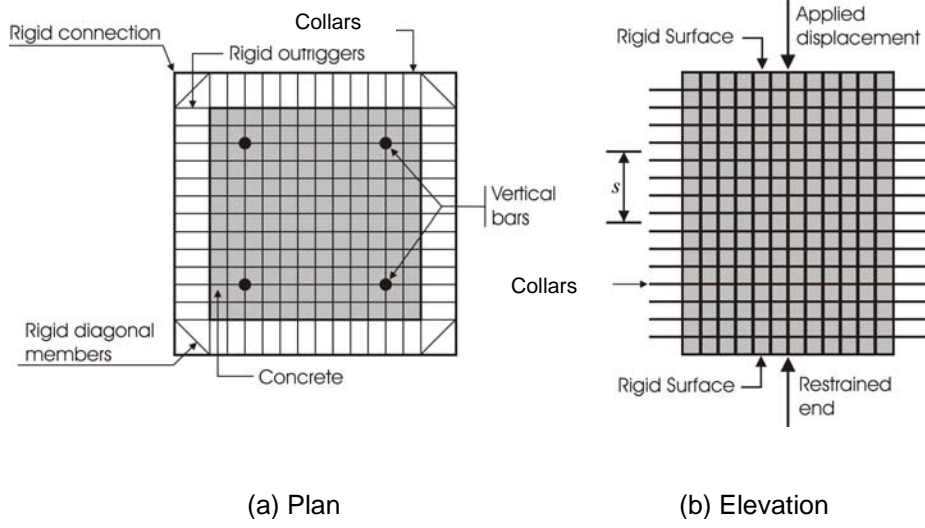


Figure 6-4: Plan and elevation of a typical finite element model for a column confined externally by steel collars

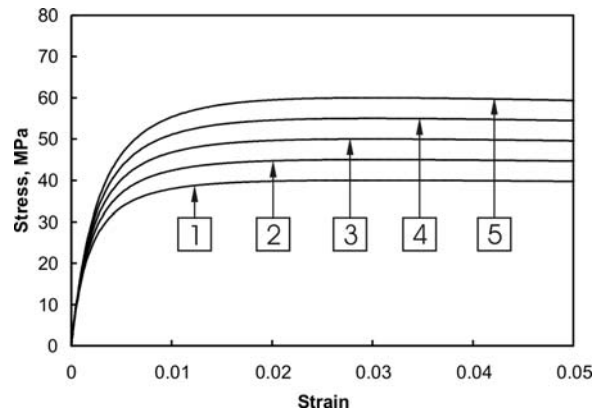


Figure 6-5: Concrete material curves without descending branches

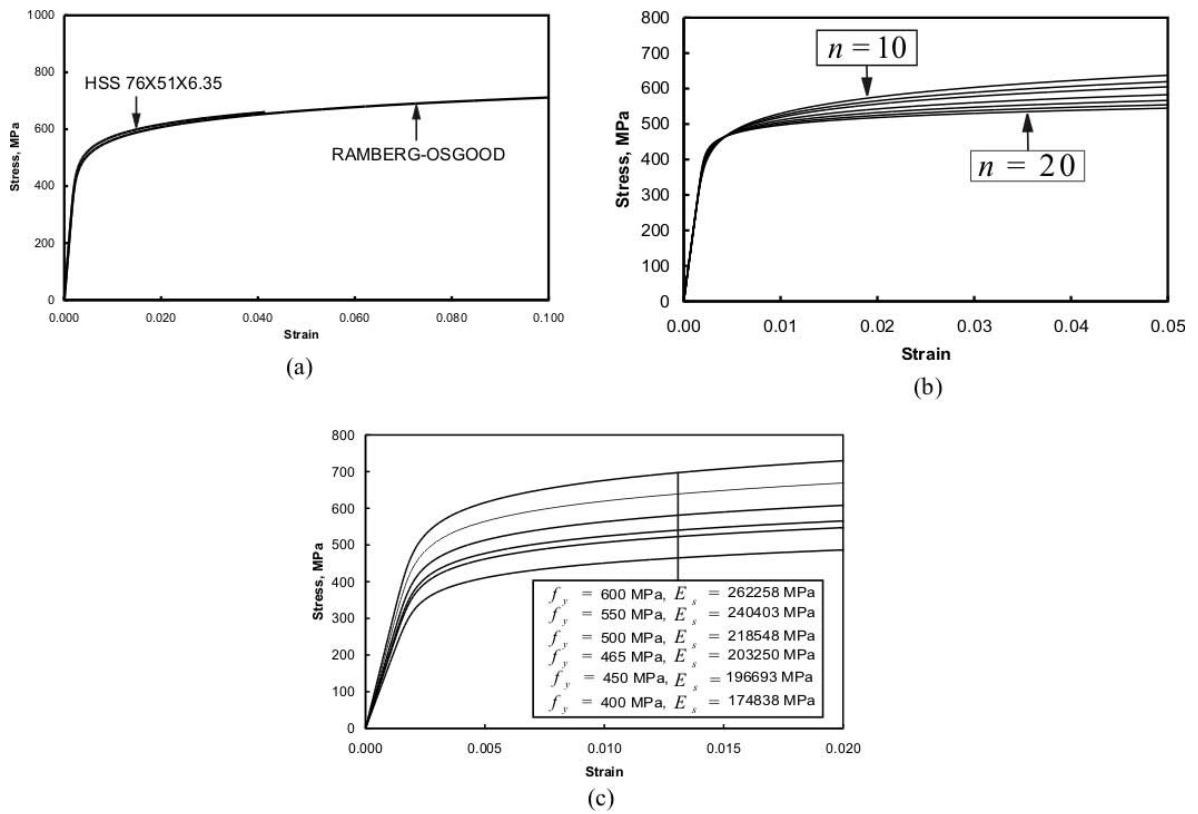


Figure 6-6: (a) Calibration of Ramberg-Osgood model; (b) variation of  $n$  keeping  $f_y$  and  $E_s$  constant; and (c) variation of  $f_y$  and  $E_s$  such that their ratio remains constant at constant value of  $n$

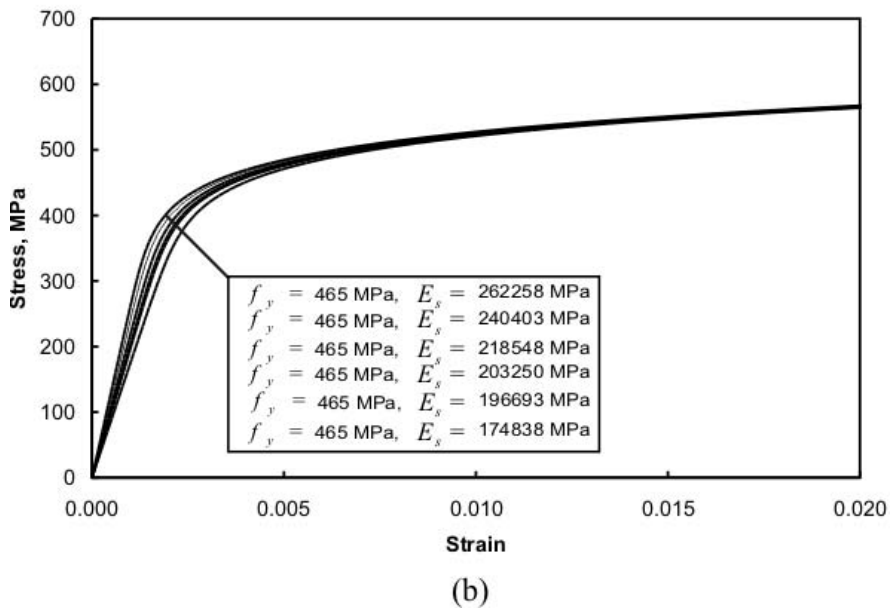
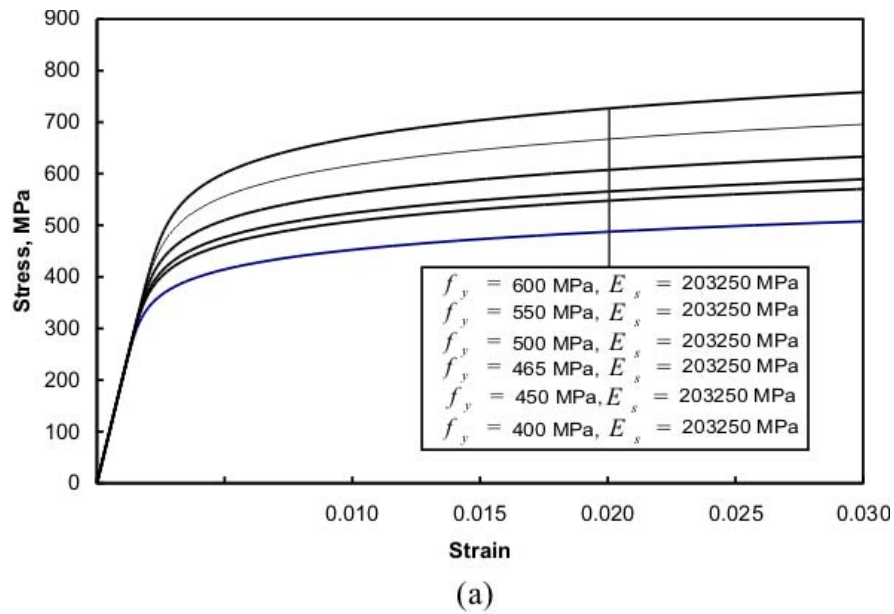
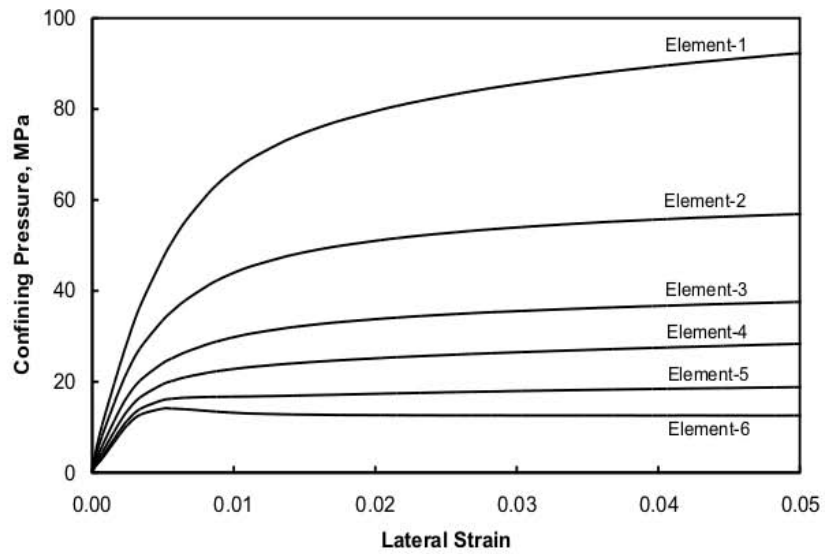
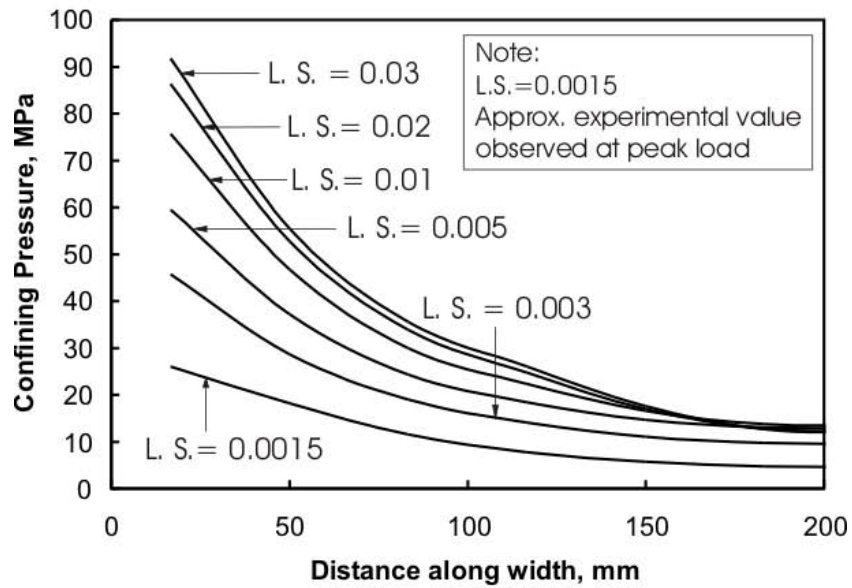


Figure 6-7: HSS steel material curves: (a) having different values of  $f_y$  keeping  $E_s$  and  $n$  constant; and (b) having different values of  $E_s$  keeping  $f_y$  and  $n$  constant.



(a)



(b)

Figure 6-8: (a) Average confining pressure on elements vs. average lateral strain; (b) Distribution of confining pressure along the width of the column

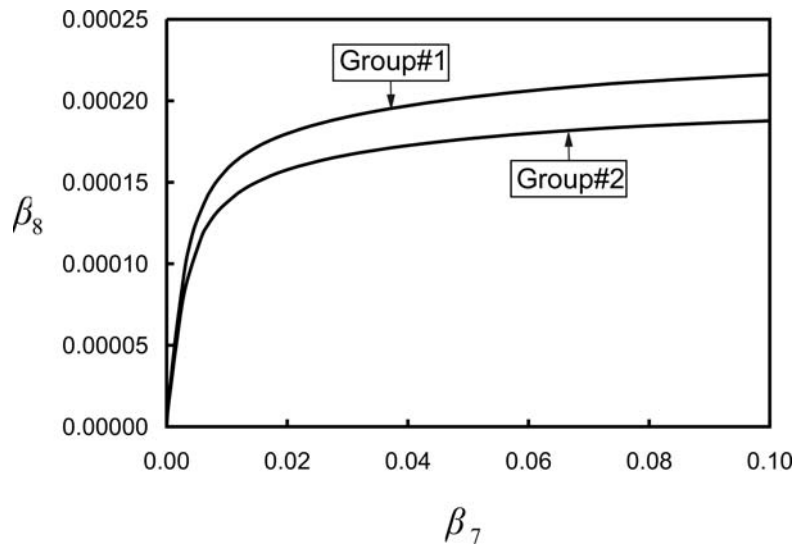


Figure 6-9 The dimensionless parameters independent of scale effect

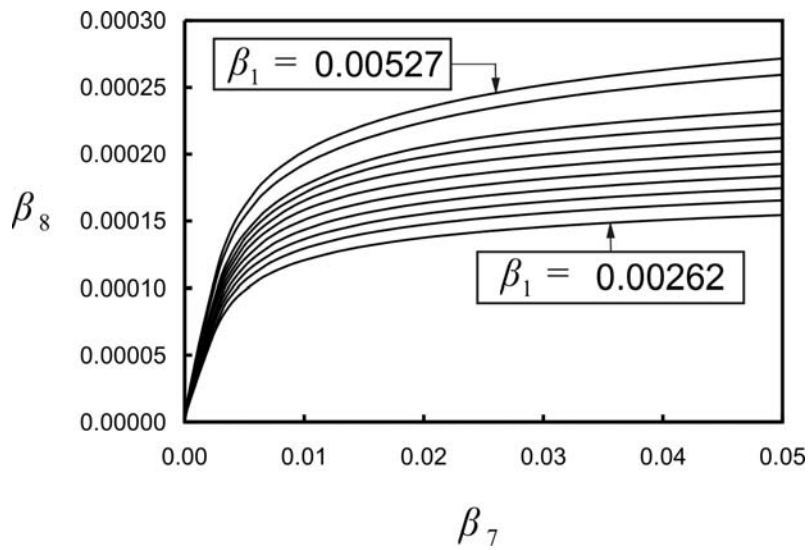
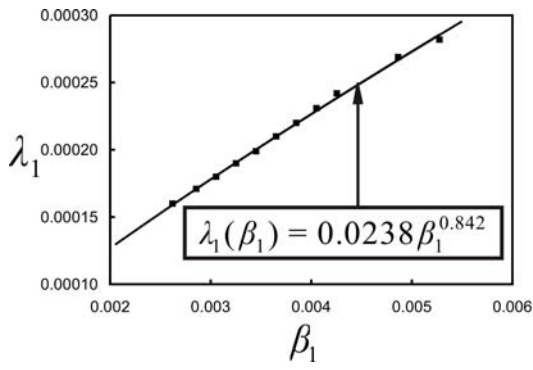
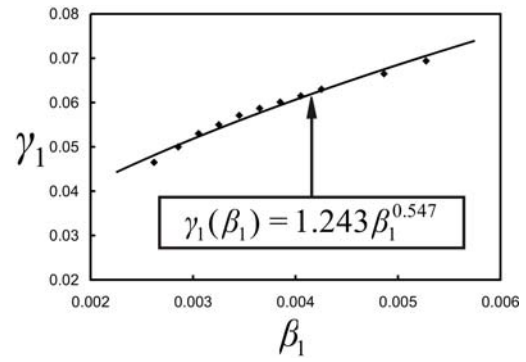


Figure 6-10: Effect of  $\beta_1$  on the confining behaviour



(a)



(b)

Figure 6-11: Relationship between: (a)  $\lambda_1$  and  $\beta_1$ ; and (b)  $\gamma_1$  and  $\beta_1$

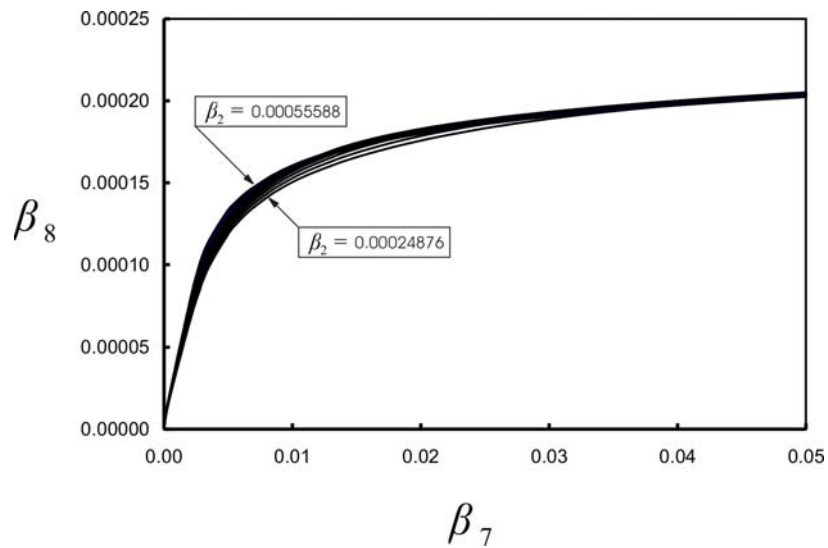


Figure 6-12: Effect of variation of  $\beta_2$  on the confining behaviour

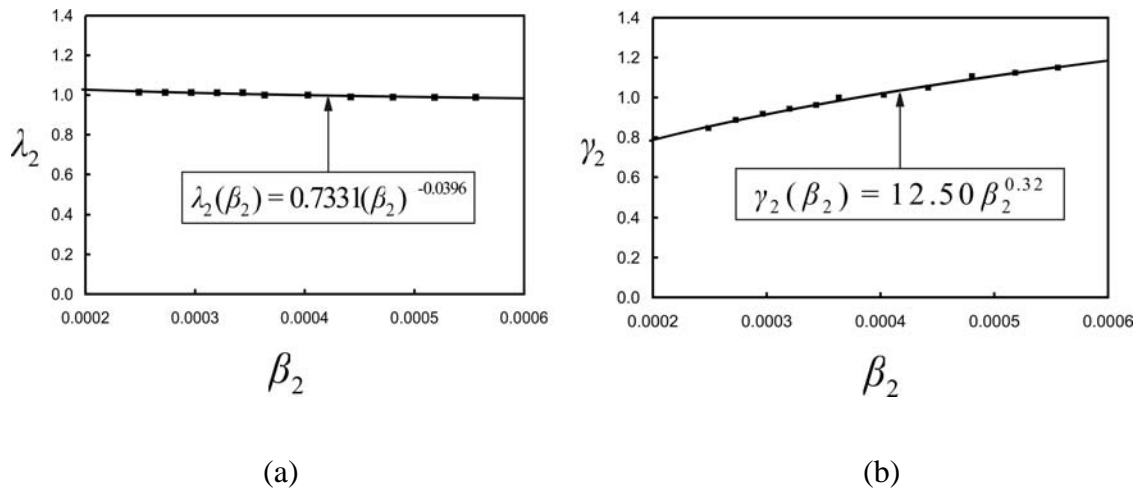


Figure 6-13: Relationship between: (a)  $\lambda_2$  and  $\beta_2$ ; and (b)  $\gamma_2$  and  $\beta_2$

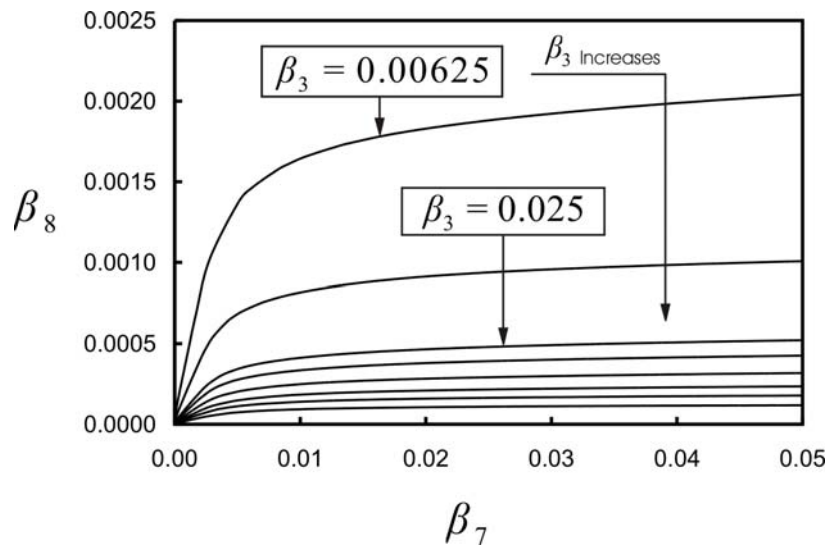


Figure 6-14: Effect of variation of  $\beta_3$  on the confining behaviour

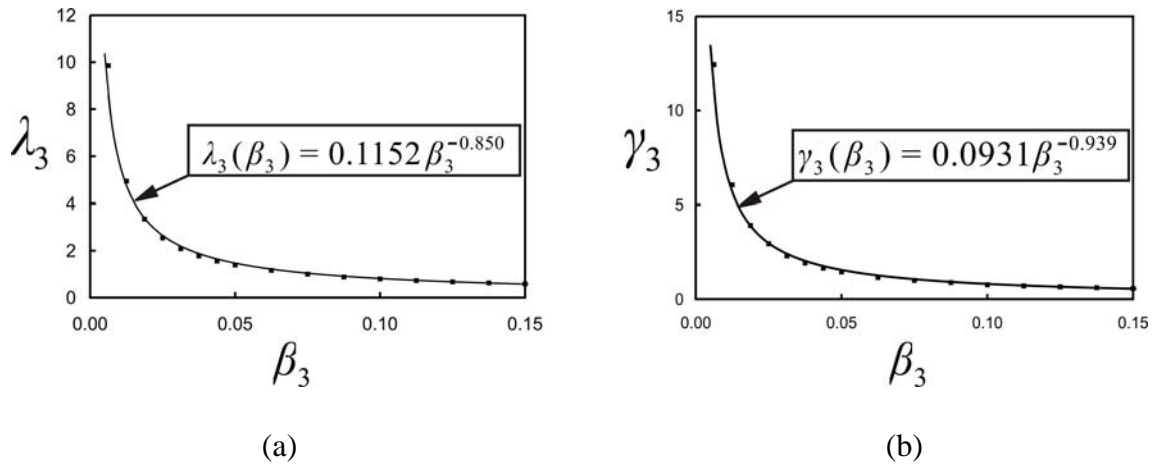


Figure 6-15: Relationship between: (a)  $\lambda_3$  and  $\beta_3$ ; (b)  $\gamma_3$  and  $\beta_3$

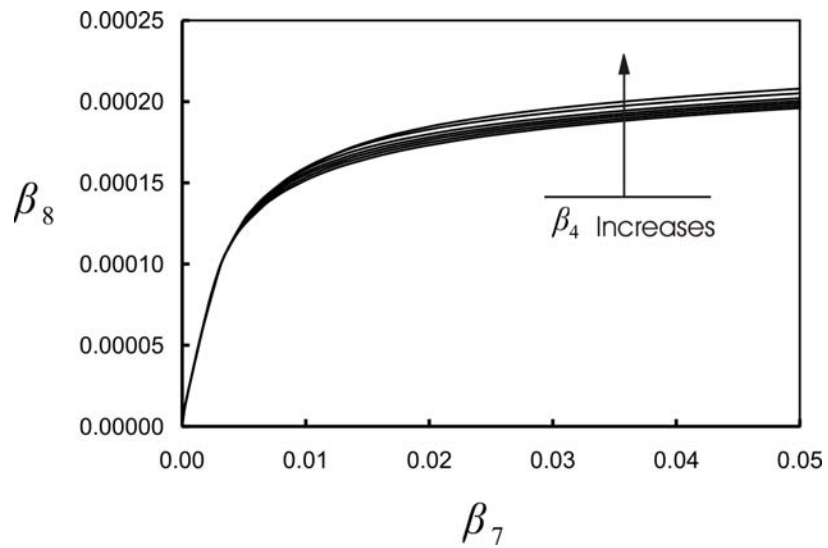


Figure 6-16: Effect of  $\beta_4$  on the confining behaviour

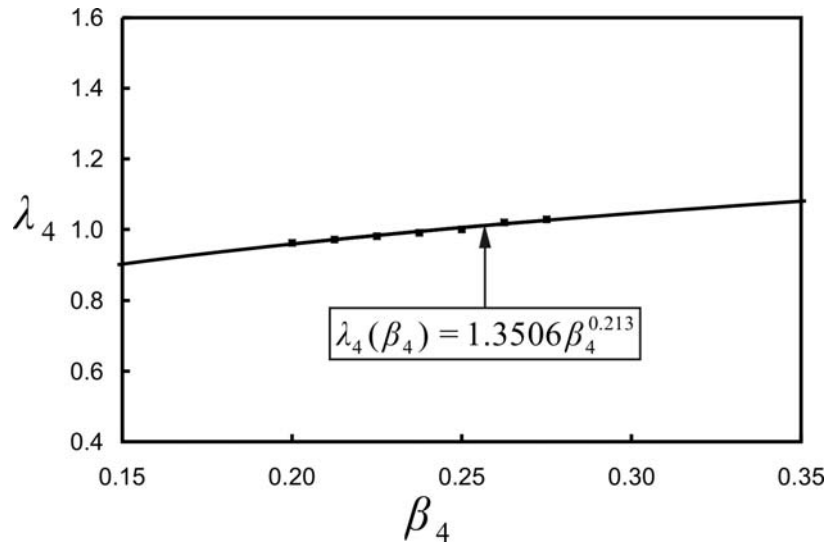


Figure 6-17: Relationship between  $\lambda_4$  and  $\beta_4$

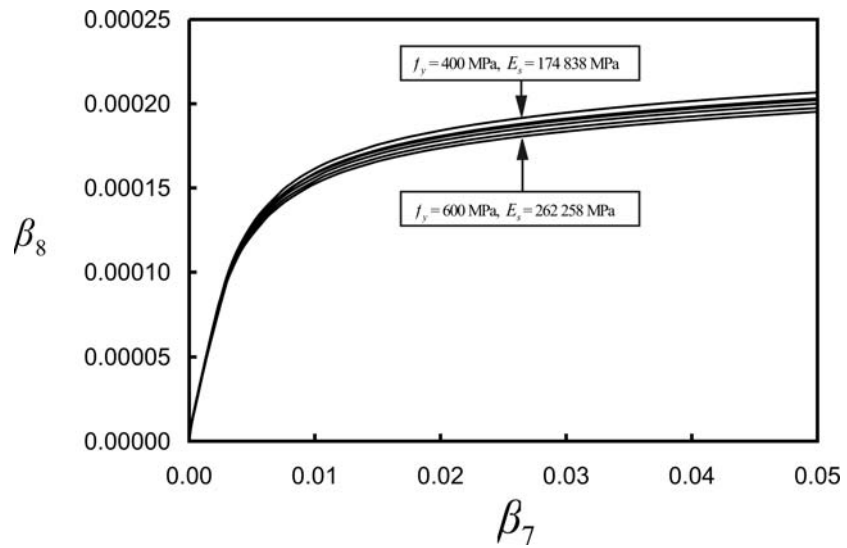


Figure 6-18: Effect of variation of  $f_y$  and  $E_s$  such that  $\beta_5$  remains constant

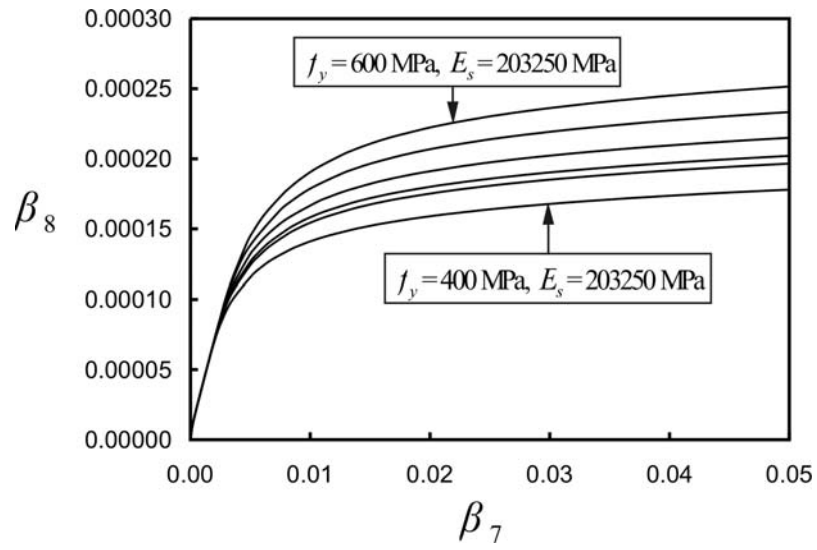


Figure 6-19: Effect of variation of  $f_y$  keeping  $E_s$  constant on the confining behaviour

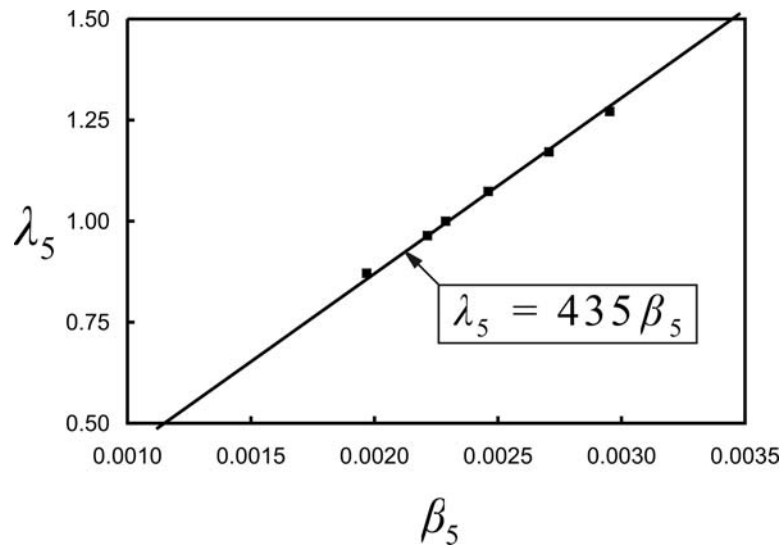


Figure 6-20: Relationship between  $\lambda_5$  and  $\beta_5$

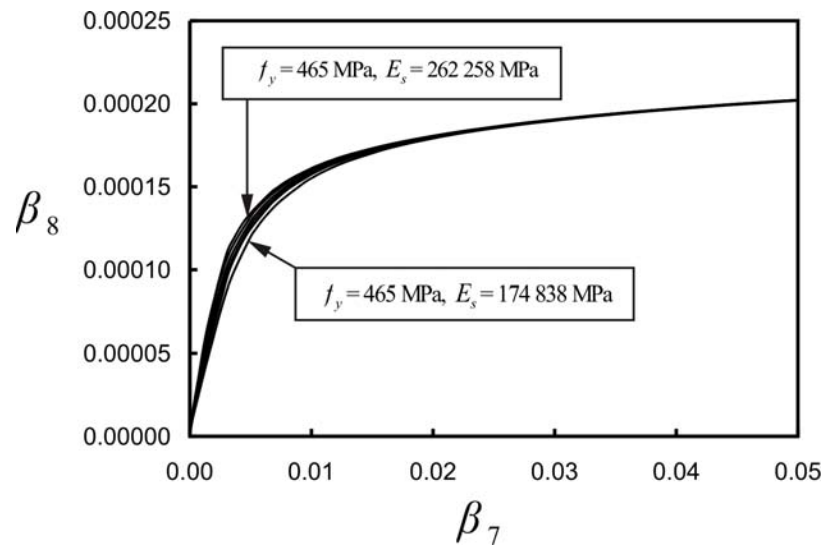


Figure 6-21: Effect of change of modulus of elasticity  $E_s$  keeping  $f_y$  constant on the confining behaviour

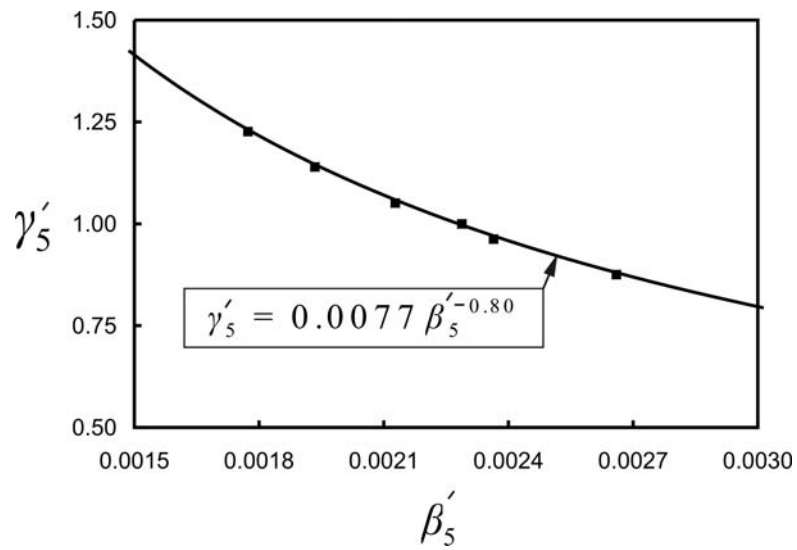


Figure 6-22: Relationship between  $\gamma_5$  and  $\beta_5$

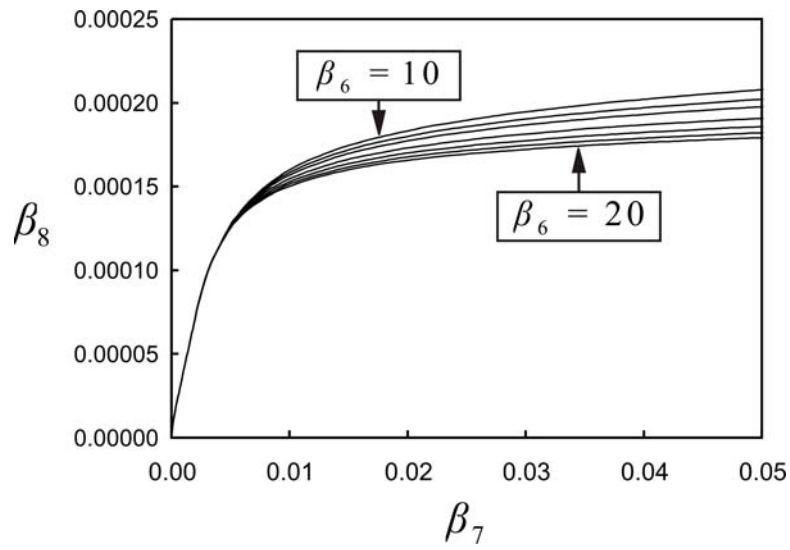


Figure 6-23: Effect of  $\beta_6$  on the confining behaviour of HSS collars

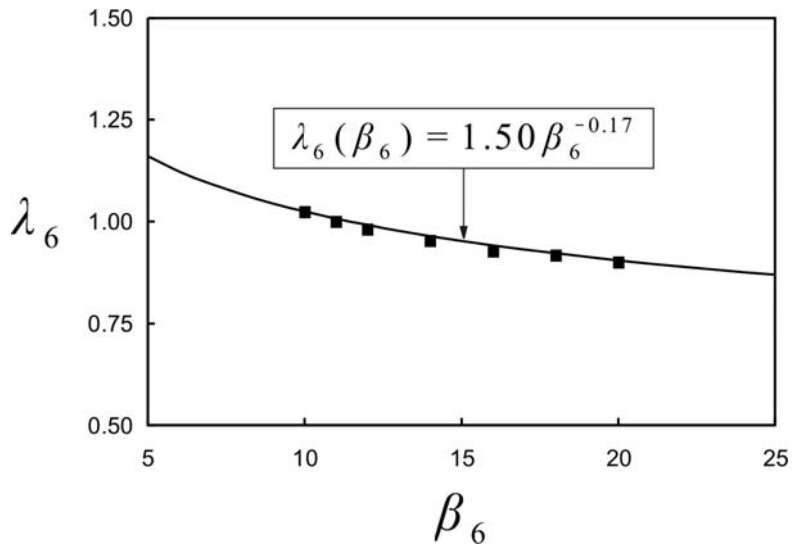


Figure 6-24: Relationship between  $\beta_6$  and  $\lambda_6$  for HSS collars

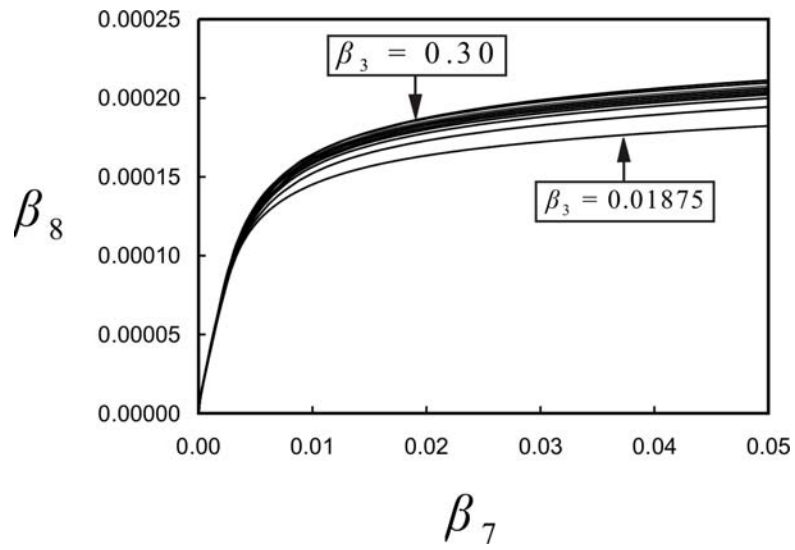


Figure 6-25: Effect of collar smearing on the confining of collars

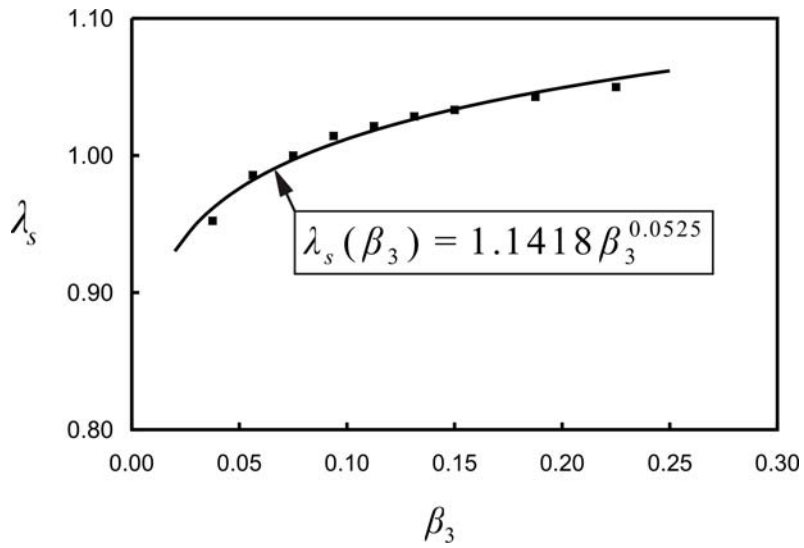


Figure 6-26: Relationship between  $\lambda_s$  and  $\beta_3$

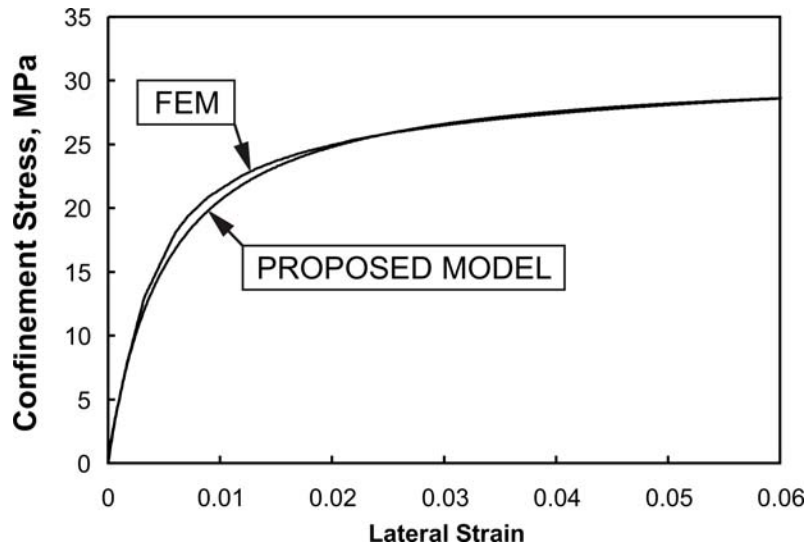


Figure 6-27: Confinement stress vs. lateral strain curves for case 1 (Table 6-20)

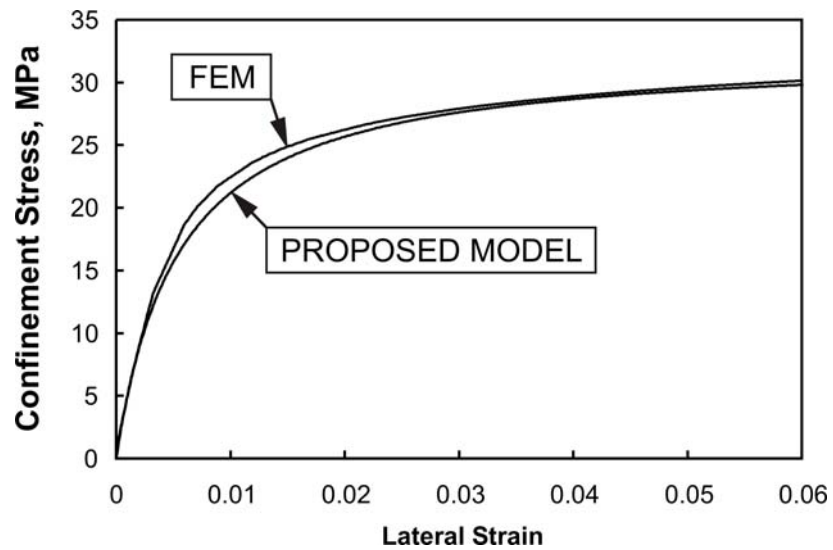


Figure 6-28: Confinement stress vs. lateral strain curves for case 2 (Table 6-20)

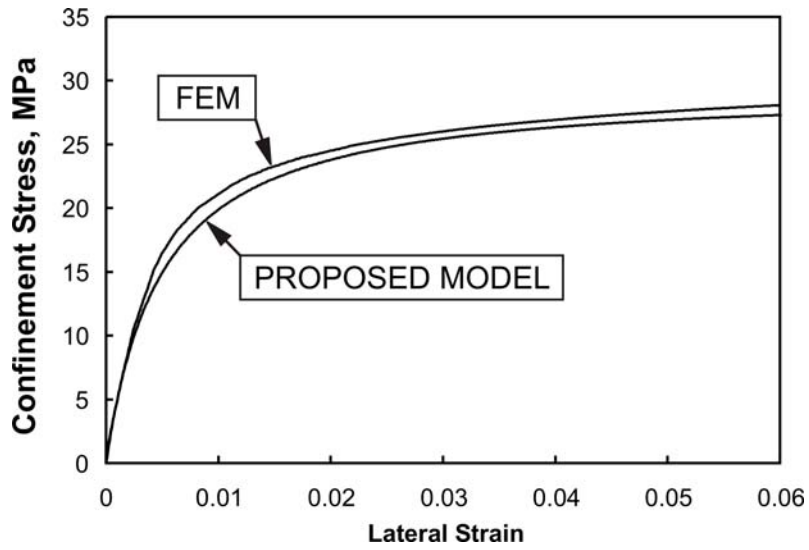


Figure 6-29: Confinement stress vs. lateral strain curves for case 3 (Table 6-20)

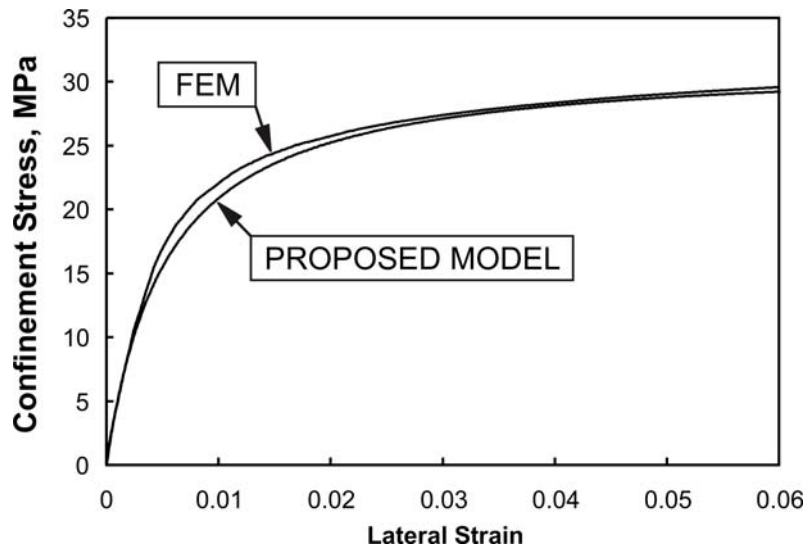


Figure 6-30: Confinement stress vs. lateral strain curves for case 4 (Table 6-20)

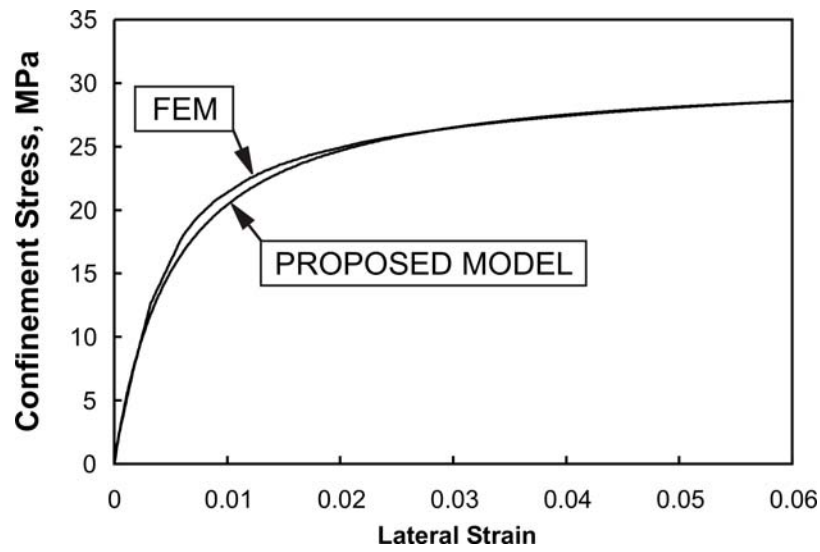


Figure 6-31: Confinement stress vs. lateral strain curves for case 5 (Table 6-20)

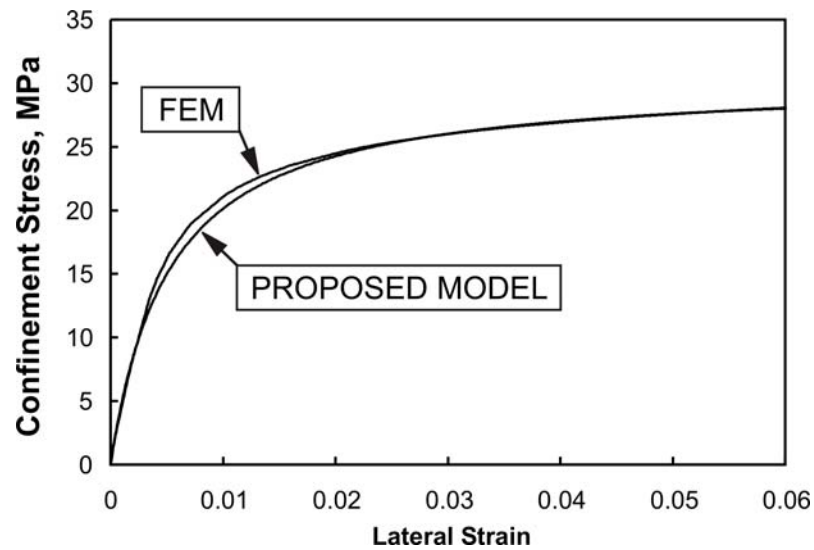


Figure 6-32: Confinement stress vs. lateral strain curves for case 6 (Table 6-20)

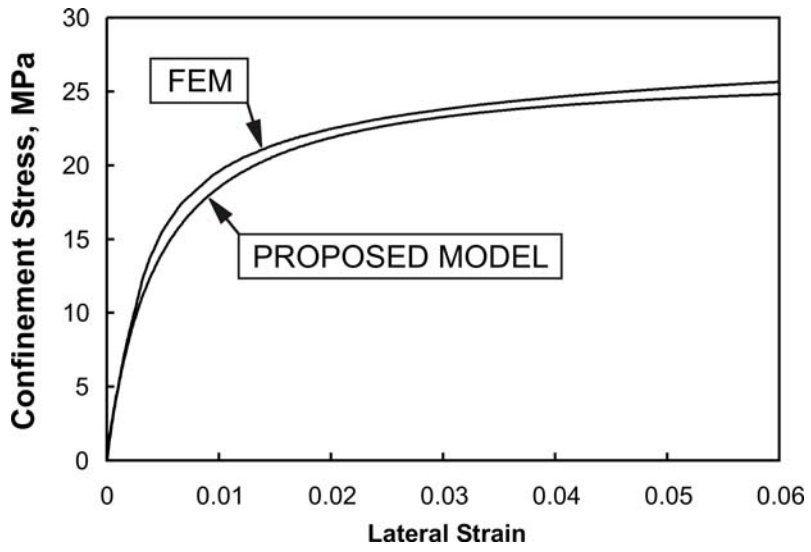


Figure 6-33: Confinement stress vs. lateral strain curves for case 7 (Table 6-20)

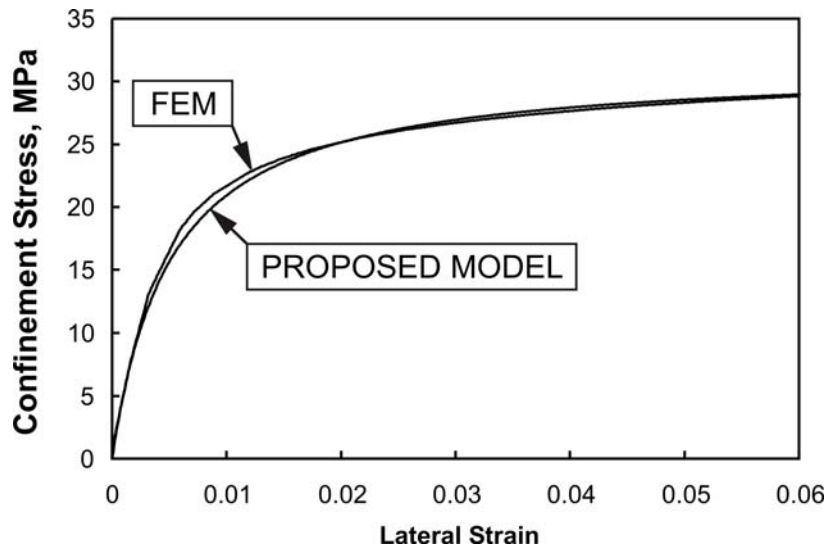


Figure 6-34: Confinement stress vs. lateral strain curves for case 8 (Table 6-20)

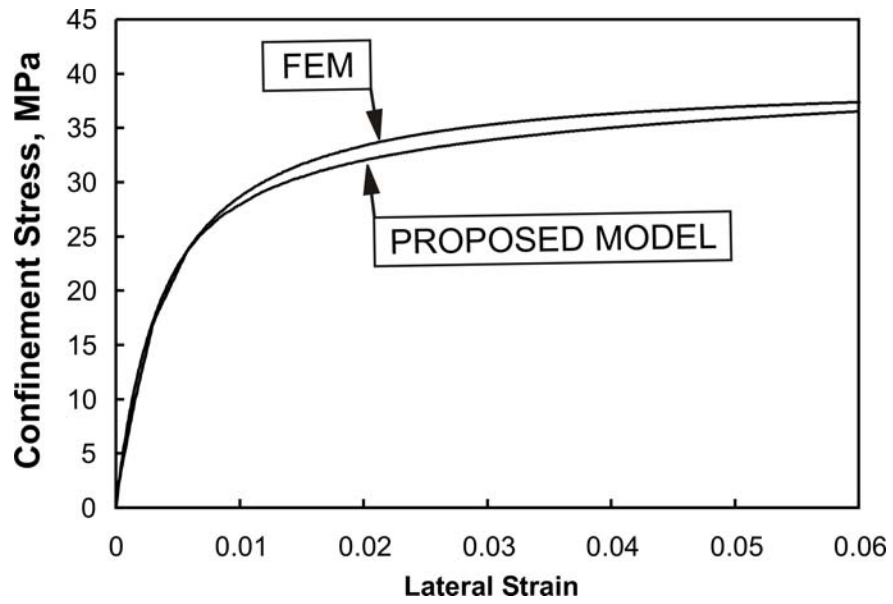


Figure 6-35: Confinement stress vs. lateral strain curves for case 9 (Table 6-20)

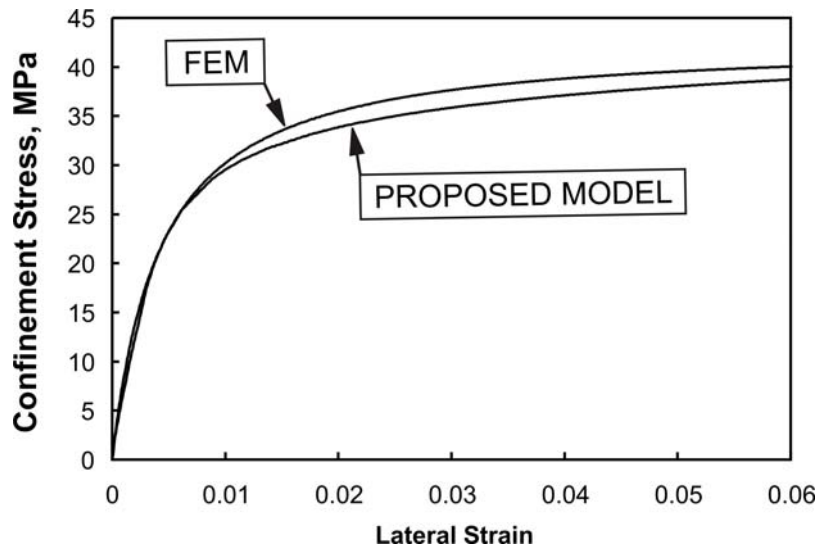


Figure 6-36: Confinement stress vs. lateral strain curves for case 10 (Table 6-20)

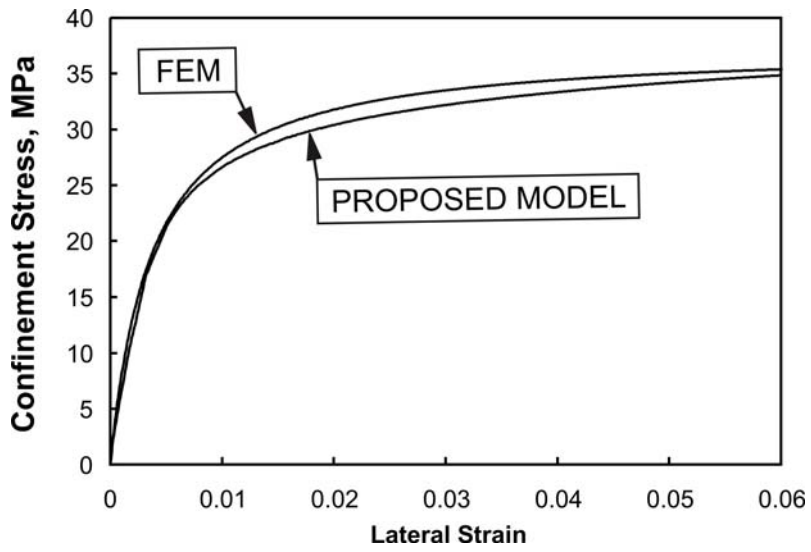


Figure 6-37: Confinement stress vs. lateral strain curves for case 11 (Table 6-20)

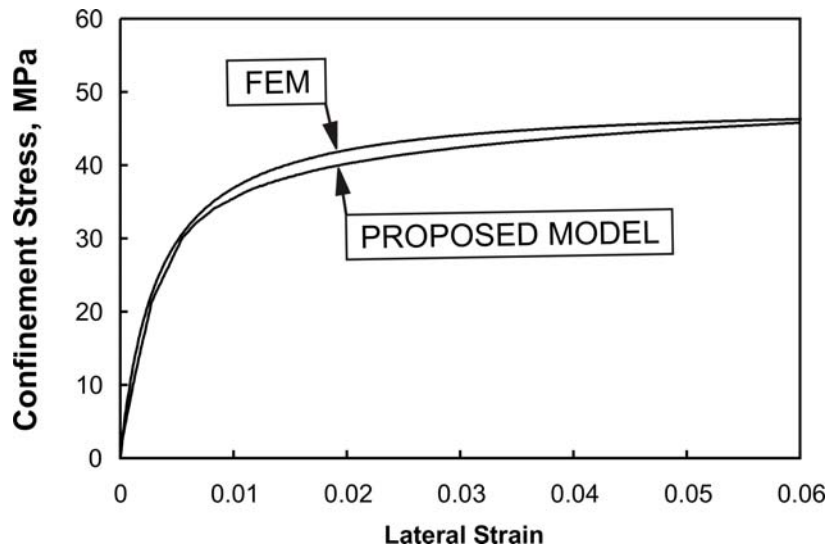


Figure 6-38: Confinement stress vs. lateral strain curves for case 12 (Table 6-20)

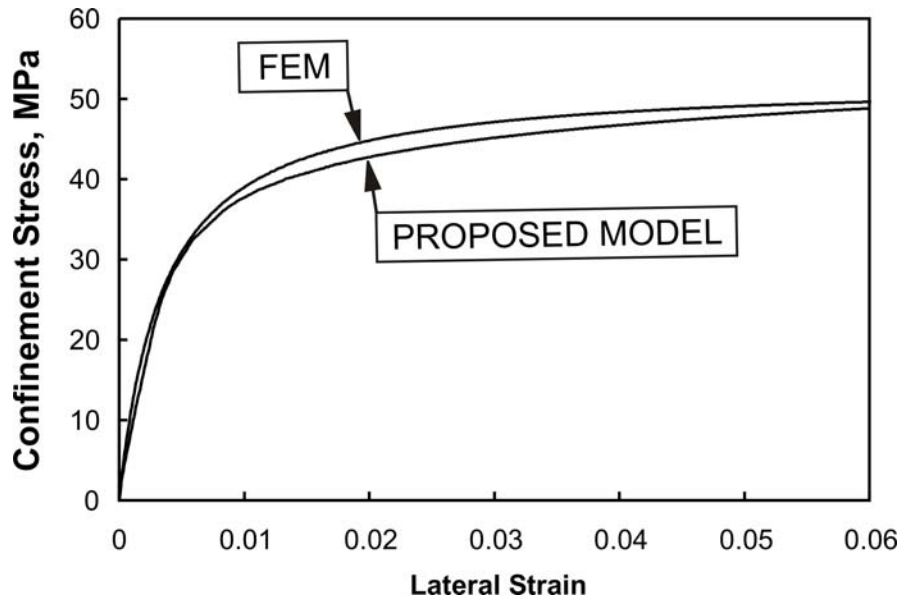


Figure 6-39: Confinement stress vs. lateral strain curves for case 13 (Table 6-20)

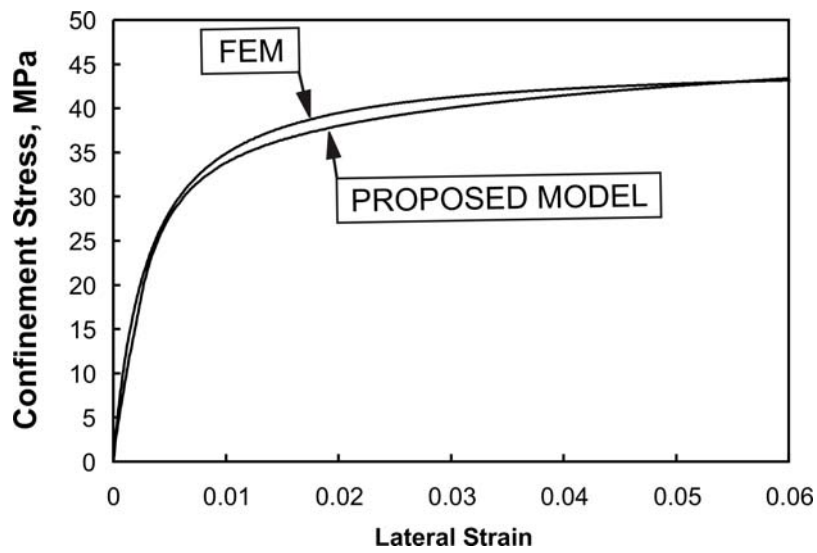


Figure 6-40: Confinement stress vs. lateral strain curves for case 14 (Table 6-20)

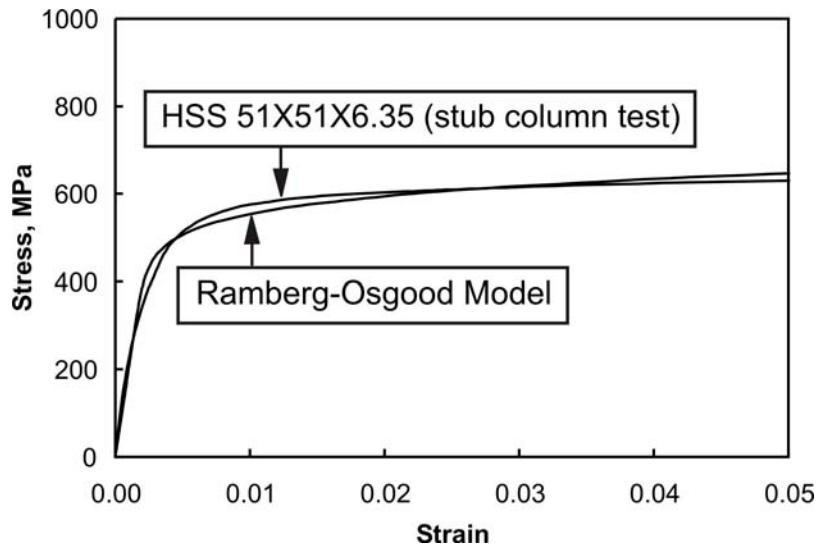


Figure 6-41: Stress vs. strain curve for HSS 51x51x6.35 mm

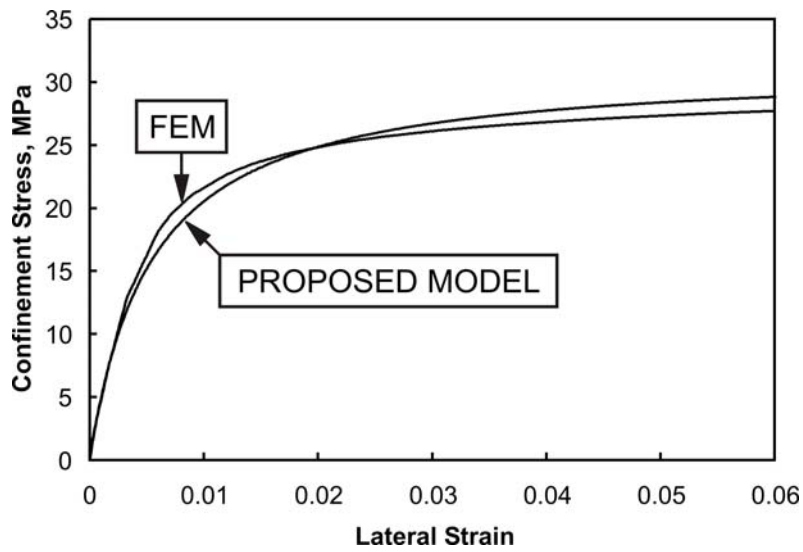


Figure 6-42: Confinement stress vs. lateral strain curves for column C06

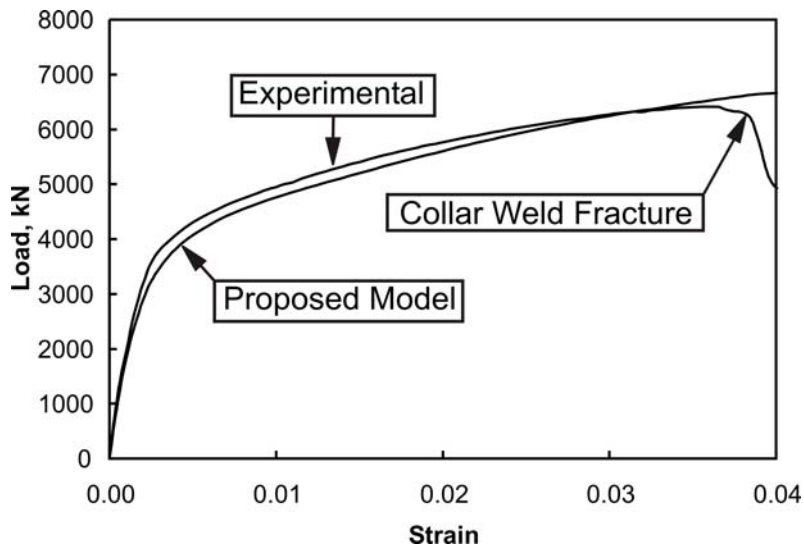


Figure 6-43: Load vs. strain curves for column C06

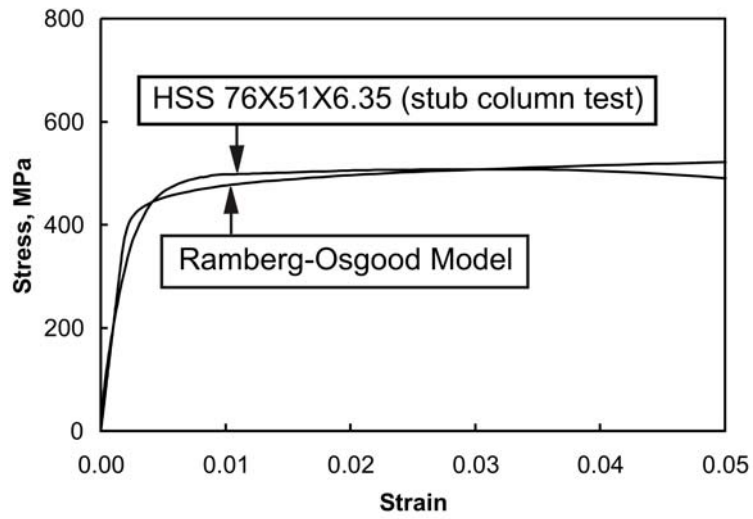


Figure 6-44: Stress vs. strain curve for HSS 76x51x6.35 mm

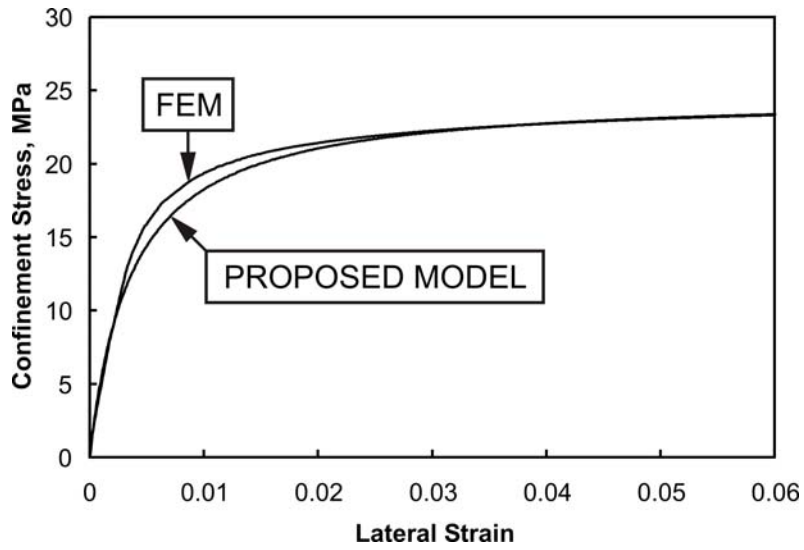


Figure 6-45: Confinement stress vs. lateral strain curves for column C09

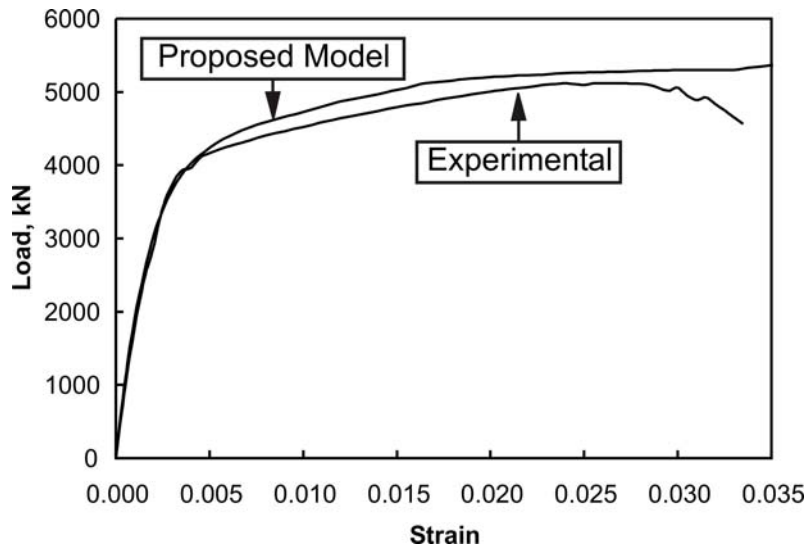


Figure 6-46: Load vs. strain curves of column C09

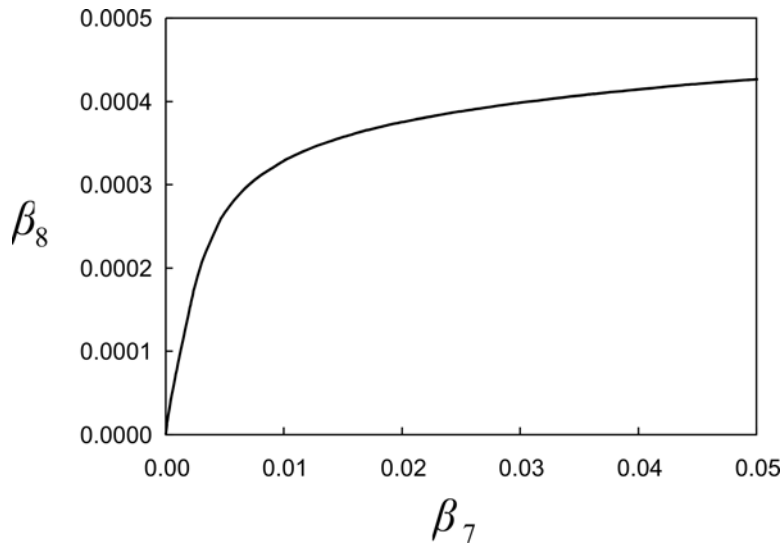


Figure 6-47: Effect of scale on the confining behaviour of solid collars

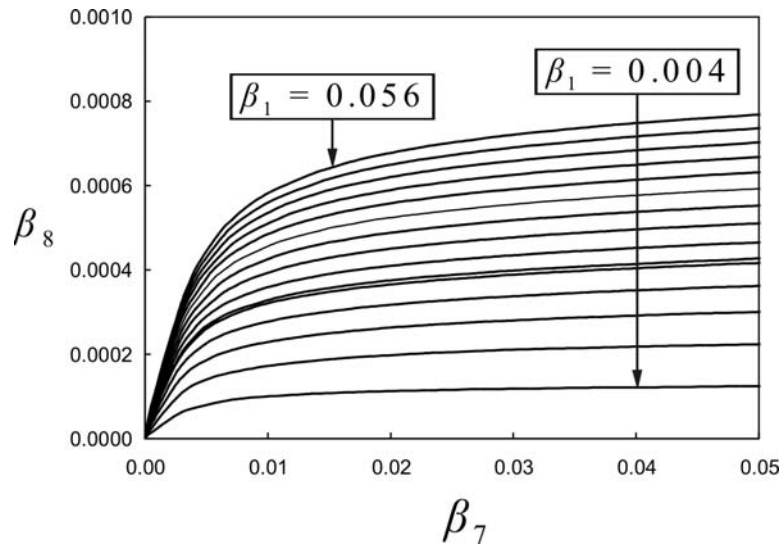
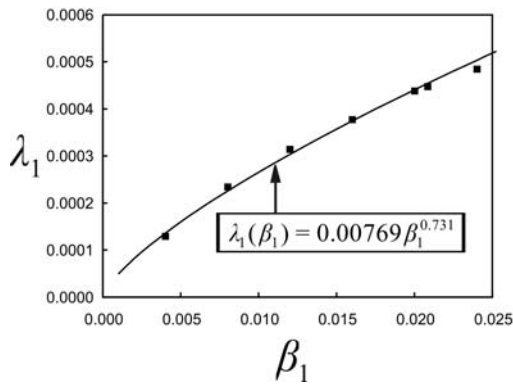
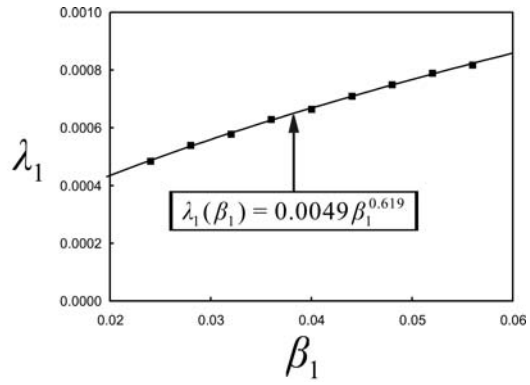


Figure 6-48: Effect of variation of  $\beta_1$  on the confining behaviour of solid collars

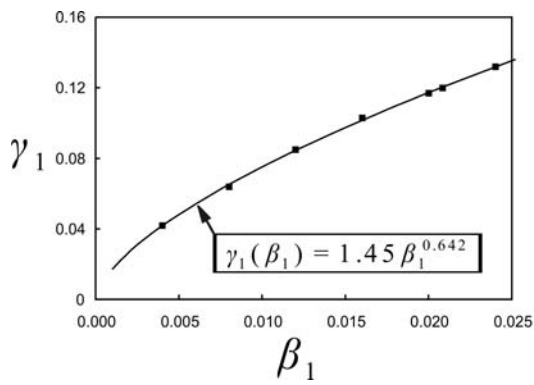


(a)

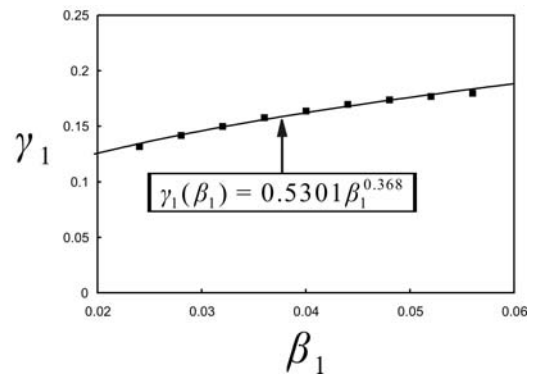


(b)

Figure 6-49 Relationship between  $\lambda_1$  and  $\beta_1$  for  $\beta_1$  ranges: (a)  $\beta_1 = 0.004$  to 0.024; and (b)  $\beta_1 = 0.024$  to 0.056.



(a)



(b)

Figure 6-50 Relationship between  $\gamma_1$  and  $\beta_1$  for  $\beta_1$  ranges: (a)  $\beta_1 = 0.004$  to 0.024; and (b)  $\beta_1 = 0.024$  to 0.056.

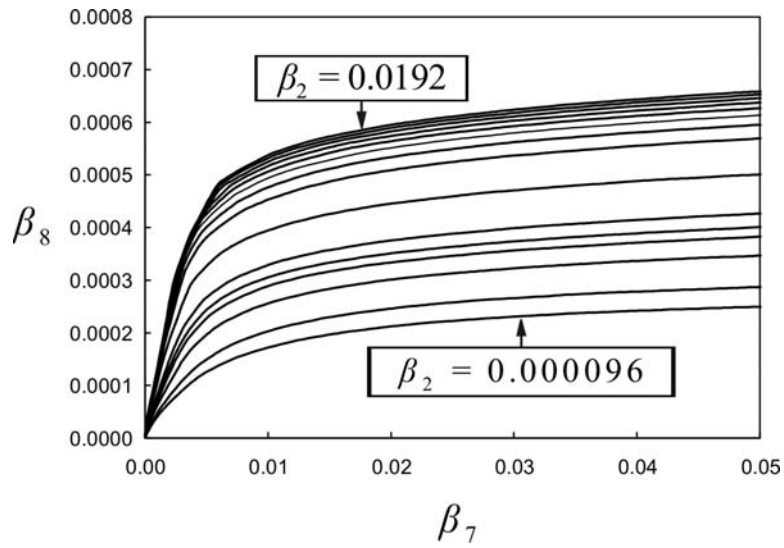


Figure 6-51 Effect of  $\beta_2$  on the confining behaviour of solid collars

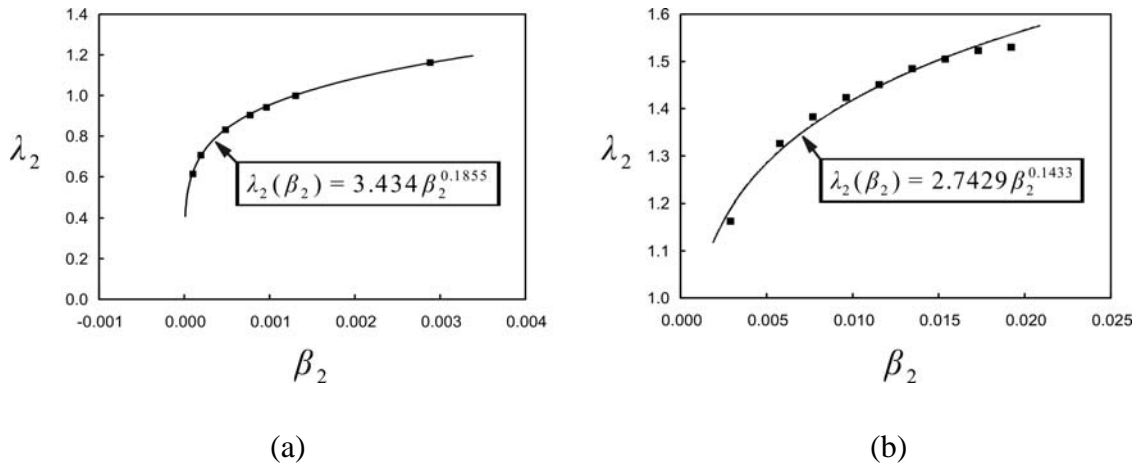
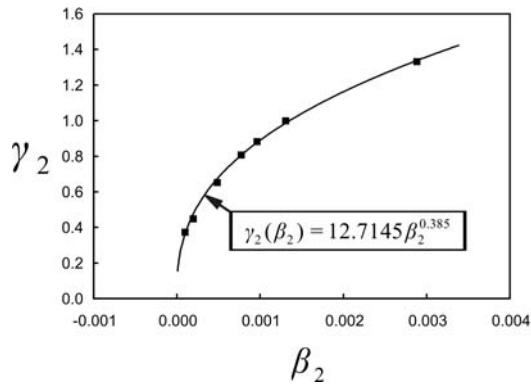
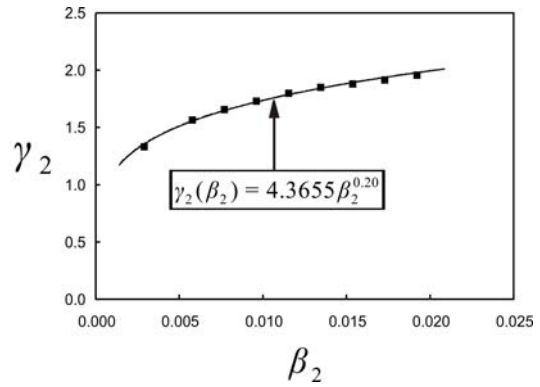


Figure 6-52: Relationship between  $\lambda_2$  and  $\beta_2$  for  $\beta_2$  ranges:  
 (a)  $\beta_2 = 0.000096$  to  $0.00288$ ; and (b)  $0.00288$  to  $0.0192$



(a)



(b)

Figure 6-53: Relationship between  $\gamma_2$  and  $\beta_2$  for  $\beta_2$  ranges:  
 (a)  $\beta_2 = 0.000096$  to  $0.00288$ ; and (b)  $0.00288$  to  $0.0192$

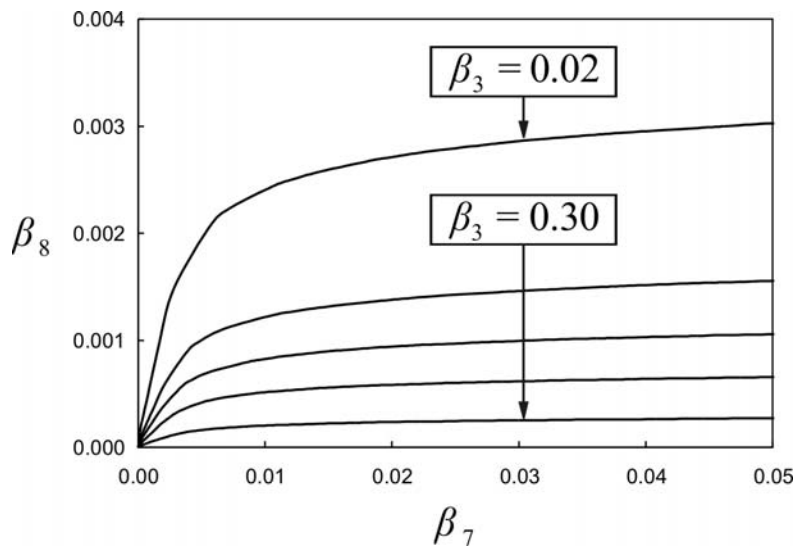
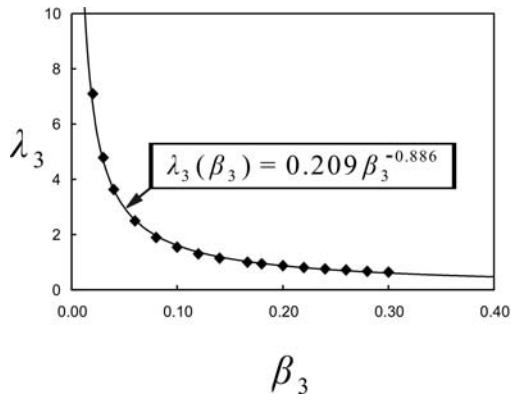
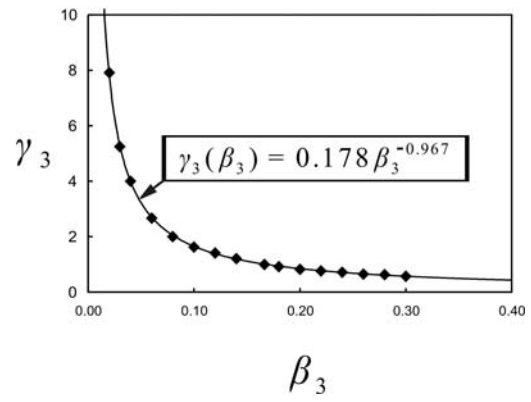


Figure 6-54: Effect of  $\beta_3$  on the confining behaviour of solid collars



(a)



(b)

Figure 6-55: Relationship between: (a)  $\lambda_3$  and  $\beta_3$  and (b)  $\gamma_3$  and  $\beta_3$  for solid collars

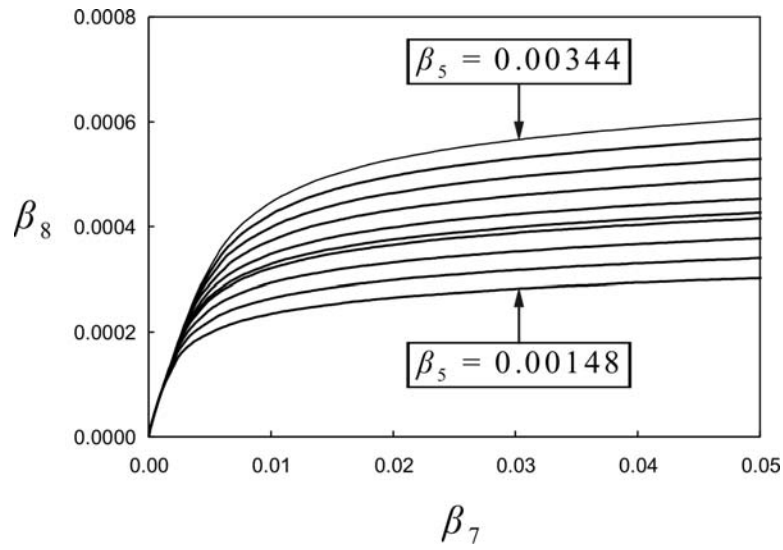


Figure 6-56: Effect of variation of  $\beta_5$  on the confining behaviour of solid collars

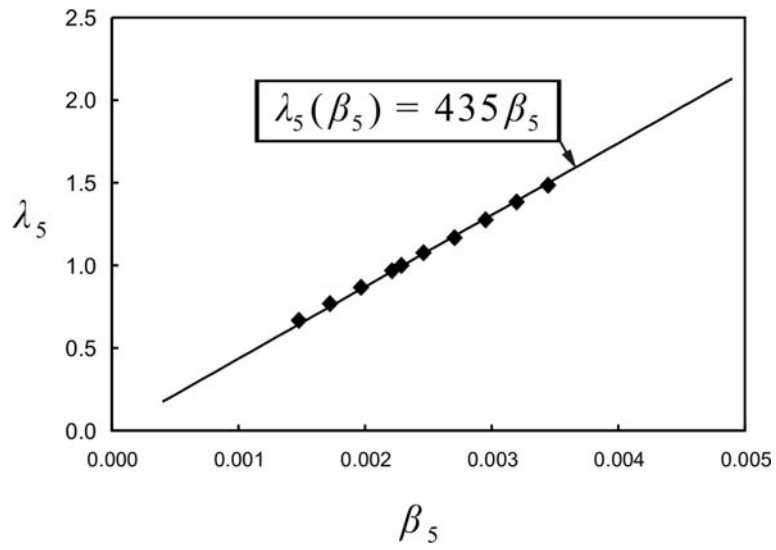


Figure 6-57: Relationship between  $\lambda_5$  and  $\beta_5$  for solid collars

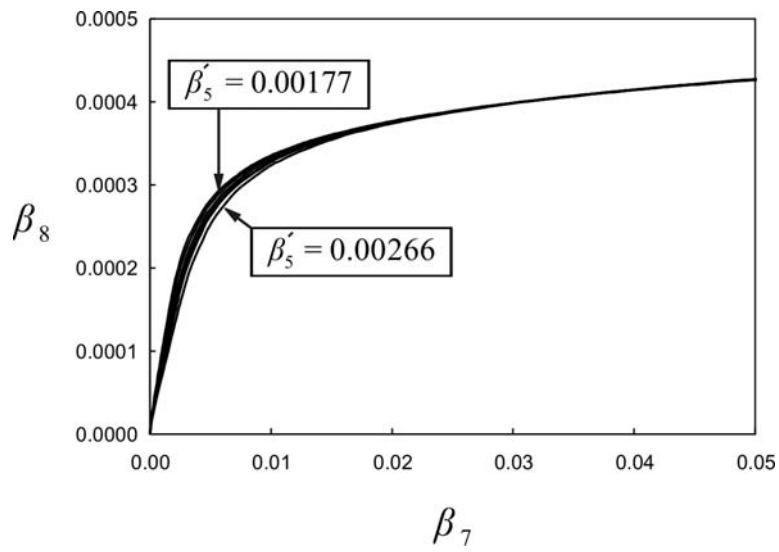


Figure 6-58: Effect of variation of  $\beta_5$  on the confining behaviour of solid collars

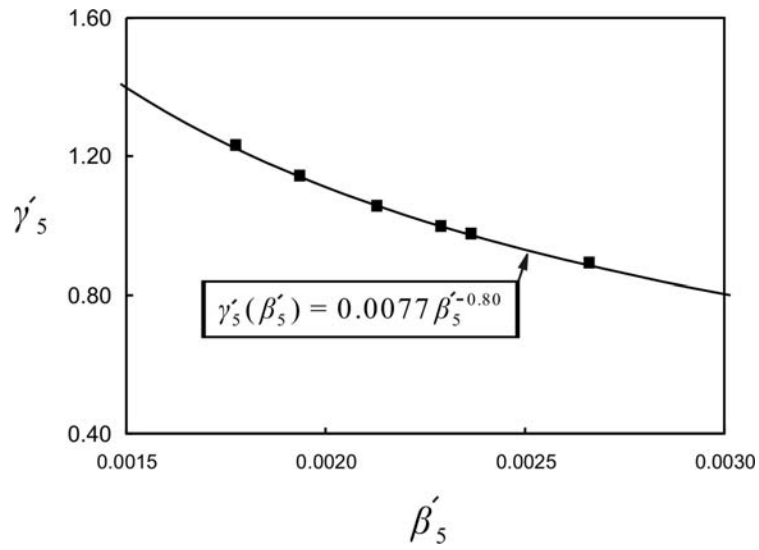


Figure 6-59: Relationship between  $\gamma_5$  and  $\beta_5$  for solid collars

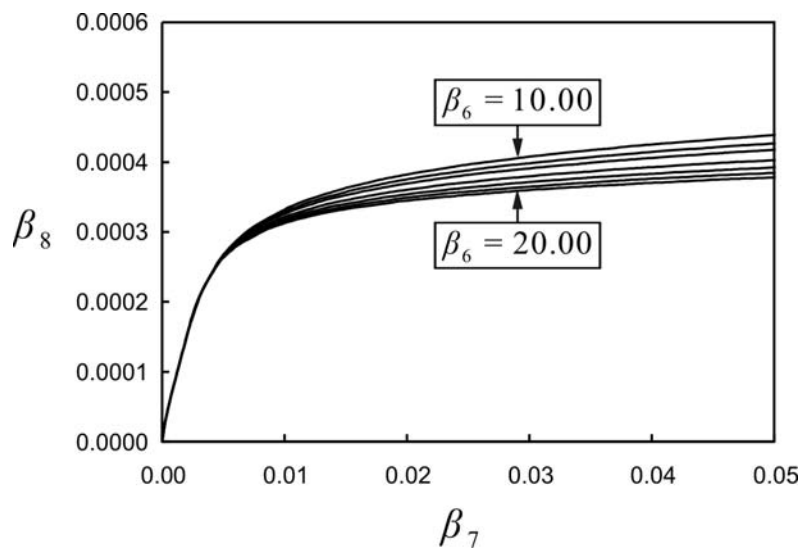


Figure 6-60: Effect of variation of  $\beta_6$  on the confining behaviour of solid collars

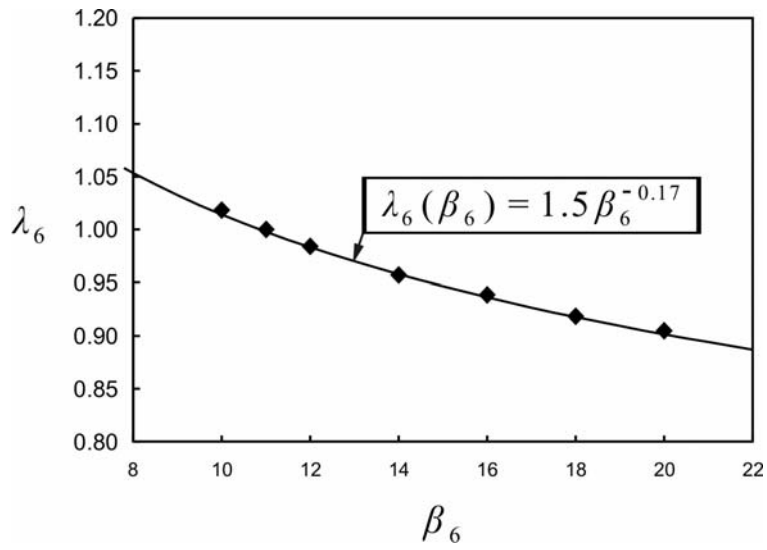


Figure 6-61: Relationship between  $\lambda_6$  and  $\beta_6$  for solid collars

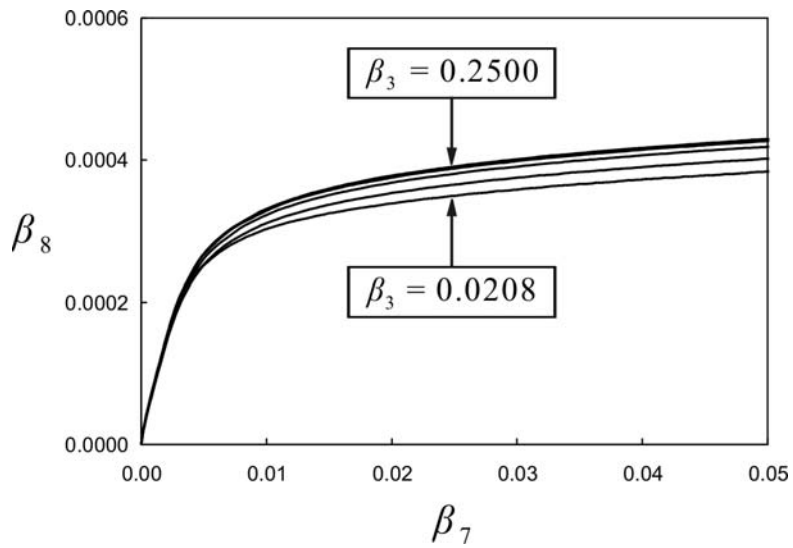


Figure 6-62: Effect of smearing on the confining behaviour of solid collars

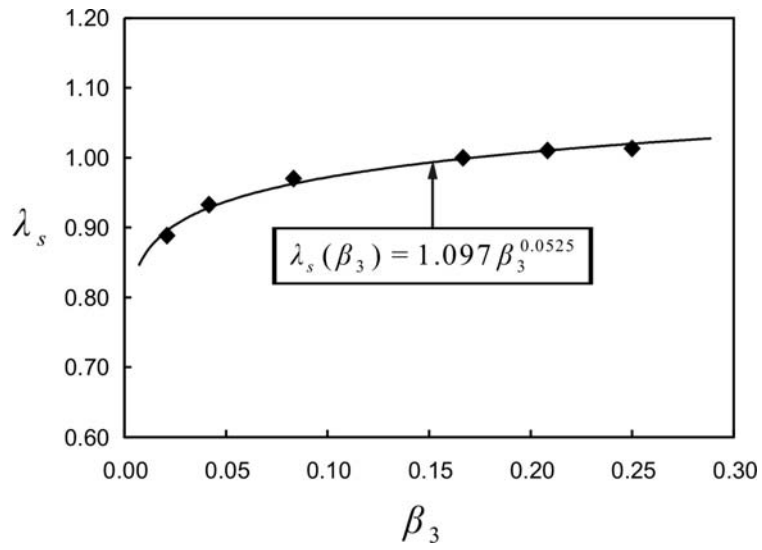


Figure 6-63: Relationship between  $\lambda_s$  and  $\beta_3$  for solid collars

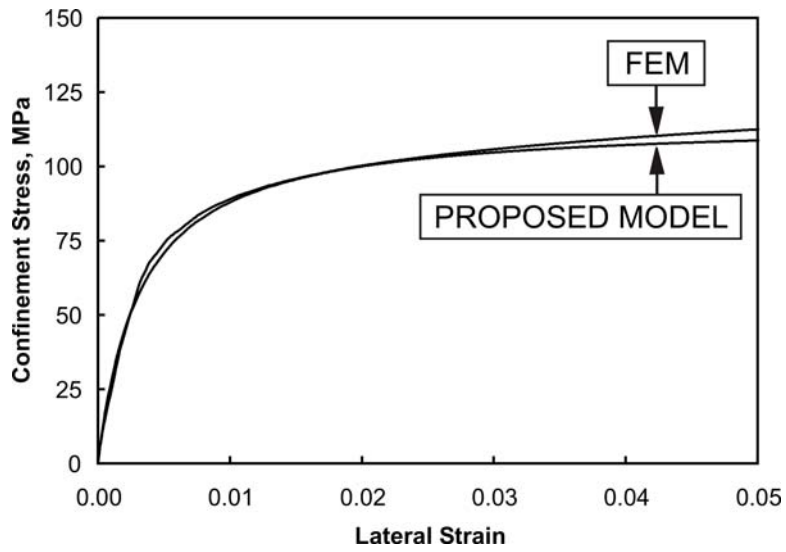


Figure 6.64: Confinement stress vs. lateral strain curve for case 1 (Table 6.35)

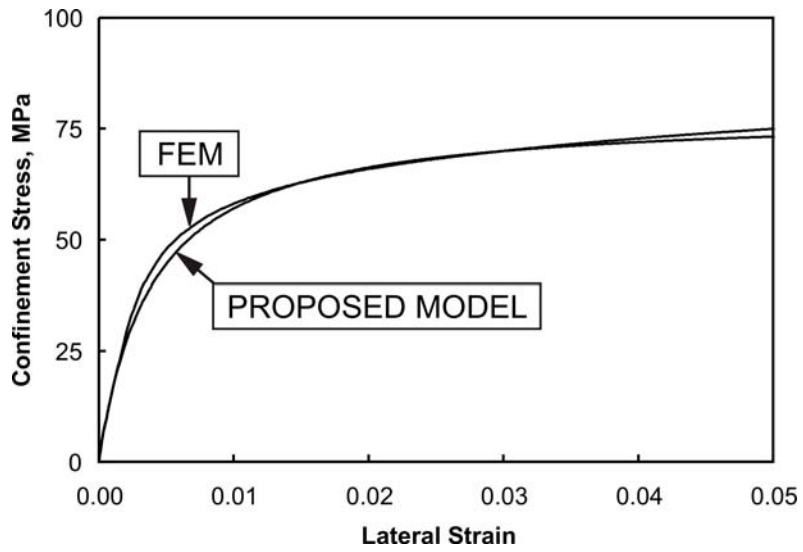


Figure 6.65: Confinement stress vs. lateral strain curve for case 2 (Table 6.35)

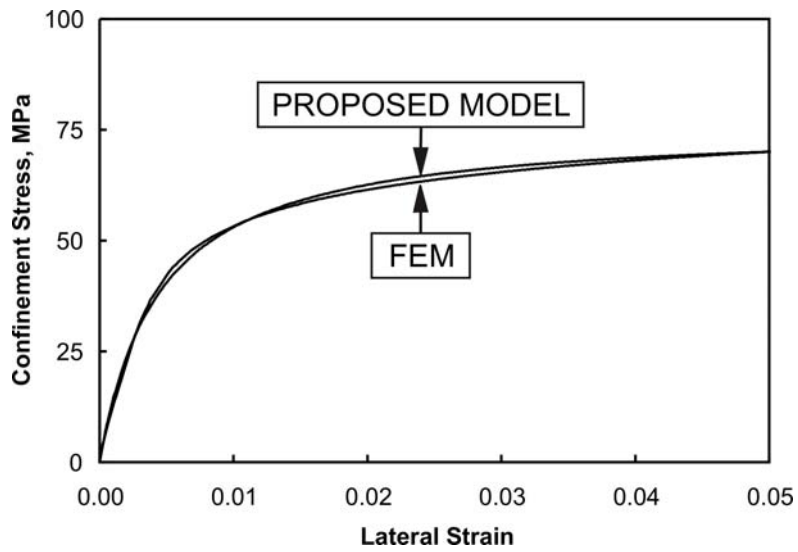


Figure 6.66: Confinement stress vs. lateral strain curve for case 3 (Table 6.35)

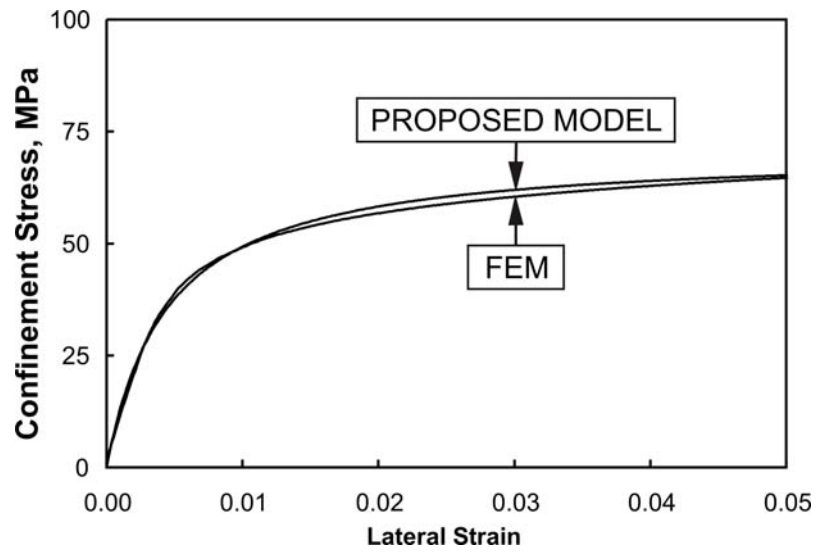


Figure 6.67: Confinement stress vs. lateral strain curve for case 4 (Table 6.35)

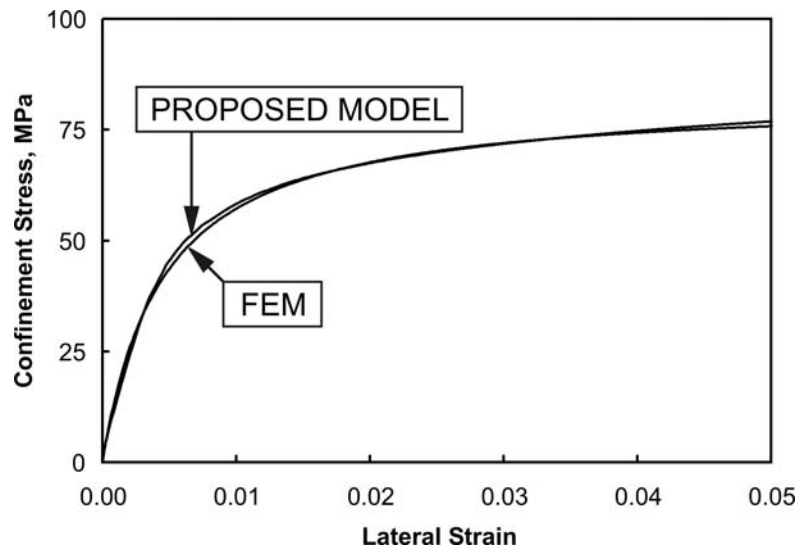


Figure 6.68: Confinement stress vs. lateral strain curve for case 5 (Table 6.35)

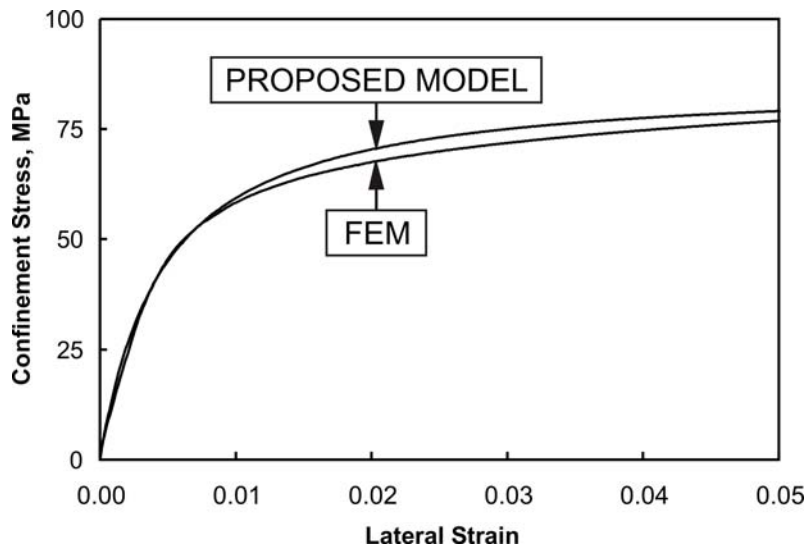


Figure 6.69: Confinement stress vs. lateral strain curve for case 6 (Table 6.35)

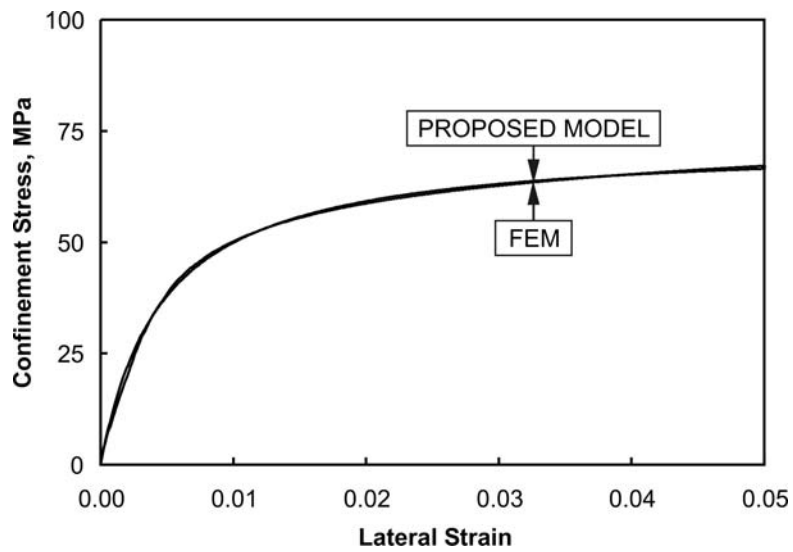


Figure 6.70: Confinement stress vs. lateral strain curve for case 7 (Table 6.35)

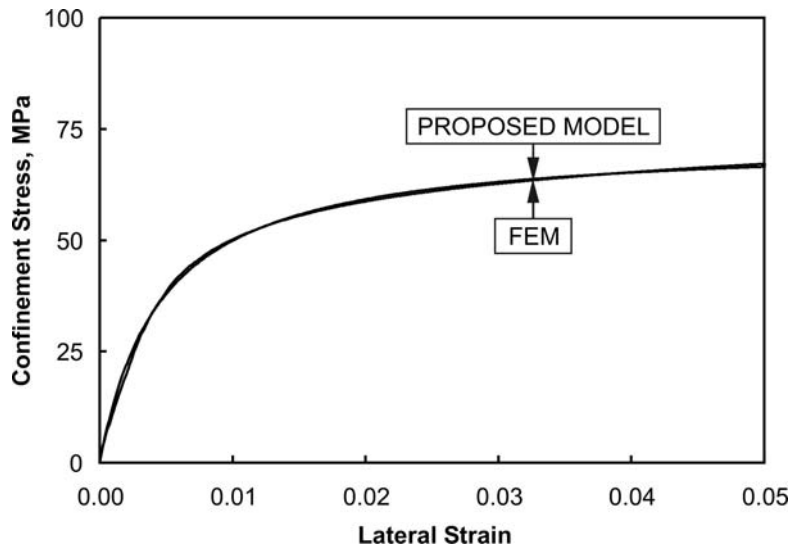


Figure 6.71: Confinement stress vs. lateral strain curve for case 8 (Table 6.35)

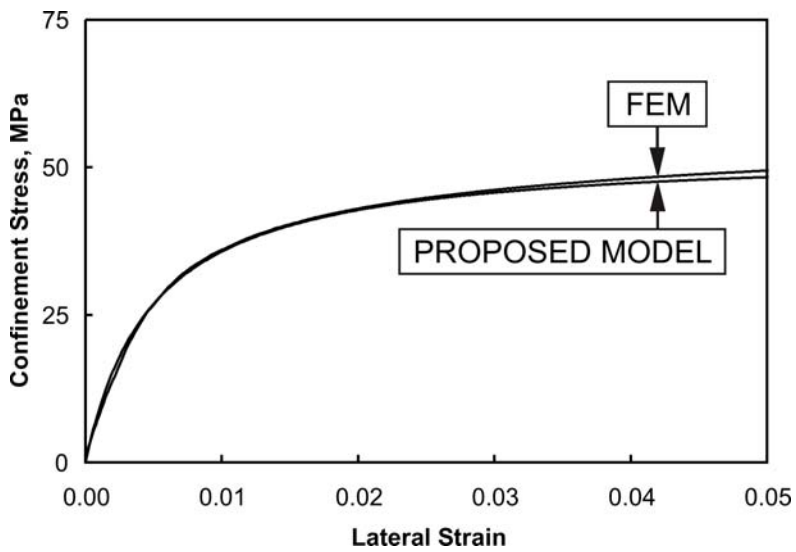


Figure 6.72: Confinement stress vs. lateral strain curve for case 9 (Table 6.35)

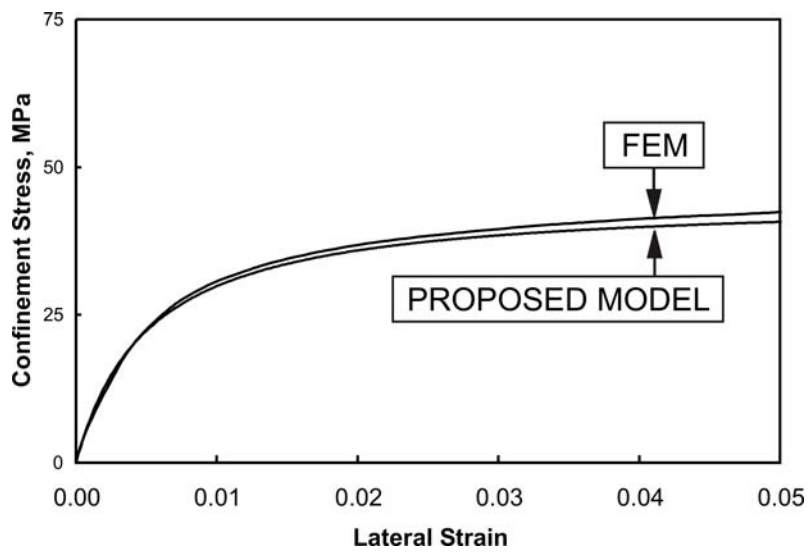


Figure 6.73: Confinement stress vs. lateral strain curve for case 10 (Table 6.35)

## 6.9 References

- Caner, F.C. and Bažant, Z.P. 2002. Lateral confinement needed to suppress softening of concrete in compression. ASCE, Journal of Engineering Mechanics, Vol. 128, No. 12, pp. 1304-1313.
- Chen, W.F. and Han, D.J. 1988. Plasticity in structural engineering. Springer-Verlag.
- Chung., H., Yang, K., Lee, Y., and Eun, H. 2002. Stress-strain curve of laterally confined concrete. Engineering Structures. Vol. 24, pp. 1153-1163.
- Fam, A.Z. and Rizkalla, S.H. 2001. Confinement models for axially loaded concrete confined by circular fiber-reinforced polymer tubes. ACI Structural Journal, Vol. 98, No. 4, pp. 451-461.
- Hibbitt, Karlsson & Sorensen, Inc. 2004a. *ABAQUS/Standard Version 6.2 User's Manual*, Pawtucket, R.I.
- Hibbitt, Karlsson & Sorensen, Inc. 2004b. *ABAQUS/Standard Version 6.2 Theory Manual*, Pawtucket, R.I.
- Hussain, M.A., and Driver, R.G. 2001. Finite element study on the strength and ductility of externally confined rectangular and square concrete columns. 29th Annual Conference of Canadian Society for Civil Engineering, Victoria, B.C., Canada, May 30-June 2.
- Kent, D.C. and Park, R. 1971. Flexural members with confined concrete. ASCE, Journal of the Structural Division, Vol. 97, No. ST7, pp. 1969-1990.
- Langhaar, H.L. 1951. Dimensional analysis and theory of models. John Wiley and Sons, N.Y.
- Légeron, F., and Paultre, P. 2003. Uniaxial confinement model for normal- and high-strength concrete columns. ASCE, Journal of Structural Engineering, Vol. 129, No. 2, pp. 241-252.
- Mander, J.B., Priestley, M.J.N. and Park, R. 1988. Theoretical stress-strain model for confined concrete. ASCE, Journal of Structural Engineering, Vol. 114, No. 8, pp. 1804-1826.
- Popovics, S.A. 1973. A numerical approach to the complete stress-strain curve of concrete. Cement and Concrete Research, Pergamon Press, Inc., No. 3, pp. 583-599.
- Saatcioglu, M. and Razvi, S.R. 1992. Strength and ductility of confined concrete. ASCE, Journal of Structural Engineering, Vol. 118, No. 6, pp. 1590-1607.
- Samaan, M., Mirmiran, A. and Shahawy, M. 1998. Model of concrete confined by fiber composites. Journal of Structural Engineering, ASCE, Vol. 124, No. 9, pp. 1025-1031.
- Sheikh, S.A. and Uzumeri, S.M. 1982. Analytical model for concrete confinement in tied columns. Journal of the Structural Division, ASCE, Vol. 108, No. ST12, pp. 2703-2722.
- Taylor, E.S., 1974. Dimensional analysis for engineers. Oxford University Press, London, U.K.

## 7. SUMMARY, CONCLUSIONS, AND RECOMMENDATIONS

### 7.1 Introduction

Existing structures can be seismically deficient due to various reasons such as changes in zoning of seismic activity in the area, changes in the performance objectives of the buildings due to, for example, a change in building function, and changes in the seismic design codes themselves due to advancements in knowledge of structural behaviour. During recent earthquakes, a large number of seismically deficient reinforced concrete structures received severe structural and non-structural damage. Many techniques have been developed for the upgrade of seismically deficient existing reinforced concrete buildings. Some techniques work through the enhancement of strength and stiffness, others through the enhancement in deformability and robustness, and still others by reducing seismic input through base isolation.

Stiffened steel plate shear walls have been used for the seismic upgrade of existing seismically deficient reinforced concrete buildings such as the Oregon State Library Building (Robinson, 2000) and the Veterans Administration Hospital in Charleston, South Carolina (Baldelli, 1983). The connection of the steel plates to the reinforced concrete frame was made with help of mechanical and adhesive type anchor bolts, which require chipping of the surface concrete to expose the bars, drilling to install the anchor bolts, and subsequent grouting. Steel plate shear walls were selected because the structures could be rehabilitated without abandoning the operation of the buildings. In both of these buildings, the rehabilitation objectives were achieved through enhancement in strength and stiffness. The inherent ductility of the steel plate shear walls could not be utilized due to the ductility incompatibility between the steel plate and the existing seismically deficient reinforced concrete frame.

A new scheme has been proposed that makes use of steel plate shear walls that resist lateral load through the development of a diagonal tension field after out-of-plane buckling of the plate. The new rehabilitation scheme should make use of the ductility of the steel plate wall. The problem of ductility incompatibility is solved by improving the ductility of the concrete frames through confinement using steel collars. The collars not only provide confinement, but also provide a means of connection of the steel plate shear wall to the reinforced concrete frames.

The ultimate aim of the broad research program is to study the composite performance of seismically deficient reinforced concrete frames rehabilitated using steel collars and thin steel

plate shear wall infill plates. However, it was considered that the confined behaviour of the collared concrete columns plays a critical role in the performance of the overall rehabilitation scheme. Therefore, the scope of the present research project was focused on the behaviour of the columns confined externally by steel collars (HSS collars were used both in the experimental and analytical work and solid steel collars were used in the analytical work only) under concentric axial loading and under combined axial and lateral cyclic loading.

## 7.2 Summary

In Chapter 2, a literature review related to the key areas of the present research is presented. Brief summaries of existing models for predicting the behaviour of concrete members confined by conventional internal reinforcement and by fibre reinforced composites are given and although many are available, existing confinement models are unable to predict the behaviour of concrete confined by HSS collars. This is primarily because of the lack of an explicit flexural stiffness parameter and/or because these models cannot account for variations in confining pressure through the axial load history of the columns. Collars provide confinement not only through axial stiffness, but also through their flexural stiffness that is significantly higher than that of conventional rebars ties. Moreover, the confining pressure under collars varies appreciably through the axial load history. Due to certain similarities with the behaviour of concrete confined by steel collars, some research into confinement using steel jackets is also summarized in this chapter. Although good behaviour of columns confined by various configurations of jackets is reported in the literature, few exploit the benefits of the flexural stiffness of steel collars.

In Chapter 3, the behaviour of reinforced concrete columns under concentric axial loading that are confined externally by HSS collars is discussed based on an experimental study under quasi-static concentric axial loading of 11 full-scale test specimens. The columns were typical of those that would be present in a two to three story building. Two control columns with conventional tie reinforcement (one satisfying the gravity load design criteria of ACI 318-02 and CSA Standard A23.3-94 and the other satisfying the seismic plastic hinge requirements of these codes), five columns confined by steel HSS collars with bolted corner connections, and four columns confined by steel HSS collars with welded collar connections were tested. In order to study the effect of external collar confinement separately, no internal tie reinforcement was provided in the test regions of the collared columns. All the columns were 300 x 300 mm in cross section and 1500 mm in height. One column with bolted collars and one column with welded collars were tested under multiple load cycles that verified the robustness of the confinement mechanism. The major parameters included in this experimental study were collar size, collar

spacing, and type of collars (collars with bolted or welded corner connections). Conclusions drawn from this experimental program are presented in the next section.

In Chapter 4, the behaviour of concrete columns under cyclic loading that are confined externally by HSS collars are discussed based on an experimental program consisting of a total of nine full-scale reinforced concrete columns typical of two to three story buildings. One control column had conventional tie reinforcement in the rest region and it satisfied the seismic plastic hinge requirements of both ACI 318-02 and CSA Standard A23.3-94 and the remaining eight columns had external collar confinement in the test regions. In order to study the effect of external collar confinement separately, no internal tie reinforcement was provided in the test regions of the collared columns. All the columns were 300 x 300 mm in cross section and about 2100 mm in height and were tested in a cantilever manner. The variables included in this study were axial load, collar spacing, collar size, and shear-span. In addition, envelope curves to the hysteresis of the columns are predicted by using the existing analytical models for flexural deformations and anchorage slip. Conclusions drawn from this experimental program are presented in the next section.

Because existing confinement models are unable to predict the stress versus strain behaviour of concrete confined externally by HSS collars, in Chapter 5 a new model has been proposed. The proposed model makes use of behavioural curves of the collars in terms of average confining pressure versus average lateral strain. A finite element model using the general-purpose finite element program ABAQUS (HKS, 2004a, 2004b) has been developed to determine these behavioural curves. The model predictions show very good agreement with the experimental results of the externally confined columns tested under concentric axial loading (Chapter 3).

The application of the confinement model proposed in Chapter 5 requires the behavioural curves of collars in terms of average confining pressure versus average lateral strain, which are obtained through finite element analysis that is not always convenient. In order to make the proposed confinement model practical, empirical models for the confining behaviour of collars are required. In Chapter 6, two empirical models have been proposed for the confining behaviour of collars with rigid corner connections for providing confinement to square concrete columns: one for collars made from hollow structural sections (HSS); and one for collars made from solid steel sections. The proposed models are based on a comprehensive finite element study using a wide variety of input parameters. For this purpose, non-dimensional parameters were identified and validated. Parametric studies were then performed in terms of these non-dimensional parameters and multiple nonlinear regressions were performed on the data obtained through finite element analyses to develop multi-dimensional empirical equations for defining the

confining behaviour of collars. The non-dimensional models provide good predictions of the behavioural curves of HSS and solid collars with rigid corner connections and eliminate the need for finite element modelling.

## **7.3 Conclusions**

### **7.3.1 Concentrically Loaded Columns**

External confinement by HSS collars has excellent potential for rehabilitation of reinforced concrete structures through enhancement in both strength and ductility. The collared columns exhibited a maximum strength enhancement factor of 3.12 (column C07; strain at peak stress equal to 0.026), calculated based on the reduced core of the column, and a maximum observed strain at peak stress of 0.043 (column C05; strength enhancement factor equal to 2.57). By comparison, a conventionally confined column satisfying the plastic hinge requirements of ACI 318 and CSA Standard A23.3 (column C00B) exhibited a strength enhancement factor of 2.70 and a strain at peak stress of 0.030. Clearly, the comparative overall benefit in strength for the collared columns is much greater when considering that the size of the core itself is considerably larger. This is because external confinement by HSS collars prevents the spalling of concrete cover under the collars and inhibits spalling between the collars. The effective core area of externally confined columns is therefore significantly larger than that of conventional columns.

On average, columns confined by collars having welded corner connections show an enhancement in strength, based on the reduced core area, of 1.95 times that of equivalent columns with bolted collars. The strain at peak stress of the concrete confined by the two types of collars are comparable and generally are close to ten times that which would be expected for unconfined concrete. The lower failure strain exhibited by columns with welded collars is attributed to the lack of ductility of the welds in the collars themselves and it may be increased significantly with deeper weld penetration.

The spacing of the collars has a profound effect on the confined material curve. It was observed that by increasing the clear spacing by about 60%, the enhancement in concrete strength was cut in half. The effect of a change in collar spacing on the strain at peak stress of the confined concrete was more prominent at higher spacings (lower levels of confinement) and it became less influential at smaller spacings (higher levels of confinement). These observations are not expected to hold at very large spacings, where the degree of confinement is very low.

The mere presence of HSS collars has a large effect on column strength due, in part, to their high stiffness. By increasing the HSS stiffness, an enhancement in both strength and ductility was observed, although the benefits in strength were relatively small as compared to the increase in collar stiffness. For bolted collars, this is attributed to the fact that the behaviour is influenced by the deformations of the bolts, which are relatively flexible components of the system. For welded collars, it is attributed to the high level of confinement achieved by the presence of the rigid corner connections, which in turn reduces the impact of the moment of inertia of the HSS member itself. Therefore, when increasing the collar stiffness, there is a threshold beyond which the rate of increasing benefit diminishes rapidly.

The column with relatively high initial active confining pressure showed improved behaviour up to the peak load, but exhibited rapid softening in the post-peak part of the curve, likely due to some combination of rapid spalling of the concrete between the collars and yielding of the bolts. An enhancement in concrete strength was observed that was 1.39 times that of the otherwise similar column by increasing the initial confining pressure by 2.24 times.

### **7.3.2 Columns Under Cyclic Loading**

All the collared columns showed very good behaviour under severe cyclic loading. The desired enhancement in strength and ductility was achieved through confinement of concrete and the presence of the collars made the columns very resistant to degradation under severe cyclic loading. External confinement by HSS collars is therefore an effective means of rehabilitating columns in seismically deficient reinforced concrete buildings.

In the collared columns, very little spalling of concrete between the collars was observed at the end of the first 20 cycles, a ductility level equal to 4, which is common in the design of new reinforced concrete structures. In the case of the conventionally tied column, most of the spalling of the concrete cover occurred at a displacement ductility level of 1.5. Hence, collared columns possess a larger effective core than that of conventionally tied columns.

Fracture of some vertical bars due to low-cycle fatigue was observed in several collared columns. However, it was more pronounced in columns with wider collar spacings. No slippage of the collars was observed in the test regions of the collared columns at the end of the tests, a feature that is highly desirable for the success of this rehabilitation scheme.

In the collared columns, most of the spalling was confined to the lower half of the test region while in the conventional column, spalling took place over a wider range. One reason could be

the upward shift in the location of the hinge formation. Collars tend to provide restraint to the spread of damage in the test region of collared columns.

The normalized peak moment of the conventionally tied column is less than that of collared columns used in the present study. The normalized modulus of toughness of the conventionally tied column is less than that of the collared columns having the same shear-span as that of the conventionally tied column. However, some collared columns with the short shear-span exhibited a lower modulus of toughness than that of the conventionally tied column.

All the collared columns exhibited a higher level of stiffness retention than the conventionally tied column. Hence, collared columns are more resistant to degradation under severe cyclic loading.

The energy dissipation in a cycle depends on the displacement amplitude, level of axial load, and the moment capacity of the columns. With an increase of each of these variables, the energy dissipation in a cycle increases. The moment capacity of the column cannot be varied at the time of testing, so this cannot be considered as a variable in the present context. Hence, the energy dissipation in a cycle can be varied by varying either axial load or displacement amplitude (which is usually related under the testing protocol to the yield displacement). That is, the slope of the cumulative energy dissipation (or normalized cumulative energy dissipation) versus cycle number curve depends on the amount of energy dissipated in each successive cycle. Increasing the energy dissipation in a cycle does not mean that the total energy dissipated by the column at the end of the test or at failure will also increase. Increasing the axial load will increase the energy dissipation in a cycle, but the deteriorating effect of axial load tends to make the column fail earlier. Therefore, the number of cycles sustained by the specimen at failure can be reduced considerably, in turn reducing the total energy dissipated by the specimen. Similarly, the energy dissipation in a cycle with a large displacement amplitude will be high. Since the displacement amplitudes are related to the yield displacement, if the yield displacement is higher the slope of the energy dissipation curve will also increase. However, this does not mean that the overall energy dissipated by the column at the end of the test will also increase, as the number of cycles sustained by the specimen will likely reduce leading to an overall reduction in the total energy dissipated at failure. In addition, the energy dissipated in primary cycles is higher than that dissipated in secondary cycles at the same level of displacement ductility. If a large number of cycles are performed at the same displacement ductility, the energy dissipation in subsequent cycles decreases due to degradation in strength and stiffness of the column.

The rate of increase of cumulative normalized energy dissipation with respect to cycle number is generally higher for conventionally tied column as compared to that of collared columns. The

cumulative normalized energy dissipated at the end of the tests is higher for conventionally tied column as compared to that of collared columns with a short shear-span. The comparison between conventionally tied columns and collared columns with a long shear-span cannot be made with respect to cumulative normalized energy dissipated at the end of the tests because the tests of most of the collared columns with long shear-span were stopped prematurely due to the limitation of jack stroke. Had the tests not stopped prematurely, the cumulative normalized energy dissipated at the end of the tests of collared columns with long shear-span would likely have been higher than that of the conventionally tied column.

The hysteretic damping ratio increases with the increase of lateral drift for all the columns. The hysteretic damping ratio of the conventionally tied column is generally higher than that of collared columns. Very rarely, the hysteretic damping ratio of collared columns became higher than that of conventionally tied columns.

The curvature ductility of the conventionally tied column was higher than that of the collared columns. The cumulative ductility ratio and cumulative energy damage indicator at the end of the test are significantly higher for conventionally tied column than those of collared columns. The collared columns exhibited less ductility because the damage is concentrated within a smaller length of the test region as compared to the length of the damaged region in the conventionally tied column.

In addition, the following conclusions are drawn with respect to the effect of various parameters on the behaviour of the collared columns.

### **7.3.2.1 Effect of Axial Load**

Based on the test results of collared columns with short and long shear-spans, it can be concluded that the presence of axial load on the columns causes an increase in the rate of degradation in strength and a decrease in the stiffness retention of the columns. The presence of axial load in columns with long and short shear-spans caused a reduction in the cumulative normalized dissipated energy at the end of the tests.

With an increase in axial load, the hysteretic damping ratio of collared columns decreased. However, this effect was more pronounced in collared columns with short shear-spans than with long shear-spans.

The application of axial loads in the range of  $0.15P_0$  to  $0.23P_0$  generally caused an improvement in the ductility of the collared columns expressed in terms of the normalized modulus of toughness (as defined in the present research), curvature ductility, cumulative ductility ratio, and cumulative energy damage indicator. It is assumed that in columns within this range of axial loads, the axial load will help improve the ductility by mobilizing confinement more rapidly as compared to columns without axial load and its improving effect on ductility is greater than its deterioration effect.

### **7.3.2.2 Effect of Collar Spacing**

In the regime of both long and short shear-span columns, columns with a wider spacing of collars exhibited lower values of normalized peak moments, normalized modulus of toughness up to the peak moment condition, and normalized modulus of toughness up to the failure of the columns as compared to those of columns with closer spacing. The rate of deterioration of strength is higher in columns with widely spaced collars than with closely spaced collars.

In the regime of both long and short shear-span columns, the effect of collar spacing on the stiffness retention of the columns was marginal; columns with closely spaced collars exhibited slightly higher stiffness retention as compared to columns with relatively wider collar spacing.

For both long and short shear-span columns, the cumulative energy dissipated and cumulative normalized energy dissipated at the end of the tests is significantly lower for columns with widely spaced collars as compared to columns with closely spaced collars.

In columns with long shear spans, the hysteretic damping ratio of columns with widely spaced collars is slightly higher than that of columns with closely spaced collars. However, in columns with short shear spans, the columns with wider spacing of collars exhibited significantly higher hysteretic damping ratios at a certain level of lateral drift than columns with closely spaced collars.

In the regimes of both long and short shear span columns, columns with widely spaced collars exhibited lower curvature ductility, cumulative ductility ratio, and cumulative energy damage indicator as compared to columns with widely spaced collars.

### 7.3.2.3 Effect of Collar Size

In the case of columns with long shear spans, the stiffness retention was slightly higher for columns with large size collars as compared to that of columns with small size collars. Conversely, in the case of columns with short shear spans, the stiffness retention was slightly higher for columns with small size collars than for columns with large size collars. The energy dissipation characteristics of the columns were not particularly sensitive to the change in the size of the collars in the range in which this study was made.

In the case of columns with long shear-spans, the normalized cumulative energy dissipated at the end of the test for the column with small size collars was higher than that of the column with large size collars, although the very low concrete strength in the latter column prevents a direct comparison. The columns behaved very similarly in this respect up to about 30 cycles of load. In the case of columns with short shear-spans, columns with different sizes of collars exhibited similar energy dissipation characteristics in terms of cumulative normalized energy dissipated versus cycle number. It appears as though the energy dissipation characteristics of the columns were not particularly sensitive to the change in the size of the collars in the range in which this study was conducted.

For columns with long shear-spans, the hysteretic damping ratio was slightly higher for columns with large size collars as compared to that of columns with small size collars. In the case of columns with short shear-spans, the hysteretic damping ratio was slightly higher for columns with small size collars as compared to that of columns with large size collars. This means that the hysteretic damping ratio was not sensitive to the change in the size of collars in the range in which this study was made.

In the case of columns with long shear-spans, the columns with large size collars exhibited higher moduli of toughness as compared to columns with small size collars. The columns with large size collars exhibited lower values of curvature ductility, cumulative ductility ratio, and cumulative normalized energy damage indicator. This discrepancy is attributed to the relatively higher value of axial load index in columns with large size collars as compared to that in columns with small size collars. In the case of columns with short shear spans, the columns with large size collars exhibited higher moduli of toughness, curvature ductility, cumulative ductility ratio, and energy damage indicator as compared to those of columns with small size collars. Based on the above, it can be concluded that the columns with large size collars exhibited higher ductility as compared to columns with small size collars.

### **7.3.2.4 Effect of Shear-Span**

The rate of strength deterioration is higher in collared columns with a short shear-span as compared to that in columns with a long shear-span. Moreover, the collared columns with a long shear-span exhibited higher stiffness retention and higher energy dissipation characteristics.

Generally, the hysteretic damping ratio exhibited by columns with shorter shear spans was higher than that of columns with long shear spans.

Based on parameters such as normalized modulus of toughness, curvature ductility, cumulative ductility ratio, and cumulative energy damage indicator, the collared columns with long shear-spans are more ductile as compared to collared columns with short shear-spans.

### **7.3.2.5 Conclusions Based on Analytical Results**

The envelope to the hysteresis curves (Chapter 4) of the conventionally tied column, the collared columns with long shear-spans, and the collared columns with short shear-spans were predicted analytically. The predicted envelope curves showed very good agreement with that of the average experimental envelope curves for the conventionally tied column and for the collared columns with long shear-spans. However, in the case of collared columns with short shear-spans, the predicted envelope curves showed very good agreement with the experimental envelope curves up to a lateral drift of about 5%. After this level of lateral drift, the predicted envelope curves over-estimate the capacity of the columns. This is because in columns with short shear-spans, more rapid spalling of concrete takes place as compared to columns with long shear-spans. Rapid spalling of concrete between the collars results in a reduced column cross section due to which the experimental capacity of the columns also reduces rapidly. However, this reduction of cross section due to spalling of concrete is not taken into account in the model. In addition, the effect of cyclic loads on the properties of the concrete and steel reinforcing bars and the effect of lateral bending of the longitudinal bars due to the expansion of the concrete were not included in the model.

### **7.3.3 Concrete Confinement and Empirical Collar Models**

The proposed confinement model (Chapter 5) for predicting the stress versus strain behaviour of collared columns was validated by applying it to columns confined externally by steel HSS collars with bolted and welded corner connections tested in phase 1 of the project (Chapter 3). Some

columns with bolted collars had initial active confining pressure due to the pre-stressing of the bolts. The results predicted by the model show good agreement with the experimental results. Equations for establishing the descending branches of the confined concrete material curves have also been proposed that show good results but they need more experimental data for calibration outside of the range of the confinement index considered.

The proposed empirical models (Chapter 6) in terms of non-dimensional parameters for the confining behaviour of HSS and solid collars with rigid corner connections were verified with the help of several case studies, including physical tests conducted as part of this research program. The results predicted by the proposed empirical models were found to correlate very well with the finite element and test results. Therefore, the empirical models represent a viable alternate to the more onerous finite element analyses for predicting confining pressure vs. lateral strain curves.

## **7.4 Recommendations for Future Research**

In Chapter 3, the behaviour of concrete columns confined externally by HSS collars under concentric axial loading was studied. The columns confined by bolted HSS collars exhibited highly ductile behaviour and the columns confined by welded HSS collars failed prematurely due to rupture of the corner welds. Therefore, the descending branch for these latter columns, with a very high level of confinement, could not be traced. However, the failure happened at a very high level of axial strain. According to the conclusion of Canar and Bažant (2002) based on tube squash tests, if the volumetric ratio of confining steel is more than 14.5%, which is similar to the columns with welded collars, then the confined concrete should not exhibit a descending branch provided lateral bending of the longitudinal bars does not take place. The idea of having no degradation with high confinement levels needs to be confirmed for collared columns with more experimental testing in which premature failure of the corner welds does not take place. However, it is expected that due to the presence of the gaps between the collars, even columns with a large amount of confining steel would exhibit a descending branch at a high level of axial strain.

The equations for establishing the descending branch of the proposed confinement model were calibrated with a database consisting of few columns. Therefore, it is recommended that additional tests of collared columns that exhibit a descending branch be conducted for the calibration of the proposed equations.

Empirical models have been developed for the confining behaviour of HSS and solid steel collars with rigid corner connections for square concrete columns in terms of their non-dimensional

parameters based on the finite element results. Currently, solid steel collars with bolts on two diagonally opposite corners and continuous at the remaining two corners (Figure 7-1) are under investigation at the University of Alberta. Such collars are fabricated by cutting thick steel plates using an oxy-gas flame cutting method. It is anticipated that these collars would be economical with respect to both fabrication and field application. It is therefore recommended that the non-dimensional parameters for these collars be identified and a model be developed for predicting the confining behaviour in terms of the non-dimensional parameters.

When the collared columns are subjected to combined axial loads and moments (the same can be achieved by subjecting the columns to eccentric loading), the column cross-section goes under a strain gradient. It has been observed from the literature review that concrete under eccentric loading achieves a higher strain. Experimental evidence is required to confirm this phenomenon for collared columns that may lead to the modification of the proposed confinement models for concrete under a strain gradient that is confined by collars.

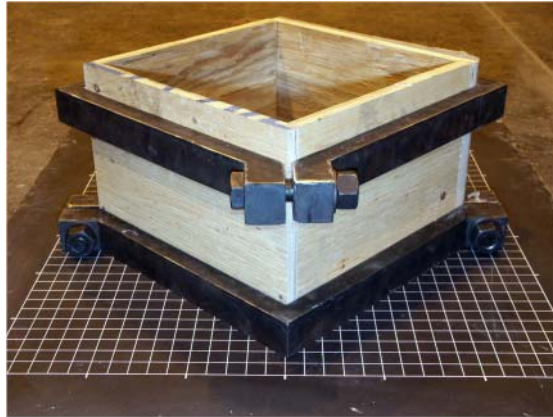
It is recommended that a comprehensive experimental study be conducted to investigate the shear behaviour of collared columns under simulated seismic loading and develop equations for predicting the shear behaviour. A research project is underway at the University of Alberta in this direction.

Existing reinforced concrete frames may have short lap splices at the location of plastic hinges. According to the literature review, the behaviour of columns with short lap splices is significantly improved by confining the splice region. The behaviour of concrete columns with short lap splices in longitudinal bars under collar confinement has not yet been studied. Therefore, it is recommended that an experimental study be carried out to investigate the behaviour of concrete columns with short lap splices in longitudinal bars confined externally by steel collars.

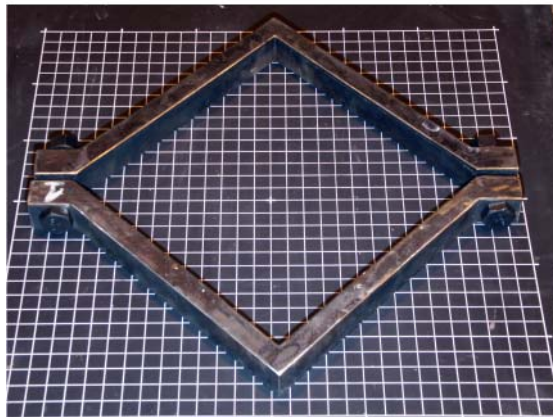
So far, the focus of the present research has been on square concrete columns. However, reinforced concrete columns with rectangular cross-sections are also frequently employed, often to satisfy architectural requirements. Therefore, it is recommended that the behaviour of rectangular concrete columns confined externally by steel collars under concentric monotonic axial loading and under cyclic lateral loading be investigated. Analytical and/or empirical confinement models are also required to predict the behaviour of rectangular concrete columns confined externally by steel collars.

Knowing the flexural and shear behaviour of collared columns under cyclic loading according to the research mentioned above, the next step is to investigate the behaviour of a seismically

deficient reinforced concrete frame rehabilitated with both collars and a steel plate shear wall. A schematic diagram of a possible single storey test specimen is shown in Figure 7-2. For this test frame, the connection of the steel plate shear wall to the beam could be made by threaded rods or steel collars passing through the slab. Based on previous research on the seismic behaviour of steel plate shear walls, it is apparent that the performance of the proposed composite test frame will be highly dependent on the thickness of the steel infill plate. The determination of the optimum plate thickness for the best performance of the composite frame requires the knowledge of the seismic shear strength and curvature ductility capacity of the boundary columns confined by steel collars. To determine the shear demand and curvature ductility demand on the boundary elements of the test frame imposed by the diagonal tension field of the steel plate shear walls, a pushover analysis of the system can be performed. As the prime objective of the proposed research is to extend the seismic benefits of the steel plate shear wall to reinforced concrete frames, existing methods for strengthening non-ductile frame joint regions should be incorporated to bring them to the same level of ductility as that of the remainder of the composite frame. After design and fabrication of the test specimen, the next step is to test the frame under simulated seismic loading to determine the composite performance of the rehabilitated system.



(a) Elevation



(b) Plan

Figure 7-1: Plan and elevation of new solid steel collars having two diagonally opposite corners with bolted connections and the remaining two corners continuous.

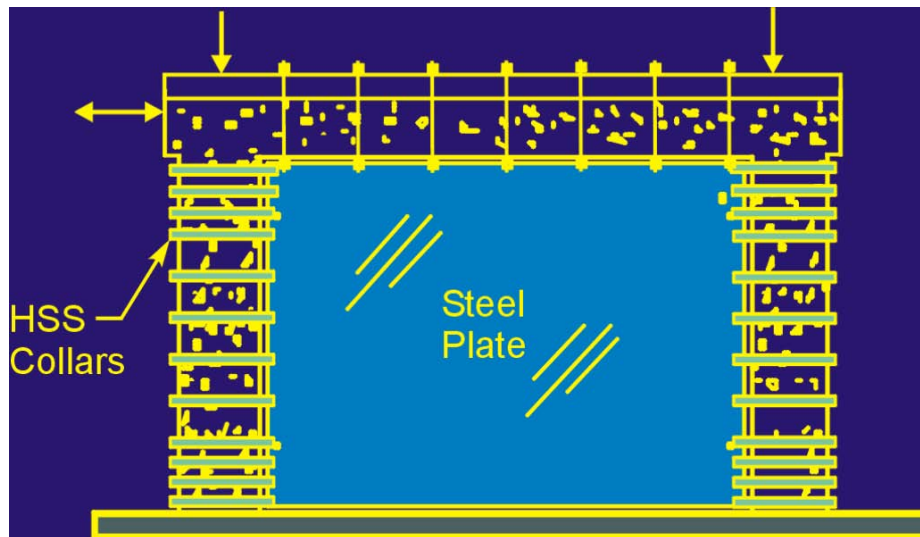


Figure 7-2: Elevation of schematic test frame

## 7.5 REFERENCES

- Baldelli, J. A. 1983. Steel shear walls for existing buildings. *Engineering Journal*, AISC, Second Quarter, pp. 70-77.
- Caner, F.C. and Bažant, Z.P. 2002. Lateral confinement needed to suppress softening of concrete in compression," *Journal of Engineering Mechanics*, ASCE, V. 128, No. 12, December 1, pp. 1304-1313
- Hibbitt, Karlsson & Sorensen, Inc. 2004a. *ABAQUS/Standard Version 6.2 User's Manual*, Pawtucket, R.I.
- Hibbitt, Karlsson & Sorensen, Inc. 2004b. *ABAQUS/Standard Version 6.2 Theory Manual*, Pawtucket, R.I.
- Robinson, K. and Ames, D. 2000. Steel Plate shear Walls (Library Seismic Upgrade). *Modern Steel Construction*, pp. 56-60.

## A. DERIVATION OF EQUATIONS FOR CONFINING STEEL

### A.1 Introduction

In this Appendix, the equations for the confining steel for circular columns and for square/rectangular columns are derived based on the assumptions of ACI 318. The equations are derived on the basis that loss in load carrying capacity of the column due to the spalling of concrete cover is compensated by the enhancement of core concrete strength due to confinement. Because of the ability in circular columns of the circular ties or spirals to resist expansion of the concrete by means of tensile forces only, they are fully effective in developing the confining pressure. However, in the case of square/rectangular columns, the ties are not fully effective in developing the confining pressure due to their lack of flexural stiffness.

### A.2 Derivation of Equation 2.8

According to earlier investigations, the strength of concrete confined by active fluid pressures is given by the following equation (all notation is presented at the end of the appendix for convenience:

$$[A.1] \quad f'_{cc} = f'_{co} + k_1 f_l$$

The value of  $k_1$  depends on the concrete constituents and proportions, as well as the lateral pressure itself. Based on experimental results, the average value of this coefficient was found to be 4.1 by Richart *et al.* (1928). Balmer (1949) reported that the value of this coefficient varied from 4.5 to 7.0, with an average value of 5.6, based on additional experimental work. The higher values of this coefficient occur at low confining pressure.

The maximum load carried by the concrete shell,  $(P_s)_{max}$ , can be calculated by the following equation:

$$[A.2] \quad (P_s)_{max} = (A_g - A_c) f'_{co}$$

The additional load,  $P_{add}$ , carried by the core concrete due to strength enhancement is given by the following equation:

$$[A.3] \quad P_{add} = k_1 f_l (A_c)$$

According to the requirement of the ACI 318, the maximum load carried by the unconfined concrete cover shell, shall be compensated by the enhancement of concrete strength in the core due to confinement:

$$[A.4] \quad P_{add} = (P_s)_{max}$$

$$[A.5] \quad k_1 f_l A_c = (A_g - A_c) f'_{co}$$

With the help of Figure A.1, the confining pressure after the yielding of the spiral steel can be calculated from the following equilibrium equation, where  $f_l = \sigma_s$ :

$$[A.6] \quad f_l = \frac{2A_{sp} f_{yh}}{s d_c}$$

According to Richart *et al.* (1928),  $k_1 = 4.1$ . Substituting the values of  $k_1$  and  $f_l$  into Equation A.5, results in the following:

$$[A.7] \quad \frac{8.2A_{sp}}{s d_c} = \left[ \frac{A_g}{A_c} - 1 \right] \frac{f'_{co}}{f_{yh}}$$

$$[A.8] \quad \frac{8.2A_{sp} \pi (d_c - d_s + d_s)}{s d_c (\pi d_c)} = \left[ \frac{A_g}{A_c} - 1 \right] \frac{f'_{co}}{f_{yh}}$$

$$[A.9] \quad \frac{A_{sp} \pi (d_c - d_s)}{s \left( \frac{\pi d_c^2}{4} \right)} + \frac{A_{sp} \pi d_s}{s \left( \frac{\pi d_c^2}{4} \right)} = 0.488 \left[ \frac{A_g}{A_c} - 1 \right] \frac{f'_{co}}{f_{yh}}$$

$$[A.10] \quad \rho_s + \frac{A_{sp} \pi d_s}{s A_c} = 0.488 \left[ \frac{A_g}{A_c} - 1 \right] \frac{f'_{co}}{f_{yh}}$$

$$[A.11] \quad \rho_s = 0.488 \left[ \frac{A_g}{A_c} - 1 \right] \frac{f'_{co}}{f_{yh}} - \frac{A_{sp} \pi d_s}{s A_c}$$

The second term on the right hand side of Equation A.11 is very small in magnitude relative to the first. Therefore, neglecting the second term and substituting,  $f'_{co} = 0.85 f'_c$  results in the following relationship:

$$[A.12] \quad \rho_s = 0.414 \left[ \frac{A_g}{A_c} - 1 \right] \frac{f'_c}{f_{yh}}$$

The coefficient 0.414 was increased to 0.45 and the equation was adopted by ACI 318. The final form of the equation (Equation 2.8) is given below:

$$[A.13] \quad \rho_s = 0.45 \left[ \frac{f'_c}{f_{yh}} \right] \left[ \frac{A_g}{A_c} - 1 \right]$$

### A.3 Derivation of Equation 2.10

This equation was derived based on the assumption that the efficiency of rectangular hoops is 50% that of spiral steel. The derivation of this equation is given in the commentary of ACI 318-71, which is reproduced here:

The following equilibrium equation can be deduced from the free body diagram shown in Figure A.1:

$$[A.14] \quad \sum V = 0 = \sigma_s s d_c - 2 A_{sp} f_{yh}$$

which simplifies to the following:

$$[A.15] \quad \sigma_s = \frac{2 A_{sp} f_{yh}}{s d_c}$$

Similarly, for the free body diagram shown in Figure A.2:

$$[A.16] \quad \sum V = 0 = \sigma_h s L_u - 2 A_{tie} f_{yh}$$

which simplifies to the following:

$$[A.17] \quad \sigma_h = \frac{2 A_{tie} f_{yh}}{s L_u}$$

According to the assumption of 50% efficiency, for equal confining pressure:

$$[A.18] \quad \sigma_s = 0.5 \sigma_h$$

Substituting Equations A.15 and A.17 into A.18:

$$[A.19] \quad \frac{2 A_{sp} f_{yh}}{s d_c} = \frac{A_{tie} f_{yh}}{s L_u}$$

$$[A.20] \quad \frac{2 A_{sp}}{d_c} = \frac{A_{tie}}{L_u}$$

For an equivalent spiral column:

$$[A.21] \quad \rho_s \approx \frac{A_{sp} \pi d_c}{s \left( \frac{\pi d_c^2}{4} \right)} \approx \frac{4 A_{sp}}{s d_c}$$

Combining Equation A.20 and Equation A.21 gives Equation 2.10:

$$[A.22] \quad A_{tie} = \frac{L_u \rho_s s}{2}$$

In later versions of the ACI code, the efficiency of the hoop reinforcement was considered to be high and it was assumed that the efficiency of the hoops is 75% of that of spirals. With this increased efficiency of the hoop, the above equation is modified to the following:

$$[A.23] \quad A_{tie} = \frac{L_u \rho_s s}{3}$$

## Appendix A Notation

$A_c$	=	area of concrete measured to outside diameter of spiral;
$A_{ch}$	=	area of rectangular core of column measured out-to-out of hoop;
$A_g$	=	gross area of the section;
$A_{sp}$	=	cross-sectional area of the spiral;
$A_{tie}$	=	cross-sectional area of one leg of the hoop reinforcement;
$d_c$	=	diameter of concrete core measured out to out of spiral;
$d_s$	=	diameter of spiral steel;
$f'_c$	=	specified compressive strength of concrete as measured from standard cylinders;
$f'_{co}$	=	compressive strength of unconfined concrete; $f'_{co} = 0.85 f'_c$ ;
$f_l$	=	lateral confining pressure;
$f_{yh}$	=	specified yield strength of spiral or hoop reinforcement;
$L_u$	=	unsupported length of rectangular hoop measured between perpendicular legs of the hoop or supplementary crossties;
$P_{add}$	=	additional load capacity due to enhancement in strength of core concrete;
$(P_s)_{max}$	=	Maximum load carried by concrete shell;
$s$	=	centre-to-centre spacing of spirals or hoops;
$\rho_s$	=	volumetric ratio of spiral steel;
$\sum V$	=	sum of all the horizontal forces;

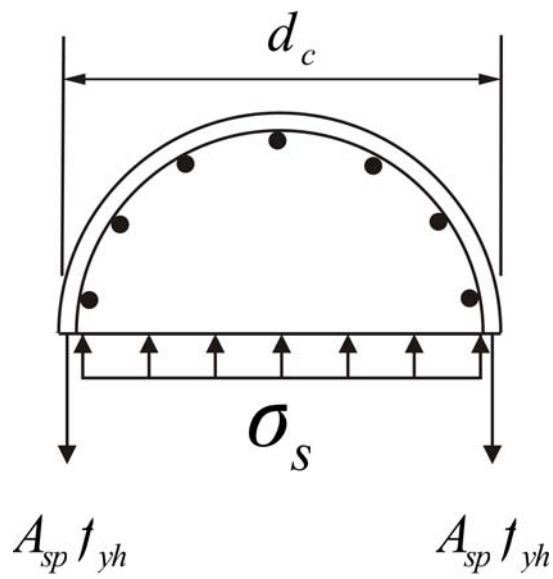


Figure A.1: Confining pressure for circular columns

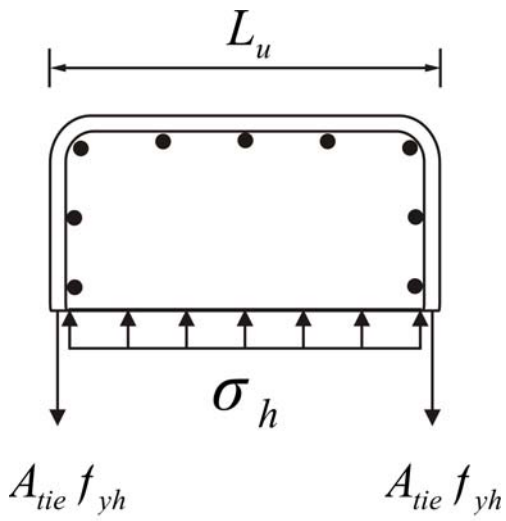


Figure A.2: Confining pressure for rectangular columns

### **A.3 References**

- Balmer, G.G. 1949. Shearing strength of concrete under high triaxial stress-computation of Mohr's envelope as a curve. Structural Research Laboratory Report sp-23, Denver, Colorado, October.
- Richart, F.E., Brandtzaeg, A., and Brown, R.L. 1928. A study of the failure of concrete under combined compressive stresses. University of Illinois, Engineering Experimental Station, Bulletin No. 185, 1928, 104 pp.

## B. PROGRAM MCP

### B.1 OBJECTIVE

The objective of this program is to add, subtract and find averages of the curves. In addition, the abscissas of different curves can be made same with the help of this program using linear interpolation technique, which then can then be added or subtracted or averaged in spreadsheets. This program has been widely used in Chapter 3 and Chapter 4.

### B.2 FORTRAN SOURCE CODE

```
C*****
C*****
C*****
CCC      DEVELOPED BY MUNAWAR A. HUSSAIN,
CCC      DEPARTMENT OF CIVIL ENGINEERING,
CCC      UNIVERSITY OF ALBERTA, EDMONTON, CANADA.
CCC      FOR ADDING AND SUBTRACTING CURVES
CCC      JULY 2002
C*****
C*****
C*****
C      For the partial fulfillment of the requirement
C      for the degree of Doctor of Philosophy
C*****
C*****
C*****
CCC*****
CCC      DEDICATED TO SABINA AND ALI
CCC*****
C*****
C*****
      PROGRAM MCURVE
      DIMENSION NCOUNT(15),WAITF(15)
      DIMENSION CURVE(3,16000,2)
      DIMENSION KOUNTG(15),STRAIN(15)
C*****
      OPEN(UNIT=1,FILE='MCP1.INP')
      OPEN(UNIT=2,FILE='MCP2.INP')
      OPEN(UNIT=3,FILE='MCP3.INP')
      OPEN(UNIT=4,FILE='MCP4.INP')
      OPEN(UNIT=5,FILE='MCP5.INP')
CCC      OPEN(UNIT=6,FILE='MCP6.INP')
CCC      OPEN(UNIT=7,FILE='MCP7.INP')
CCC      OPEN(UNIT=8,FILE='MCP8.INP')
CCC      OPEN(UNIT=9,FILE='MCP9.INP')
CCC      OPEN(UNIT=10,FILE='MCP10.INP')
C*****
      OPEN(UNIT=11,FILE='MCP1.OUT')
      OPEN(UNIT=12,FILE='MCP2.OUT')
CCC      OPEN(UNIT=13,FILE='VCURVE.DAT')
```

```

OPEN(UNIT=14,FILE='MCP.OUT')
C*****
CCC      REWIND(10)
          REWIND(11)
          REWIND(12)
          REWIND(14)
C*****
          NCOORD=2
C*****
1000      FORMAT(I10)
1010      FORMAT(2F25.10)
C*****
          WRITE(*,501)
501      FORMAT(5X,'PROGRAM FOR'/
          .5X,'FINDING WEIGHTED AVERAGE OF CURVES'/
          .5X,'AND ADDITION OF CURVES'//)
          WRITE(*,2001)
2001     FORMAT(5X,'FOR WEIGHTED AVERAGE, OPTION=1'/
          .,5X,'FOR ADDITION OF CURVES, OPTION=2'//)
          WRITE(*,2010)
2010     FORMAT(10X,'BY'//5X,'MUNAWAR HUSSAIN'/
          .5X,'DEPARTMENT OF CIVIL ENGINEERING'/
          .5X,'UNIVERSITY OF ALBERTA'/
          .5X,'EDMONTON, ALBERTA, CANADA'/
          .5X,'JULY 2002'//)
CCC      WRITE(*,505)
CCC505   FORMAT('****DEDICATED TO SABINA AND ALI*****'//)
          WRITE(*,502)
502     FORMAT(5X,'PLEASE ENTER THE DATA BELOW')
          WRITE(*,505)
505     FORMAT(5X,'NUMBER OF CURVES      X-INTERVAL      OPTION')
          READ(*,*)NCURVE,SINT,LOPT
*****
          WRITE(*,*)'PLEASE ENTER WEIGHT FACTORS FOR COMBINATION'
          READ(*,*)(WAITF(ICURVE),ICURVE=1,NCURVE)
*****
          DO 200 ICURVE=1,NCURVE
          READ(ICURVE,*)NCOUNT(ICURVE)
          NPOIN=NCOUNT(ICURVE)
          DO 300 IPOIN=1,NPOIN
          READ(ICURVE,*)XCOD1,YCOD1
          CURVE(ICURVE,IPOIN,1)=XCOD1
          CURVE(ICURVE,IPOIN,2)=YCOD1
CCC      WRITE(14,*)XCOD1,YCOD1
          IF(IPOIN.EQ.NPOIN)THEN
          STRAIN(ICURVE)=XCOD1
          ENDIF
300      CONTINUE
200      CONTINUE
*****
C        WRITE(14,1010)(STRAIN(ICURVE),ICURVE=1,NCURVE)
*****
          SMIN=STRAIN(1)
          DO 700 ICURVE=1,NCURVE
          SDIFF=SMIN-STRAIN(ICURVE)
          IF(SDIFF.GT.0)SMIN=STRAIN(ICURVE)
700      CONTINUE

```

```

SMIN=SMIN
LMIN=SMIN/SINT
*****
REWIND(11)
REWIND(12)
*****
WRITE(11,350)
350  FORMAT(/'THIS PROGRAM WAS DEVELOPED BY MUNAWAR HUSSAIN'
./'DEPARTMENT OF CIVIL ENGINEERING'/'UNIVERSITY OF ALBERTA,
.EDMONTON, CANADA'/)
WRITE(11,355)
355  FORMAT(/'THE DATA FOR ALL THE GENERATED CURVES HAVE BEEN DUMPED'
./'IN THIS FILE')
CC*****
CC*****
CC*****
CC*****
DO 7777 ICURVE=1,NCURVE
CALL ANAME
WRITE(11,1050)ICURVE
1050  FORMAT(/'GENERATED DATA FOR CURVE NO.',I3,2X,'FOLLOWS:-')
NPOIN=NCOUNT(ICURVE)
NINT=STRAIN(ICURVE)/SINT
MINT=NINT+1
WRITE(11,1060)MINT
1060  FORMAT('NUMBER OF DATA POINTS IN THIS GENERATED CURVE=',I5/)
XCOD0=0.000
YCOD0=0.000
KONT=0
XCOD=0.000
WRITE(11,1010)XCOD0,YCOD0
WRITE(12,1010)XCOD0,YCOD0
CC*****
DO 5555 KINT=1,NINT
XCOD=XCOD+SINT
DO 4444 IPOIN=1,NPOIN
XCOD2=CURVE(ICURVE,IPOIN,1)
YCOD2=CURVE(ICURVE,IPOIN,2)
IF(XCOD2.GE.XCOD)THEN
LPOIN=IPOIN-1
XCOD1=CURVE(ICURVE,LPOIN,1)
YCOD1=CURVE(ICURVE,LPOIN,2)
GOTO 6666
ENDIF
4444  CONTINUE
6666  KONT=KONT+1
YCOD=YCOD1+(YCOD2-YCOD1)*(XCOD-XCOD1)/(XCOD2-XCOD1)
WRITE(11,1010)XCOD,YCOD
WRITE(12,1010)XCOD,YCOD
5555  CONTINUE
KOUNTG(ICURVE)=KONT+1
7777  CONTINUE
*****
JMIN=SMIN/SINT+1
*****
CCCCC  WRITE(14,*)(KOUNTG(ICURVE),ICURVE=1,NCURVE)
*****

```

```

WRITE(14,311)
311  FORMAT('XY-DATA FOR RESULTANT CURVE FOLLOWS')
WRITE(11,312)
312  FORMAT('XY-DATA FOR RESULTANT CURVE FOLLOWS')
WRITE(11,313)JMIN
313  FORMAT('NUMBER POINTS IN THE RESULTANT CURVE=',I5)
*****
REWIND(12)
*****
DO 1922 ICURVE=1,NCURVE
NPOIN=KOUNTG(ICURVE)
DO 2344 IPOIN=1,NPOIN
CURVE(ICURVE,IPOIN,1)=0
CURVE(ICURVE,IPOIN,2)=0
2344  CONTINUE
1922  CONTINUE
*****
DO 8888 ICURVE=1,NCURVE
NPOIN=KOUNTG(ICURVE)
DO 8822 IPOIN=1,NPOIN
READ(12,*)XCOD1,YCOD1
CURVE(ICURVE,IPOIN,1)=XCOD1
CURVE(ICURVE,IPOIN,2)=YCOD1
8822  CONTINUE
8888  CONTINUE
*****
C      DO 3344 ICURVE=1,NCURVE
C      NPOIN=KOUNTG(ICURVE)
C      DO 2345 IPOIN=1,NPOIN
C      XCOD1=CURVE(ICURVE,IPOIN,1)
C      YCOD1=CURVE(ICURVE,IPOIN,2)
C      WRITE(13,1010)XCOD1,YCOD1
C2345  CONTINUE
C3344  CONTINUE
C*****
NPOIN=SMIN/SINT+1
***INCREASE BY 1 IS FOR FIRST COORDINATE WHICH IS (0.000,0.000)
*****
IF(LOPT.EQ.1)THEN
GOTO 1934
ELSE
GOTO 2311
ENDIF
*****
1934  DO 9999 IPOIN=1,NPOIN
SFACT=0.0
SUMM=0.0
DO 9911 ICURVE=1,NCURVE
XCOD1=CURVE(ICURVE,IPOIN,1)
YCOD1=CURVE(ICURVE,IPOIN,2)
FACT=WAITF(ICURVE)
SFACT=SFACT+FACT
SUMM=SUMM+FACT*YCOD1
9911  CONTINUE
XCOD=XCOD1
YCOD=SUMM/SFACT
WRITE(11,1010)XCOD,YCOD

```

```

WRITE(12,1010)XCOD,YCOD
WRITE(14,1010)XCOD,YCOD
9999 CONTINUE
GOTO 5000
C*****
2311 DO 1166 IPOIN=1,NPOIN
SUMM=0.0
DO 9111 ICURVE=1,NCURVE
XCOD1=CURVE(ICURVE,IPOIN,1)
YCOD1=CURVE(ICURVE,IPOIN,2)
FACT=WAITF(ICURVE)
SUMM=SUMM+FACT*YCOD1
9111 CONTINUE
XCOD=XCOD1
YCOD=SUMM
WRITE(11,1010)XCOD,YCOD
WRITE(12,1010)XCOD,YCOD
WRITE(14,1010)XCOD,YCOD
1166 CONTINUE
*****
5000 CONTINUE
CALL JOB
*****
CLOSE(1)
CLOSE(2)
CLOSE(3)
CLOSE(4)
CLOSE(5)
CCC CLOSE(6)
CCC CLOSE(7)
CCC CLOSE(8)
CCC CLOSE(9)
CCC CLOSE(10)
CCC CLOSE(11)
CCC CLOSE(12)
CCC CLOSE(14)
*****
STOP
END
C*****
C*****
C*****
C*****
SUBROUTINE ANAME
REWIND (103)
C*****
WRITE(*,10)
10 FORMAT(/////5X, 'DEVELOPED BY MUNAWAR A. HUSSAIN, U OF A,
.EDMONTON, CANADA')
RETURN
END
C*****
C*****
C*****
SUBROUTINE JOB
WRITE(*,10)
10 FORMAT(/5X, 'JOB COMPLETED! JOB COMPLETED!')

```

```
                RETURN
                END
C*****
C*****
C*****
```

### **B.3 OPERATION**

The program works in interactive mode. On execution, the program asks for the number of input files to be engaged (The file names are *MCP1.INP*, *MCP2.INP*, *MCP3.INP* and so on). Then the program asks about the type of operation to be performed on these files such as addition/subtraction or finding average of the given input files. The program also asks for the required size of interval between the data points of the resulting output file. Two sample input files such as *MCP1.INP* and *MCP2.INP* and the resulting output file (*MCP.OUT*) containing the average of the two input files are given in Table B.1. It can be seen that the data points of the input files are at random locations and the data points of the output file are at constant interval specified by the user. The number 18 and 17 in the first lines of the input data files *MCP1.INP*, and *MCP2.INP* represent the number of data points in these files, respectively.

Table B.1: Sample input and output files

MCP1.INP		MCP2.INP		MCP.OUT	
18		17			
0.00	0.00	0.00	0.00	0.00	0.00
0.16	21.70	0.19	26.91	0.50	53.92
0.35	38.36	0.34	40.45	1.00	98.43
0.62	64.28	0.54	58.98	1.50	139.34
0.84	84.56	0.83	86.22	2.00	166.38
0.99	95.61	1.07	106.16	2.50	182.76
1.14	107.78	1.12	107.63	3.00	191.01
1.32	122.36	1.19	114.74	3.50	198.08
1.52	137.78	1.38	133.30	4.00	204.92
1.84	155.00	1.73	160.00	4.50	210.68
2.02	160.00	2.06	176.00	5.00	215.93
2.58	178.00	2.18	180.00	5.50	219.04
3.04	186.09	2.42	189.00	6.00	222.15
3.92	199.80	2.55	191.00	6.50	225.26
4.90	210.00	4.94	221.00	7.00	228.37
7.30	214.00	7.24	245.84	7.50	237.43
9.74	217.00	10.11	254.50	8.00	231.50
15.61	208.00			8.50	232.56
				9.00	233.62
				9.50	234.67
				10.00	235.40

### C. YIELDING OF LONGITUDINAL BARS AT YIELD DISPLACEMENT

A procedure for the determination of the yield displacement of columns has been described in Chapter 4. In this appendix, a brief investigation is presented on whether yielding of longitudinal bars in tension is likely to occur at the displacement  $\Delta_y$ . A singly reinforced rectangular concrete section of 300 mm width and 600 mm overall depth is chosen to study bar yielding behaviour. The section is reinforced with 3- $\phi$ 25 mm bars with a 540 mm effective depth. The yield strength,  $f_y$ , and modulus of elasticity,  $E_s$ , of the reinforcing bars are 500 MPa and 200 000 MPa, respectively. The effect of the strength of concrete,  $f'_c$ , on the nominal moment strength,  $M_{nuc}$ , and the moment strength of the section at the first yield of tensile steel,  $M_{yuc}$  (based on unconfined concrete), was studied. The nominal moment strengths,  $M_{nuc}$ , were calculated based on the ACI 318 Whitney stress block. The moment capacities of the section at the first yield of the steel were calculated using the strain compatibility analysis. This analysis requires the complete stress vs. strain curves of concrete and the equation proposed by Popovics (1973) was used. The strain equal to 0.003 was considered as the failure strain of concrete. The results of these calculations are given in Table C.1. The values of other parameters such as the coefficient  $\beta_1$ , the steel ratio,  $\rho$ , and the balanced steel ratio,  $\rho_b$ , are also given in the table. The definitions of these terms can be found in ACI 318-02.

Figure C-1 shows the plot of values of  $M_{nuc}$  and  $M_{yuc}$  with respect to  $f'_c$ . For concrete strengths varying from 20 to 45 MPa, the given section is under-reinforced, *i.e.*, crushing of the concrete will take place after the yielding of the tensile steel takes place. This is also clear from Table C-1, which shows that the values of steel ratios,  $\rho$ , are less than the corresponding balanced steel ratios,  $\rho_b$ . Hence, for an under-reinforced section, the nominal moment strengths,  $M_{nuc}$ , are always more than the corresponding yield moment capacity,  $M_{yuc}$ , of the section. Figure C-1 also shows that with the increase of concrete strength, both the nominal moment strength,  $M_{nuc}$ , and the moment capacity at the first yield of steel,  $M_{yuc}$ , increase. This figure also shows that  $M_{nuc}$  and  $M_{yuc}$  converge when the steel ratio,  $\rho$ , approaches the balanced steel ratios,  $\rho_b$ . When the steel ratio,  $\rho$ , becomes equal to the balanced steel ratio,  $\rho_b$ , yielding of the steel and the crushing of the concrete happen simultaneously and the nominal moment capacity,  $M_{nuc}$ , and yield moment capacity,  $M_{yuc}$ , are equal. In over-reinforced

concrete sections, crushing of the concrete happens before yielding of the steel and the nominal moment strength,  $M_{nuc}$ , will be controlled by the crushing of the concrete.

Figure C-2 shows the plot of the ratio of  $M_{yuc}$  to  $M_{nuc}$ , expressed in percentage, with respect to the cylinder strength of concrete. For low strength concrete,  $M_{yuc}$  tends to approach  $M_{nuc}$ , but as the strength of concrete increases,  $M_{yuc}$  becomes a smaller percentage of  $M_{nuc}$ . In the present case, it levels off at about 96% of  $M_{nuc}$ . The procedure used for the determination of yield displacements,  $\Delta_y$ , in Chapter 4 requires that the yielding of the section take place between  $0.75M_{nuc}$  and  $M_{nuc}$  (assuming  $M_{nuc} = M_{if}$ ). In balanced and over-reinforced sections, the chance of yielding of the tensile steel occurring at the yield displacement,  $\Delta_y$ , determined by this procedure is nil. Moreover, in under-reinforced sections, the chance of yielding the tensile steel at the yield displacement,  $\Delta_y$ , is also unlikely because  $M_{yuc}$  can go as high as 96% of  $M_{nuc}$ . Therefore, the procedure for the determination of the yield displacement in Chapter 4 does not guarantee that the yielding of the tensile steel will take place at the yield displacement. Hence, the yield displacement should refer to the yielding of the section as a whole. This seems viable because in over-reinforced sections, the damage starts in the concrete and the member goes into the nonlinear range and starts absorbing energy prior to yielding of the steel.

Table C.1: Nominal flexural strength and moment capacities at first yield of longitudinal tensile steel bars of a singly reinforced section

$f'_c$ (MPa)	$\beta_1$	$\rho$	$\rho_b$	$M_{yuc}$ (kN·m)	$M_{nuc}$ (kN·m)	Ratio $M_{yuc} / M_{nuc}$ (%)
20	0.85	0.0093	0.0158	347.65	349.85	99.37
25	0.85	0.0093	0.0197	353.29	360.88	97.90
30	0.85	0.0093	0.0236	356.75	368.24	96.88
35	0.81	0.0093	0.0263	359.10	371.93	96.55
40	0.77	0.0093	0.0286	361.16	374.56	96.42
45	0.73	0.0093	0.0305	362.76	376.46	96.36

Notes:

Width of the section: 300 mm

Overall depth of the section: 600 mm

Effective depth of the section: 540 mm

Yield stress of steel: 500 MPa

Modulus of elasticity of steel: 200 000 MPa

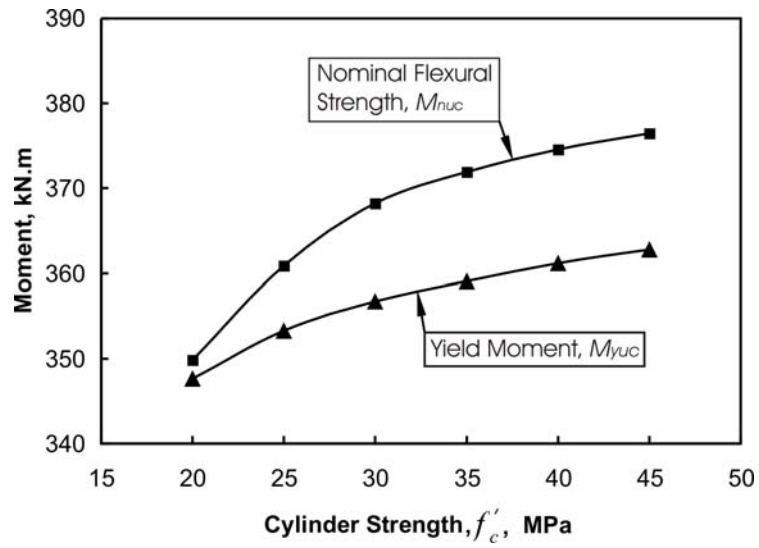


Figure C-1: Effect of strength of concrete on  $M_{nuc}$  and  $M_{yuc}$  of a singly reinforced section

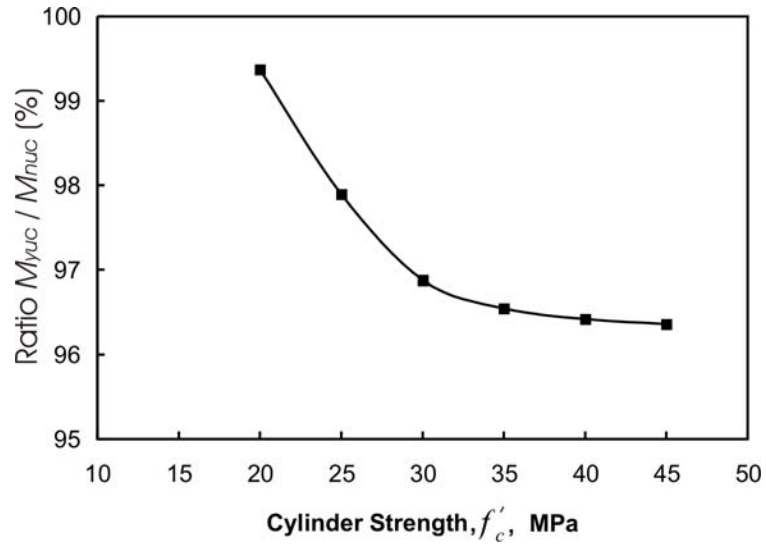


Figure C-2: Effect of strength of concrete on the ratio of  $M_{yuc}$  to  $M_{nuc}$  of a singly reinforced concrete section

## **C.2 References**

ACI Committee 318. 2002. Building code requirements for structural concrete (318-02) and commentary (318R-02). American Concrete Institute, Detroit, 391 pp.

Popovics, S.A. 1973. A numerical approach to the complete stress-strain curve of concrete. Cement and Concrete Research, Pergamon Press, Inc., No. 3, pp. 583-599.

## D. MOMENT VERSUS REINFORCING BAR STRAIN RELATIONSHIPS

In this section, the strain data of the tie bars of specimen CL0 and of the longitudinal bars of all the specimens are presented. Figure D-1 shows the location of strain gages on the longitudinal bars of each column. The locations of strain gauges on the longitudinal bars of the columns are identified with notation L1, L2, L3 and so on (L1 means the location of strain gage number 1, for example). These strain gages are divided into five groups based on their locations: group 1 consists of strain gages at locations L1, L2, and L3; group 2 consists of strain gages at locations L8, L9, and L10; group 3 consists of strain gages at locations L6 and L7; group 4 consists of strain gages at locations L4 and L5; and group 5 consists of strain gages at locations L11 and L12. The strain gages were affixed on the neutral axis of the rebars to cancel the effect of the strain gradient in the rebars. The data of the strain gauges within a certain group were similar. Therefore, it was decided to present the data of one strain gage from each group. Generally, the data from a strain gauge that sustained a greater number of cycles before debonding or malfunctioning in a certain group was selected for presentation. The selection of the number of cycles for presentation depends on the availability of the data and the clarity of figures. From 10 to 20 cycles are presented. In the present study, all the columns were first pushed towards the north in all the cycles they sustained. The moments corresponding to the north push are specified as positive and those corresponding to the south push are negative. Similarly, the tensile rebar strains are positive and the compressive rebar strains are negative. For the location of strain gauges on the tie bars in specimen CL0, the ties are numbered from bottom to top. The first tie close to the footing is given number 1 and the second tie is given number 2 and so on. The strain gauges on the tie bars are located at mid-depth of the column section on either its north or east face.

### D.1 Specimen CL0

Figure D-2 shows the relationships between the moment at the column base and longitudinal bar strains for column CL0. For this column, a gravity load of 1470 kN was maintained up to the end of the 16<sup>th</sup> cycle and was reduced to 720 kN for the remaining cycles. The yielding of the longitudinal bars of the column is clear from this figure. The nominal moment capacity of the column based on the unconfined concrete,  $M_{nuc}$ , is 180.3 kN·m (Table 4.5). The moment at first yield considering confined concrete in compression,  $M_{ycc}$ , is 246.8 kN·m (Table 4.5).

Figure D-2(a) shows the relationship between the moment at the column base vs. strain of a longitudinal bar at location L3 on the south face of the column. The tensile and compressive strains of this longitudinal bar in the first 15 cycles are similar.

Figure D-2(b) shows the relationship between moment at the column base and strain of a longitudinal bar at location L10 on the north face of the column. In the first 10 cycles, the tensile and compressive strains are similar. In cycles 11 through 15, the compressive strain in the bar at location L3 increases gradually with the increase in the number of cycles and it becomes much higher than the tensile strains at the end of 15<sup>th</sup> cycle. Similar behaviour was observed for strains at location L5 and L11. At these locations, the tensile and compressive strains in the rebars are similar up to the end of the first five cycles. The compressive strains become much higher than the tensile strains in cycles 6 through 15. The compressive strains in the rebars at level 2 are much higher than those at level 1. This can be explained with the help of Figure 4-18, which shows that the most damaged region occurs between 300 to 550 mm above the footing.

Figure D-2(c) shows the relationship between the moment and the rebar strain at location L6. In the first five cycles, the strains remain compressive. In the sixth cycle, the rebar is subjected to a small tensile strain when the column is at the extreme north. Thereafter, the loops shift towards the left with the increase in the number of cycles.

In Figures D-2(b), D-2(c), D-2(d), and D-2(e), the loops shift towards the left with the increase in the number of cycles. This is because the concrete sheds its load due to damage imparted to the concrete due to cycling, which is then carried by the longitudinal bars of the column. The strain at location L3 does not show this behaviour. The reason of this discrepancy is not known.

Figure D-3 shows the relationships between moment at the column base and strains in ties 1, 2, and 3, respectively. The strain gages were installed on the neutral axis of the tie bars to cancel the effect of the strain gradient from bending as the ties are pushed out due to concrete dilation. The strains in the tie bars are tensile as shown in Figures D-3(b) through D-3(f). Figure D-3(a) shows tensile as well as compressive strains in the tie bars under cyclic loading. The reason for this discrepancy is attributed to the error in placing strain gauge exactly at the neutral axis of the tie bar. The tensile strain of tie 5 is much higher than that of tie 1 and tie 3. This is because tie 5 is located in the most damage region (location of hinge formation) of the column.

## **D.2 Specimens CL1 and CL5**

First the specimen CL1 will be discussed and then specimen CL5 will be discussed. Both of these specimens were tested without gravity load.

Figure D-4 shows the relationships between moment and strains of longitudinal bars at different locations for specimen CL1. The yielding of the longitudinal bars of the column is clear from this

figure. The moment at the first yield of the tensile steel considering confined concrete in the compression zone,  $M_{ycc}$ , is 151.1 kN·m (Table 4.6).

The bars on the north and south faces receive tensile and compressive strains in the first five or sometime first ten cycles. However, tensile strains are higher in magnitude than compressive strains (Figures D-4(a), D-4(b), D-4(d), and D-4(e)). In cycles 6 through 15, the strains in the rebars are generally tensile. However, the magnitude of tensile strains varies during cycling.

In the first five cycles, the crushing of concrete does not take place because the applied moment in these cycles is much less than the nominal moment strength of the section,  $M_{nuc}$  ( $M_{nuc}=142.56$  kN.m, Table 4.5), calculated based on the unconfined concrete strength. As the crushing of unconfined concrete does not take place in these five cycles, the collar confinement is not activated in these cycles because collar confinement is passive.

Therefore, the bond between concrete and rebars remains intact and the column section behaves like a composite column section. Hence, the longitudinal steel bars receive compressive as well as tensile strains in these cycles and the magnitude of tensile and compressive strains are comparable.

In cycles 6 through 15, the longitudinal bars of the column, generally, do not receive compressive strains. However, they receive high tensile strains. This is because in these cycles the applied moment on the column is more than  $M_{nuc}$  ( $M_{nuc}=142.6$  kN.m, Table 4.5), which means that the crushing of unconfined concrete takes place in these cycles and, due to outward pressure of the crushed concrete on the collars, the collar confinement becomes effective. With each additional cycle, the outward pressure increases and the confining pressure from the collars on the concrete also increases. The column section is over-reinforced if unconfined concrete is considered and it becomes under-reinforced if confined concrete is considered. Up to about the first 20 cycles, the spalling of concrete is very limited. Hence, the full cross-section of the column takes part in resisting the applied moments.

Figure D-4(a) shows a relationship between moment and strain of a longitudinal bar located on the south face of the column. In cycles 6 through 15, the strain of this bar never becomes compressive. When the column is pushed towards the north in these cycles, the bars on the south face of the column go into tension and tension cracks are created on the south face of the column. As the concrete is under high confining pressure, the gaps created by tension cracks are immediately filled by the crushed confined concrete. When the column is pushed towards south,

the crushed concrete starts taking load immediately. The stretched bars just relax and do not take compression. As the columns do not carry gravity load, the need of these bars to take compressive load does not arise because the presence of concrete is sufficient to take compressive loads. Hence, these rebars do not show compressive strains.

Figure D-4(c) shows the moment vs. strain of a longitudinal bar at mid-depth of the column. These bars receive only tensile strain during cyclic loading, which increases with the increase in the displacement ductility level.

The relationships between moment at the column base and strains of longitudinal bars for column CL5 are given in Figure D-8. The yielding of longitudinal bars of the column is clear from this figure. The nominal moment capacity of the section,  $M_{nuc}$ , based on the unconfined concrete is 164.3 kN·m (Table 4.5). This is the only column in which yielding of the tensile steel can take place before the crushing of unconfined concrete in the compression zone. The moment at the first yield calculated based on the unconfined concrete,  $M_{yuc}$ , is 135.5 kN·m (Table 4.5). The moment capacity of the section based on the first yield of the tensile steel considering confined concrete material,  $M_{ycc}$ , is calculated to be 163.8 kN·m (Table 4.5). The interpretation of results given above for column CL1 applies to this specimen also.

### **D.3 Specimens CL2, CL3, CL4, CL6, CL7, and CL8**

Each of these columns was tested under gravity loads of 720 kN. The moment vs. longitudinal bar strain relationships for these columns are shown in Figures D-5, D-6, D-7, D-9, D-10, and D-11, respectively, which are similar for all the columns with a few exceptions that are attributed to the malfunctioning or debonding of strain gages. The values of  $M_{nuc}$  and  $M_{ycc}$  for these columns are given in Table 4.5. Yielding of the longitudinal bars in both tension and compression is obvious from these figures. The bars receive both tension and compressive strains due to cyclic loading; however, the tensile strains are higher than the compressive strains. The reason for this discrepancy is that in tension the load is resisted by the steel alone because concrete cannot resist tensile forces after cracking, whereas in the compression zone the load is resisted by both concrete and steel. In the columns without gravity loads, practically the bars do not go into compression. In the present case, the compressive forces are high due to the presence of gravity loads. The confined concrete starts resisting compressive load, as described before, during a cycle. The compressive forces are high and the confined concrete is strained considerably. Due to high strains in the compression zone, the resisting capacity of the

longitudinal bars is also mobilized. Hence, the longitudinal bars of the columns (with gravity loads) show considerable compressive strains under horizontal cyclic loading.

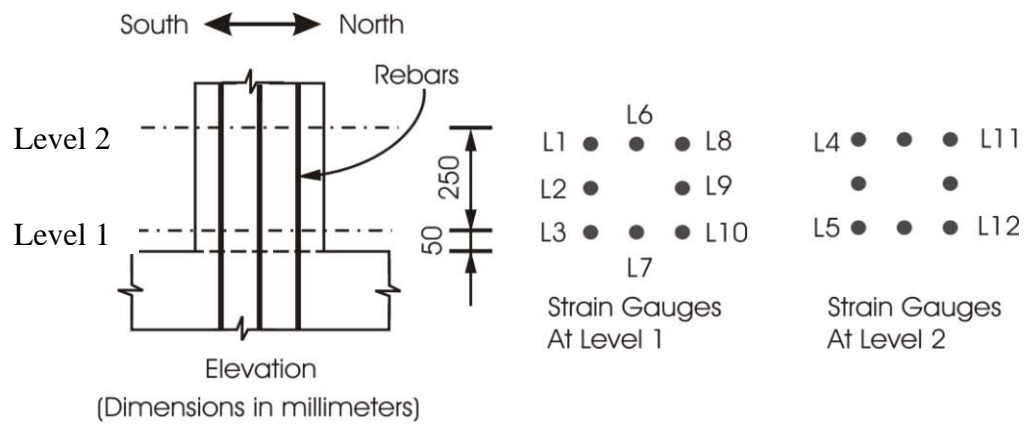
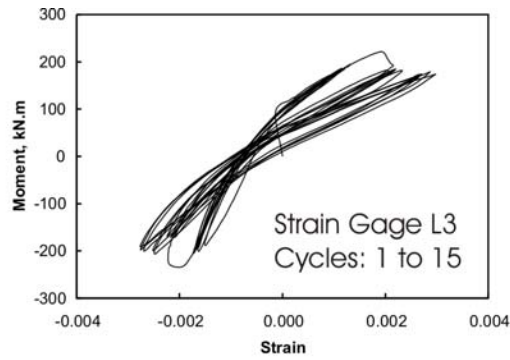
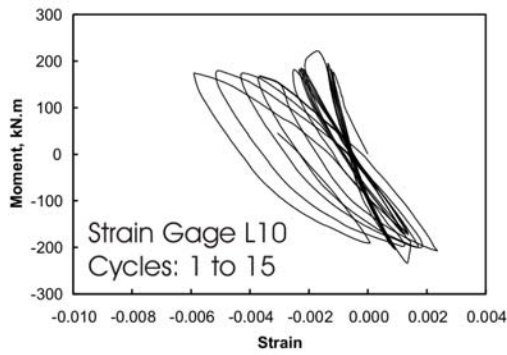


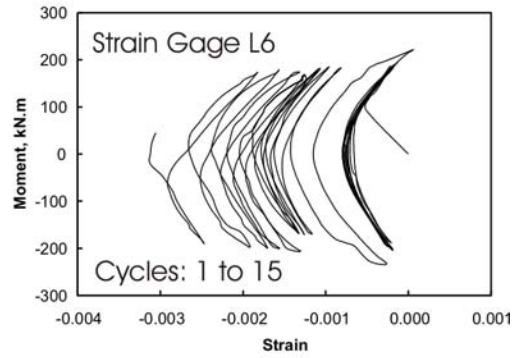
Figure D-1: Location of strain gages on the longitudinal bars of the columns (collars not shown for clarity).



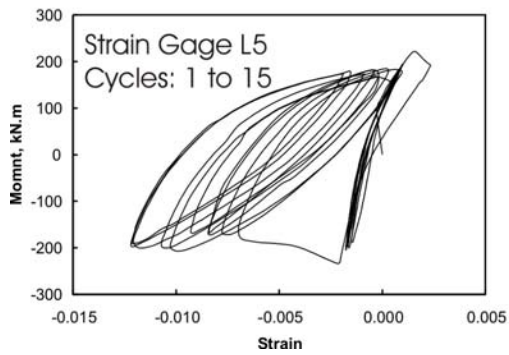
(a)



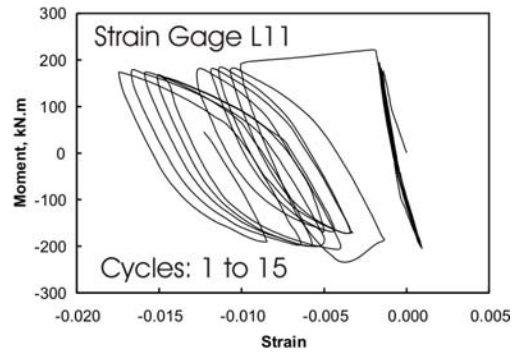
(b)



(c)



(d)



(e)

Figure D-2: Moment at column base vs. longitudinal bar strains for column CL0

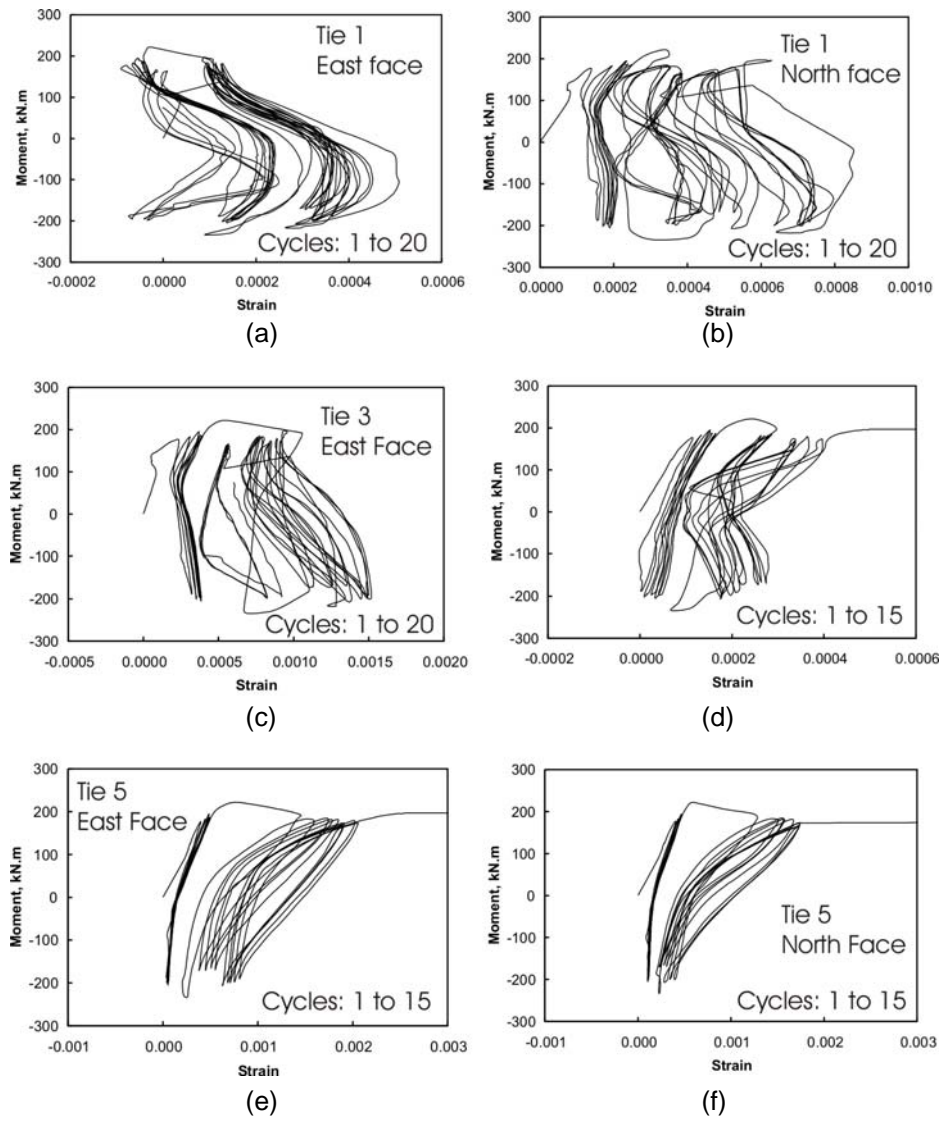
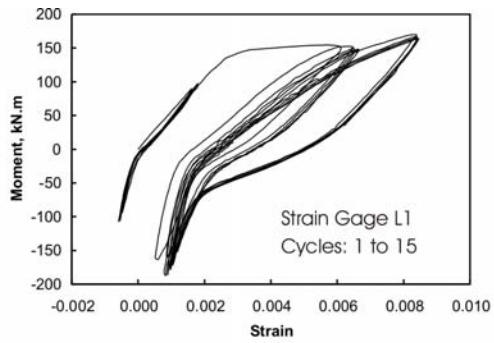
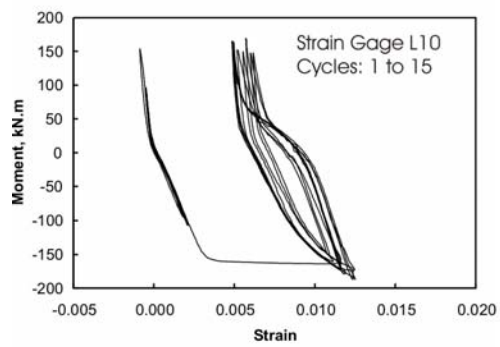


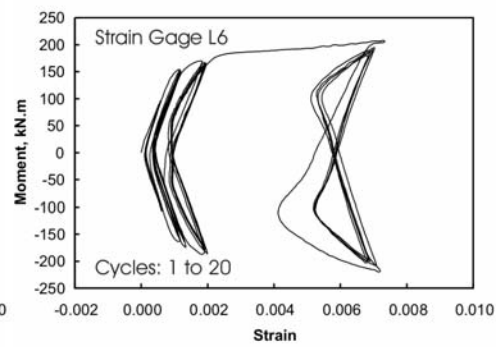
Figure D-3: Moment at the column base vs. strains of tie bars for column CL0



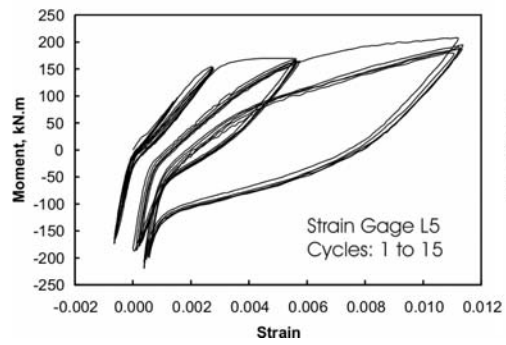
(a)



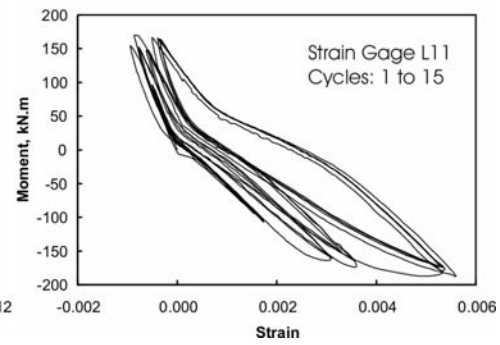
(b)



(c)

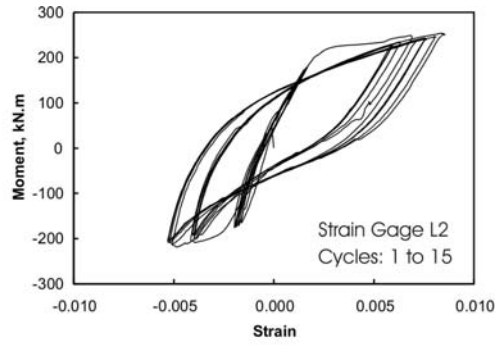


(d)

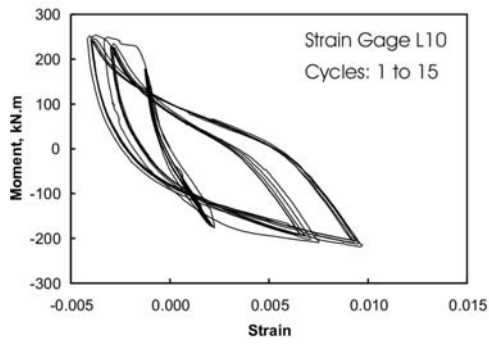


(e)

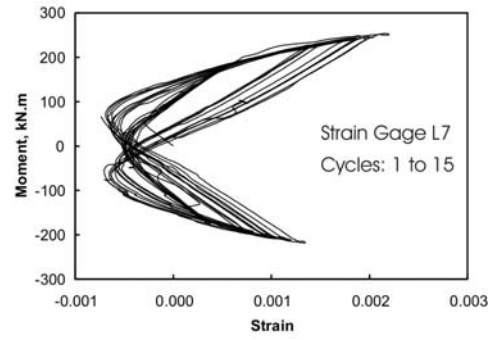
Figure D-4: Moment at column base vs. longitudinal bar strain for column CL1



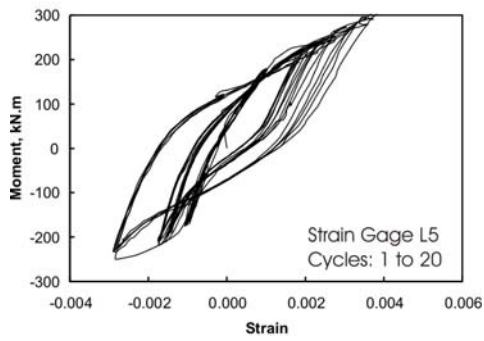
(a)



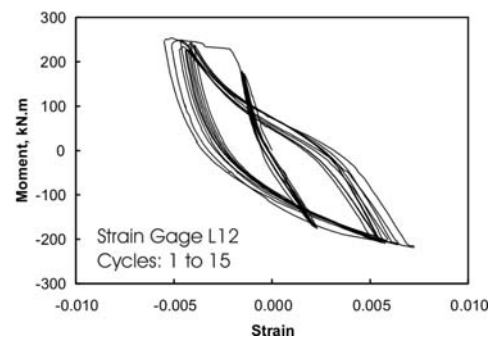
(b)



(c)

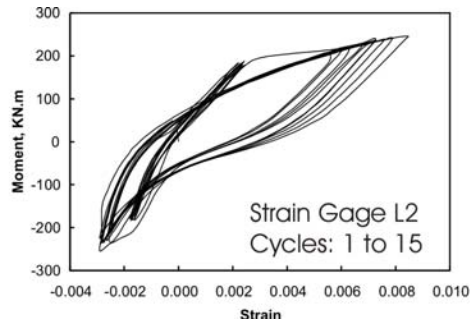


(d)

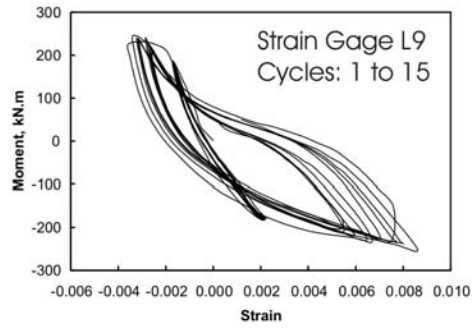


(e)

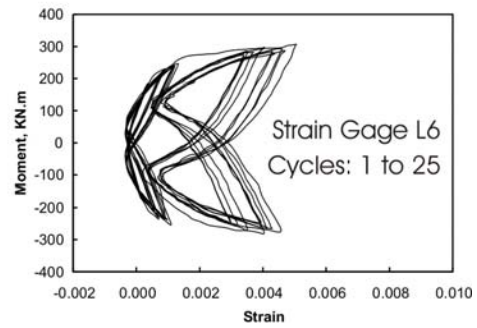
Figure D-5: Moment at column base and the strain on longitudinal bars for column CL2



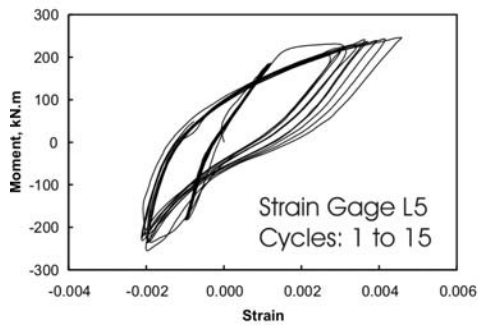
(a)



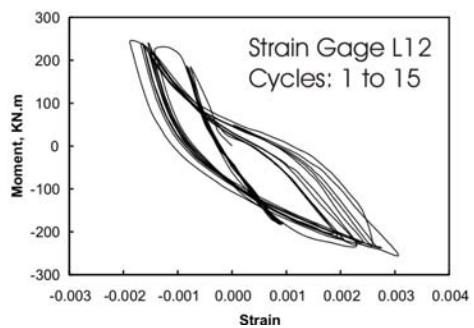
(b)



(c)

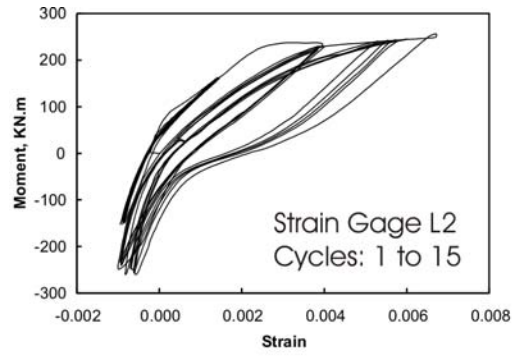


(d)

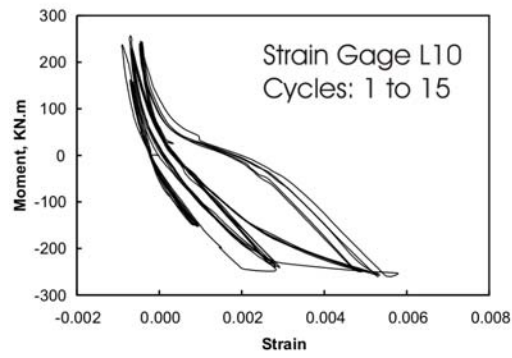


(e)

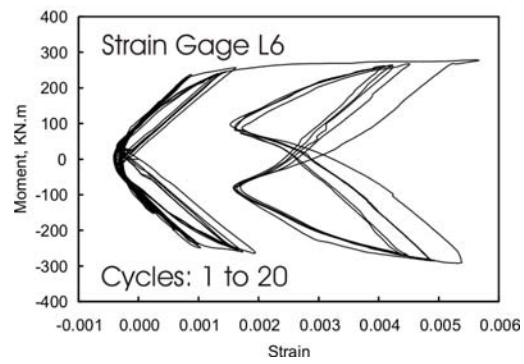
Figure D-6: Moment at column base vs. longitudinal bars for column CL3



(a)

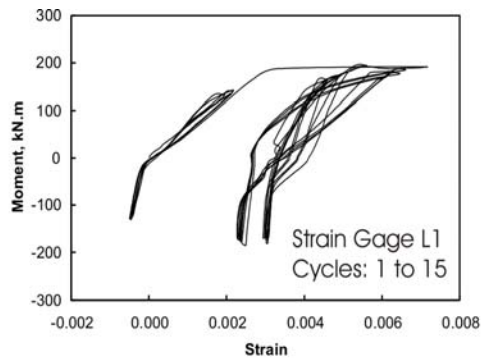


(b)

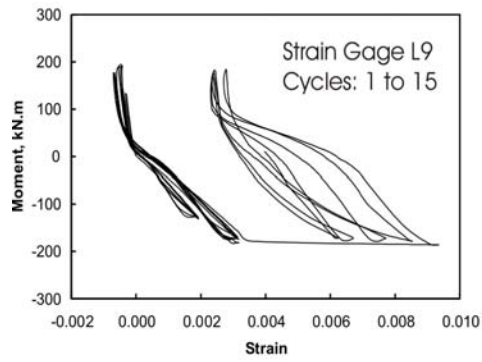


(c)

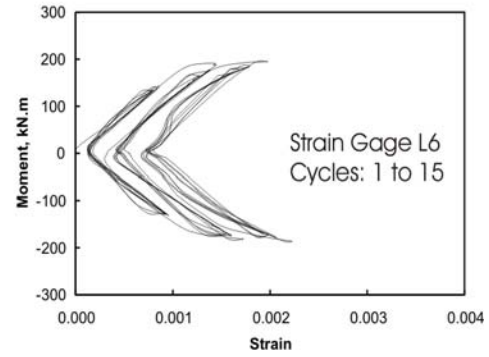
Figure D-7: Moment at column base vs. longitudinal bars for column CL4



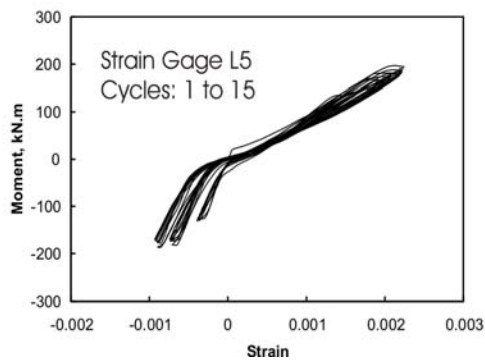
(a)



(b)

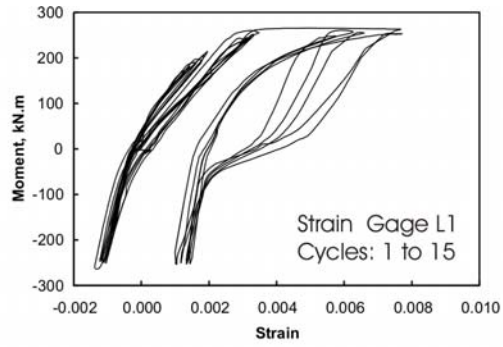


(c)

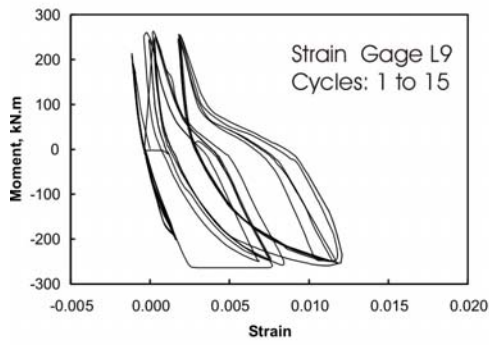


(d)

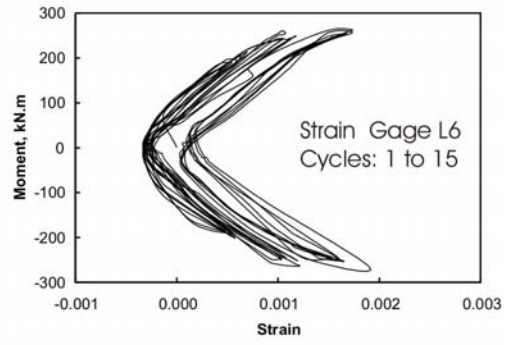
Figure D-8: Moment at column base and the strain on longitudinal bars for column CL5



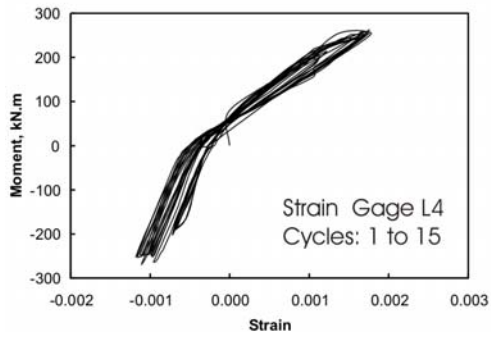
(a)



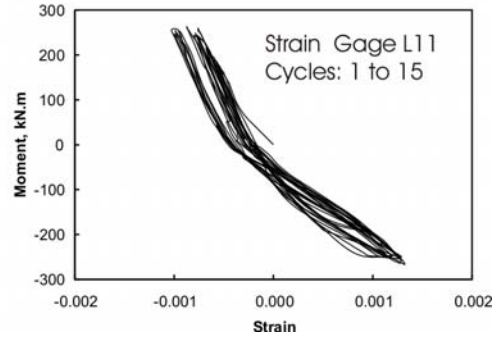
(b)



(c)

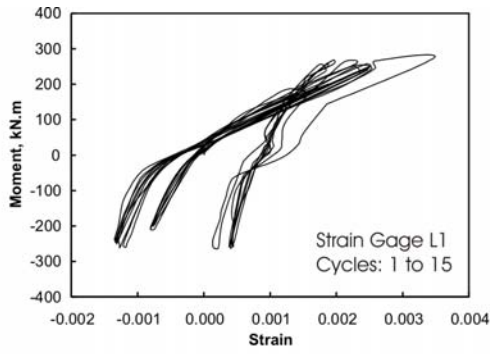


(d)

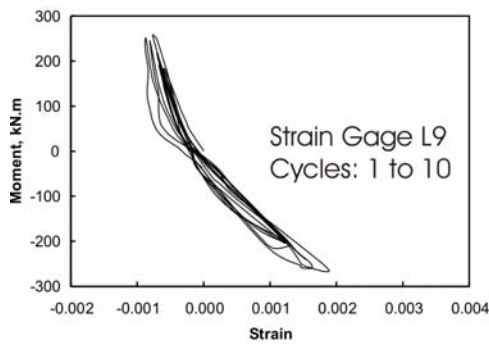


(e)

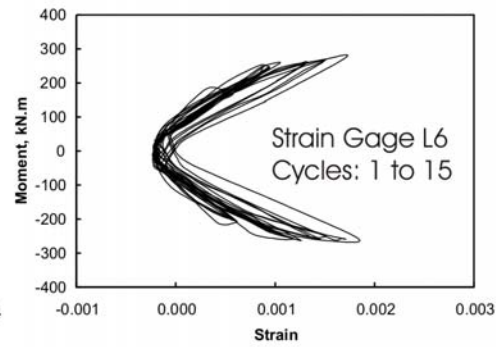
Figure D-9: Moment at column base vs. longitudinal bars for column CL6



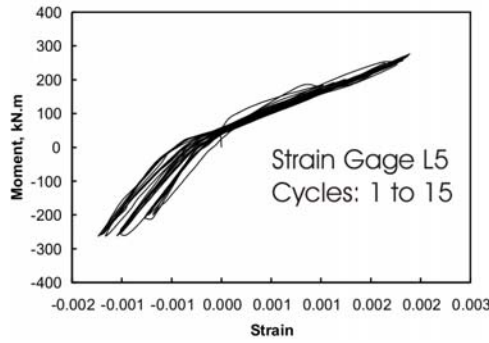
(a)



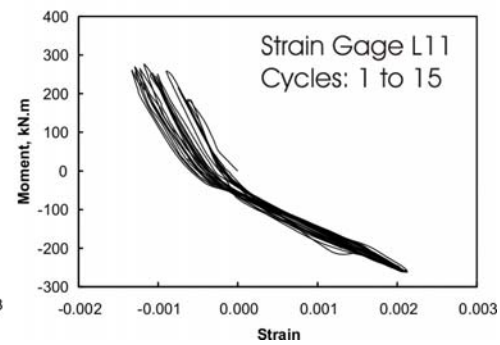
(b)



(c)

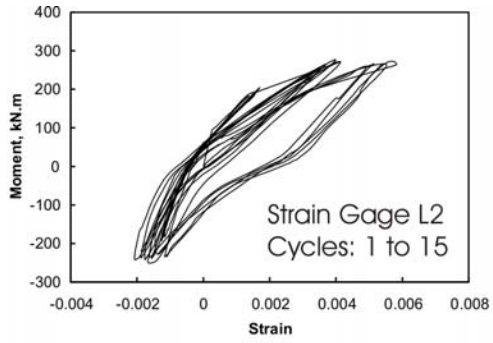


(d)

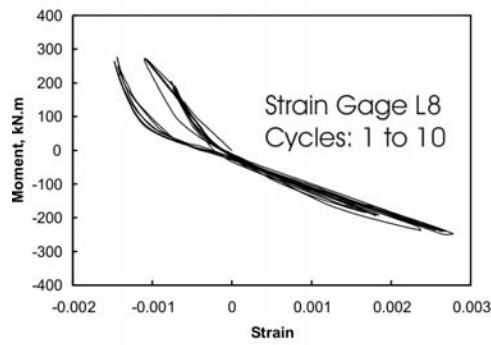


(e)

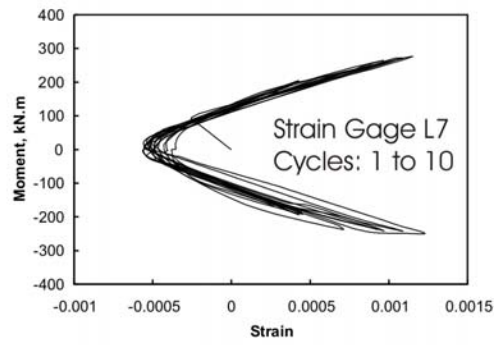
Figure D-10: Moment at column base vs. longitudinal bars strains for column CL7



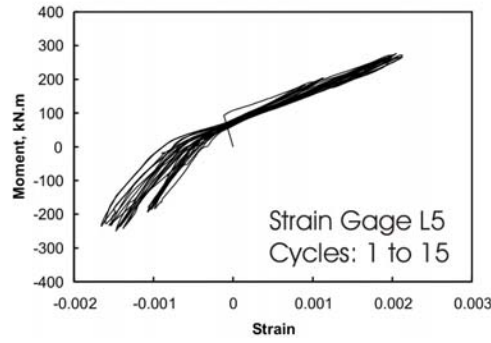
(a)



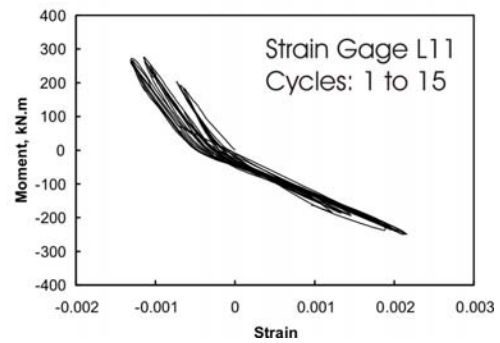
(b)



(c)



(d)



(e)

Figure D-11: Moment at column base vs. longitudinal bar strains for column CL8

**E. AVERAGE ENVELOPES TO MOMENT VERSUS DRIFT HYSTERESES**

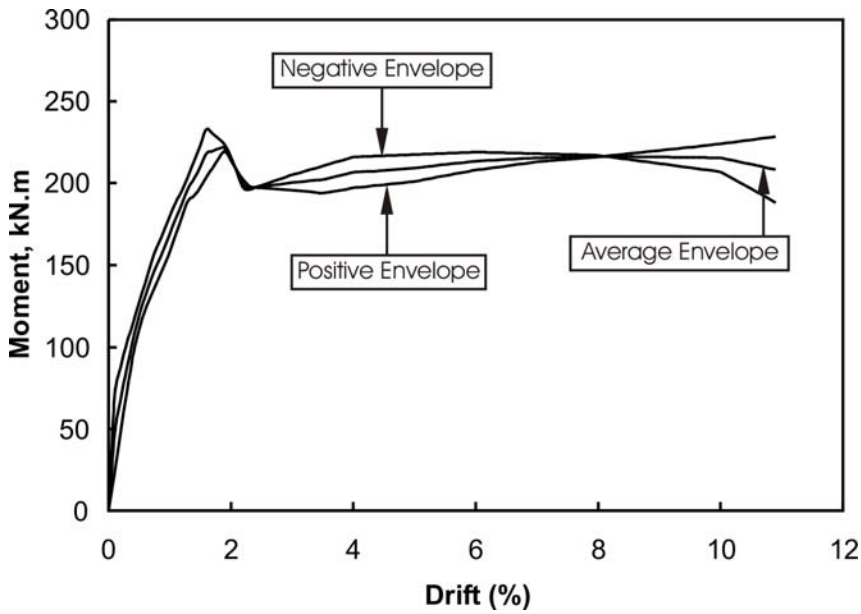


Figure E-1: Envelopes to moment vs. lateral drift hysteresis for column CL0

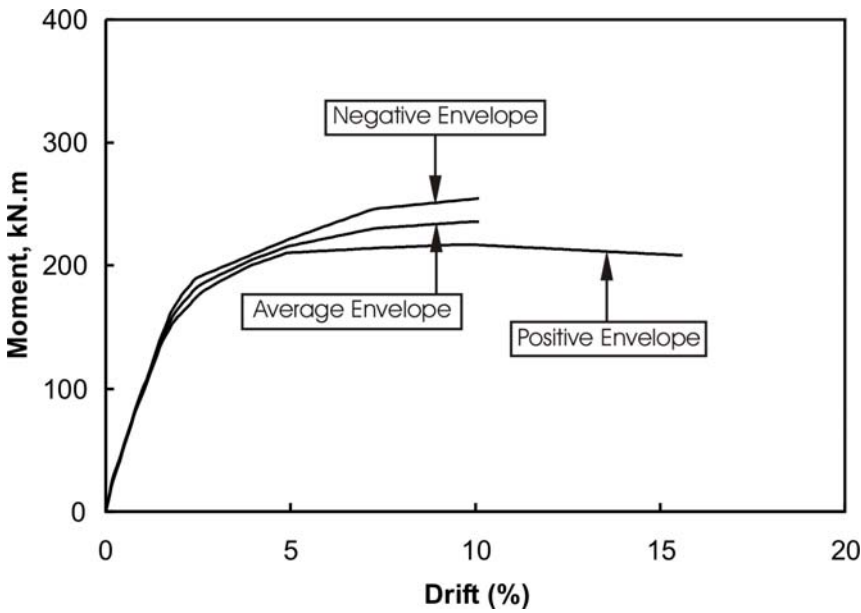


Figure E-2: Envelopes to moment vs. lateral drift hysteresis for specimen CL1

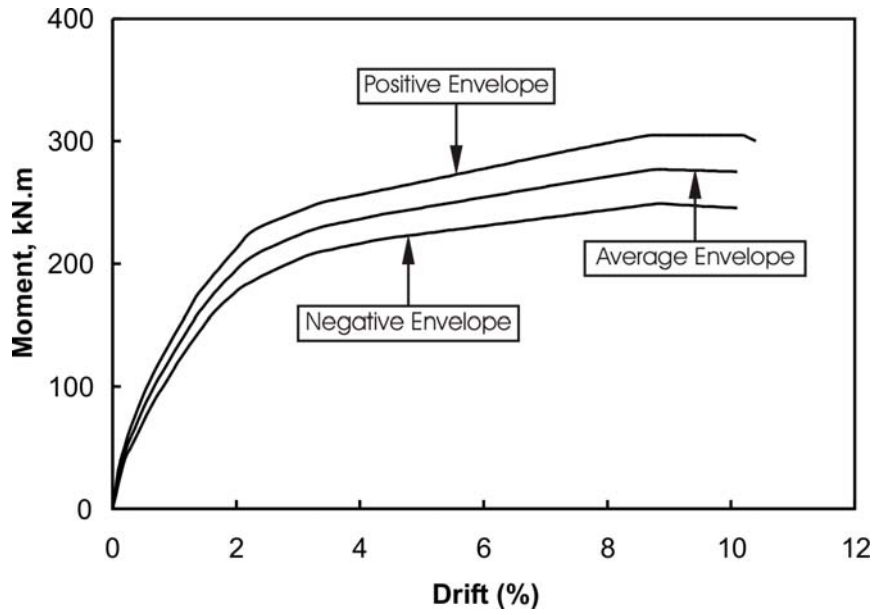


Figure E-3: Envelopes to moment vs. lateral drift hysteresis for specimen CL2

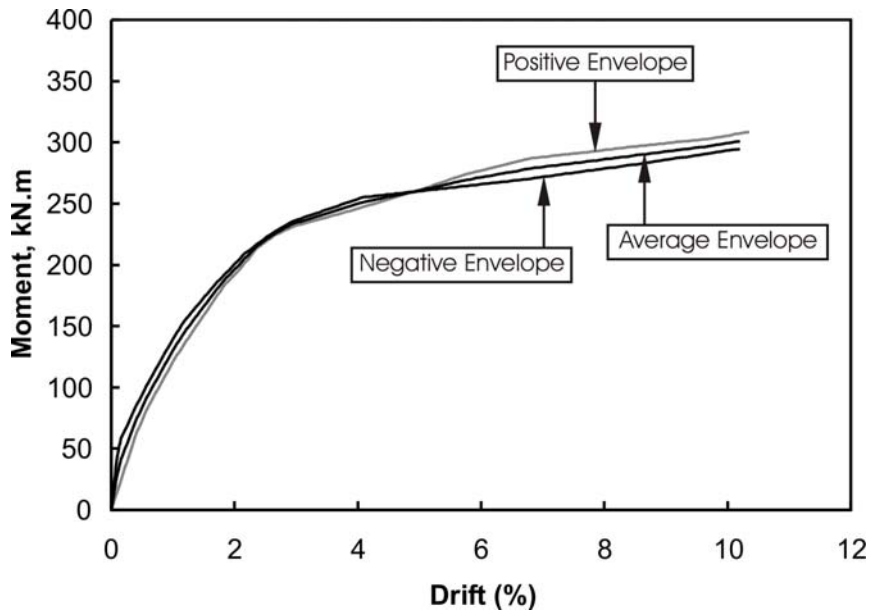


Figure E-4: Envelopes to moment vs. lateral drift hysteresis for specimen CL3

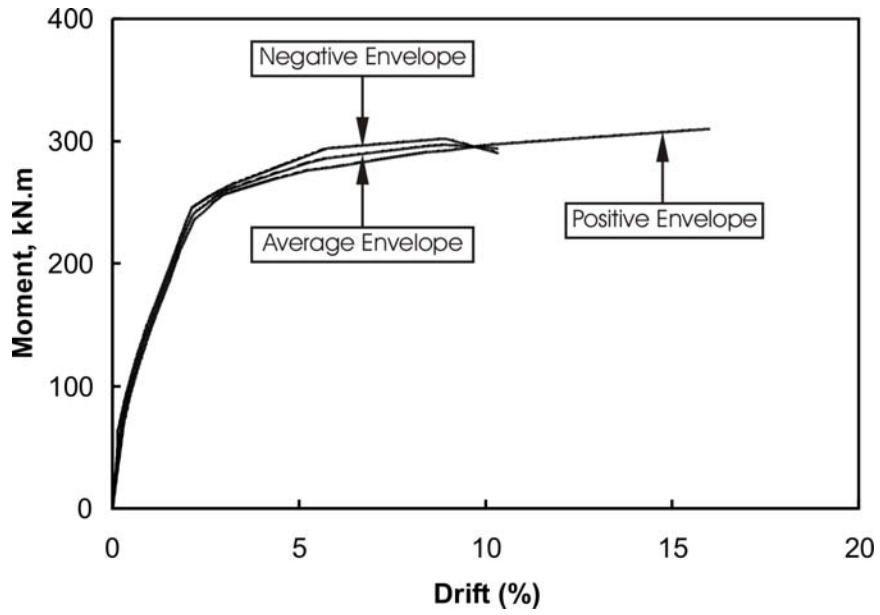


Figure E-5: Envelopes to moment vs. lateral drift hysteresis for specimen CL4

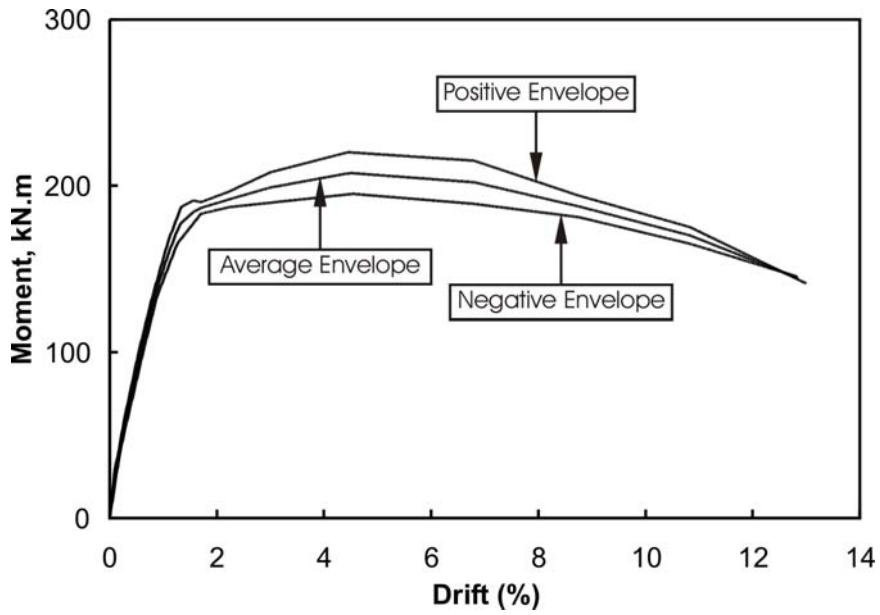


Figure E-6: Envelopes to moment vs. lateral drift hysteresis for specimen CL5

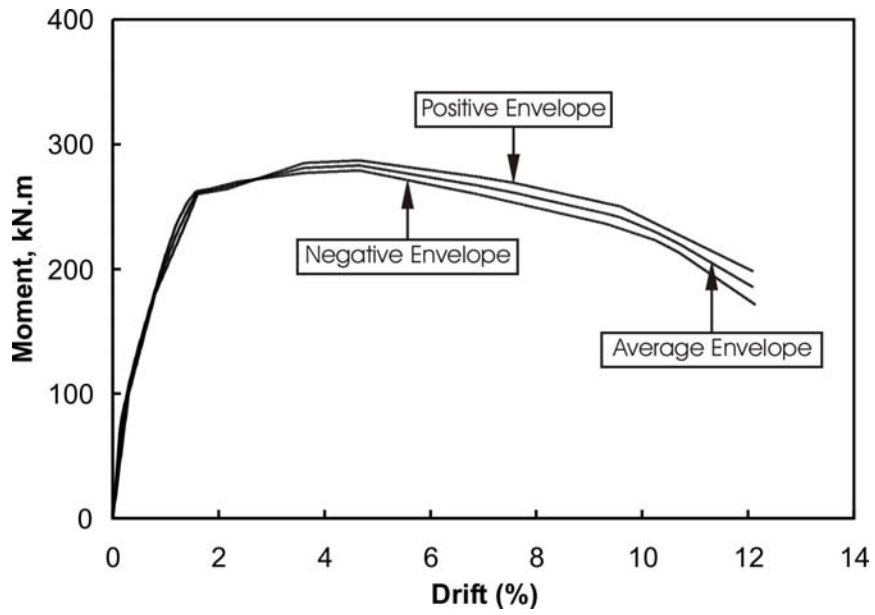


Figure E-7: Envelopes to moment vs. lateral drift hysteresis for specimen CL6

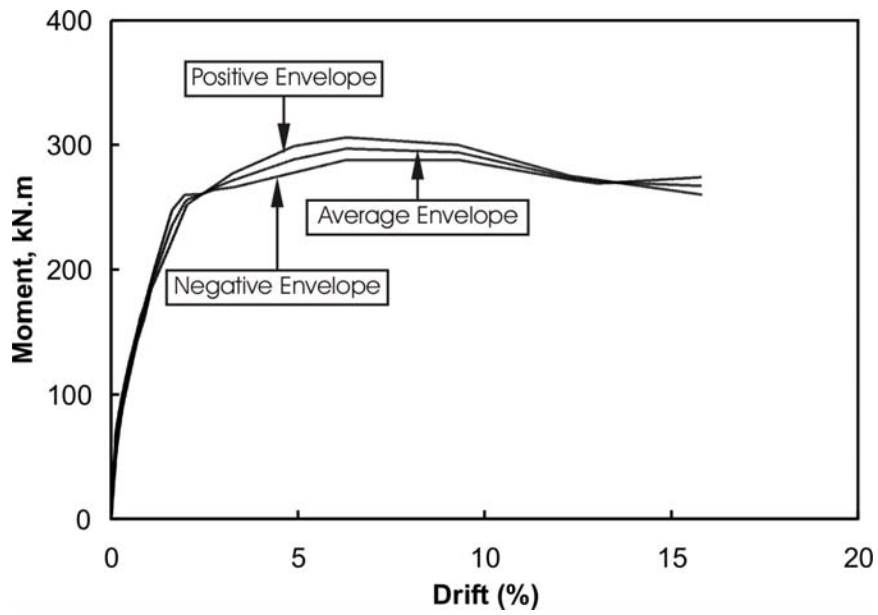


Figure E-8: Envelopes to moment vs. lateral drift hysteresis for specimen CL7

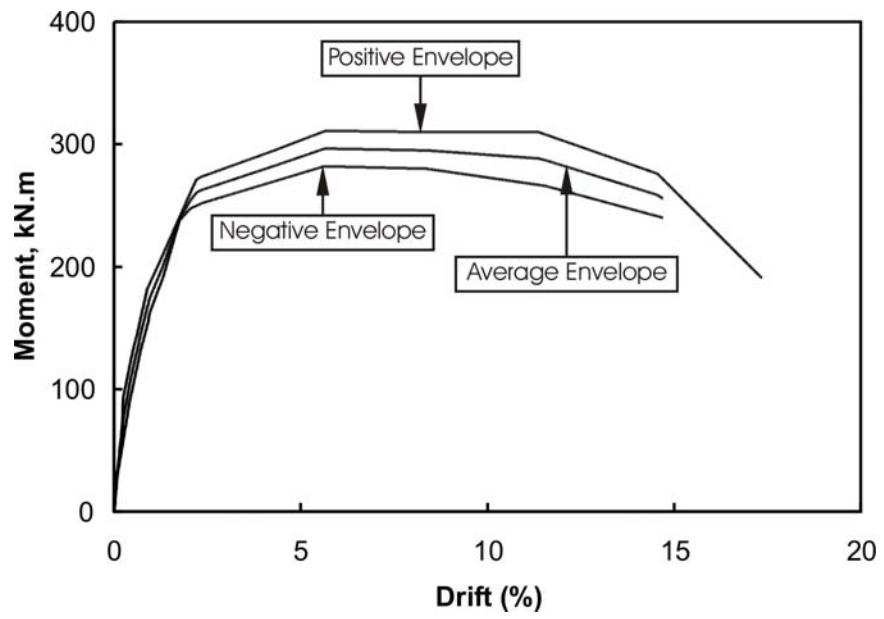


Figure E-9: Envelopes to moment vs. lateral drift hysteresis for specimen CL8

## F. DETERMINATION OF YIELD DISPLACEMENTS

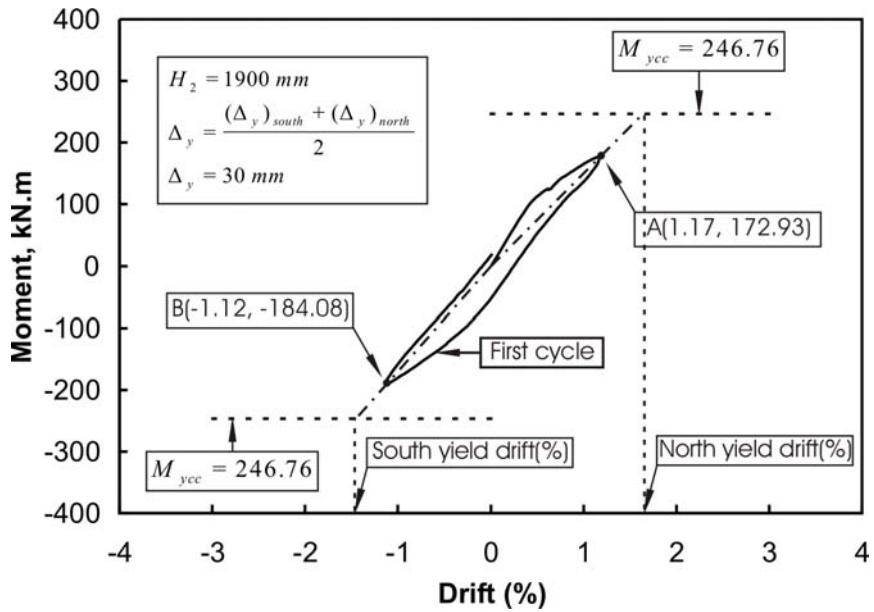


Figure F-1: Determination of yield displacement for column CL0 using the first cycle (method 1(alternative 2))

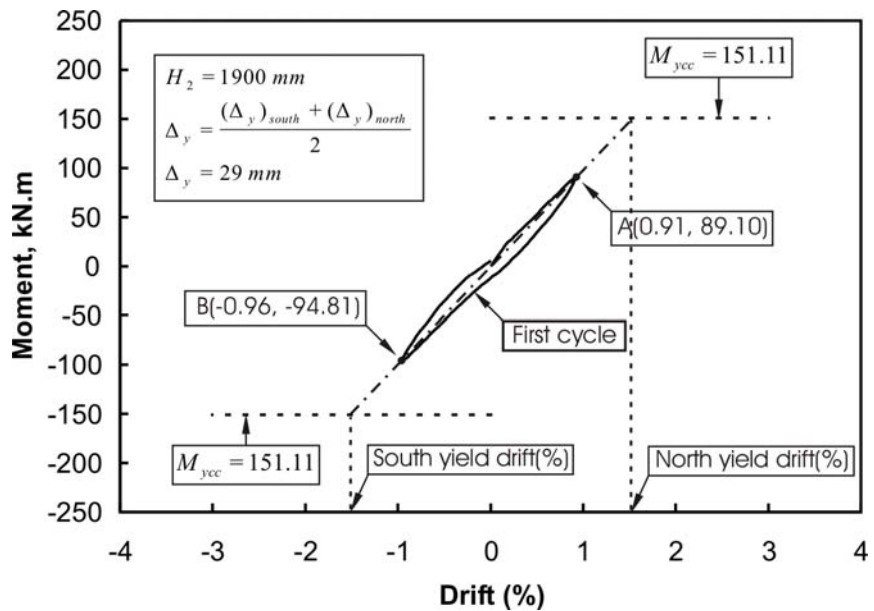


Figure F-2: Determination of yield displacement for column CL1 using the first cycle (method 1(alternative 2))

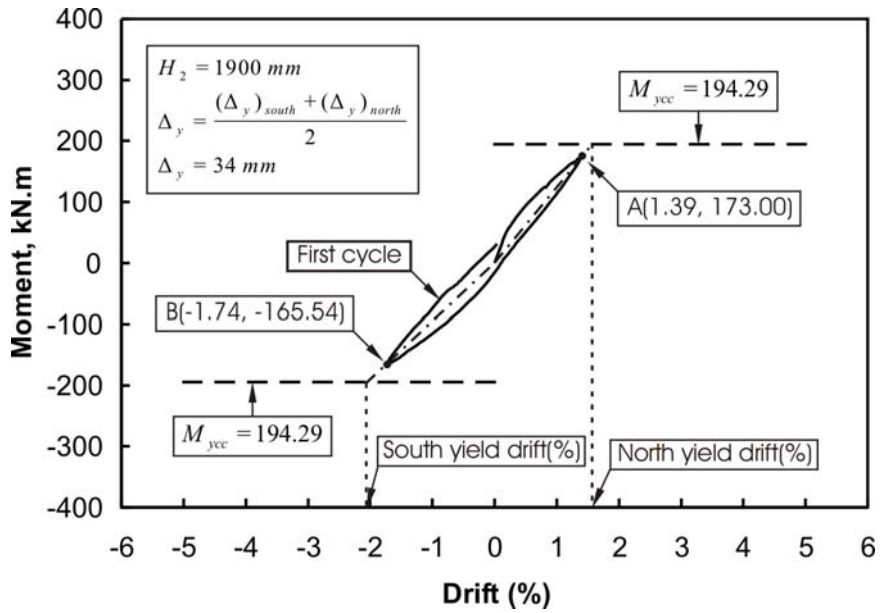


Figure F-3: Determination of yield displacement for column CL2 using the first cycle (method 1(alternative 2))

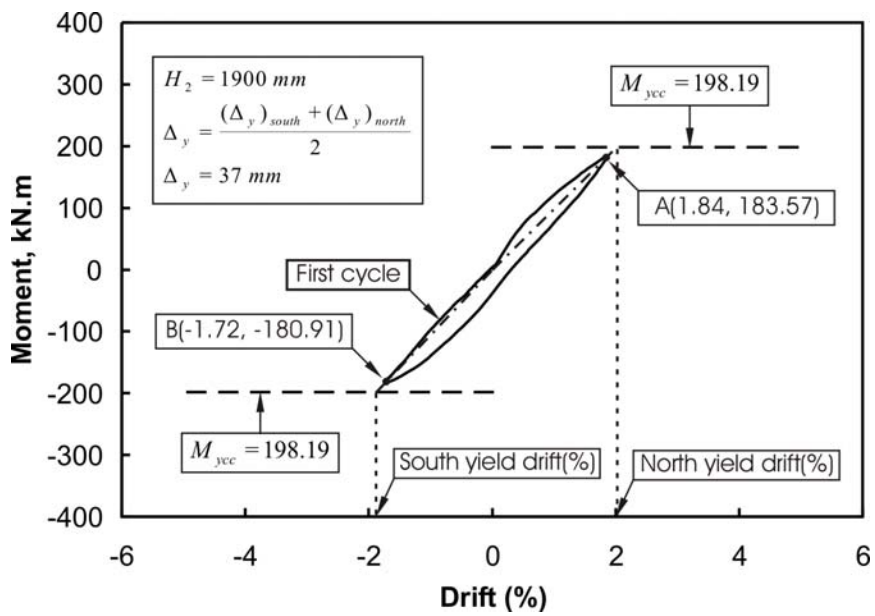


Figure F-4: Determination of yield displacement for column CL3 using the first cycle (method 1(alternative 2))

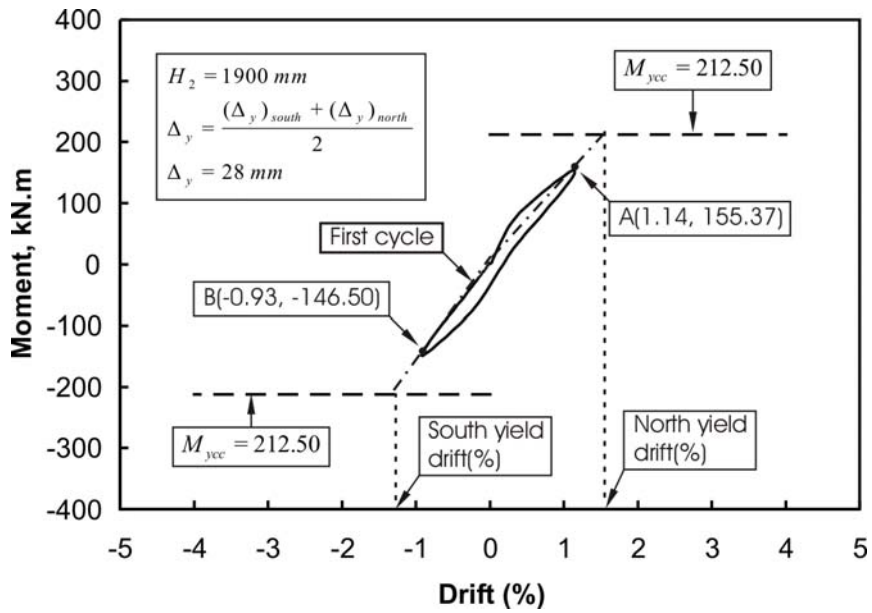


Figure F-5: Determination of yield displacement for column CL4 using the first cycle (method 1(alternative 2))

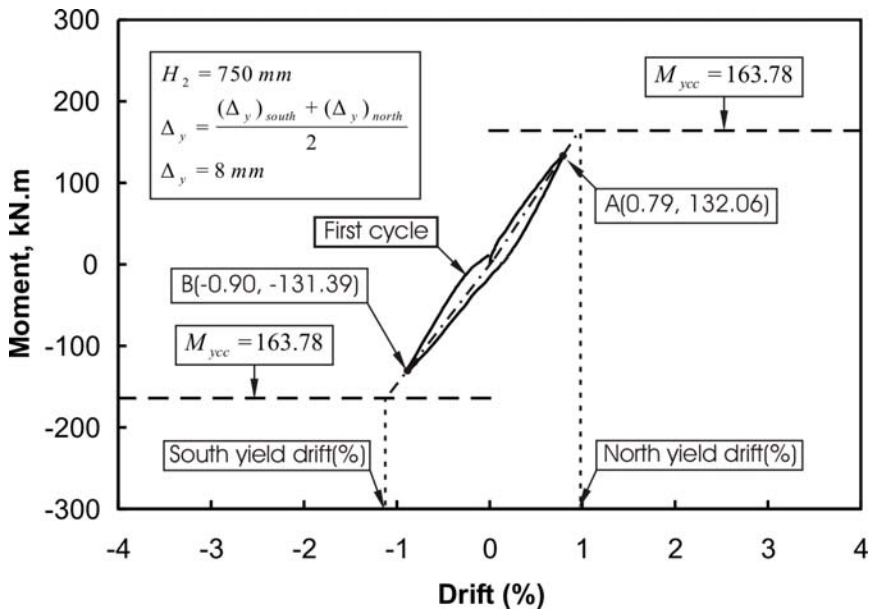


Figure F-6 Determination of yield displacement for column CL5 using the first cycle (method 1(alternative 2))

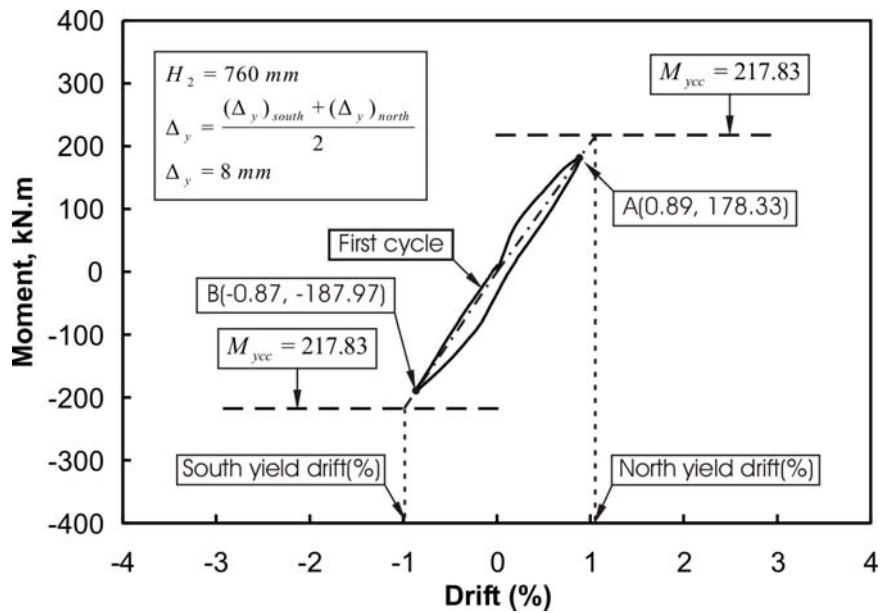


Figure F-7: Determination of yield displacement for column CL6 using the first cycle(method 1(alternative 2))

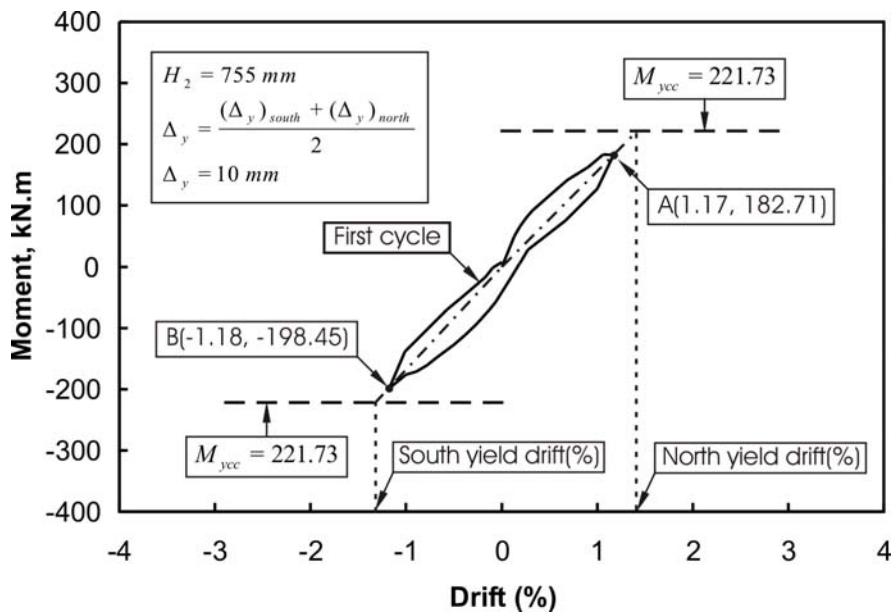


Figure F-8: Determination of yield displacement for column CL7 using the first cycle (method 1(alternative 2))

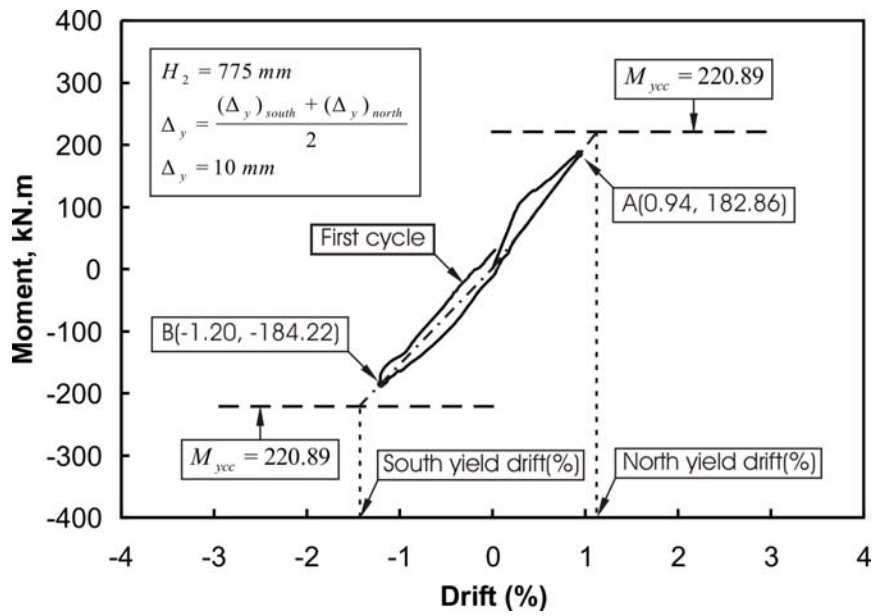


Figure F-9: Determination of yield displacement for column CL8 using the first cycle (method 1(alternative 2))

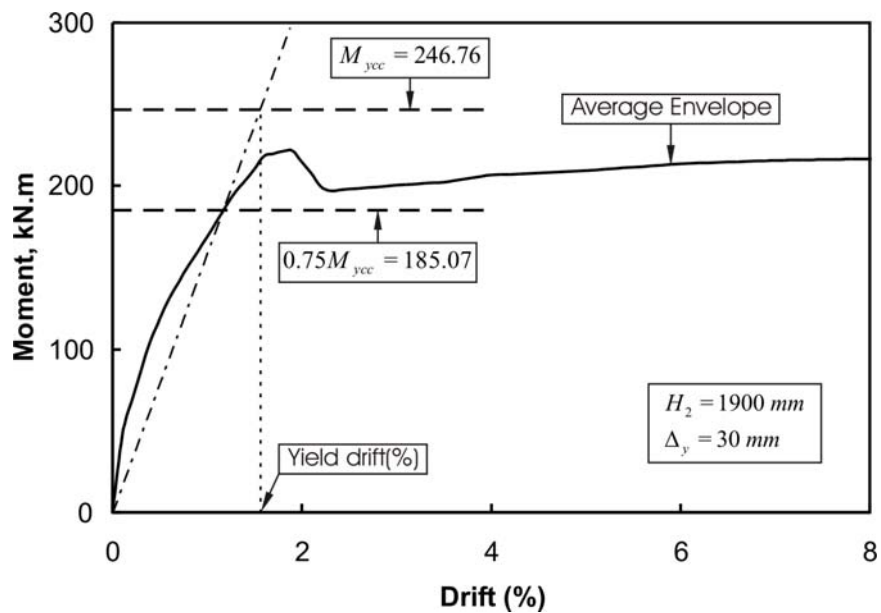


Figure F-10: Determination of yield displacement for column CL0 using average envelope (method 1(alternative 3))

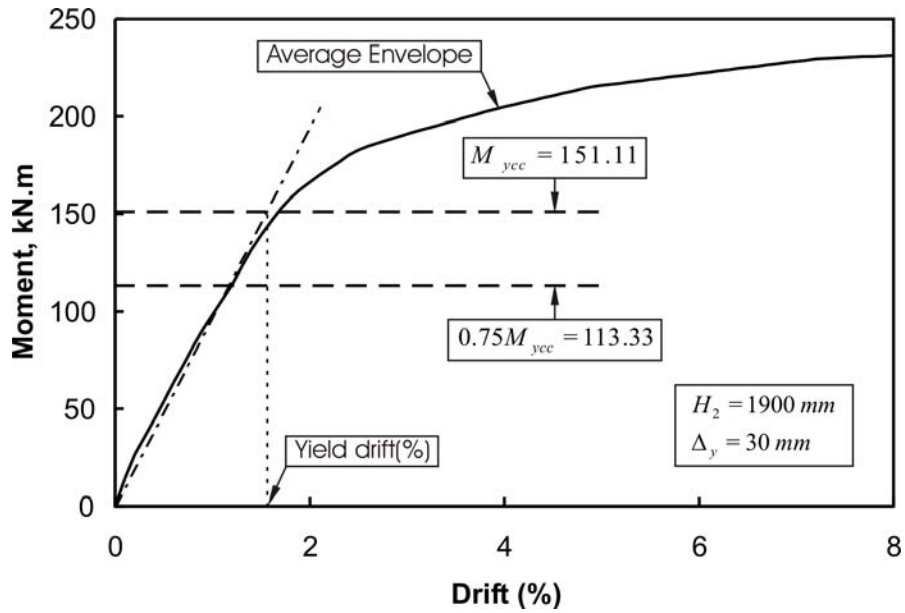


Figure F-11: Determination of yield displacement for column CL1 using average envelope (method 1(alternative 3))

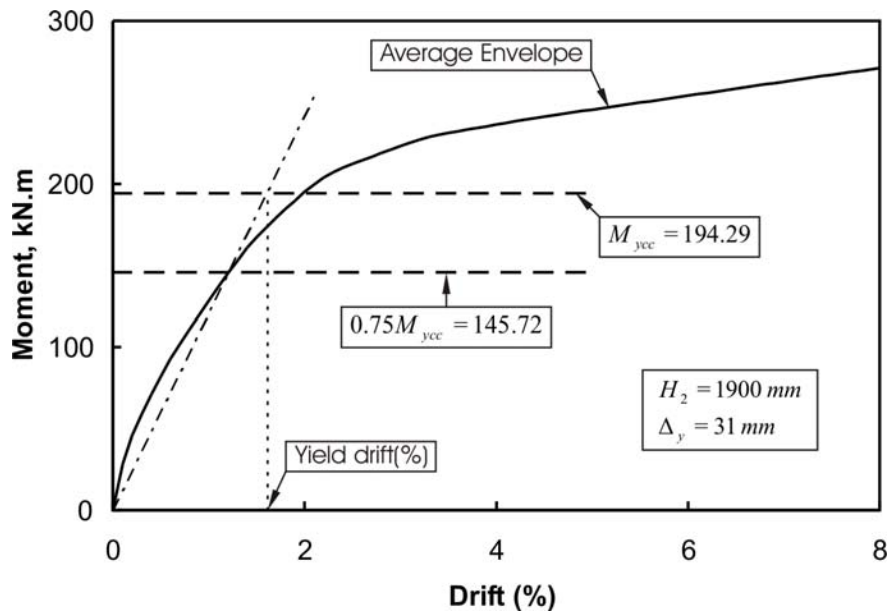


Figure F-12: Determination of yield displacement for column CL2 using average envelope (method 1(alternative 3))

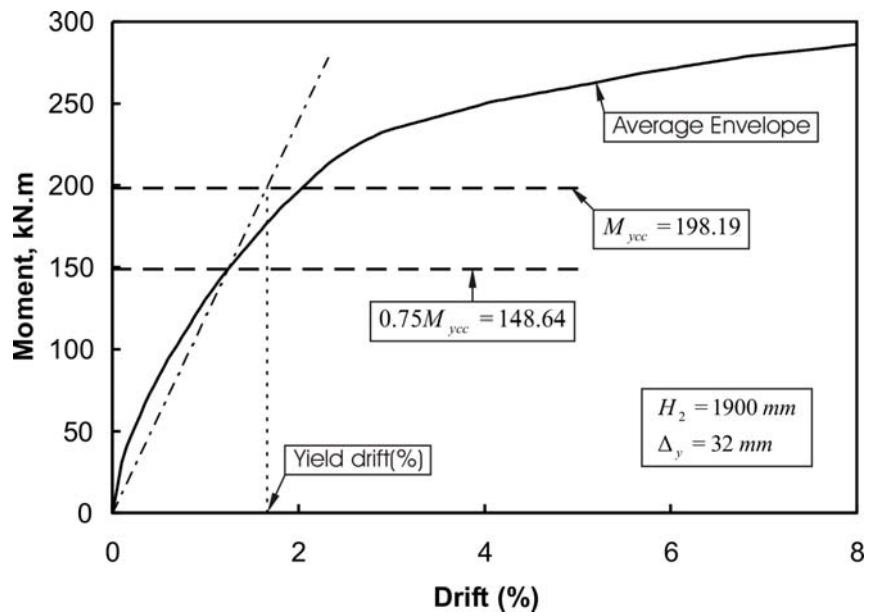


Figure F-13: Determination of yield displacement for column CL3 using average envelope (method 1(alternative 3))

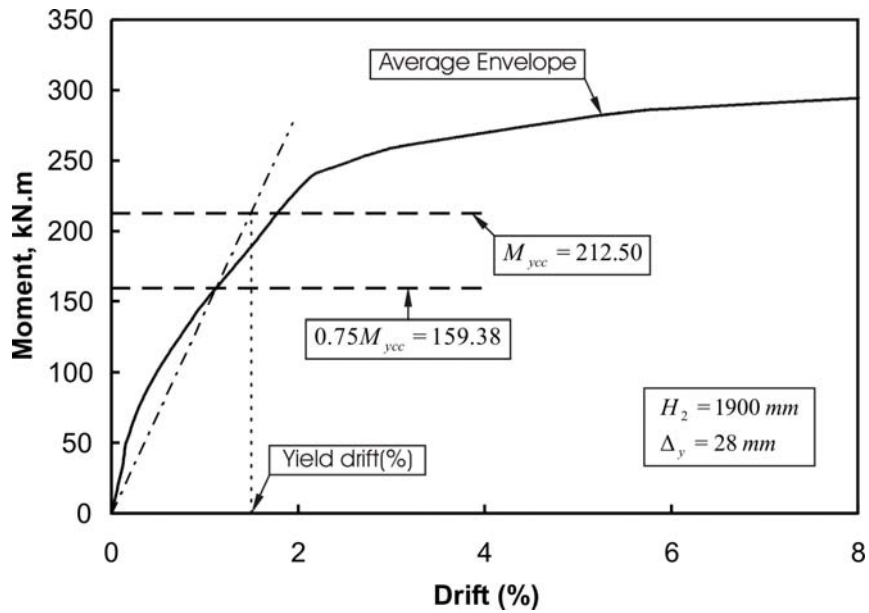


Figure F-14: Determination of yield displacement for column CL4 using average envelope (method 1(alternative 3))

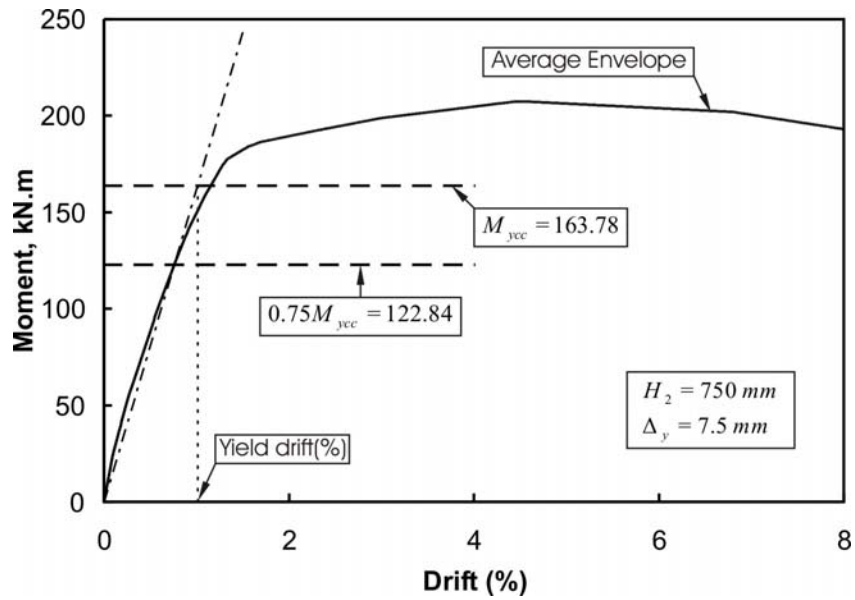


Figure F-15: Determination of yield displacement for column CL5 using average envelope (method 1(alternative 3))

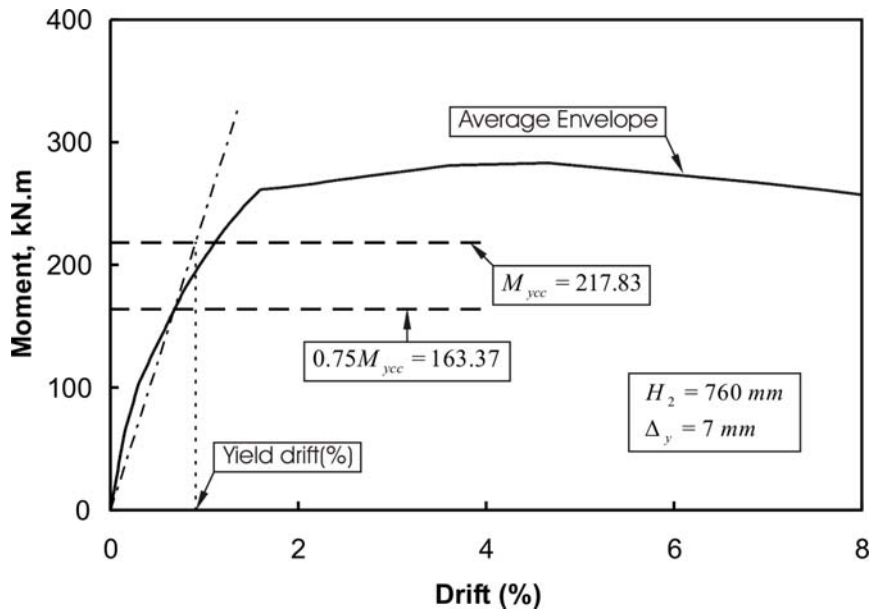


Figure F-16: Determination of yield displacement for column CL6 using average envelope (method 1(alternative 3))

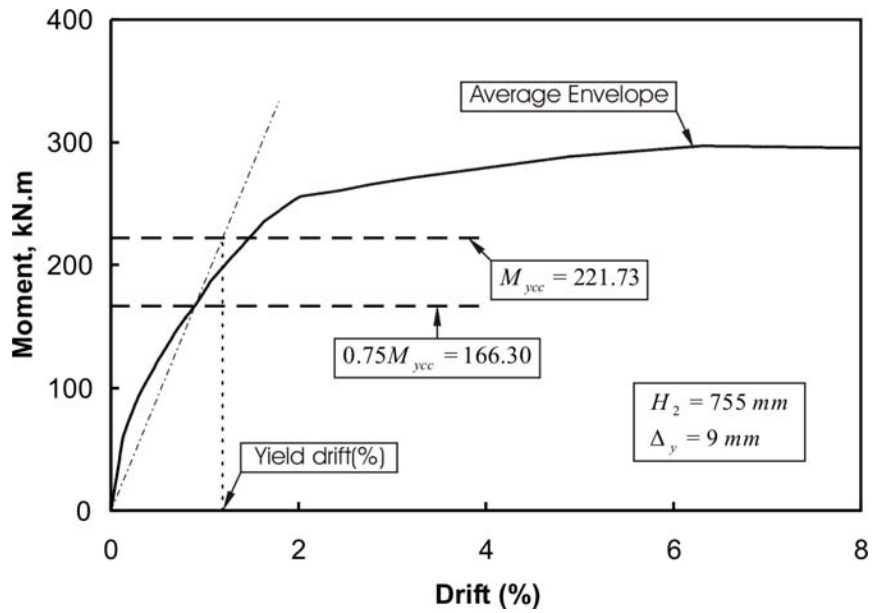


Figure F-17: Determination of yield displacement for column CL7 using average envelope (method 1(alternative 3))

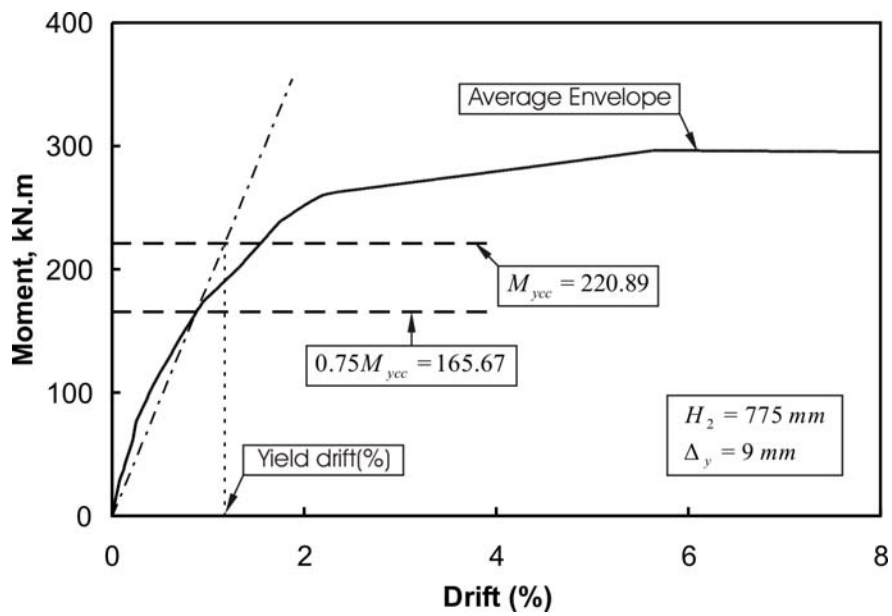


Figure F-18: Determination of yield displacement for column CL8 using average envelope (method 1(alternative 3))

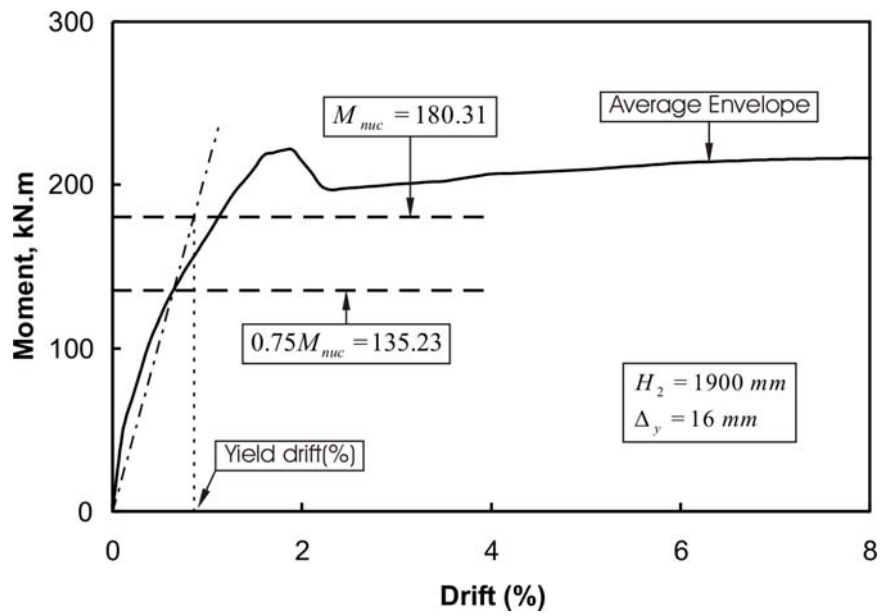


Figure F-19: Determination of yield displacement for column CL0 using average envelope (method 1(alternative 4))

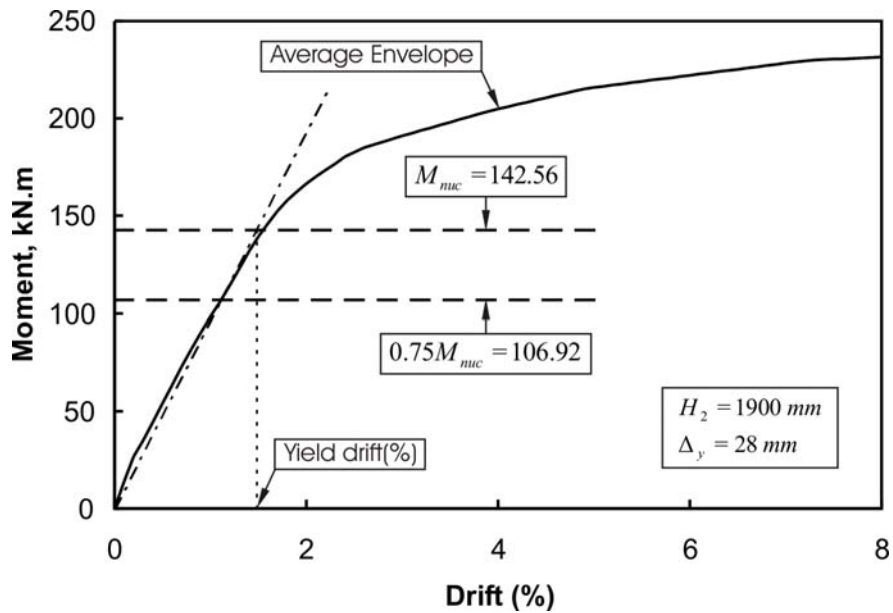


Figure F-20: Determination of yield displacement for column CL1 using average envelope (method 1(alternative 4))

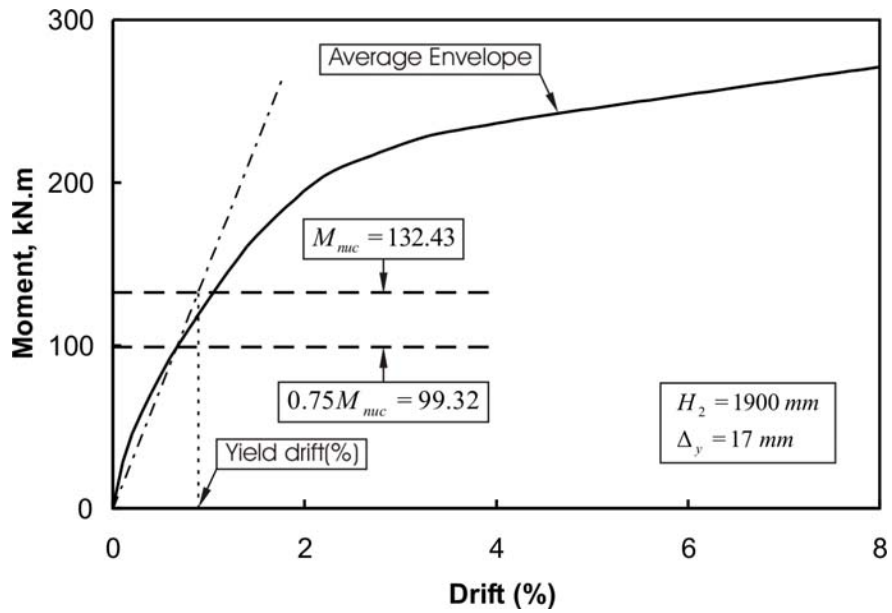


Figure F-21: Determination of yield displacement for column CL2 using average envelope (method 1(alternative 4))

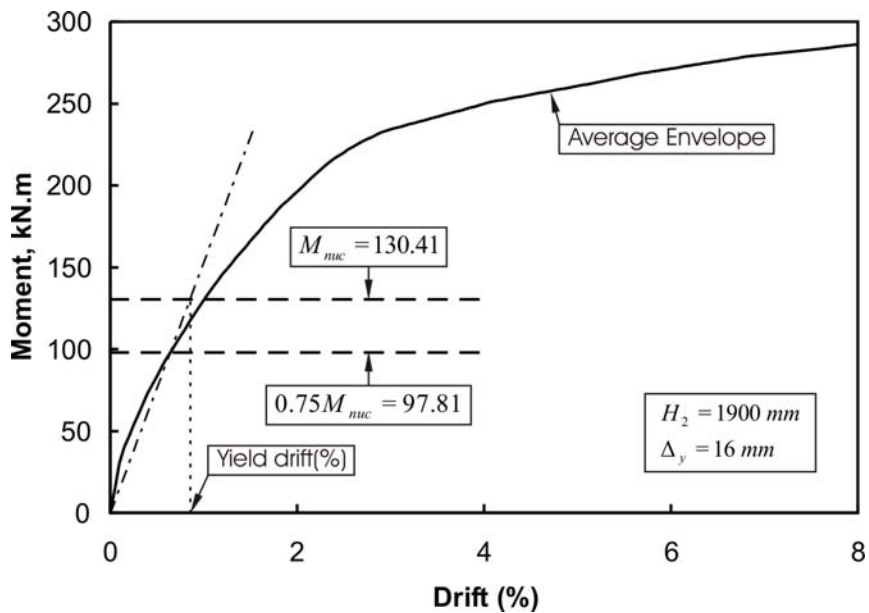


Figure F-22: Determination of yield displacement for column CL3 using average envelope (method 1(alternative 4))

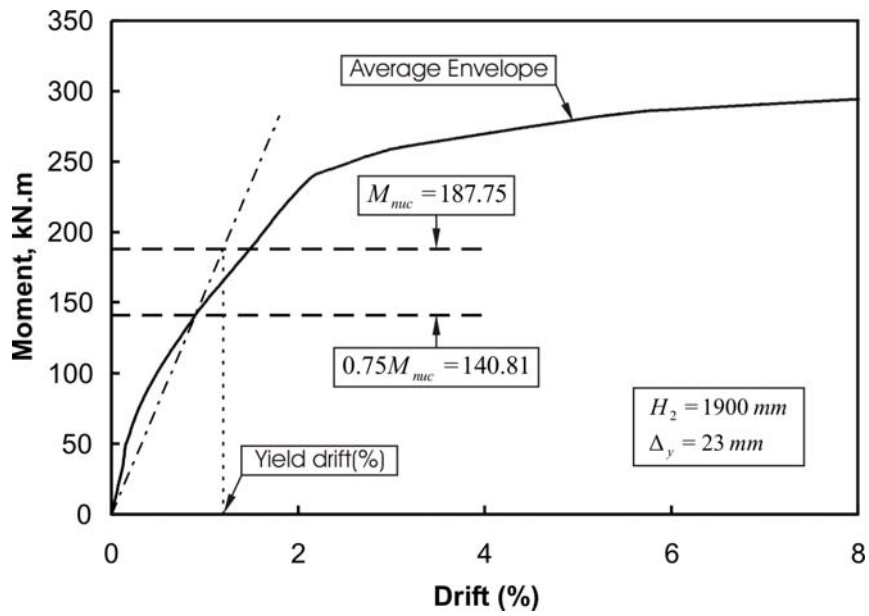


Figure F-23: Determination of yield displacement for column CL4 using average envelope (method 1(alternative 4))

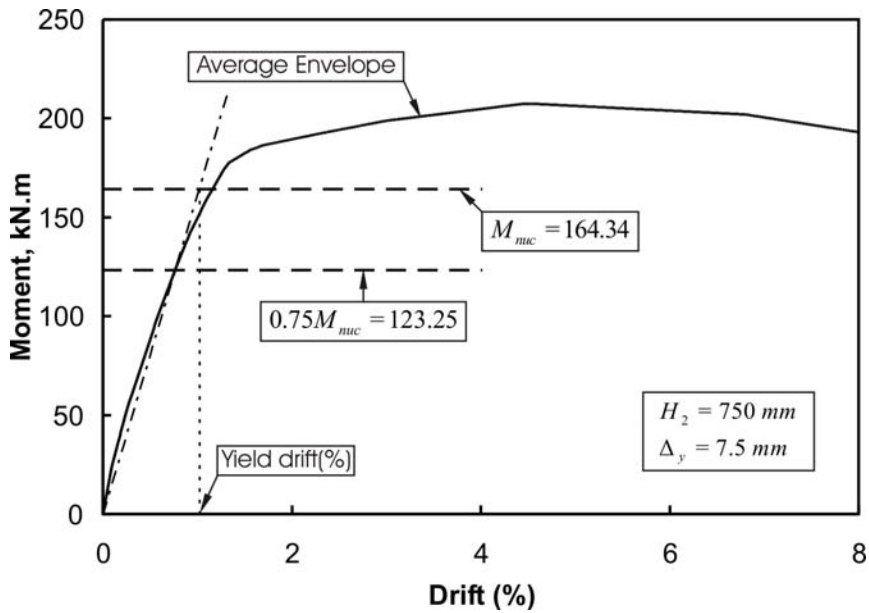


Figure F-24: Determination of yield displacement for column CL5 using average envelope (method 1(alternative 4))

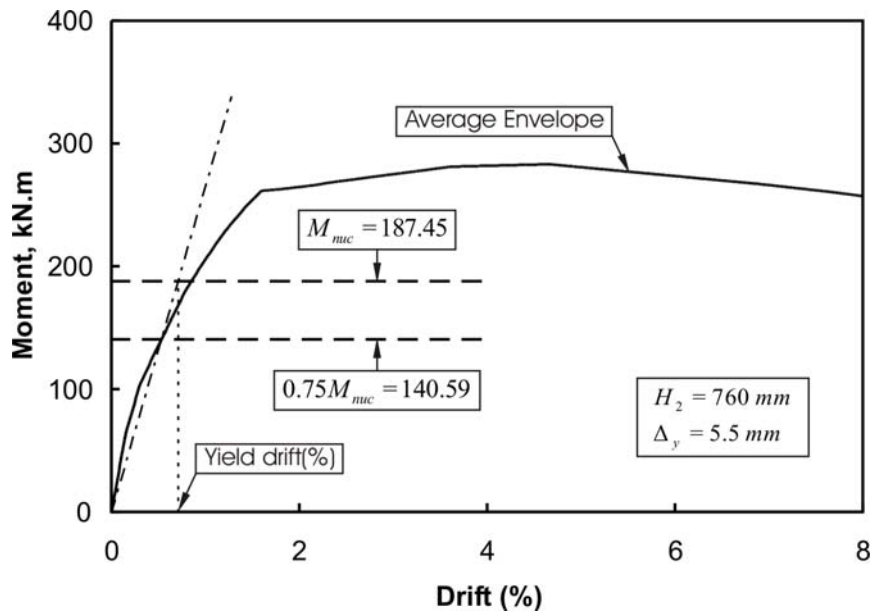


Figure F-25: Determination of yield displacement for column CL6 using average envelope (method 1(alternative 4))

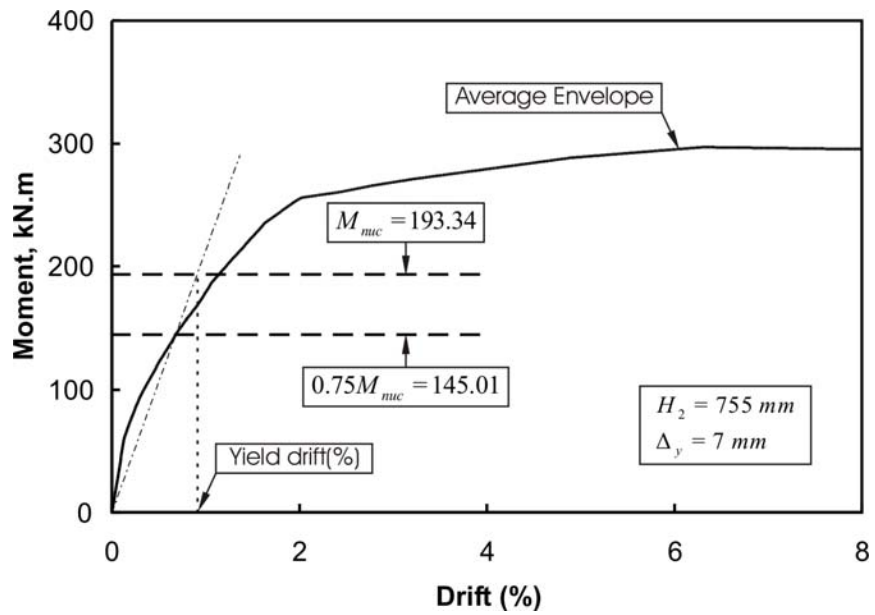


Figure F-26: Determination of yield displacement for column CL7 using average envelope (method 1(alternative 4))

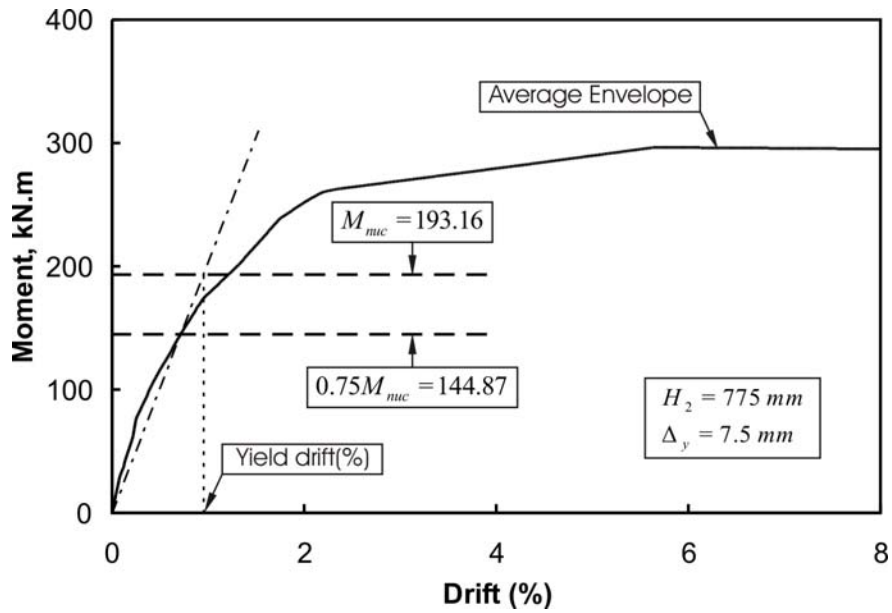


Figure F-27: Determination of yield displacement for column CL8 using average envelope (method 1(alternative 4))

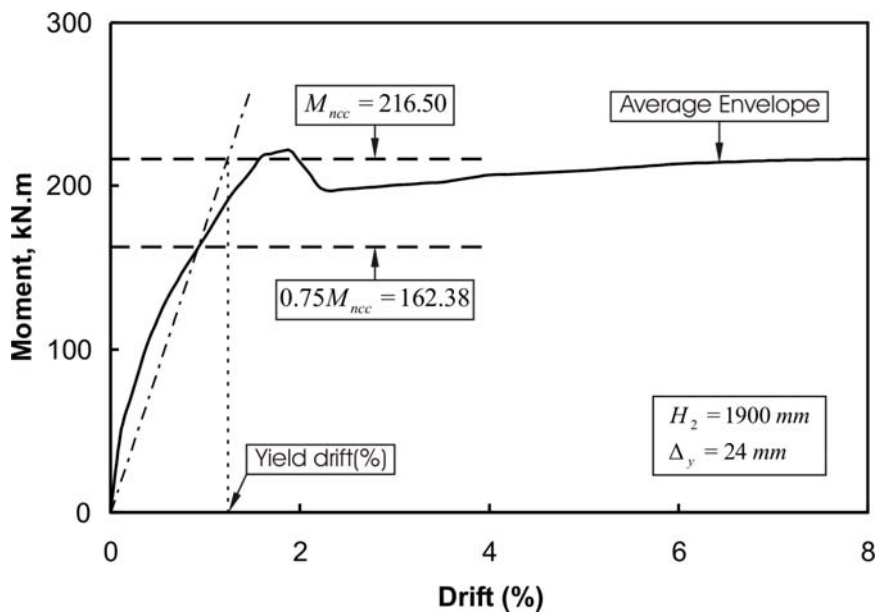


Figure F-28: Determination of yield displacement for column CL0 using average envelope (method 1(alternative 5))

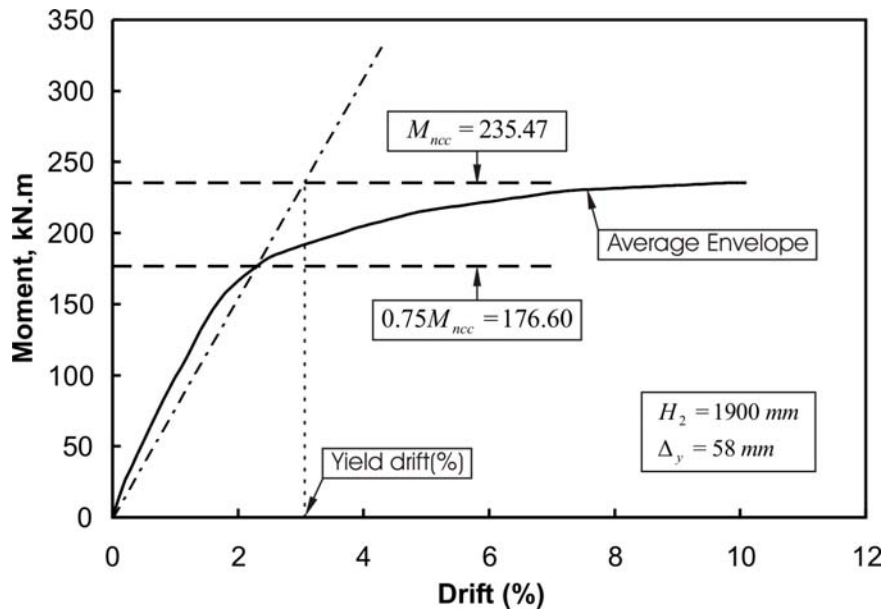


Figure F-29: Determination of yield displacement for column CL1 using average envelope (method 1(alternative 5))

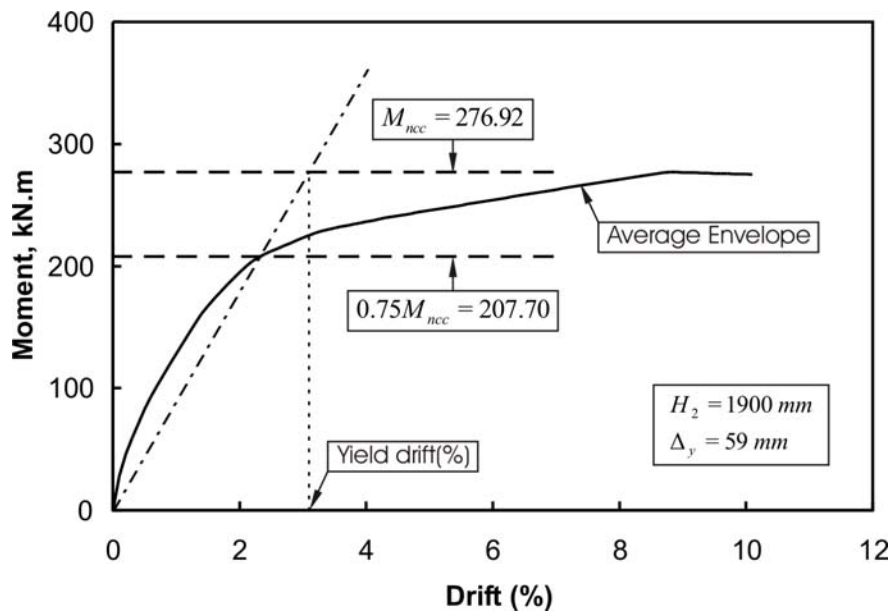


Figure F-30: Determination of yield displacement for column CL2 using average envelope (method 1(alternative 5))

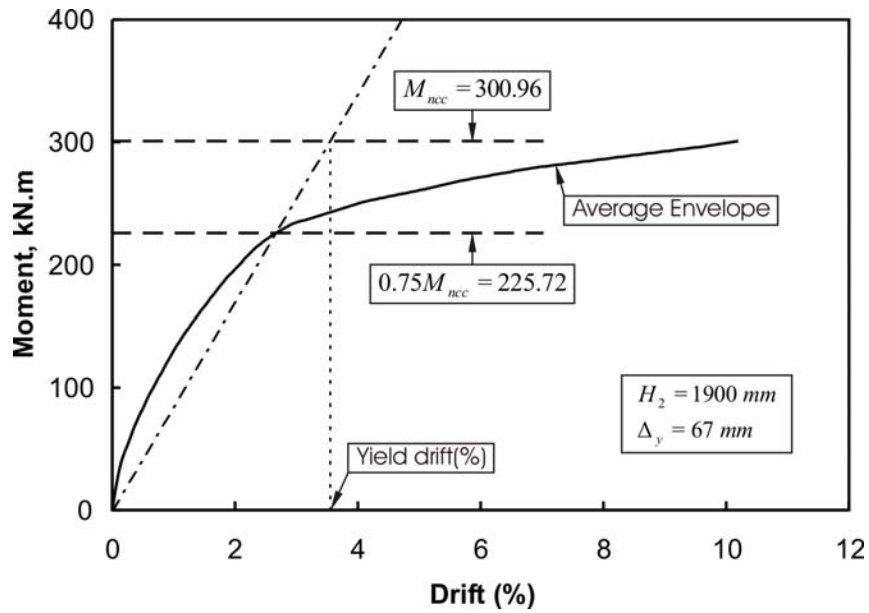


Figure F-31: Determination of yield displacement for column CL3 using average envelope (method 1(alternative 5))

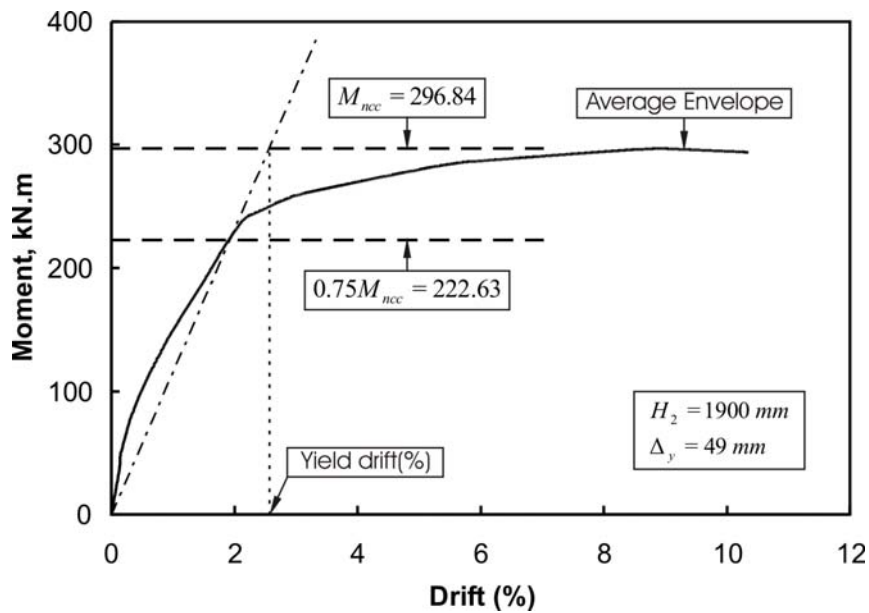


Figure F-32: Determination of yield displacement for column CL4 using average envelope (method 1(alternative 5))

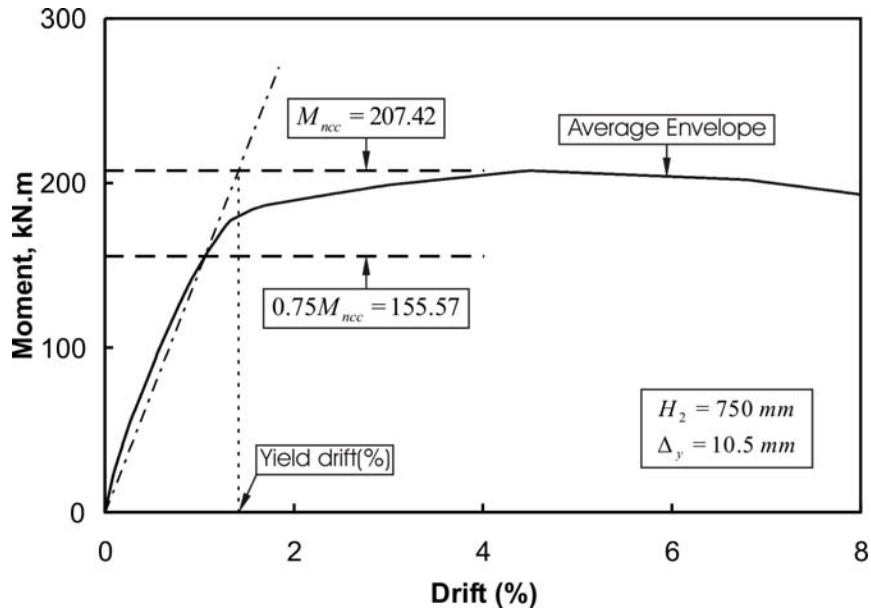


Figure F-33: Determination of yield displacement for column CL5 using average envelope (method 1(alternative 5))

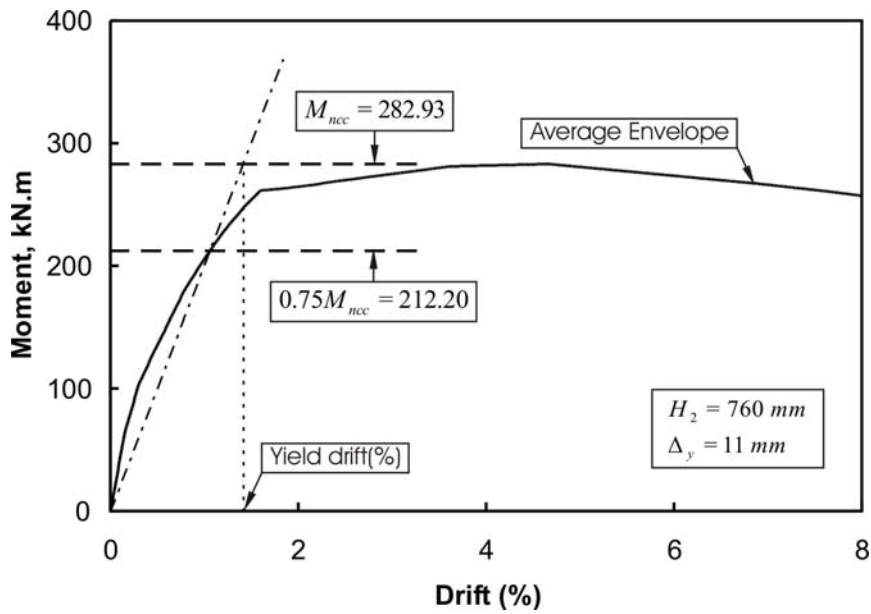


Figure F-34: Determination of yield displacement for column CL6 using average envelope (method 1(alternative 5))

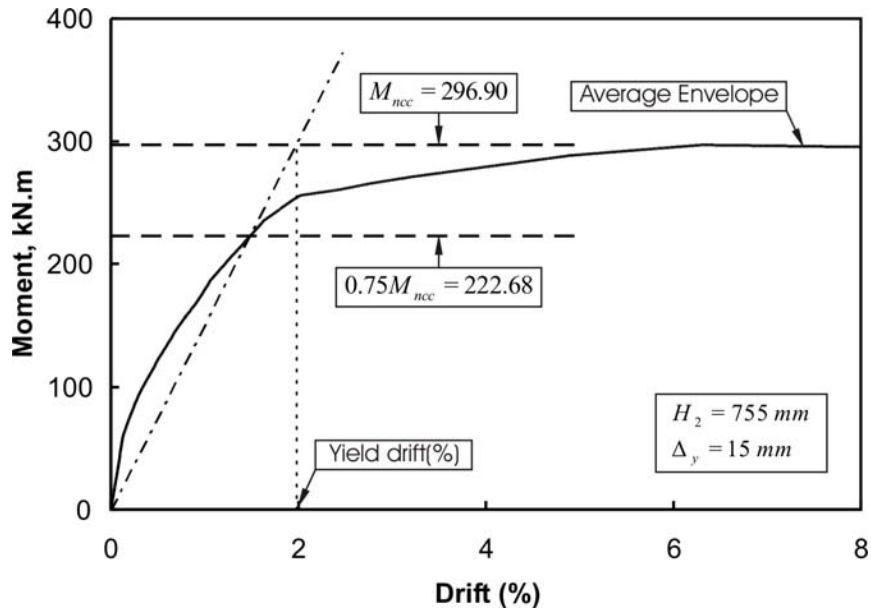


Figure F-35: Determination of yield displacement for column CL7 using average envelope (method 1(alternative 5))

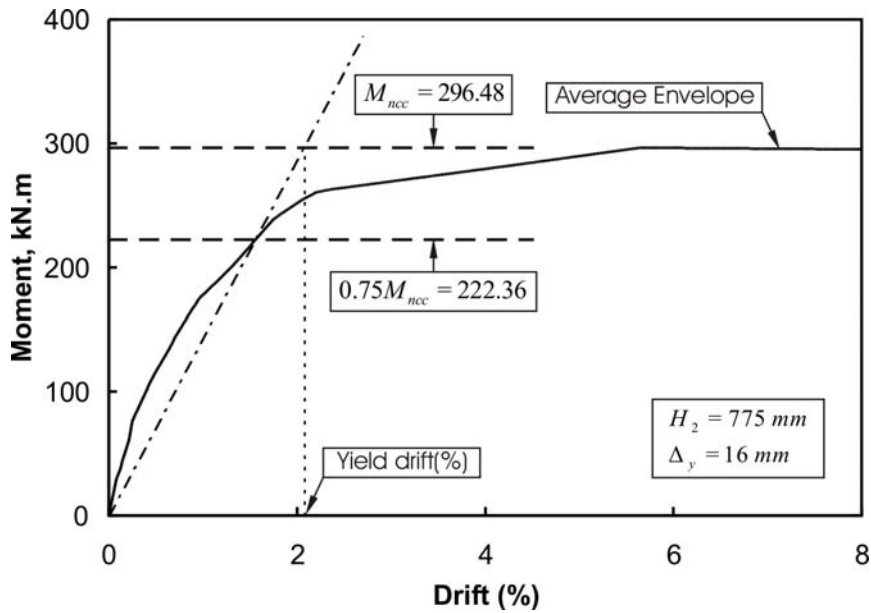


Figure F-36: Determination of yield displacement for column CL8 using average envelope (method 1(alternative 5))

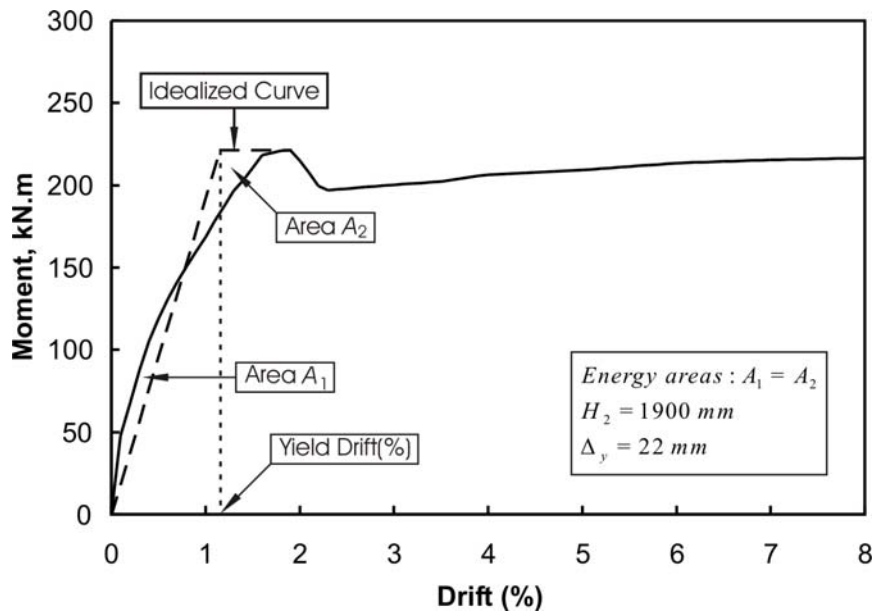


Figure F-37: Determination of yield displacement for column CL0 using area equalization method (case 1)

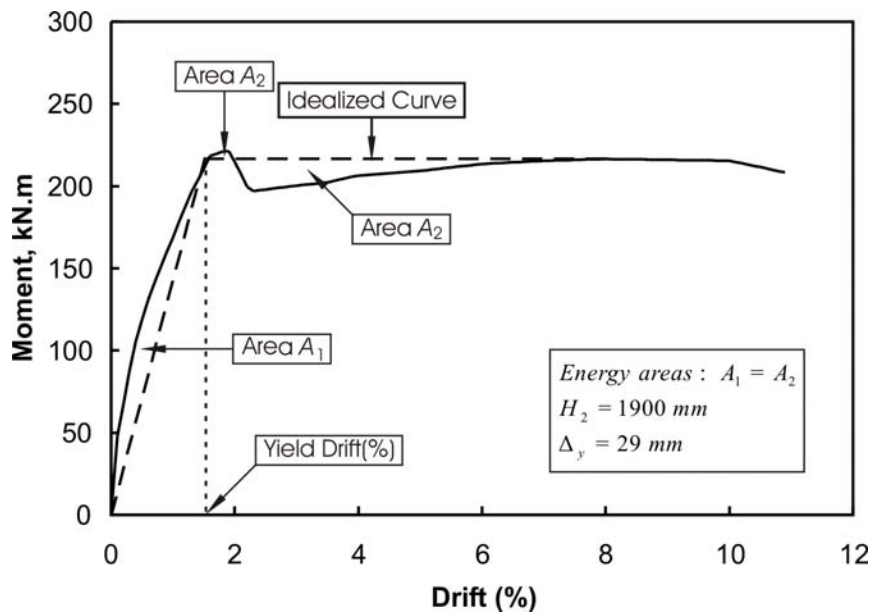


Figure F-38: Determination of yield displacement for column CL0 using area equalization method (case 2)

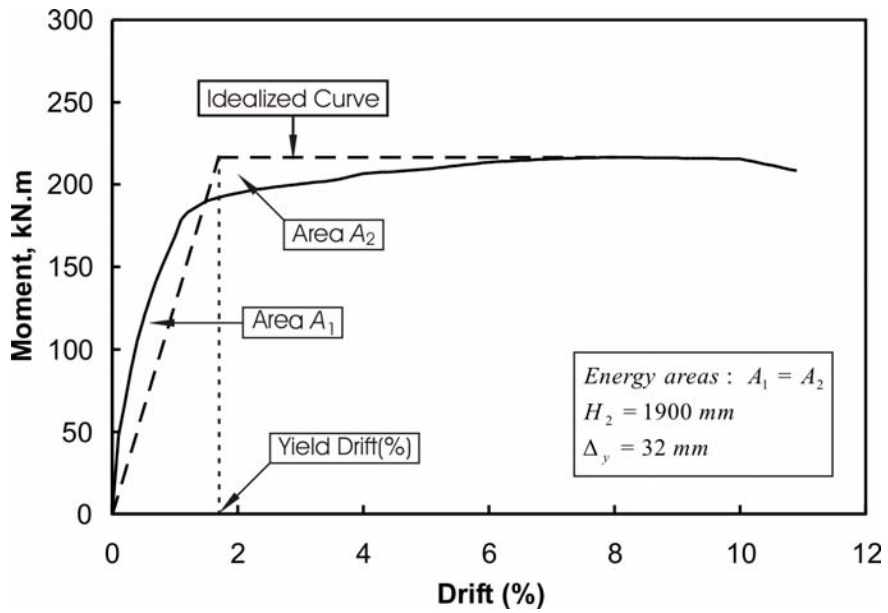


Figure F-39: Determination of yield displacement for column CL0 using area equalization method (case 3).

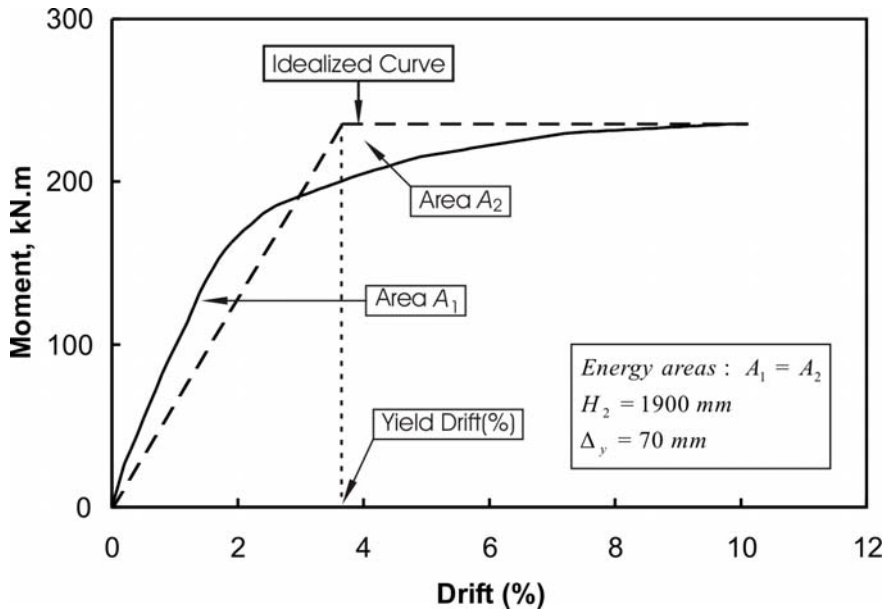


Figure F-40: Determination of yield displacement for column CL1 using area equalization method

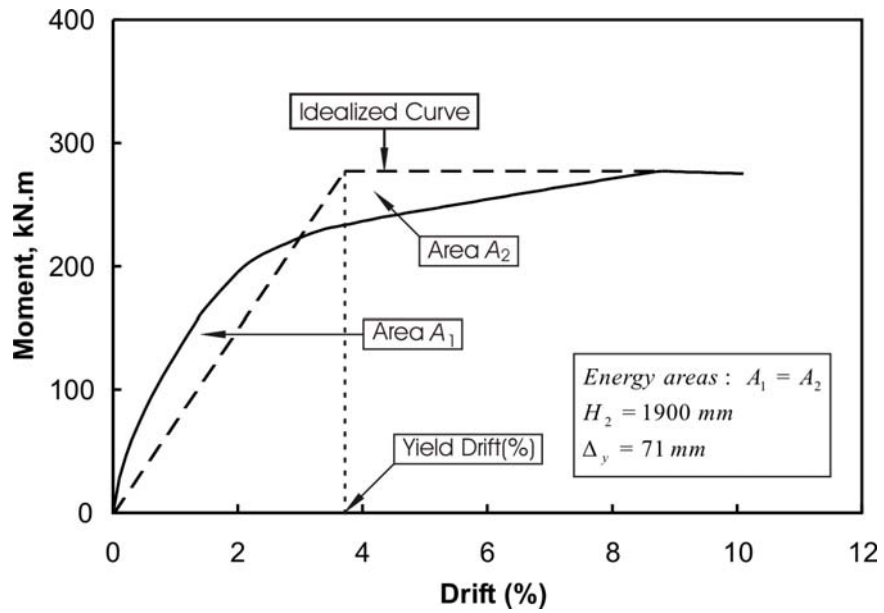


Figure F-41: Determination of yield displacement for column CL2 using area equalization method

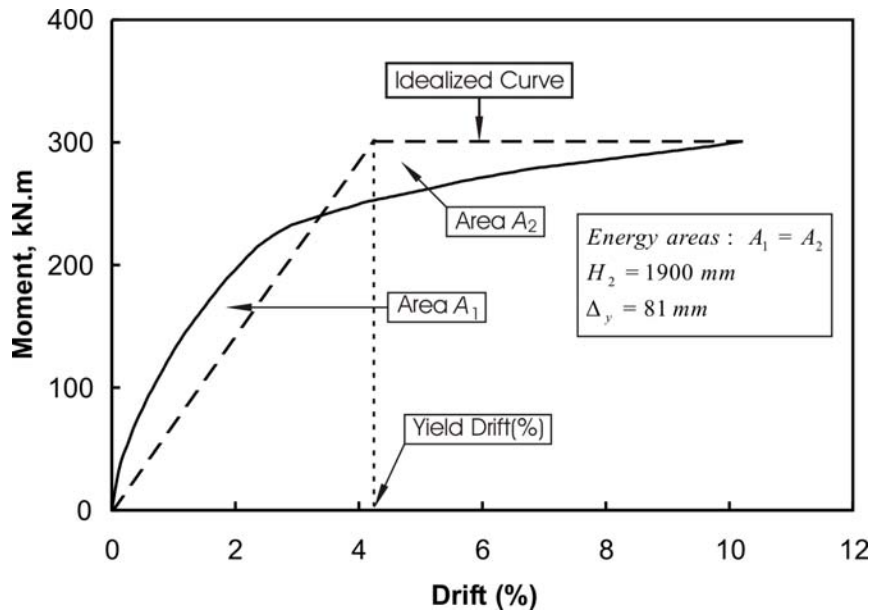


Figure F-42: Determination of yield displacement for column CL3 using area equalization method

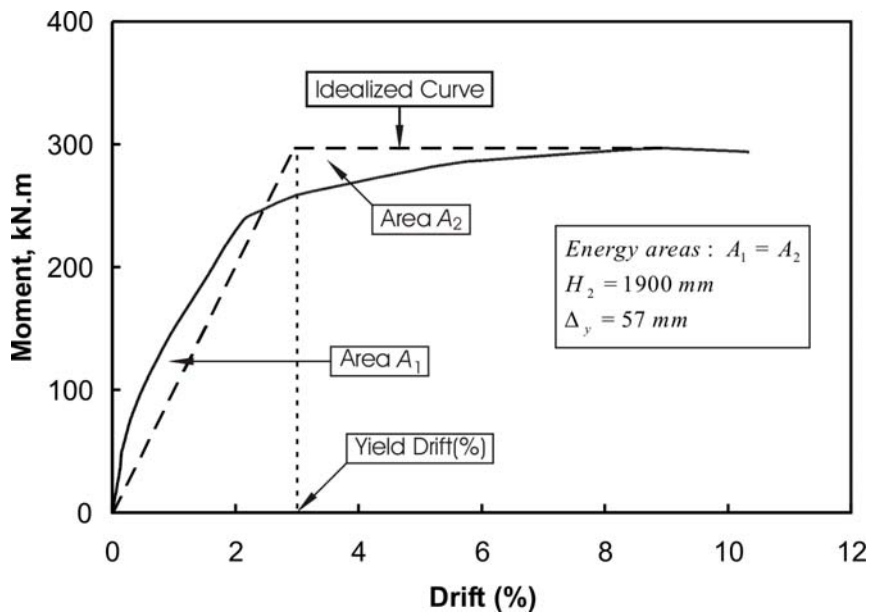


Figure F-43: Determination of yield displacement for column CL4 using area equalization method

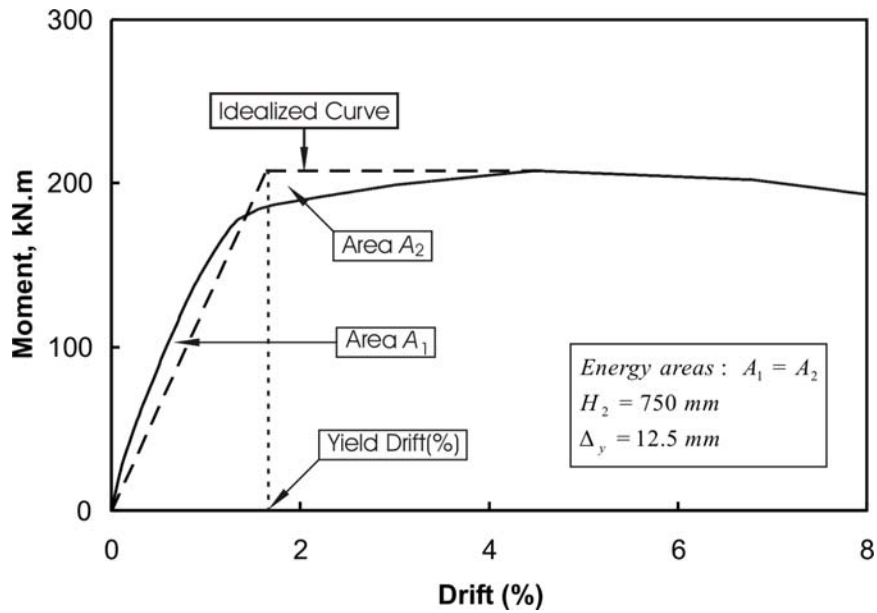


Figure F-44: Determination of yield displacement for column CL5 using area equalization method

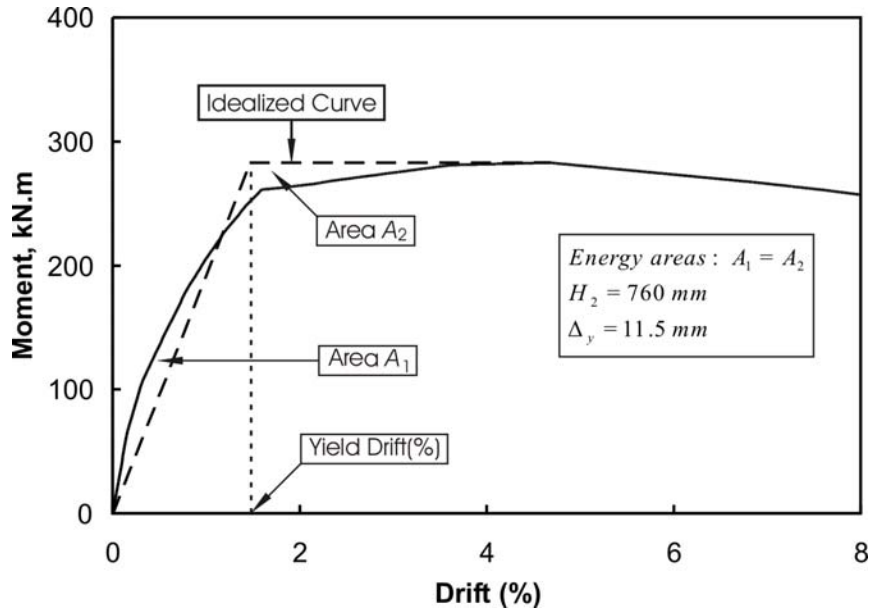


Figure F-45: Determination of yield displacement for column CL6 using area equalization method

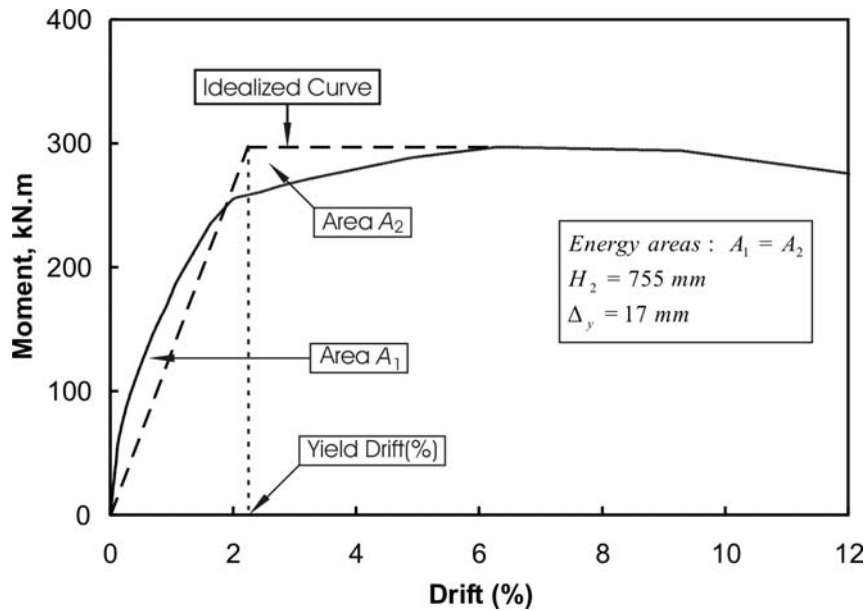


Figure F-46: Determination of yield displacement for column CL7 using area equalization method

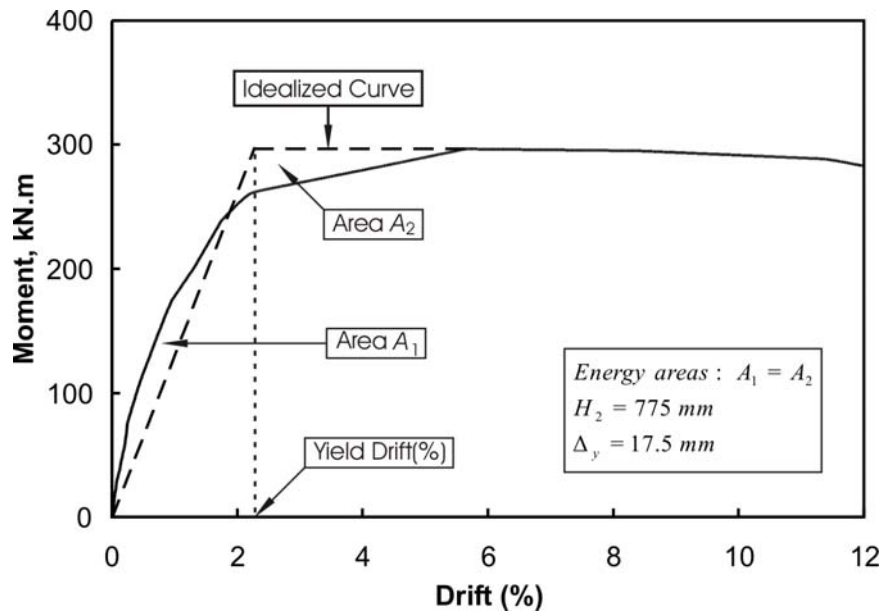


Figure F-47: Determination of yield displacement for column CL8 using area equalization method

## G. ENERGY DISSIPATION

Table G.1: Energy dissipated by specimen CL0 based on overall system

Cycle number	Energy dissipated per cycle (kN.m)	Cumulative energy dissipated (kN.m)	Cumulative norm. energy dissipated
1	1.09	1.09	0.32
2	0.84	1.93	0.56
3	0.83	2.76	0.81
4	0.78	3.54	1.04
5	0.70	4.24	1.24
6	5.69	9.93	2.90
7	3.46	13.38	3.92
8	3.23	16.61	4.86
9	2.85	19.46	5.69
10	3.66	23.12	6.76
11	6.43	29.55	8.64
12	5.42	34.97	10.23
13	6.33	41.30	12.08
14	6.07	47.37	13.86
15	5.39	52.76	15.43
16	26.19	78.95	23.10
17	17.50	96.46	28.22
18	17.50	113.96	33.34
19	16.74	130.70	38.23
20	16.56	147.27	43.08
21	33.43	180.70	52.86
22	35.48	216.18	63.24
23	33.89	250.07	73.15
24	34.50	284.57	83.25
25	36.03	320.59	93.78
26	39.43	360.02	105.32
27	40.62	400.65	117.20
28	40.62	441.27	129.09
29	39.34	480.61	140.59
30	39.14	519.74	152.04
31	39.30	559.04	163.54
32	39.77	598.81	175.17
33	39.17	637.98	186.63
34	39.39	677.37	198.15
35	39.14	716.51	209.60
36	39.70	756.21	221.22
37	39.30	795.50	232.71
38	37.67	833.17	243.73
39	35.66	868.83	254.16
40	34.25	903.07	264.18
41	34.54	937.61	274.28
42	34.39	972.00	284.34
43	35.66	1007.66	294.77
44	34.25	1041.91	304.79

Note: Experimental  $\Delta_y = 30$  mm;  $H_2 = 1900$  mm; and  $M_{\max} = 216.50$  kN.m

Table G.2: Energy dissipated by specimen CL1 based on overall system

Cycle number	Energy dissipated per cycle (kN.m)	Cumulative energy dissipated (kN.m)	Cumulative norm. energy dissipated
1	0.31	0.31	0.11
2	0.20	0.51	0.18
3	0.15	0.66	0.23
4	0.11	0.78	0.27
5	0.11	0.89	0.31
6	0.97	1.86	0.65
7	0.68	2.54	0.89
8	0.53	3.07	1.08
9	0.45	3.52	1.24
10	0.36	3.88	1.36
11	1.80	5.68	1.99
12	1.54	7.22	2.53
13	1.39	8.61	3.02
14	1.34	9.95	3.49
15	1.31	11.26	3.95
16	11.03	22.29	7.82
17	8.98	31.27	10.97
18	8.80	40.08	14.06
19	8.64	48.72	17.09
20	8.07	56.79	19.92
21	19.81	76.59	26.87
22	18.43	95.02	33.34
23	18.17	113.19	39.71
24	18.81	132.00	46.31
25	17.21	149.21	52.35
26	31.77	180.98	63.49
27	31.93	212.91	74.70
28	29.88	242.80	85.18
29	28.89	271.69	95.32
30	28.20	299.89	105.21
31	29.68	329.57	115.62
32	28.91	358.48	125.76
33	29.48	387.96	136.11
34	29.53	417.49	146.47
35	29.76	447.26	156.91
36	28.44	475.70	166.89
37	28.56	504.26	176.91
38	28.30	532.57	186.84
39	28.32	560.88	196.77
40	28.88	589.76	206.90
41	28.16	617.92	216.78
42	28.69	646.60	226.84
43	28.59	675.20	236.88
44	28.63	703.83	246.92
45	28.59	732.42	256.95

Note: Experimental  $\Delta_y = 23$  mm;  $H_2 = 1900$  mm, and  $M_{max} = 235.47$  kN.m

Table G.3: Energy dissipated by specimen CL2 based on overall system

Cycle number	Energy dissipated per cycle (kN.m)	Cumulative energy dissipated (kN.m)	Cumulative Norm. energy dissipated
1	1.10	1.10	0.18
2	0.64	1.74	0.29
3	0.68	2.42	0.40
4	0.61	3.03	0.51
5	0.73	3.76	0.63
6	5.51	9.27	1.55
7	4.34	13.61	2.28
8	3.97	17.58	2.94
9	4.10	21.68	3.63
10	4.10	25.78	4.31
11	8.20	33.98	5.69
12	8.12	42.10	7.05
13	7.90	50.00	8.37
14	7.94	57.94	9.70
15	7.93	65.87	11.02
16	32.21	98.08	16.41
17	30.32	128.41	21.49
18	28.14	156.55	26.20
19	28.76	185.31	31.01
20	29.09	214.40	35.88
21	39.58	253.98	42.50
22	40.44	294.42	49.27
23	40.23	334.65	56.00
24	40.00	374.65	62.70
25	39.83	414.48	69.36
26	36.81	451.29	75.52
27	26.85	478.14	80.01

Note: Experimental  $\Delta_y = 41$  mm;  $H_2 = 1900$  mm, and  $M_{max} = 276.92$  kN.m

Table G.4: Energy dissipated by specimen CL3 based on overall system

Cycle number	Energy dissipated per cycle (kN.m)	Cumulative energy dissipated (kN.m)	Cumulative Norm. energy dissipated
1	1.35	1.35	0.22
2	0.72	2.07	0.34
3	0.62	2.69	0.45
4	0.56	3.25	0.54
5	0.59	3.84	0.64
6	3.80	7.64	1.27
7	3.14	10.78	1.79
8	2.97	13.75	2.28
9	2.84	16.59	2.76
10	2.86	19.45	3.23
11	6.92	26.37	4.38
12	6.32	32.69	5.43
13	6.05	38.74	6.44
14	6.89	45.63	7.58
15	6.29	51.92	8.63
16	31.34	83.26	13.83
17	26.33	109.59	18.21
18	25.26	134.85	22.40
19	24.74	159.59	26.51
20	23.74	183.33	30.46
21	37.99	221.32	36.77
22	36.79	258.11	42.88
23	36.26	294.37	48.90
24	35.93	330.30	54.87
25	36.66	366.96	60.96
26	35.99	402.95	66.94
27	36.00	438.95	72.92
28	35.24	474.19	78.78
29	35.69	509.88	84.71
30	35.36	545.23	90.58
31	35.31	580.55	96.45
32	35.90	616.45	102.41
33	35.33	651.77	108.28
34	35.22	687.00	114.13
35	35.05	722.05	119.96
36	35.09	757.14	125.79
37	35.06	792.21	131.61
38	35.01	827.21	137.43
39	35.16	862.37	143.27
40	34.98	897.35	149.08
41	34.98	932.33	154.89
42	35.01	967.33	160.71
43	34.92	1002.26	166.51
44	35.22	1037.48	172.36
45	34.74	1072.22	178.13

Note: Experimental  $\Delta_y = 38$  mm;  $H_2 = 1900$  mm, and  $M_{max} = 300.96$  kN.m

Table G.5: Energy dissipated by specimen CL4 based on overall system

Cycle number	Energy dissipated per cycle (kN.m)	Cumulative energy dissipated (kN.m)	Cumulative Norm. energy dissipated
1	0.68	0.68	0.16
2	0.46	1.14	0.26
3	0.39	1.53	0.35
4	0.36	1.89	0.43
5	0.36	2.25	0.51
6	1.87	4.12	0.94
7	1.24	5.36	1.23
8	1.14	6.50	1.49
9	1.10	7.60	1.74
10	1.02	8.62	1.97
11	3.57	12.18	2.79
12	2.83	15.01	3.43
13	2.64	17.65	4.03
14	2.68	20.33	4.65
15	3.22	23.55	5.38
16	18.34	41.88	9.57
17	14.36	56.25	12.86
18	14.72	70.97	16.22
19	13.94	84.91	19.41
20	13.91	98.82	22.59
21	32.23	131.05	29.96
22	29.44	160.49	36.69
23	29.07	189.56	43.33
24	29.19	218.75	50.01
25	30.50	249.25	56.98
26	37.59	286.84	65.57
27	36.75	323.59	73.97
28	36.41	360.00	82.29
29	36.24	396.24	90.58
30	36.08	432.32	98.83
31	35.87	468.19	107.03
32	36.01	504.20	115.26
33	35.56	539.76	123.39
34	35.28	575.04	131.45
35	35.44	610.48	139.55
36	35.01	645.49	147.63
37	34.94	680.43	155.71
38	34.54	714.97	163.79
39	35.34	750.32	171.87
40	35.34	785.66	179.95
41	35.14	820.80	187.98
42	35.24	856.05	196.02
43	34.67	890.72	203.94
44	34.53	925.25	211.84
45	34.58	959.83	219.74

Note: Experimental  $\Delta_y = 28$  mm;  $H_2 = 1900$  mm, and  $M_{max} = 296.84$  kN.m

Table G.6: Energy dissipated by specimen CL5 based on overall system

Cycle number	Energy dissipated per cycle (kN.m)	Cumulative energy dissipated (kN.m)	Cumulative Norm. energy dissipated
1	0.43	0.43	0.20
2	0.23	0.66	0.30
3	0.16	0.82	0.37
4	0.15	0.97	0.44
5	0.14	1.12	0.51
6	1.96	3.08	1.39
7	0.72	3.79	1.72
8	0.65	4.45	2.01
9	0.51	4.96	2.24
10	0.50	5.46	2.47
11	2.44	7.90	3.57
12	1.78	9.68	4.37
13	1.76	11.44	5.17
14	1.60	13.04	5.89
15	1.50	14.53	6.57
16	12.39	26.93	12.17
17	9.13	36.06	16.30
18	8.84	44.90	20.29
19	8.11	53.01	23.96
20	7.89	60.90	27.53
21	19.86	80.76	36.50
22	17.23	98.00	44.29
23	17.23	115.23	52.08
24	15.33	130.55	59.01
25	14.42	144.98	65.53
26	24.75	169.73	76.71
27	24.80	194.53	87.92
28	23.12	217.65	98.37
29	22.89	240.54	108.72
30	21.38	261.92	118.38
31	31.18	293.10	132.48
32	28.92	322.02	145.55
33	29.47	351.49	158.87
34	27.29	378.78	171.20
35	26.49	405.27	183.18
36	32.77	438.05	197.99
37	28.44	466.49	210.84

Note: Experimental  $\Delta_y = 8$  mm;  $H_2 = 750$  mm, and  $M_{max} = 207.42$  kN.m

Table G.7: Energy dissipated by specimen CL6 based on overall system

Cycle number	Energy dissipated per cycle (kN.m)	Cumulative energy dissipated (kN.m)	Cumulative Norm. energy dissipated
1	0.69	0.69	0.22
2	0.39	1.08	0.34
3	0.43	1.51	0.48
4	0.38	1.89	0.60
5	0.33	2.22	0.70
6	2.11	4.33	1.37
7	1.20	5.53	1.75
8	1.26	6.79	2.15
9	1.32	8.11	2.56
10	1.18	9.29	2.94
11	3.42	12.71	4.02
12	2.83	15.53	4.91
13	2.35	17.89	5.65
14	2.37	20.25	6.40
15	2.62	22.88	7.23
16	14.70	37.58	11.88
17	11.92	49.50	15.64
18	11.40	60.90	19.24
19	11.72	72.62	22.95
20	11.38	84.00	26.55
21	24.49	108.50	34.29
22	22.62	131.11	41.43
23	24.54	155.65	49.19
24	27.79	183.45	57.97
25	25.84	209.29	66.14
26	40.47	249.76	78.93
27	38.25	288.01	91.02
28	39.75	327.76	103.58
29	40.16	367.92	116.27
30	38.90	406.82	128.56
31	43.79	450.61	142.40

Note: Experimental  $\Delta_y = 8.5$  mm;  $H_2 = 760$  mm, and  $M_{max} = 282.93$  kN.m

Table G.8: Energy dissipated by specimen CL7 based on overall system

Cycle number	Energy dissipated per cycle (kN.m)	Cumulative energy dissipated (kN.m)	Cumulative Norm. energy dissipated
1	1.26	1.26	0.28
2	0.75	2.00	0.44
3	0.63	2.63	0.58
4	0.75	3.38	0.75
5	0.84	4.22	0.93
6	3.24	7.46	1.65
7	2.15	9.61	2.12
8	1.24	10.84	2.40
9	1.39	12.23	2.70
10	1.65	13.87	3.07
11	5.24	19.11	4.23
12	4.41	23.52	5.20
13	4.54	28.06	6.20
14	3.72	31.78	7.03
15	3.62	35.40	7.83
16	20.68	56.08	12.40
17	16.86	72.94	16.13
18	15.86	88.81	19.64
19	15.59	104.40	23.09
20	14.66	119.06	26.33
21	31.65	150.72	33.33
22	30.68	181.40	40.11
23	29.99	211.39	46.74
24	29.81	241.19	53.33
25	31.90	273.10	60.39
26	50.00	323.09	71.44
27	46.96	370.06	81.83
28	41.95	412.00	91.10
29	40.90	452.91	100.15
30	42.10	495.01	109.46
31	61.23	556.24	123.00
32	58.81	615.05	136.00
33	58.30	673.35	148.89
34	57.52	730.87	161.61
35	51.80	782.67	173.07

Note: Experimental  $\Delta_y = 11.5$  mm;  $H_2 = 755$  mm, and  $M_{max} = 296.90$  kN.m

Table G.9: Energy dissipated by specimen CL8 based on overall system

Cycle number	Energy dissipated per cycle (kN.m)	Cumulative energy dissipated (kN.m)	Cumulative Norm. energy dissipated
1	0.71	0.71	0.17
2	0.56	1.27	0.30
3	0.56	1.83	0.43
4	0.67	2.50	0.59
5	0.65	3.15	0.75
6	1.53	4.68	1.11
7	2.46	7.14	1.70
8	2.26	9.40	2.23
9	1.50	10.90	2.59
10	1.72	12.62	3.00
11	2.39	15.01	3.57
12	3.46	18.48	4.39
13	2.72	21.20	5.04
14	4.27	25.47	6.05
15	3.61	29.07	6.91
16	17.30	46.37	11.02
17	15.88	62.26	14.79
18	15.86	78.12	18.56
19	14.23	92.34	21.94
20	13.64	105.98	25.19
21	29.67	135.65	32.24
22	28.98	164.63	39.12
23	27.96	192.59	45.77
24	29.70	222.29	52.82
25	28.71	251.00	59.65
26	43.94	294.94	70.09
27	42.80	337.74	80.26
28	41.04	378.77	90.01
29	41.22	419.99	99.81
30	40.28	460.27	109.38
31	57.62	517.89	123.07
32	57.03	574.92	136.62
33	54.55	629.48	149.59
34	54.80	684.27	162.61
35	54.19	738.46	175.49

Note: Experimental  $\Delta_y = 11$  mm;  $H_2 = 775$  mm, and  $M_{max} = 296.48$  kN.m

## H. DISTRIBUTION OF ENERGY DISSIPATION IN COLUMNS

Although the curvature distributions give a general idea of damage distribution in the test regions of the columns, it is difficult to quantify the level of damage in a certain segment of the test region using only these diagrams. Conversely, the distribution of energy dissipation in columns gives a better idea of the damage distribution and the location of the most damaged region,  $h_f$ , of the column. In addition, it helps to estimate the effective plastic hinge lengths,  $L_p$ , in the columns.

Figures H-1 through H-8 shows the distribution of energy dissipation along the test regions of collared columns (CL1 to CL8) for different levels of displacement ductility. These figures also give insight into the variation of energy dissipation in different parts of the column with the increase of displacement ductility. The energy dissipated at a particular displacement ductility level is the sum of energy dissipated in all the cycles to that level.

The values of energy dissipated per cycle based on the overall systems are given in Appendix-G. The energy dissipated per loop based on the overall system is equal to the area enclosed by the moment at column base vs. lateral drift hysteresis loop. The values of energy dissipated up to the centreline of the first collar and the second and/or third collar are given in Tables H.1 through H.8 for columns CL1 through CL8. The energy dissipated per cycle is equal to the area enclosed by the moment vs. collar rotation (in radians) hysteresis loop. However, for these hysteresis loops, the moment was calculated at a point located midway between the top of the footing and the centreline of the collar under consideration.

### H.1 Column CL1

Figure H-1 shows the distribution of energy dissipation along column CL1 at different levels of displacement ductility. The centreline of collars 1 and 3 are located at 55 mm and 256 mm, respectively, from the top of the footing (Table 4.4). The energy dissipation below the first collar was only calculated up to cycle 20 because the stroke of the LVDTs used for measuring the rotation of the collar was exhausted in one direction. Figure 4-91 shows the curvature distribution for this column. The curvature distributions for ductility levels  $\mu = 4.6$  and  $\mu = 6.59$  were calculated using the data of the LVDTs for one direction only. The calculations for the distribution of energy dissipation in this column presented below are based on the sum of energy dissipated in cycles 16 through 20, cycles 21 through 25, and in cycles 1 through 45. The reason for choosing cycles 16 through 20 and cycles 21 through 25 is that the corresponding displacement

ductilities are  $\mu = 3.1$  and  $\mu = 4.6$ , respectively, which encompass the displacement ductility level  $\mu = 4$ , that is often used for the design of reinforced concrete frames in zones of high seismic activity.

Based on the sum of energy dissipated in cycles 16 through 20 in different parts of the column, the energy dissipated below the first and third collar is 47.06% and 78.34%, respectively, of the energy dissipated in the overall system, and the remaining 21.66% is dissipated in the region between the third collar and the point of application of horizontal load. Based on the above, the energy dissipated between collar 1 and collar 3 is 31.28% of the total energy dissipated. Based on the sum of energy dissipated in cycles 21 through 25 in different parts of the column, the energy dissipated below the third collar is 77.67% and the remaining 22.33% is dissipated in the region between the third collar and the point of application of horizontal load.

Based on the cumulative energy dissipated from cycle 1 through 45, the energy dissipated below the third collar is 80.22% of the energy dissipated in the overall system and 19.78% is dissipated above the third collar. Figure 4-19 shows the extent of damage in different parts of column CL1 at different stages of the test.

## H.2 Column CL2

Figure H-2 shows the distribution of energy dissipation along column CL2 at different levels of displacement ductility. The distances from the centreline of collars 1 and 2 are 76 mm and 240 mm, respectively, from the top of the footing (Table 4.4). The calculations for the distribution of energy dissipation in this column are based on the sum of energy dissipated in cycles 11 through 15, cycles 16 through 20, and in cycles 1 through 27. The reason for choosing cycles 11 through 15 and 16 through 20 is that the displacement ductilities are  $\mu = 2.65$  and  $\mu = 5.29$ , respectively, which encompass the ductility level  $\mu = 4$ .

Based on the sum of energy dissipated in cycles 11 through 15 in different parts of the column, the energy dissipated below the first and second collar is 28.09% and 75.08%, respectively, of the energy dissipated in the overall system, and the remaining 24.92% is dissipated in the region between the second collar and the point of application of horizontal load. Therefore, the energy dissipated between collars 1 and 2 is 46.99% of the energy dissipated in the overall system. Based on cycles 16 through 20 in different parts of the column, the energy dissipated below the first and second collars is 13.81% and 76.74%, respectively, of the energy dissipated in the overall system, and the remaining 23.26% is dissipated in the region between the second collar

and the point of application of horizontal load. The energy dissipated between collars 1 and 2 is 62.93% of the total energy dissipated in these cycles.

Based on the sum of energy dissipated in cycles 1 through 27, the energy dissipated below the first and second collars is 12.13% and 81.83%, respectively, of the energy dissipated in the overall system, and the remaining 18.17% is dissipated in the region between the second collar and the point of application of horizontal load. The energy dissipated between collars 1 and 2 is 69.70% of the total energy dissipated in these cycles.

The energy dissipation between the first and second collar is much higher than that below the first collar. This is in accordance with the curvature distributions of the column along the test region at different levels of displacement ductility (Figure 4-92). The rupture of vertical bars between collars 1 and 2 support these observations (Figure 4-20).

### **H.3 Column CL3**

Figure H-3 shows the distribution of energy dissipation along column CL3 at different levels of displacement ductility. The distance to the centreline of collars 1 and 3 are 64 mm and 294 mm, respectively, from the top of the footing (Table 4.4). The calculations for the distribution of energy dissipation in this column are based on the sum of energy dissipated in cycles 11 through 15, cycles 16 through 20, and in cycles 1 through 45. Cycles 11 through 15 and cycles 16 through 20 were selected because the displacement ductility levels of these cycles are  $\mu = 2.38$  and  $\mu = 4.75$ , respectively, which encompass the ductility level  $\mu = 4$ .

Based on the sum of energy dissipated in cycles 11 through 15 in different parts of the column, the energy dissipated below the first and third collars is 25.90% and 62.85%, respectively, of the energy dissipated in the overall system in these cycles, and the remaining 37.15% is dissipated in the region between the third collar and the point of application of horizontal load. The energy dissipated between collars 1 and 3 is 36.95% of the total energy dissipated in these cycles. Based on the sum of energy dissipated in cycles 16 through 20, the energy dissipated below the first and third collars is 16.55% and 61.33%, respectively, of the energy dissipated in the overall system in these cycles, and the remaining 38.67% is dissipated in the region between the third collar and the point of application of horizontal load. The energy dissipated between collars 1 and 3 is 44.78% of the total energy dissipated in these cycles.

Based on the sum of energy dissipated in cycles 1 through 45, the energy dissipated below the first and third collars is 12.15% and 61.77%, respectively, of the energy dissipated in the overall system in these cycles, and the remaining 38.23% is dissipated in the region between the third collar and the point of application of horizontal load. The energy dissipated between collars 1 and 3 is 49.62% of the total energy dissipated in these cycles.

The energy dissipation between the first and third collars is higher than that below the first collar. The appearance of the test region of the column shows considerable damage above the third collar (Figure 4-21(d)), which supports the calculated distribution of energy dissipation.

#### **H.4 Column CL4**

Figure H-4 shows the distribution of energy dissipation along column CL4 at different levels of displacement ductility. The distance from the centreline of collars 1 and 3 are 66 mm and 285 mm, respectively, from the top of the footing (Table 4.4). The calculations for the distribution of energy dissipation in this column are based on the sum of energy dissipated in cycles 16 through 20, and energy dissipated in cycles 1 through 45. The reason for choosing cycles 16 through 20 is that these cycles were performed at a ductility level of,  $\mu = 4$ .

Based on the sum of energy dissipated in cycles 16 through 20, the energy dissipated below the first and third collars is 30.65% and 81.40%, respectively, of the energy dissipated in the overall system in these cycles, and the remaining 18.60% is dissipated in the region between the third collar and the point of application of horizontal load. The energy dissipated between collars 1 and 3 is 50.75% of the total energy dissipated in these cycles.

Based on the sum of energy dissipated in cycles 1 through 45, the energy dissipated below the first and third collars is 30.62% and 79.10%, respectively, of the energy dissipated in the overall system in these cycles, and the remaining 20.90% is dissipated in the region between the third collar and the point of application of horizontal load. The energy dissipated between collars 1 and 3 is 48.48% of the total energy dissipated in these cycles.

The data above indicate that the distribution of energy dissipation along the column is relatively uniform, calculated based on cycles 16 through 20 and based on cycles 1 through 45. From Figure H-4 and the sum of energy dissipated from cycles 1 through 45, it can be seen that 30.62%, 48.48%, and 20.90% of the total energy is dissipated below the first collar, between the first and third collars, and between the third collar and the point of application of horizontal load.

The appearance of the test region of the column shows some damage above the third collar (Figure 4-22(d)), which supports the calculated distribution of energy dissipation.

## H.5 Column CL5

Figure H-5 shows the distribution of energy dissipation along column CL5 at different levels of displacement ductility. The distance of centerline of collar 1 and collar 3 are 50 and 260 mm, respectively, from the top of footing (Table 4.4). The calculations for the distribution of energy dissipation in this column are based on the sum of energy dissipated in cycles 16 through 20, and the sum of energy dissipated in cycles 1 through 37. The reason for choosing cycles 16 through 20 is that these cycles were performed at a displacement ductility level of  $\mu = 4.27$ , which is close to  $\mu = 4$ , generally used for the design of reinforced concrete frames in the zones of high seismic activity.

Based on the sum of energy dissipated in cycles 16 through 20 in different parts of the column, the energy dissipated below the first and third collar is 77.87 and 82.75%, respectively, of the energy dissipated in the overall system in these cycles, and the remaining 17.25% is dissipated in the region between the third collar and the point of application of horizontal load. Based on the above, the energy dissipated between collar 1 and collar 3 is 4.88% of the energy dissipated in the overall system.

Based on the sum of energy dissipated in cycles 1 through 37 in different parts of the column, the energy dissipated below the first and third collar is 60.79 and 76.82%, respectively, of the energy dissipated in the overall system in these cycles, and the remaining 23.18% is dissipated in the region between the third collar and the point of application of horizontal load. Based on the above, the energy dissipated between collar 1 and collar 3 is 16.03% of the energy dissipated in the overall system.

From Figure H-5 and the data above, it is evident that 60.79%, 16.03%, and 23.18% of the total energy dissipated in the system is dissipated below the first collar, between the first and the third collars, and between the third collar and the point of application of horizontal load. An increase in the energy dissipation above the third collar takes place with the increase in the displacement ductility level. Figure 4-23 shows that most of the damage occurs below the first collar and between first and second collars.

## H.6 Column CL6

Figure H-6 shows the distribution of energy dissipation along column CL6 at different levels of displacement ductility. The energy dissipation below the first collar is generally higher than the energy dissipated below the second collar. This discrepancy is explained as follows: rotation takes place only below the first collar and the remainder of the test region just rotates as a rigid body. Hence, the rotation of the first collar and second collar are almost identical. However, the moment corresponding to the first collar is higher than that corresponding to the second collar. As a result, the energy dissipation below the second collar is lower than the energy dissipation below the first collar. Based on this, it can be deduced that the energy dissipation between the first and second collars is very small. Figure 4-24(d) shows the appearance of column CL6 at the end of the test; the damage is visible only below first collar.

The distance of the centerline of collar 1 and collar 2 are 97 and 254 mm, respectively, from the top of footing (Table 4.4). The calculations for the distribution of energy dissipation in this column are based on the sum of energy dissipated in cycles 11 through 15, cycles 16 through 20, and energy dissipated in cycles 1 through 31. The reason for choosing cycles 11 through 15, and cycles 16 through 20 is that the displacement ductility level of cycles 11 through 15, and cycles 16 through 20 are  $\mu = 2.43$  and  $\mu = 4.86$ , respectively, which encompass the ductility level  $\mu = 4$ , that is generally used for the design of reinforced concrete frames in zones of high seismic activity.

Based on the sum of energy dissipated in cycles 11 through 15 in different parts of the column, the energy dissipated below the first collar is 87.86% of the energy dissipated in the overall system, and the remaining 12.14% is dissipated in the region between the first collar and the point of application of horizontal load. Based on the sum of energy dissipated in cycles 16 through 20 in different parts of the column, the energy dissipated below the first collar is 92.21% of the energy dissipated in the overall system, and the remaining 7.79% is dissipated in the region between the first collar and point of application of horizontal load.

Based on the sum of energy dissipated in cycles 1 through 31 in different parts of the column, the energy dissipated below the first collar is 87.01% of the energy dissipated in the overall system, and the remaining 12.99% is dissipated in the region between the first collar and the point of application of horizontal load.

Hence, most of the energy is dissipated below the first collar, which is also clear from the curvature distributions along the test region of the column at different levels of displacement ductility (Figure 4-96).

## H.7 Column CL7

Figure H-7 shows the distribution of energy dissipation along column CL7 at different levels of displacement ductility. The energy dissipation below the third collar is lower than that dissipated below the second collar. The reason for this discrepancy has already been given in section H.6. Figure 4-26(d) shows the damage below the first collar and between first and second collars. The distance of the centerline of collar 1, 2, and 3 are 51, 152, and 252 mm, respectively, from the top of footing (Table 4.4). The calculations for the distribution of energy dissipation in this column are based on the sum of energy dissipated in cycles 11 through 15, cycles 16 through 20, and energy dissipated in cycles 1 through 35. The reason for choosing cycles 11 through 15, and cycles 16 through 20 is that the displacement ductility level of cycle 11 through 15, and cycles 16 through 20 are  $\mu = 2.44$  and  $\mu = 4.89$ , respectively, which encompass the ductility level  $\mu = 4$ , that is generally used for the design of reinforced concrete frames in zones of high seismic activity.

Based on the sum of energy dissipated in cycles 11 through 15 in different parts of the column, the energy dissipated below the first and second collar is 66.05 and 67.95%, respectively, of the energy dissipated in the overall system in these cycles, and the remaining 32.05% is dissipated in the region between the second collar and the point of application of horizontal load. The energy dissipated between the first and second collar is 1.90% of the energy dissipated in the overall system. Based on the sum of energy dissipated in cycles 16 through 20 in different parts of the column, the energy dissipated below the first and second collar is 59.81 and 70.69%, respectively, of the energy dissipated in the overall system, and the remaining 29.31% is dissipated in the region between the second collar and the point of application of the horizontal load. The energy dissipated between the first and second collar is 10.88% of the energy dissipated in the overall system.

Based on the sum of energy dissipated in cycles 1 through 35 in different parts of the column, the energy dissipated below the first and second collar is 54.23 and 66.68%, respectively, of the energy dissipated in the overall system in these cycles, and the remaining 33.32% is dissipated in the region between the third collar and the point of application of horizontal load. The energy dissipated between collar 1 and collar 2 is 12.45% of the energy dissipated in the overall system.

Based on the above data, a significant amount of the overall energy is dissipated below the first collar.

## H.8 Column CL8

Figure H-8 shows the distribution of energy dissipation along column CL8 at different levels of displacement ductility. The energy dissipation below the third collar is lower than that dissipated below the second collar. The reason for this discrepancy has been given in section 4.3.11.6. Other similar discrepancies in energy dissipation are also seen at ductility level  $\mu = 2.44$ .

The distance of the centerline of collar 1, 2, and 3 are 65, 170, and 270 mm, respectively, from the top of footing (Table 4.4). The calculations for the distribution of energy dissipation in this column are based on the sum of energy dissipated in cycles 16 through 20 and energy dissipated in cycles 1 through 35. The reason for choosing cycles 16 through 20 is that the displacement ductility level of cycles 16 through 20 is  $\mu = 4.89$ , which is close to the ductility level  $\mu = 4$ , that is generally used for the design of reinforced concrete frames in zones of high seismic activity.

Based on the sum of energy dissipated in cycles 16 through 20 in different parts of the column, the energy dissipated below the first and second collar is 53.91 and 84.93%, respectively, of the energy dissipated in the overall system in these cycles, and the remaining 15.07% is dissipated in region between the second collar and point of application of horizontal load. Based on the above, the energy dissipated between the first and second collar is 31.02% of the energy dissipated in the overall system.

Based on the sum of energy dissipated in cycles 1 through 35 in different parts of the column, the energy dissipated below the second collar is 63.60% of the energy dissipated in the overall system in these cycles, and the remaining 36.40% is dissipated in the region between the second collar and the point of application of horizontal load.

The appearance of the test region of the column in Figure 4-27(d), shows considerable damage below the first collar and between first and second collars, which is in accordance with the calculations of energy dissipation in different parts of the column given above.

Table H.1: Energy dissipated up to different heights of the test region for column CL1

Cycle number	Energy dissipated per cycle below 3rd collar (kN.m)	Cumulative energy dissipated below 3rd collar (kN.m)	Energy dissipated per cycle below 1st collar (kN.m)	Cumulative energy dissipated below 1st collar (kN.m)
1	0.14	0.14	0.08	0.08
2	0.09	0.23	0.06	0.14
3	0.06	0.29	0.05	0.19
4	0.05	0.34	0.03	0.22
5	0.05	0.39	0.03	0.25
6	0.65	1.04	0.47	0.73
7	0.36	1.40	0.28	1.01
8	0.43	1.83	0.33	1.33
9	0.36	2.19	0.27	1.60
10	0.28	2.47	0.22	1.82
11	1.41	3.88	0.93	2.75
12	1.19	5.07	0.81	3.56
13	1.08	6.15	0.73	4.29
14	1.03	7.18	0.70	4.99
15	1.00	8.18	0.69	5.69
16	8.48	16.67	5.07	10.75
17	7.08	23.75	4.21	14.97
18	6.92	30.67	4.14	19.11
19	6.79	37.46	4.17	23.28
20	6.39	43.85	3.84	27.12
21	15.13	58.98	-	-
22	14.26	73.24	-	-
23	14.11	87.35	-	-
24	14.71	102.06	-	-
25	13.58	115.63	-	-
26	24.57	140.20	-	-
27	25.16	165.36	-	-
28	23.69	189.05	-	-
29	22.89	211.94	-	-
30	22.48	234.42	-	-
31	23.70	258.13	-	-
32	23.16	281.28	-	-
33	23.69	304.97	-	-
34	23.80	328.77	-	-
35	24.07	352.84	-	-
36	23.09	375.93	-	-
37	23.21	399.14	-	-
38	23.14	422.28	-	-
39	23.19	445.47	-	-
40	23.80	469.27	-	-
41	23.20	492.47	-	-
42	23.76	516.23	-	-
43	23.66	539.89	-	-
44	23.87	563.77	-	-
45	23.79	587.55	-	-

Table H.2: Energy dissipated up to different heights of the test region for column CL2

Cycle number	Energy dissipated per cycle below 2 <sup>nd</sup> collar (kN.m)	Cumulative energy dissipated below 2 <sup>nd</sup> collar (kN.m)	Energy dissipated per cycle below 1st collar (kN.m)	Cumulative energy dissipated below 1st collar (kN.m)
1	0.53	0.53	0.35	0.35
2	0.31	0.84	0.20	0.55
3	0.31	1.16	0.22	0.77
4	0.30	1.45	0.20	0.96
5	0.37	1.82	0.25	1.21
6	4.07	5.89	1.81	3.02
7	3.25	9.14	1.45	4.47
8	2.97	12.11	1.31	5.79
9	3.05	15.16	1.35	7.14
10	3.06	18.22	1.35	8.48
11	6.13	24.35	2.39	10.87
12	6.09	30.45	2.31	13.18
13	5.92	36.37	2.20	15.37
14	5.99	42.36	2.17	17.54
15	5.96	48.32	2.15	19.69
16	24.33	72.65	5.25	24.94
17	23.17	95.82	4.42	29.36
18	21.57	117.39	3.74	33.10
19	22.23	139.63	3.63	36.73
20	22.68	162.30	3.47	40.20
21	32.03	194.34	4.05	44.25
22	33.42	227.76	3.56	47.81
23	33.94	261.70	3.19	51.00
24	34.59	296.28	2.77	53.76
25	35.37	331.66	2.28	56.04
26	34.07	365.73	1.46	57.50
27	25.51	391.24	0.51	58.01

Table H.3: Energy dissipated up to different heights of the test region for column CL3

Cycle number	Energy dissipated per cycle below 3 <sup>rd</sup> collar (kN.m)	Cumulative energy dissipated below 3 <sup>rd</sup> collar (kN.m)	Energy dissipated per cycle below 1st collar (kN.m)	Cumulative energy dissipated below 1st collar (kN.m)
1	0.62	0.62	0.41	0.41
2	0.32	0.94	0.21	0.62
3	0.29	1.23	0.19	0.82
4	0.26	1.49	0.18	0.99
5	0.25	1.74	0.19	1.19
6	2.59	4.33	1.21	2.40
7	2.12	6.45	1.04	3.44
8	2.00	8.45	0.96	4.41
9	1.91	10.36	0.91	5.32
10	1.92	12.28	0.91	6.23
11	4.44	16.72	1.89	8.12
12	4.05	20.77	1.68	9.79
13	3.89	24.66	1.58	11.38
14	4.35	29.01	1.71	13.09
15	3.99	33.00	1.55	14.64
16	19.49	52.49	5.41	20.04
17	16.19	68.69	4.44	24.48
18	15.42	84.11	4.16	28.64
19	15.04	99.14	3.97	32.61
20	14.45	113.59	3.78	36.39
21	23.39	136.98	5.99	42.37
22	22.52	159.50	5.64	48.01
23	22.11	181.61	5.47	53.48
24	21.76	203.38	5.27	58.75
25	22.20	225.58	5.40	64.15
26	22.76	248.34	5.35	69.50
27	21.82	270.16	5.16	74.66
28	21.33	291.49	4.97	79.63
29	21.94	313.43	2.78	82.41
30	21.80	335.23	2.60	85.01
31	21.79	357.02	2.47	87.48
32	22.17	379.19	2.72	90.21
33	21.83	401.02	2.57	92.78
34	21.80	422.82	2.57	95.35
35	21.72	444.54	2.54	97.89
36	21.77	466.31	2.64	100.54
37	21.72	488.03	2.64	103.17
38	21.75	509.78	2.58	105.75
39	21.76	531.54	2.84	108.59
40	21.68	553.23	5.51	114.10
41	21.75	574.98	2.85	116.95
42	21.78	596.76	2.49	119.44
43	21.78	618.55	2.32	121.75
44	22.00	640.55	4.10	125.85
45	21.73	662.28	4.39	130.24

Table H.4: Energy dissipated up to different heights of the test region for column CL4

Cycle number	Energy dissipated per cycle below 3 <sup>rd</sup> collar (kN.m)	Cumulative energy dissipated below 3 <sup>rd</sup> collar (kN.m)	Energy dissipated per cycle below 1 <sup>st</sup> collar (kN.m)	Cumulative energy dissipated below 1 <sup>st</sup> collar (kN.m)
1	0.35	0.35	0.14	0.14
2	0.26	0.60	0.13	0.27
3	0.18	0.79	0.13	0.40
4	0.18	0.97	0.12	0.52
5	0.18	1.14	0.12	0.64
6	1.14	2.28	0.78	1.42
7	0.70	2.99	0.49	1.91
8	0.67	3.65	0.46	2.38
9	0.65	4.31	0.43	2.81
10	0.57	4.87	0.41	3.22
11	2.80	7.67	1.92	5.14
12	2.19	9.87	1.48	6.62
13	2.08	11.94	1.37	7.99
14	2.09	14.03	1.35	9.34
15	2.60	16.63	1.51	10.85
16	14.81	31.44	5.78	16.63
17	11.70	43.14	4.54	21.16
18	11.99	55.12	4.51	25.68
19	11.40	66.52	4.15	29.83
20	11.38	77.90	4.09	33.92
21	24.82	102.73	8.30	42.22
22	22.97	125.69	7.23	49.45
23	22.64	148.34	6.91	56.36
24	22.69	171.03	6.77	63.13
25	23.86	194.89	8.69	71.82
26	35.64	230.53	12.58	84.40
27	28.68	259.21	9.29	93.69
28	28.44	287.65	9.04	102.73
29	28.33	315.98	8.73	111.46
30	28.15	344.12	8.37	119.83
31	28.15	372.27	8.50	128.33
32	28.18	400.45	10.87	139.20
33	27.91	428.36	9.66	148.86
34	27.62	455.98	9.05	157.91
35	27.84	483.82	11.70	169.61
36	26.44	510.27	14.54	184.15
37	28.43	538.70	14.26	198.41
38	27.65	566.35	13.76	212.16
39	27.99	594.34	14.66	226.82
40	26.55	620.88	12.68	239.49
41	27.93	648.81	12.98	252.48
42	27.87	676.68	11.54	264.02
43	27.51	704.19	10.21	274.23
44	27.53	731.72	8.28	282.51
45	27.55	759.27	11.37	293.88

Table H.5: Energy dissipated up to different heights of the test region for column CL5

Cycle number	Energy dissipated per cycle below 3rd collar (kN.m)	Cumulative energy dissipated below 3rd collar (kN.m)	Energy dissipated per cycle below 1st collar (kN.m)	Cumulative energy dissipated below 1st collar (kN.m)
1	0.34	0.34	0.26	0.26
2	0.16	0.49	0.14	0.40
3	0.11	0.60	0.11	0.51
4	0.14	0.74	0.11	0.62
5	0.09	0.82	0.09	0.72
6	1.57	2.40	1.57	2.28
7	0.49	2.89	0.61	2.90
8	0.52	3.41	0.59	3.48
9	0.27	3.68	0.46	3.95
10	0.26	3.94	0.47	4.42
11	1.72	5.67	2.25	6.67
12	1.35	7.02	1.68	8.35
13	1.38	8.40	1.66	10.01
14	1.28	9.68	1.50	11.51
15	1.26	10.94	1.41	12.92
16	10.44	21.38	9.90	22.82
17	7.59	28.97	7.07	29.89
18	7.45	36.42	6.80	36.69
19	6.70	43.12	6.25	42.94
20	6.39	49.51	6.09	49.03
21	17.12	66.62	13.33	62.36
22	15.63	82.25	13.49	75.85
23	14.53	96.78	12.69	88.55
24	12.67	109.45	10.71	99.26
25	11.95	121.40	10.05	109.31
26	20.53	141.93	15.10	124.41
27	20.21	162.14	15.37	139.79
28	18.78	180.92	14.38	154.16
29	18.06	198.98	14.31	168.47
30	16.67	215.65	13.98	182.45
31	24.24	239.88	19.05	201.51
32	22.21	262.09	18.97	220.47
33	21.21	283.30	18.87	239.34
34	19.20	302.50	9.53	248.87
35	17.69	320.19	20.12	268.98
36	21.28	341.47	6.33	275.32
37	16.89	358.36	8.25	283.57

Table H.6: Energy dissipated up to different heights of the test region for column CL6

Cycle number	Energy dissipated per cycle below 2nd collar (kN.m)	Cumulative energy dissipated below 2nd collar (kN.m)	Energy dissipated per cycle below 1st collar (kN.m)	Cumulative energy dissipated below 1st collar (kN.m)
1	0.55	0.55	0.41	0.41
2	0.24	0.78	0.22	0.63
3	0.13	0.92	0.15	0.77
4	0.43	1.35	0.35	1.12
5	0.04	1.39	0.09	1.21
6	1.67	3.06	1.57	2.78
7	0.65	3.70	0.67	3.45
8	0.82	4.52	0.82	4.27
9	0.72	5.24	0.77	5.04
10	0.65	5.89	0.72	5.76
11	2.66	8.55	2.87	8.63
12	2.43	10.98	2.56	11.19
13	1.99	12.97	2.12	13.31
14	1.86	14.83	2.04	15.35
15	2.19	17.02	2.35	17.70
16	12.66	29.68	13.69	31.39
17	10.50	40.18	11.13	42.52
18	9.95	50.14	10.52	53.04
19	10.26	60.40	10.79	63.83
20	9.79	70.19	10.24	74.06
21	21.53	91.72	21.27	95.34
22	19.93	111.65	19.48	114.82
23	21.80	133.45	21.36	136.18
24	24.47	157.92	24.21	160.39
25	22.58	180.51	22.62	183.01
26	35.35	215.86	35.79	218.80
27	32.83	248.69	34.00	252.80
28	33.68	282.36	35.61	288.40
29	33.82	316.18	36.24	324.64
30	32.98	349.16	35.70	360.35
31	29.20	378.37	31.76	392.10

Table H.7: Energy dissipated up to different heights of the test region for column CL7

Cycle number	Energy dissipated per cycle below 3rd collar (kN.m)	Cumulative energy dissipated below 3rd collar (kN.m)	Energy dissipated per cycle below 2nd collar (kN.m)	Cumulative energy dissipated below 2nd collar (kN.m)	Energy dissipated per cycle below first collar (kN.m)	Cumulative energy dissipated below first collar (kN.m)
1	0.77	0.77	0.66	0.66	0.49	0.49
2	0.45	1.22	0.42	1.08	0.26	0.76
3	0.36	1.59	0.33	1.41	0.23	0.99
4	0.46	2.05	0.43	1.84	0.22	1.20
5	0.53	2.57	0.49	2.33	0.24	1.44
6	2.01	4.59	2.08	4.41	1.81	3.25
7	1.35	5.94	1.38	5.79	1.21	4.46
8	0.77	6.71	0.82	6.61	0.93	5.39
9	0.87	7.57	0.90	7.51	0.82	6.22
10	1.03	8.61	1.09	8.60	0.94	7.16
11	3.30	11.90	3.50	12.10	3.47	10.62
12	2.81	14.71	3.01	15.11	2.80	13.43
13	2.88	17.59	3.09	18.20	2.94	16.36
14	2.37	19.97	2.52	20.72	2.46	18.82
15	2.31	22.28	2.51	23.23	2.56	21.38
16	13.49	35.77	14.55	37.78	12.18	33.56
17	11.10	46.87	11.93	49.71	9.93	43.49
18	10.45	57.33	11.26	60.97	9.75	53.24
19	10.28	67.61	11.00	71.97	9.24	62.48
20	9.73	77.34	10.40	82.37	8.94	71.42
21	20.90	98.24	21.80	104.18	18.28	89.69
22	20.28	118.52	21.04	125.21	17.27	106.96
23	19.78	138.30	20.50	145.71	17.04	124.00
24	19.66	157.96	20.38	166.10	16.95	140.95
25	20.96	178.92	21.77	187.86	18.03	158.97
26	32.30	211.22	33.04	220.91	25.91	184.89
27	30.46	241.68	31.28	252.18	24.35	209.24
28	27.06	268.74	27.77	279.96	22.59	231.83
29	26.30	295.05	27.09	307.05	22.45	254.28
30	26.96	322.00	27.74	334.79	23.09	277.37
31	39.29	361.30	40.14	374.92	30.51	307.88
32	37.40	398.69	38.18	413.10	29.82	337.70
33	36.95	435.64	37.74	450.84	29.90	367.59
34	36.34	471.99	37.25	488.10	29.79	397.38
35	32.95	504.94	33.82	521.92	27.06	424.44

Table H.8: Energy dissipated up to different heights of the test region for column CL8

Cycle number	Energy dissipated per cycle below 3rd collar (kN.m)	Cumulative energy dissipated below 3rd collar (kN.m)	Energy dissipated per cycle below 2nd collar (kN.m)	Cumulative energy dissipated below 2nd collar (kN.m)	Energy dissipated per cycle below first collar (kN.m)	Cumulative energy dissipated below first collar (kN.m)
1	0.44	0.44	0.40	0.40	0.33	0.33
2	0.34	0.78	0.34	0.73	0.21	0.54
3	0.41	1.19	0.42	1.16	0.18	0.72
4	0.38	1.57	0.39	1.55	0.18	0.90
5	0.88	2.45	0.97	2.52	0.50	1.40
6	1.55	4.00	1.62	4.14	1.17	2.57
7	1.41	5.41	1.51	5.65	1.04	3.61
8	0.93	6.34	1.01	6.66	0.71	4.32
9	1.07	7.41	1.17	7.82	0.85	5.17
10	1.52	8.93	1.65	9.48	1.25	6.42
11	2.26	11.19	2.50	11.98	1.98	8.40
12	1.76	12.95	1.87	13.85	1.27	9.68
13	2.79	15.74	3.04	16.89	2.24	11.91
14	2.33	18.07	2.54	19.43	1.88	13.79
15	11.65	29.72	12.57	32.00	8.17	21.96
16	10.79	40.51	11.52	43.52	7.38	29.34
17	10.83	51.34	11.53	55.06	7.36	36.70
18	9.69	61.03	10.32	65.37	6.52	43.22
19	9.31	70.34	9.88	75.25	6.29	49.51
20	20.37	90.71	20.68	95.93	13.02	62.54
21	19.99	110.71	20.26	116.19	12.63	75.17
22	19.32	130.03	19.58	135.77	12.16	87.33
23	20.38	150.41	20.71	156.48	13.01	100.34
24	19.68	170.09	19.96	176.44	12.46	112.80
25	30.12	200.21	30.52	206.96	18.79	131.59
26	29.55	229.75	29.78	236.74	18.30	149.89
27	27.87	257.62	28.23	264.97	17.56	167.45
28	27.83	285.45	28.21	293.18	17.63	185.08
29	27.05	312.50	27.45	320.63	17.52	202.60
30	38.28	350.78	39.22	359.85	8.70	211.29
31	37.54	388.32	38.50	398.35	-	-
32	35.56	423.89	36.69	435.05	-	-
33	35.61	459.49	36.92	471.97	-	-
34	34.97	494.46	36.46	508.43	-	-
35	37.28	531.74	38.39	546.82	-	-

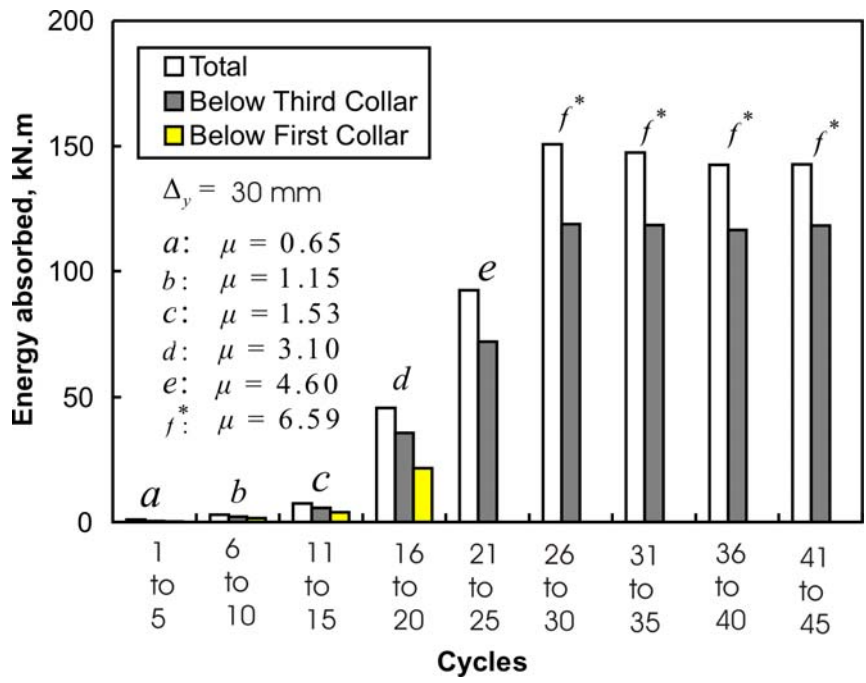


Figure H-1: Distribution of energy absorption mechanism in specimen CL1

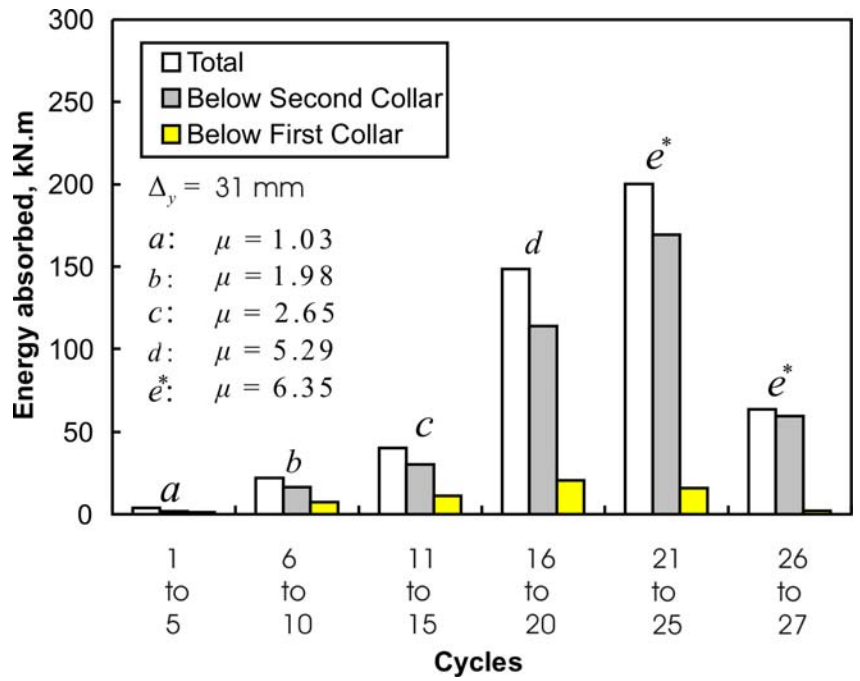


Figure H-2: Distribution of energy absorption mechanism in specimen CL2

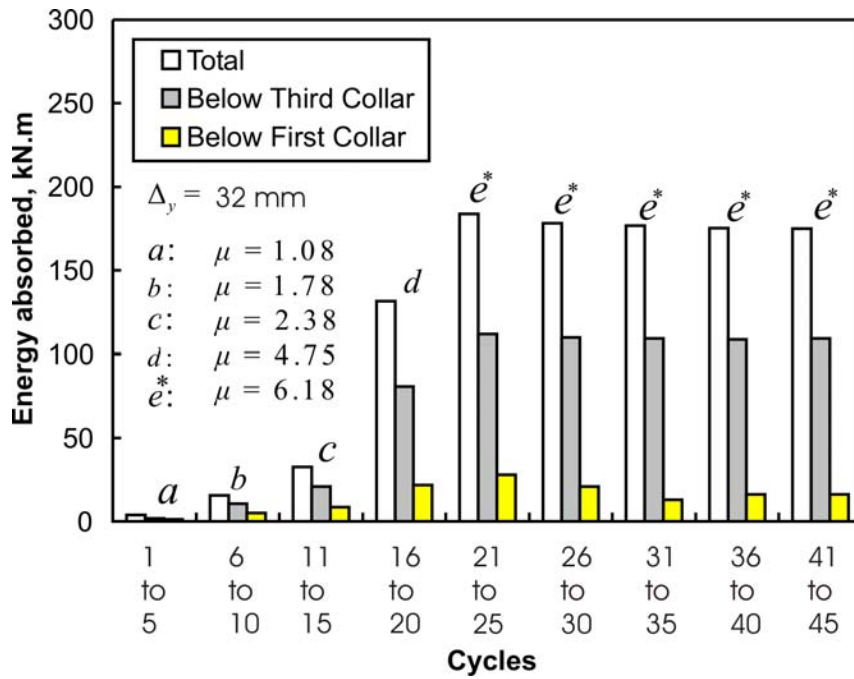


Figure H-3: Distribution of energy absorption mechanism in specimen CL3

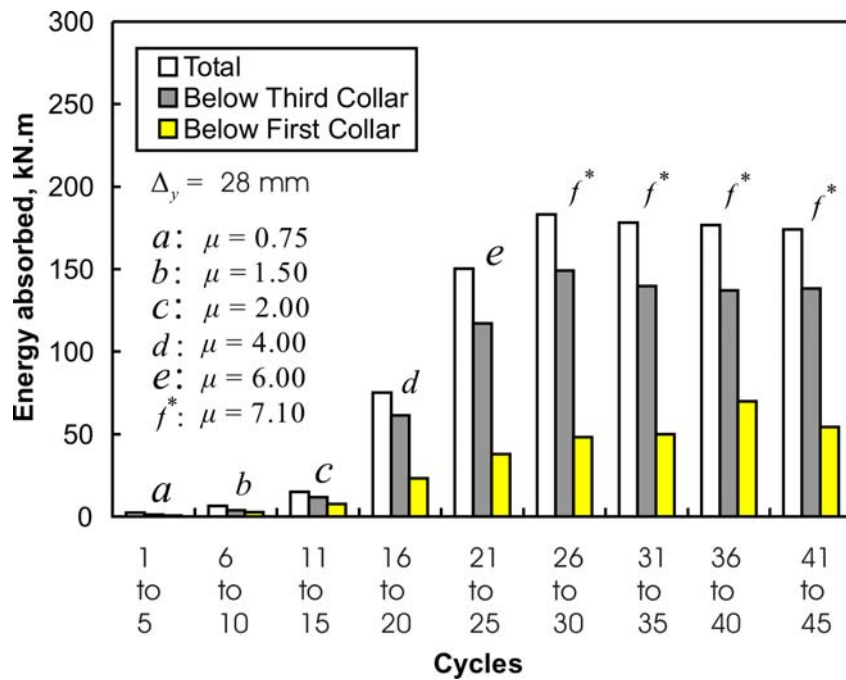


Figure H-4: Distribution of energy absorption mechanism in specimen CL4

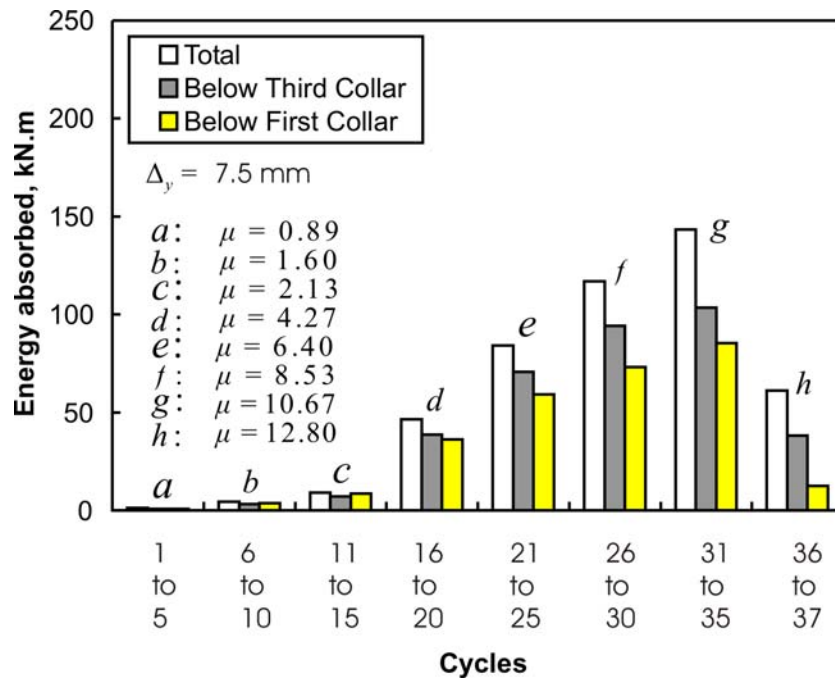


Figure H-5: Distribution of energy absorption mechanism in specimen CL5

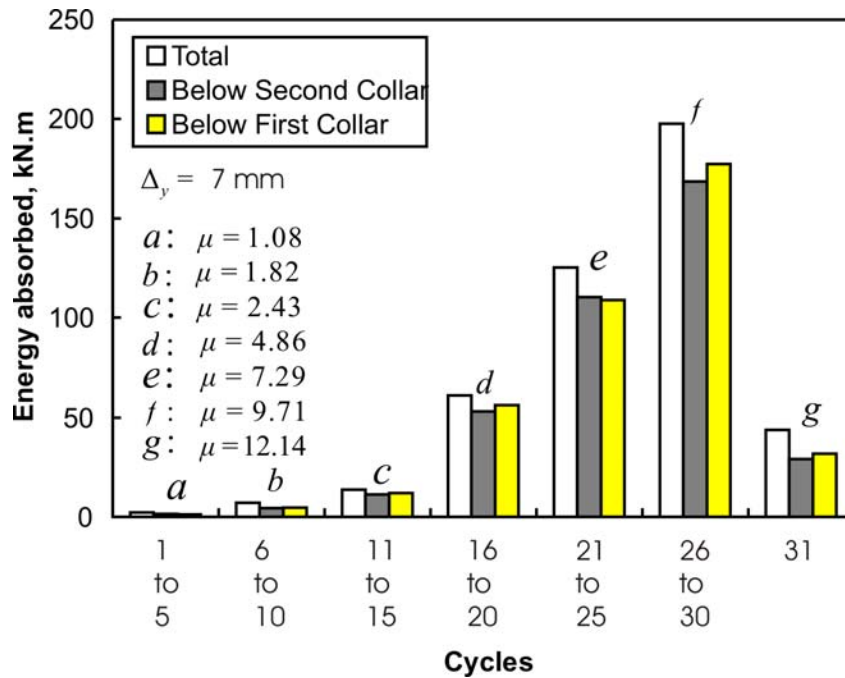


Figure H-6: Distribution of energy absorption mechanism in specimen CL6

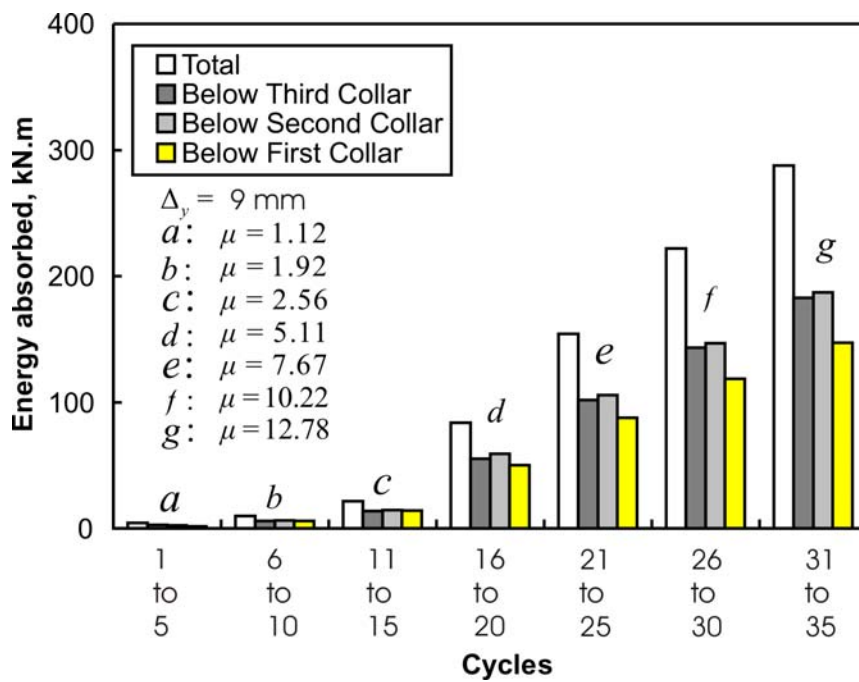


Figure H-7: Distribution of energy absorption mechanism in specimen CL7

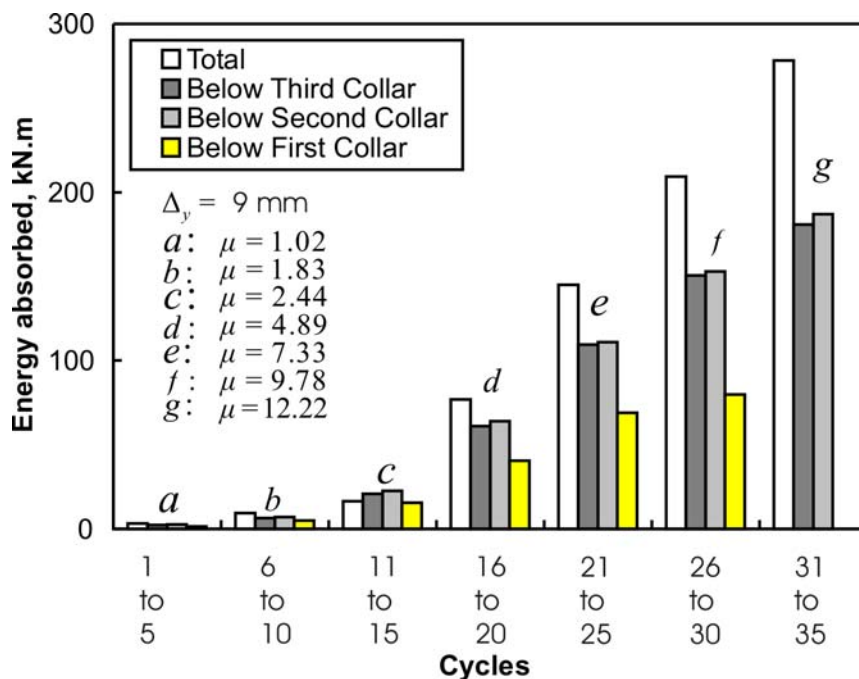


Figure H-8: Distribution of energy absorption mechanism in specimen CL8

## I. MOMENT VERSUS CURVATURE HYSTERESES

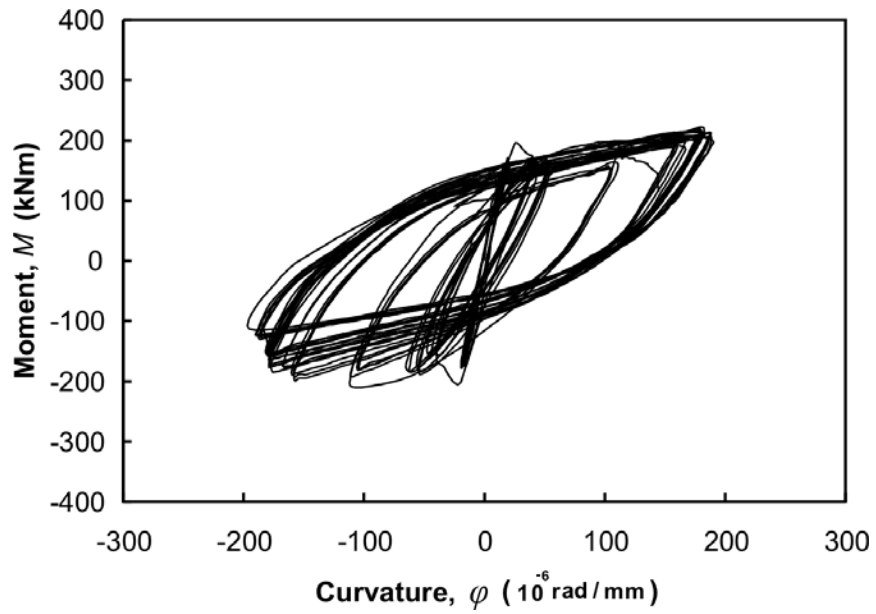


Figure I-1: Moment vs. curvature hysteresis for column CL0

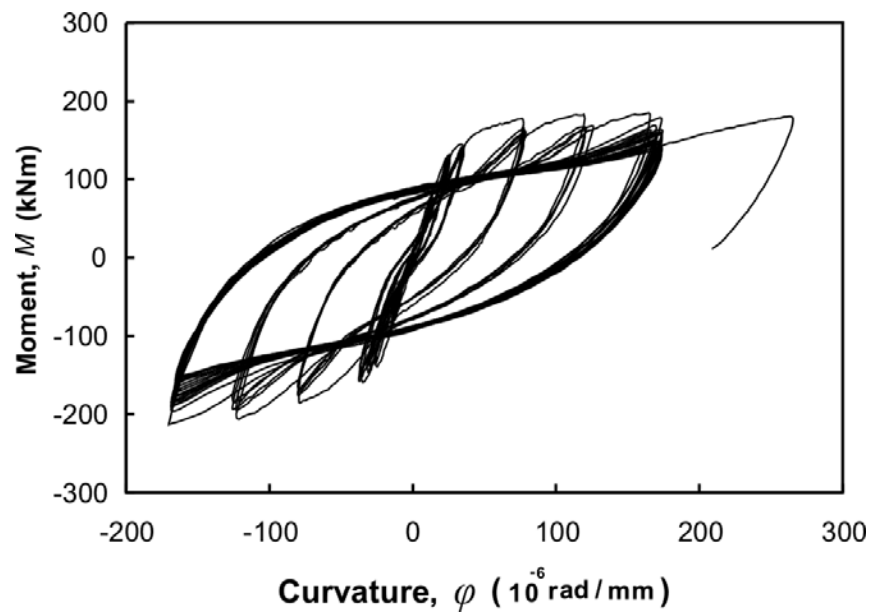


Figure I-2: Moment vs. curvature hysteresis for column CL1

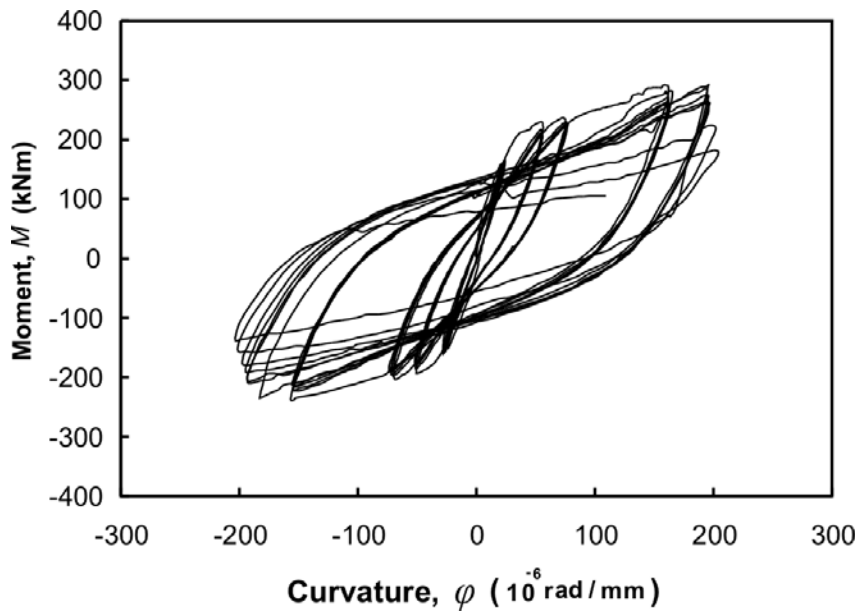


Figure I-3: Moment vs. curvature hysteresis for column CL2

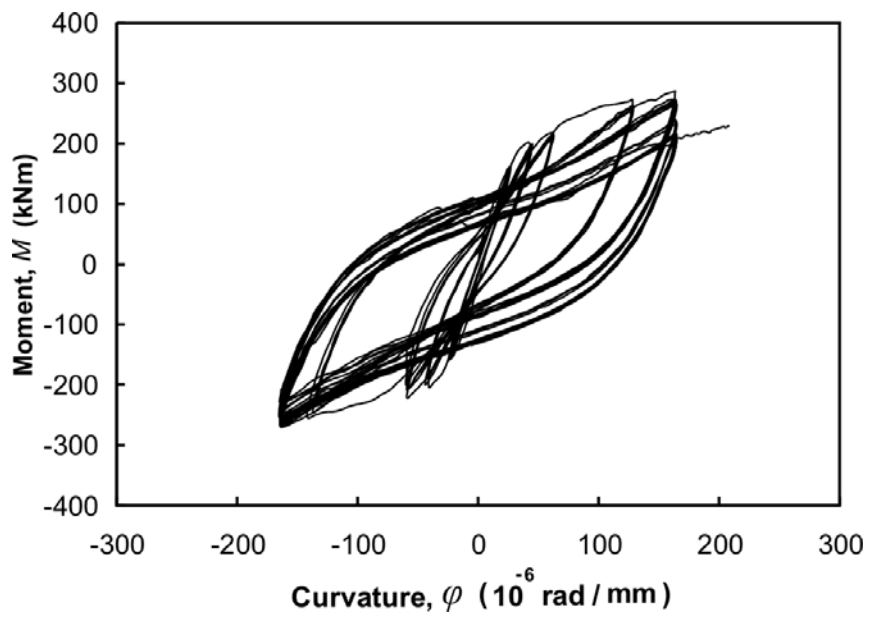


Figure I-4: Moment vs. curvature hysteresis for column CL3

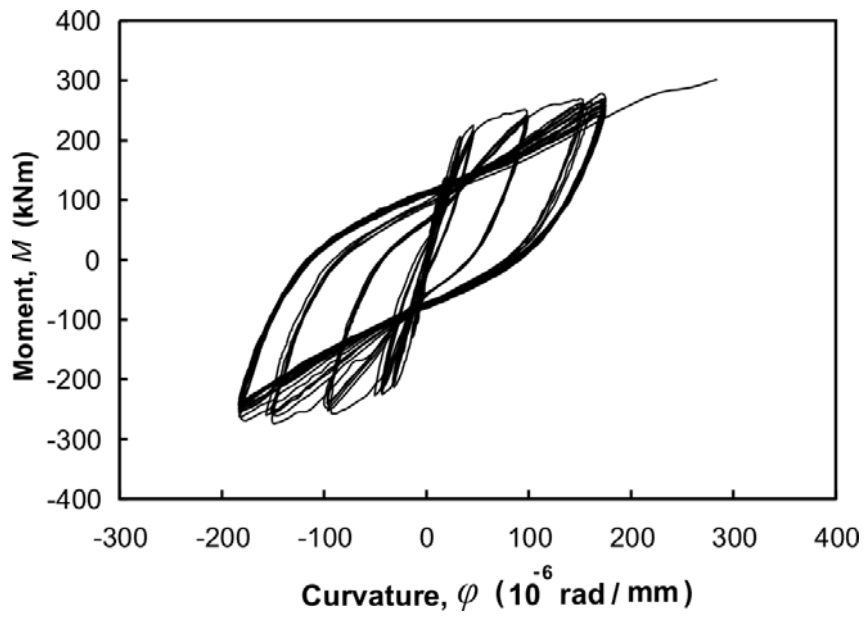


Figure I-5: Moment vs. curvature hysteresis for column CL4

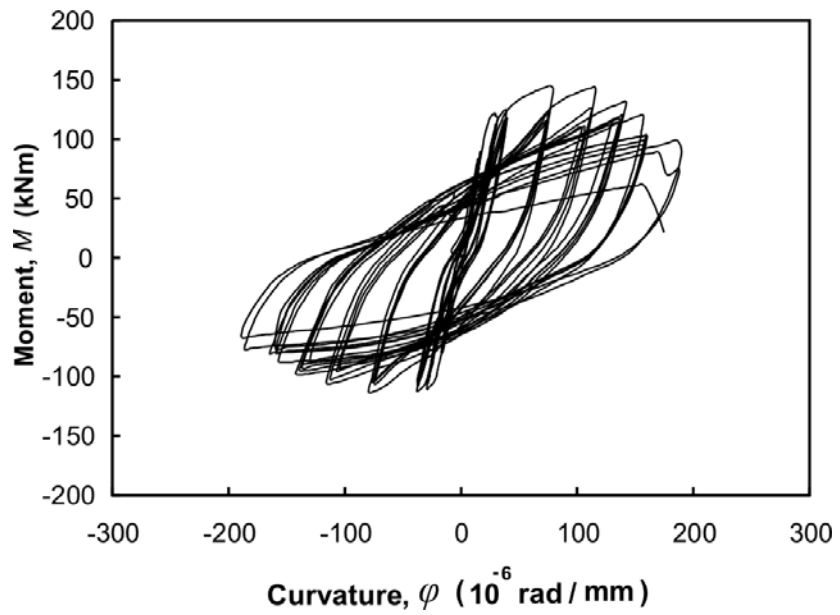


Figure I-6: Moment vs. curvature hysteresis for column CL5

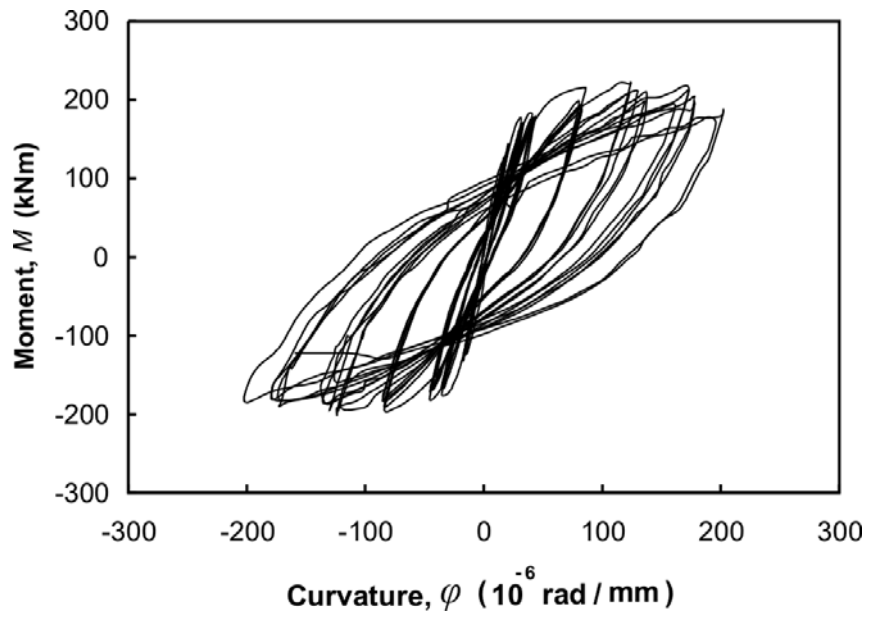


Figure I-7: Moment vs. curvature hysteresis for column CL6

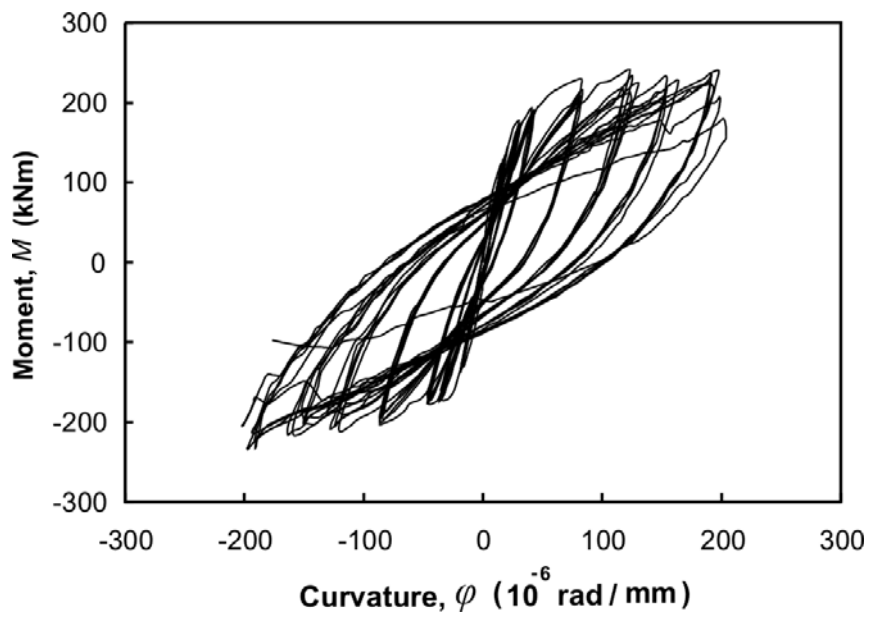


Figure I-8: Moment vs. curvature hysteresis for column CL7

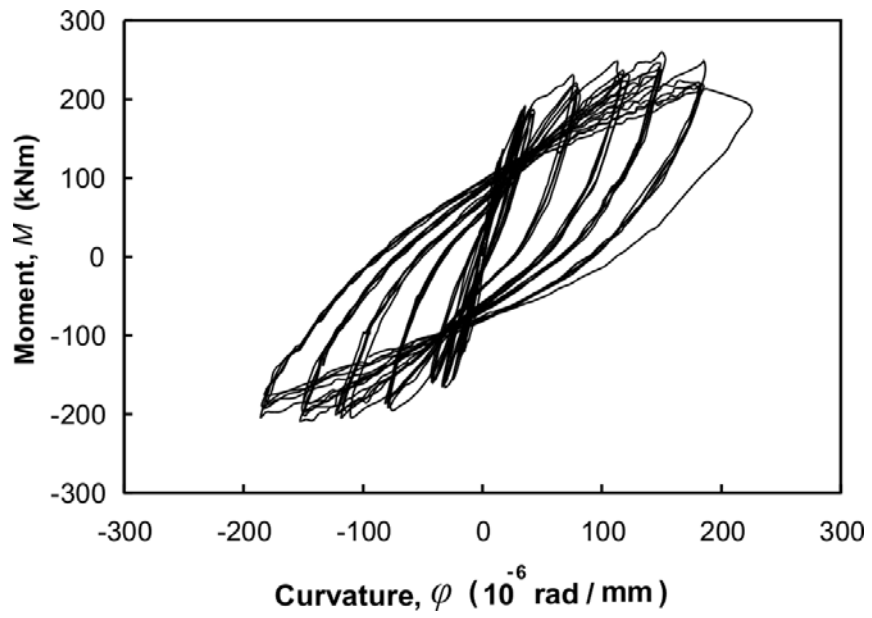


Figure I-9: Moment vs. curvature hysteresis for column CL8

## J. DUCTILITY PARAMETERS

Table J.1: Ductility ratios and energy damage indicator for column CL0.

Cycle number	Ductility Ratio	Cumulative ductility ratios	Energy damage indicator	Cumulative energy damage indicator
1	1.70	1.70	0.83	0.83
2	1.90	3.60	0.81	1.64
3	2.04	5.64	0.86	2.49
4	2.11	7.76	0.87	3.37
5	2.10	9.86	0.75	4.12
6	4.32	14.18	13.79	17.91
7	4.39	18.57	8.13	26.04
8	4.69	23.26	8.73	34.77
9	4.38	27.65	6.80	41.57
10	4.93	32.58	10.77	52.34
11	5.87	38.45	22.25	74.59
12	5.87	44.32	18.17	92.75
13	6.40	50.73	23.50	116.25
14	6.24	56.97	22.90	139.15
15	5.98	62.95	19.20	158.35
16	12.23	75.18	198.17	356.52
17	11.59	86.78	109.28	465.80
18	11.59	98.37	109.28	575.08
19	11.41	109.78	103.30	678.39
20	11.39	121.17	102.34	780.72
21	17.28	138.44	359.42	1140.14
22	17.28	155.72	376.21	1516.35
23	17.53	173.25	364.11	1880.47
24	18.30	191.55	384.99	2265.46
25	18.27	209.82	397.38	2662.84
26	19.33	229.15	462.94	3125.78
27	19.39	248.54	478.14	3603.92
28	19.39	267.93	478.14	4082.06
29	19.39	287.32	458.46	4540.52
30	19.54	306.86	453.60	4994.12
31	19.54	326.40	454.57	5448.70
32	19.64	346.04	461.61	5910.30
33	19.61	365.65	457.59	6367.90
34	19.70	385.35	459.92	6827.81
35	19.71	405.07	456.62	7284.43
36	19.80	424.87	459.91	7744.35
37	19.93	444.80	451.80	8196.15
38	19.67	464.47	508.08	8704.23
39	20.28	484.75	385.95	9090.17
40	20.44	505.19	385.34	9475.51
41	20.52	525.71	392.94	9868.45
42	20.60	546.31	389.68	10258.13
43	20.74	567.06	389.43	10647.55
44	21.15	588.20	392.75	11040.31

Table J.2: Ductility ratios and energy damage indicator for column CL1.

Cycle number	Ductility Ratio	Cumulative ductility ratios	Energy damage indicator	Cumulative energy damage indicator
1	0.57	0.57	0.01	0.01
2	0.64	1.21	0.01	0.02
3	0.64	1.85	0.01	0.03
4	0.65	2.50	0.01	0.03
5	0.65	3.15	0.01	0.04
6	1.16	4.31	0.11	0.15
7	1.17	5.48	0.08	0.23
8	1.24	6.72	0.09	0.32
9	1.21	7.93	0.07	0.39
10	1.16	9.10	0.06	0.45
11	1.60	10.70	0.32	0.77
12	1.62	12.32	0.29	1.06
13	1.60	13.92	0.25	1.31
14	1.60	15.52	0.24	1.55
15	1.63	17.15	0.24	1.79
16	3.52	20.68	5.22	7.01
17	3.56	24.23	4.12	11.13
18	3.55	27.79	3.85	14.98
19	3.58	31.36	3.78	18.76
20	3.54	34.90	3.50	22.26
21	5.46	40.37	15.69	37.95
22	5.50	45.86	13.82	51.76
23	5.52	51.39	13.56	65.33
24	5.67	57.05	13.93	79.26
25	5.44	62.50	11.66	90.92
26	7.55	70.05	35.43	126.35
27	7.70	77.75	34.06	160.41
28	7.61	85.35	30.41	190.82
29	7.51	92.86	28.65	219.47
30	7.47	100.33	27.22	246.69
31	7.69	108.02	29.76	276.45
32	7.58	115.60	27.43	303.88
33	7.68	123.27	28.66	332.54
34	7.67	130.94	28.31	360.85
35	7.66	138.60	28.18	389.03
36	7.54	146.14	25.87	414.90
37	7.52	153.66	25.57	440.47
38	7.53	161.19	24.72	465.19
39	7.55	168.74	24.37	489.56
40	7.63	176.36	24.94	514.50
41	7.52	183.89	23.01	537.51
42	7.61	191.49	24.12	561.63
43	7.61	199.10	23.70	585.33
44	7.59	206.69	23.96	609.29
45	7.60	214.29	22.94	632.23

Table J.3: Ductility ratios and energy damage indicator for column CL2.

Cycle number	Ductility Ratio	Cumulative ductility ratios	Energy damage indicator	Cumulative energy damage indicator
1	1.53	1.53	0.16	0.16
2	1.62	3.15	0.11	0.27
3	1.72	4.87	0.13	0.39
4	1.73	6.60	0.12	0.51
5	1.79	8.39	0.14	0.65
6	3.60	11.98	2.62	3.27
7	3.59	15.57	2.04	5.31
8	3.53	19.10	1.79	7.10
9	3.62	22.72	1.90	9.00
10	3.63	26.35	1.88	10.88
11	4.88	31.23	5.72	16.60
12	4.96	36.20	5.66	22.26
13	4.99	41.18	5.45	27.71
14	5.02	46.20	5.48	33.19
15	5.02	51.22	5.41	38.60
16	10.76	61.98	60.81	99.41
17	10.81	72.79	55.04	154.46
18	10.71	83.50	49.69	204.15
19	10.69	94.20	49.51	253.66
20	10.74	104.94	49.44	303.10
21	12.79	117.73	89.37	392.47
22	13.10	130.83	86.63	479.10
23	13.09	143.92	84.34	563.44
24	13.18	157.10	80.00	643.44
25	13.21	170.31	77.98	721.42
26	13.59	183.89	63.72	785.15
27	13.77	197.67	39.18	824.33

Table J.4: Ductility ratios and energy damage indicator for column CL3.

Cycle number	Ductility Ratio	Cumulative ductility ratios	Energy damage indicator	Cumulative energy damage indicator
1	1.42	1.42	0.26	0.26
2	1.48	2.90	0.16	0.43
3	1.50	4.40	0.15	0.58
4	1.52	5.92	0.14	0.72
5	1.50	7.42	0.14	0.86
6	2.52	9.93	1.90	2.76
7	2.64	12.58	1.70	4.46
8	2.58	15.16	1.50	5.96
9	2.52	17.68	1.39	7.34
10	2.44	20.12	1.30	8.65
11	3.61	23.73	5.51	14.16
12	3.65	27.38	5.02	19.18
13	3.58	30.96	4.71	23.89
14	3.56	34.52	5.23	29.12
15	3.64	38.16	4.90	34.01
16	8.04	46.20	66.67	100.68
17	7.91	54.11	53.00	153.68
18	7.79	61.91	48.88	202.56
19	7.78	69.69	46.74	249.29
20	7.78	77.47	44.12	293.42
21	9.78	87.25	98.90	392.32
22	9.77	97.02	91.17	483.48
23	9.72	106.75	87.24	570.73
24	9.71	116.46	88.33	659.05
25	9.77	126.22	85.75	744.80
26	9.77	135.99	90.45	835.26
27	9.76	145.75	84.90	920.15
28	9.76	155.51	85.72	1005.87
29	9.76	165.27	85.03	1090.90
30	9.77	175.04	82.73	1173.63
31	9.79	184.83	83.88	1257.51
32	9.77	194.60	81.68	1339.19
33	9.79	204.39	83.42	1422.61
34	9.74	214.13	82.07	1504.68
35	9.79	223.92	82.52	1587.20
36	9.71	233.64	80.65	1667.85
37	9.79	243.43	81.20	1749.05
38	9.79	253.22	80.08	1829.13
39	9.79	263.01	82.02	1911.15
40	9.79	272.80	80.96	1992.11
41	9.76	282.56	80.39	2072.50
42	9.80	292.36	79.75	2152.25
43	9.79	302.15	80.23	2232.48
44	9.80	311.94	79.83	2312.30
45	9.77	321.71	78.62	2390.93

Table J.4: Ductility ratios and energy damage indicator for column CL4.

Cycle number	Ductility Ratio	Cumulative ductility ratios	Energy damage indicator	Cumulative energy damage indicator
1	0.91	0.91	0.06	0.06
2	0.97	1.87	0.05	0.11
3	1.04	2.91	0.04	0.16
4	1.02	3.93	0.04	0.19
5	1.01	4.94	0.04	0.23
6	1.99	6.93	0.71	0.94
7	1.97	8.90	0.42	1.35
8	2.03	10.93	0.40	1.75
9	2.00	12.93	0.38	2.13
10	2.01	14.94	0.33	2.46
11	2.71	17.66	2.08	4.54
12	2.71	20.36	1.63	6.17
13	2.71	23.07	1.50	7.66
14	2.74	25.82	1.53	9.20
15	2.92	28.73	2.03	11.23
16	5.93	34.66	27.06	38.29
17	5.85	40.51	22.07	60.37
18	5.99	46.50	22.16	82.53
19	5.94	52.44	21.21	103.74
20	5.93	58.36	21.01	124.75
21	9.22	67.58	85.70	210.45
22	9.23	76.81	76.93	287.39
23	9.28	86.09	75.32	362.71
24	9.33	95.42	75.96	438.67
25	9.64	105.06	84.02	522.69
26	10.79	115.85	143.81	666.51
27	10.83	126.68	115.40	781.91
28	10.82	137.50	112.67	894.58
29	10.77	148.27	107.96	1002.53
30	10.84	159.11	109.28	1111.81
31	10.85	169.97	109.46	1221.27
32	10.86	180.82	109.31	1330.58
33	10.84	191.67	107.30	1437.88
34	10.81	202.48	103.28	1541.17
35	10.83	213.31	104.68	1645.84
36	10.83	224.14	108.26	1754.10
37	10.83	234.96	108.60	1862.70
38	10.83	245.79	108.26	1970.96
39	10.83	256.62	108.26	2079.22
40	10.83	267.45	108.26	2187.48
41	10.82	278.27	101.92	2289.40
42	10.84	289.11	102.15	2391.55
43	10.80	299.91	97.96	2489.51
44	10.83	310.74	99.52	2589.03
45	10.83	321.57	97.18	2686.22

Table J.5: Ductility ratios and energy damage indicator for column CL5.

Cycle number	Ductility Ratio	Cumulative ductility ratios	Energy damage indicator	Cumulative energy damage indicator
1	1.16	1.16	0.09	0.09
2	1.22	2.38	0.05	0.14
3	1.21	3.59	0.04	0.17
4	1.23	4.82	0.03	0.21
5	1.23	6.05	0.03	0.24
6	2.17	8.21	0.89	1.13
7	2.07	10.29	0.31	1.44
8	2.11	12.40	0.29	1.72
9	2.02	14.42	0.21	1.93
10	2.06	16.47	0.21	2.14
11	2.73	19.20	1.44	3.58
12	2.66	21.86	0.97	4.54
13	2.69	24.55	0.96	5.50
14	2.67	27.23	0.83	6.33
15	2.65	29.88	0.78	7.11
16	5.46	35.34	15.83	22.94
17	5.16	40.50	9.83	32.77
18	5.19	45.69	9.67	42.44
19	5.05	50.74	8.23	50.67
20	5.04	55.78	7.92	58.59
21	7.65	63.44	35.43	94.02
22	7.72	71.15	32.74	126.76
23	7.72	78.87	28.04	154.80
24	7.36	86.23	20.82	175.62
25	7.17	93.40	18.92	194.54
26	9.47	102.87	48.24	242.78
27	9.26	112.13	43.59	286.37
28	9.10	121.24	38.54	324.91
29	9.10	130.33	36.12	361.04
30	8.64	138.97	31.39	392.43
31	10.46	149.44	50.46	442.90
32	10.60	160.04	42.32	485.22
33	10.82	170.86	44.07	529.29
34	10.53	181.39	38.58	567.86
35	10.61	192.00	36.34	604.21
36	12.53	204.53	51.52	655.72
37	12.49	217.02	38.06	693.78

Table J.6: Ductility ratios and energy damage indicator for column CL6

Cycle number	Ductility Ratio	Cumulative ductility ratios	Energy damage indicator	Cumulative energy damage indicator
1	1.16	1.16	0.05	0.05
2	1.24	2.40	0.03	0.08
3	1.45	3.85	0.05	0.13
4	1.44	5.29	0.04	0.18
5	1.39	6.68	0.04	0.21
6	2.53	9.22	0.47	0.68
7	2.46	11.68	0.25	0.93
8	2.54	14.22	0.28	1.21
9	2.60	16.82	0.29	1.50
10	2.59	19.41	0.26	1.76
11	3.27	22.68	0.99	2.75
12	3.22	25.90	0.77	3.52
13	3.23	29.13	0.65	4.17
14	3.23	32.36	0.63	4.81
15	3.35	35.71	0.75	5.55
16	6.41	42.12	9.11	14.67
17	6.21	48.33	6.71	21.37
18	6.26	54.59	6.31	27.69
19	6.36	60.95	6.49	34.18
20	6.31	67.26	6.19	40.37
21	9.36	76.62	23.02	63.39
22	9.28	85.90	20.39	83.77
23	9.80	95.70	23.32	107.10
24	10.41	106.11	25.83	132.92
25	10.26	116.37	24.14	157.06
26	13.07	129.44	51.07	208.13
27	13.04	142.48	45.49	253.62
28	13.39	155.87	46.51	300.13
29	13.68	169.55	48.20	348.33
30	13.43	182.98	46.11	394.44
31	12.38	195.36	34.72	429.16

Table J.7: Ductility ratios and energy damage indicator for column CL7.

Cycle number	Ductility Ratio	Cumulative ductility ratios	Energy damage indicator	Cumulative energy damage indicator
1	1.24	1.24	0.09	0.09
2	1.36	2.60	0.06	0.15
3	1.41	4.01	0.06	0.21
4	1.46	5.47	0.06	0.27
5	1.55	7.03	0.06	0.33
6	2.58	9.61	0.76	1.09
7	2.63	12.24	0.54	1.62
8	2.56	14.80	0.41	2.03
9	2.49	17.30	0.34	2.37
10	2.64	19.94	0.38	2.75
11	3.45	23.39	1.78	4.54
12	3.44	26.83	1.39	5.92
13	3.52	30.35	1.47	7.39
14	3.36	33.70	1.19	8.58
15	3.48	37.18	1.30	9.88
16	6.67	43.86	15.38	25.26
17	6.60	50.45	11.86	37.12
18	6.62	57.07	11.29	48.41
19	6.59	63.65	10.47	58.87
20	6.40	70.06	9.62	68.49
21	9.61	79.67	35.62	104.11
22	9.84	89.51	33.90	138.01
23	9.67	99.18	31.88	169.89
24	9.53	108.71	29.68	199.58
25	10.28	118.99	34.48	234.05
26	12.34	131.33	68.98	303.03
27	12.89	144.22	67.02	370.06
28	12.01	156.23	52.71	422.77
29	11.96	168.19	50.08	472.85
30	11.92	180.11	50.63	523.48
31	15.58	195.68	112.06	635.53
32	15.22	210.90	94.59	730.12
33	15.09	225.99	99.43	829.55
34	15.00	240.99	97.72	927.27
35	15.81	256.80	85.14	1012.41

Table J.8: Ductility ratios and energy damage indicator for column CL8.

Cycle number	Ductility Ratio	Cumulative ductility ratios	Energy damage indicator	Cumulative energy damage indicator
1	1.03	1.03	0.07	0.07
2	1.13	2.16	0.05	0.13
3	1.13	3.28	0.05	0.18
4	1.18	4.47	0.05	0.24
5	1.29	5.76	0.06	0.30
6	2.09	7.85	0.29	0.59
7	2.33	10.18	0.61	1.20
8	2.36	12.54	0.54	1.74
9	2.23	14.77	0.35	2.09
10	2.35	17.11	0.47	2.56
11	2.42	19.53	0.58	3.13
12	2.91	22.45	1.08	4.21
13	2.84	25.29	0.73	4.94
14	3.11	28.39	1.26	6.20
15	3.02	31.41	1.09	7.29
16	5.47	36.88	11.45	18.74
17	5.67	42.55	10.42	29.15
18	5.85	48.40	10.35	39.51
19	5.68	54.08	9.08	48.58
20	5.62	59.70	8.60	57.18
21	7.97	67.66	30.09	87.27
22	8.50	76.16	30.60	117.87
23	8.38	84.54	27.67	145.54
24	8.80	93.33	31.28	176.82
25	8.65	101.98	29.13	205.96
26	10.96	112.95	62.39	268.35
27	10.69	123.64	58.22	326.57
28	10.64	134.28	52.97	379.53
29	10.73	145.00	51.73	431.26
30	10.65	155.66	50.99	482.25
31	13.32	168.97	94.80	577.05
32	13.24	182.22	84.17	661.23
33	13.04	195.26	78.58	739.81
34	13.01	208.27	75.49	815.29
35	12.93	221.20	74.88	890.18

## K. PROGRAM MCR

### K.1 OBJECTIVE

The objective of this computer program is to determine the moment versus curvature relationships of the reinforced concrete sections with and without axial load. The program requires the material curves of the steel longitudinal bars and the concrete. The program works both for confined and unconfined concrete material curves. A sample input file is given subsequently in this appendix. The explanation of various terms in the data file is given in Table K.1.

### K.2 FORTRAN SOURCE CODE

```
C*****
C*****
C*****
C*****
C      MUNAWAR ALI HUSSAIN
C      PHD. CANDIDATE
C      STRUCTURES GROUP
C      DEPARTMENT OF CIVIL ENGINEERING
C      UNIVERSITY OF ALBERTA
C      CANADA, OCTOBER 2003
C*****
C*****
C*****
C*****
C      PROGRAM MCR
C      DIMENSION TITLE(20)
C*****
C      OPEN(UNIT=101,FILE='MCR.INP')
C      OPEN(UNIT=102,FILE='MCR.DAT')
C      OPEN(UNIT=103,FILE='MCR.CON')
C      OPEN(UNIT=104,FILE='MCR.STE')
C      OPEN(UNIT=105,FILE='MCR.OUT1')
C      OPEN(UNIT=106,FILE='MCR.OUT')
C*****
C      REWIND(101)
C      REWIND(102)
C      REWIND(103)
C      REWIND(104)
C      REWIND(105)
C      REWIND(106)
C*****
1000  FORMAT(20A4)
1002  FORMAT(2F26.8)
C*****
C      CALL ANAME
C*****
```

```

      READ(101,1000)TITLE
      WRITE(102,1000)TITLE
C      WRITE(105,1000)TITLE
      WRITE(106,1000)TITLE
      READ(101,1000)TITLE
      WRITE(102,1000)TITLE
      READ(101,1000)TITLE
C*****
      READ(101,*)NPC,NPS,SNSTA,SINC,SNEND,CINC,AFORCE
      WRITE(102,1005)NPC,NPS,SNSTA,SINC,SNEND,CINC,AFORCE
1005  FORMAT(/5X,'NPC=',I6/5X,'NPS=',I6/5X,'SNSTA=',F20.6
      . /5X,'SINC=',F20.6
      . /5X,'SNEND=',F20.6/5X,'CINC=',F20.6/5X,'AFORCE=',F20.6/)
C*****
      READ(101,1000)TITLE
CCCC  WRITE(102,1000)TITLE
      READ(101,*)WIDTH,DEPTH,AS1,AS2,AS3,DST1,DST2,DST3
      WRITE(102,1010)WIDTH,DEPTH,AS1,AS2,AS3,DST1,DST2,DST3
1010  FORMAT(/5X,'COLUMN WIDTH=',F12.5/5X,'COLUMN DEPTH=',F12.5
      . /5X,'AS1=',F12.5/5X,'AS2=',F12.5/5X,'AS3=',F12.5
      . /5X,'DST1=',F12.5/5X,'DST2=',F12.5/5X,'DST3=',F12.5/)
C*****
      READ(101,1000)TITLE
      WRITE(102,1000)TITLE
      READ(101,1000)TITLE
      WRITE(102,1000)TITLE
C*****
      DO 100 IPC=1,NPC
      READ(101,*)CSTRAIN,CSTRESS
      WRITE(102,1002)CSTRAIN,CSTRESS
      WRITE(103,1002)CSTRAIN,CSTRESS
100    CONTINUE
C*****
      READ(101,1000)TITLE
      WRITE(102,1000)TITLE
      READ(101,1000)TITLE
      WRITE(102,1000)TITLE
C*****
      DO 105 IPS=1,NPS
      READ(101,*)SSTRAIN,SSTRESS
      WRITE(102,1002)SSTRAIN,SSTRESS
      WRITE(104,1002)SSTRAIN,SSTRESS
105    CONTINUE
C*****
      NITER=SSTRAIN/SINC+1
      MITER=DEPTH/CINC+1
      WRITE(102,107)NITER,MITER
107    FORMAT(/10X,'NITER=',I6,10X,'MITER=',I6)
C*****
      WRITE(102,917)
917    FORMAT(/5X,'WIDTH DEPTH SN100 CN100 FST1 FST2 FST3
      . AFORCE CDEPTH XBAR CFORCE')
C*****
      REWIND(103)
      REWIND(104)
C*****
C      WRITE(105,1235)

```

```

C1235  FORMAT(10X,'STEEL STRAIN',15X,'MOMENT'/)
C*****
      WRITE(106,1240)
1240  FORMAT(/10X,'MOMENT',10X,'SN100',10X,'CN100',
      .10X,'CDEPTH',10X,'CURVATURE'/)
C*****
      SN100=SNSTA
C*****
      DO 800 ITER=1,NITER
      CDEPTH=1.00000
      DO 900 JTER=1,MITER
      CN100=SN100*CDEPTH/(DST1-CDEPTH)
C*****
      IF(SN100.LT.0)THEN
      CN200=ABS(SN100)
      CALL SSTRES(CN200,SSTRES1)
      CALL CSTRES(CN200,CSTRES1)
      FST1=- (SSTRES1-CSTRES1)*AS1
      ELSE
      CALL SSTRES(SN100,SSTRES1)
      FST1=SSTRES1*AS1
      ENDIF
C*****
      SSTRN2=SN100*(DST2-CDEPTH)/(DST1-CDEPTH)
      IF(SSTRN2.LT.0)THEN
      CSTRN2=ABS(SSTRN2)
      CALL SSTRES(CSTRN2,SSTRES2)
      CALL CSTRES(CSTRN2,CSTRES2)
      FST2=- (SSTRES2-CSTRES2)*AS2
      ELSE
      CALL SSTRES(SSTRN2,SSTRES2)
      FST2=SSTRES2*AS2
      ENDIF
C*****
      SSTRN3=SN100*(DST3-CDEPTH)/(DST1-CDEPTH)
      IF(SSTRN3.LT.0)THEN
      CSTRN3=ABS(SSTRN3)
      CALL SSTRES(CSTRN3,SSTRES3)
      CALL CSTRES(CSTRN3,CSTRES3)
      FST3=- (SSTRES3-CSTRES3)*AS3
      ELSE
      CALL SSTRES(SSTRN3,SSTRES3)
      FST3=SSTRES3*AS3
      ENDIF
C*****
      CALL RESCON(WIDTH,CDEPTH,CN100,XBAR,CFORCE)
C*****
      FRES=FST1+FST2+FST3+AFORCE-CFORCE
C*****
      IF(ABS(FRES).LT.1000)THEN
      RESMOM=FST1*(DST1-DEPTH/2)+FST2*(DST2-DEPTH/2)+
      .FST3*(DST3-DEPTH/2)+CFORCE*(DEPTH/2-CDEPTH+XBAR)
      RESMOM=RESMOM/1000/1000
C      WRITE(105,915)SN100,RESMOM
C915  FORMAT(5X,F20.10,5X,F20.6)
      WRITE(102,909)WIDTH,DEPTH,SN100,CN100,FST1,FST2,FST3,AFORCE,
      .CDEPTH,XBAR,CFORCE

```

```

909   FORMAT(11F20.6)
C*****
      PHI=CN100/CDEPTH
      WRITE(106,111)RESMOM,SN100,CN100,CDEPTH,PHI
111   FORMAT(5E20.8)
C*****
      GOTO 950
      ENDIF
C*****
      CDEPTH=CDEPTH+CINC
900   CONTINUE
C*****
950   SN100=SN100+SINC
      IF(SN100.GT.SNEND)GOTO 2121
800   CONTINUE
      CALL JOB
C*****
2121          CLOSE(101)
              CLOSE(102)
              CLOSE(103)
              CLOSE(104)
C              CLOSE(105)
              CLOSE(106)
C*****
      STOP
      END
C*****
      SUBROUTINE CSTRES(EPSSL, CPP)
      CALL ANAME
      KOUNT=0
      NPOIN=20000
C*****
C*****
C*****
      DO 110 IPOIN=1,NPOIN
      READ(103,*)EPSSLAT,CPDATA
      KOUNT=KOUNT+1
C*****
      IF(EPSSL.EQ.EPSSLAT) THEN
      GOTO 200
      ENDIF
C*****
      IF(EPSSL.LT.EPSSLAT) THEN
      EPS2=EPSSLAT
      CP2=CPDATA
      GOTO 300
      ENDIF
110   CONTINUE
C*****
300   KOUNT=KOUNT-1
      REWIND(103)
      DO 400 K=1,KOUNT
      READ(103,*)EPSSLAT,CPDATA
400   CONTINUE
      EPS1=EPSSLAT
      CP1=CPDATA
      CPP=CP1+(CP2-CP1)*(EPSSL-EPS1)/(EPS2-EPS1)

```

```

                GOTO 500
C*****
200      CPP=CPDATA
500      REWIND(103)
                RETURN
                END
C*****
C*****
C*****
                SUBROUTINE SSTRES(EPSSL, CPP)
                CALL ANAME
                KOUNT=0
                NPOIN=20000
C*****
                DO 110 IPOIN=1, NPOIN
                READ(104, *) EPSSLAT, CPDATA
                KOUNT=KOUNT+1
C*****
                IF(EPSSL.EQ.EPSSLAT) THEN
                GOTO 200
                ENDIF
C*****
                IF(EPSSL.LT.EPSSLAT) THEN
                EPS2=EPSSLAT
                CP2=CPDATA
                GOTO 300
                ENDIF
110      CONTINUE
C*****
300      KOUNT=KOUNT-1
                REWIND(104)
                DO 400 K=1, KOUNT
                READ(104, *) EPSSLAT, CPDATA
400      CONTINUE
                EPS1=EPSSLAT
                CP1=CPDATA
                CPP=CP1+(CP2-CP1)*(EPSSL-EPS1)/(EPS2-EPS1)
                GOTO 500
C*****
200      CPP=CPDATA
500      REWIND(104)
                RETURN
                END
C*****
C*****
                SUBROUTINE RESCON(WIDTH, CDEPTH, CSTRAIN, XBAR, SFORCE)
                DIMENSION CDEPT(200), CSTS(200), FCON(200), XDIST(200)
                WIDTH=WIDTH
                CDEPTH=CDEPTH
                NITER=100
                CINC=CDEPTH/(NITER-1)
                C=0.00000
C*****
                DO 200 ITER=1, NITER
                CDEPT(ITER)=C
                CTN=CSTRAIN*C/CDEPTH
                CALL CSTRES(CTN, CSTS1)

```

```

CSTS(ITER)=CSTS1
C=C+CINC
200 CONTINUE
C*****
NITER=NITER-1
C*****
DO 300 ITER=1,NITER
FCON(ITER)=WIDTH*CINC*(CSTS(ITER)+CSTS(ITER+1))/2
XDIST(ITER)=(CDEPT(ITER)+CDEPT(ITER+1))/2
300 CONTINUE
C*****
SMOM=0.00000
SFORCE=0.0000
DO 400 ITER=1,NITER
SFORCE=SFORCE+FCON(ITER)
SMOM=SMOM+FCON(ITER)*XDIST(ITER)
400 CONTINUE
C*****
SFORCE=SFORCE
XBAR=SMOM/SFORCE
C*****
RETURN
END
C*****
C*****
C*****
C*****
SUBROUTINE ANAME
REWIND (103)
REWIND (104)
C*****
WRITE(*,10)
10 FORMAT(5X,'DEVELOPED BY MUNAWAR A. HUSSAIN, U OF A,
EDMONTON,
.CANADA')
C*****
C*****
C*****
RETURN
END
C*****
C*****
C*****
SUBROUTINE JOB
WRITE(*,10)
10 FORMAT(//5X,'JOB COMPLETED! JOB COMPLETED! JOB
COMPLETED!')
RETURN
END
C*****
C*****
C*****

```

### K.3 A SAMPLE INPUT FILE

Munawar A. Hussain

Department of Civil Engineering, University of Alberta

NPC	NPS	SNSTART	SINC	SNEND	CINC	AFORCE	
20	34	0.001	0.01	0.13	0.001	0.0000	
WIDTH	DEPTH	AS1	AS2	AS3	DST1	DST2	DST3
300.00	300.00	1500	1000	1500	240	150	60

Confined-Concrete-Curve Follows

Axial-Strain    Axial-Stress

0.000	0.00
0.005	25.77
0.010	32.03
0.015	33.58
0.020	33.70
0.025	33.41
0.030	32.96
0.035	32.43
0.040	31.84
0.045	31.34
0.050	30.90
0.055	30.49
0.060	30.07
0.065	29.76
0.070	29.44
0.075	29.12
0.080	28.85
0.085	28.59
0.090	28.33
0.095	28.14

Stress-Strain-Curve for Vertical Rebars of The Column

Axial-Strain    Axial-Stress

0.000	0.00
0.005	509.87
0.010	517.80
0.015	551.72
0.020	582.22
0.025	609.03
0.030	631.94
0.035	651.67
0.040	667.70
0.045	680.84
0.050	693.33
0.055	702.52
0.060	710.33
0.065	716.58
0.070	721.43
0.075	725.95
0.080	729.06
0.085	731.47
0.090	733.35
0.095	734.92
0.100	735.88
0.105	736.41
0.110	736.48

0.115	736.24
0.120	735.70
0.125	734.90
0.130	733.89
0.135	733.26
0.140	731.34
0.145	729.15
0.150	726.49
0.155	723.53
0.160	720.28
0.165	717.17

Table K.1: Explanation of various terms in the input file (*MCR.INP*)

TERM	EXPLANATION
NPC	Number of data points in stress versus strain curve of concrete
NPS	Number of data points in stress versus strain curve of steel longitudinal bars
SNSTART	Start strain for steel longitudinal bars
SNEND	Steel strain at which analysis is to be terminated
SINC	Increment in steel strain
CINC	Increment in $c$ , where $c$ is the distance from extreme compression fiber to the neutral axis of the column section
Width	Width of column section
Depth	Depth of column section
AS1	Area of longitudinal steel 1
AS2	Area of longitudinal steel 2
AS3	Area of longitudinal steel 3
DST1	Distance of longitudinal steel 1 from compression face
DST2	Distance of longitudinal steel 2 from compression face
DST3	Distance of longitudinal steel 3 from compression face

## L. PROGRAM C4P

### L.1 OBJECTIVE

Knowing the behaviour of collars in terms of confining pressure versus lateral strain relationships by the finite element or by the proposed empirical models, the computer program C4P is used to find the confined concrete material curve of the reduced core of the confined columns. This program is used in Chapters 5 and 6. A sample input file is also given later in this chapter. The explanation of various terms in the input file is given in Table L.1.

### L.2 FORTRAN SOURCE CODE

```
C*****
C*****
C   The acronym C4P is derived from the following:
C   Confinement of reinforced Concrete Columns by steel Collar
C*****
C*****
C       PROGRAM DEVELOPED BY MUNAWAR A. HUSSAIN
C       PHD. CANDIDATE
C       STRUCTURES GROUP
C       DEPARTMENT OF CIVIL ENGINEERING
C       UNIVERSITY OF ALBERTA
C       CANADA, MARCH 2003
C*****
C*****
C       Dedicated to Sabina and Ali
C*****
C*****
C*****
C       PROGRAM C4P
C       DIMENSION TITLE(20)
C*****
C*****C4P.INP  contains input data
C*****C4P.DAT  contains the generated data
C*****C4P.CPLS is the scratch file for confining-pressure vs lateral-
C*****strain
C*****C4P.CPAS is the scratch file for confining-pressure vs axial-
C*****strain
C*****C4P.OUT  contains data for confined-concrete-stress vs axial-
C*****strain
C*****
C       OPEN(UNIT=101,FILE='C4P.inp')
C       OPEN(UNIT=102,FILE='C4P.dat')
C       OPEN(UNIT=103,FILE='C4P.cpls')
C       OPEN(UNIT=104,FILE='C4P.cpas')
C       OPEN(UNIT=105,FILE='C4P.out')
C*****
C       REWIND(101)
```

```

        REWIND(102)
        REWIND(103)
        REWIND(104)
        REWIND(105)
C*****
1000   FORMAT(20A4)
1002   FORMAT(2F26.7)
1004   FORMAT(10E12.4)
C*****
        READ(101,1000)TITLE
        WRITE(102,1000)TITLE
        READ(101,1000)TITLE
        WRITE(102,1000)TITLE
        READ(101,1000)TITLE
CCCCC WRITE(102,1000)TITLE
C*****
        READ(101,*)NPOIN,FCOP,EC,PRCO,EPS0,CPACTIVE
        WRITE(102,1005)NPOIN,FCOP,EC,PRCO,EPS0,CPACTIVE
1005   FORMAT(/5X,'NPOIN=',I5/5X,'FCOP=',F20.6/5X,'SECANT-E=',F20.6/
        .5X,'PRCO=',F20.6/5X,'EPS0=',F20.6/5X,'CPACTIVE=',F20.6)
C*****
        READ(101,1000)TITLE
        WRITE(102,1000)TITLE
C*****
C*****
C*****
        DO 100 IPOIN=1,NPOIN
        READ(101,*)EPSLAT,CP
        WRITE(102,1002)EPSLAT,CP
        WRITE(103,1002)EPSLAT,CP
100    CONTINUE
        SLMAX=EPSLAT
        JOUNT=SLMAX/0.00001+10
C*****
C*****INITIAL VALUES FOLLOWS*****
C*****
        XCOORD=0.00000
        WRITE(102,1003)
1003   FORMAT(5X,'EPSCC',7X,'EPSCCP',7X,'PRC',8X,'CPPIN',7X,'CPPOUT',
        .7X,'EPSL',7X,'EP',7X,'FCC',7X,'R',7X,'ECC')
        WRITE(104,1002)XCOORD,CPACTIVE
        WRITE(105,1002)XCOORD,XCOORD
C*****
        EPSCC=0.0005
        EPSCCP=0.01
        ECC=1.10*EC
        ECO=1.12*EC
        CPP=0.00000
        KOUNT=30
        PRCLMT=0.50000
C*****
        DO 1200 J=1,JOUNT
        DO 1500 K=1,KOUNT
        CONSTT=1.914*(CPP/FCOP)+0.719
        PRC=PRCO*(CONSTT*(EPSCC/EPSCCP)+1)
C*****
        IF(PRC.GT.PRCLMT)THEN

```

```

      PRC=PRCLMT
      ENDIF
C*****
      EPSL=EPSCC*PRC
      IF (EPSL.GT.SLMAX)GOTO 1400
      CALL CPRESS(NPOIN, EPSL, CPP)
      CPPIN=CPP
      CPP=CPP-CPACTIVE
      EP=CPP/EPSL
      CPP=EPSL/(((1-PRC)/ECC)+1/EP)
      CPP=CPP+CPACTIVE
      CPPOUT=CPP
      FCCP=FCOP*(-1.254+2.254*SQRT(1+7.94*CPP/FCOP)-2.0*CPP/FCOP)
      SEF=FCCP/FCOP
      EPSCCP=EPS0*(1+5*(SEF-1))
      ESEC=FCCP/EPSCCP
      R=ECO/(ECO-ESEC)
      X=EPSCC/EPSCCP
      FCC=FCCP*X*R/(R-1+X**R)
      ECC=FCC/EPSCC
1500  CONTINUE
      WRITE(104,1002)EPSCC, CPP
      WRITE(102,1004)EPSCC, EPSCCP, PRC, CPPIN, CPPOUT, EPSL, EP, FCC, R, ECC
      WRITE(105,1002)EPSCC, FCC
      EPSCC=EPSCC+0.0005
1200  CONTINUE
1400  CONTINUE
C*****
C*****
      CALL JOB
C*****
C*****
      CLOSE(101)
      CLOSE(102)
      CLOSE(103)
      CLOSE(104)
      CLOSE(105)
C*****
      STOP
      END
C*****
      SUBROUTINE CPRESS(NPOIN, EPSL, CPP)
      CALL ANAME
      KOUNT=0
CCCC  WRITE(102,*)EPSL
C*****
      DO 110 IPOIN=1,NPOIN
      READ(103,*)EPSLAT, CPDATA
CCCC  WRITE(102,*)EPSLAT, CPDATA
      KOUNT=KOUNT+1
CCCC  WRITE(102,*)KOUNT
C*****
      IF (EPSL.EQ.EPSLAT) THEN
      GOTO 200
      ENDIF
C*****
      IF (EPSL.LT.EPSLAT) THEN

```

```

        EPS2=EPSLAT
        CP2=CPDATA
CCCC  WRITE(102,*)EPS2,CP2
        GOTO 300
        END IF
C*****
C*****
110  CONTINUE
C*****
300  KOUNT=KOUNT-1
        REWIND(103)
        DO 400 K=1,KOUNT
        READ(103,*)EPSLAT,CPDATA
400  CONTINUE
        EPS1=EPSLAT
        CP1=CPDATA
        CPP=CP1+(CP2-CP1)*(EPSL-EPS1)/(EPS2-EPS1)
        GOTO 500
C*****
200  CPP=CPDATA
        CALL ANAME
500  CONTINUE
        RETURN
        END
C*****
C*****
C*****
        SUBROUTINE ANAME
        REWIND (103)
C*****
        WRITE(*, 10)
10   FORMAT(5X, 'DEVELOPED BY MUNAWAR A. HUSSAIN, U OF A,
        .CANADA')
C*****
C*****
C*****
        RETURN
        END
C*****
C*****
C*****
        SUBROUTINE JOB
        WRITE(*,10)
10   FORMAT(//5X, 'JOB COMPLETED! JOB COMPLETED!')
        RETURN
        END
C*****
C*****
C*****

```

### L.3 A SAMPLE INPUT FILE

Munawar A. Hussain

Deptt. of Civil and Env. Engg, University of Alberta, Edmonton, Canada

NPOIN	f'co	Ec	POISSON	EPSILON-0	CP-ACTIVE
93	32.895	21221	0.15	0.0031	2.9162

Lateral-Strain	Confining-Pressure
----------------	--------------------

0.000	0.00
0.002	5.80
0.004	7.26
0.006	8.60
0.008	9.81
0.010	10.75
0.012	11.40
0.014	11.79
0.016	12.18
0.018	12.34
0.020	12.47
0.022	12.60
0.024	12.72
0.026	12.80
0.028	12.87
0.030	12.95
0.032	13.02
0.034	13.08
0.036	13.14
0.038	13.20
0.040	13.24
0.042	13.29
0.044	13.33
0.046	13.37
0.048	13.41
0.050	13.45
0.052	13.47
0.054	13.50
0.056	13.52
0.058	13.55
0.060	13.58
0.062	13.60
0.064	13.63
0.066	13.65
0.068	13.67
0.070	13.67
0.072	13.67
0.074	13.67
0.076	13.67
0.078	13.67
0.080	13.68
0.082	13.68
0.084	13.68
0.086	13.68
0.088	13.68
0.090	13.68
0.092	13.68
0.094	13.69

0.096	13.69
0.098	13.66
0.100	13.64
0.102	13.61
0.104	13.58
0.106	13.56
0.108	13.53
0.110	13.50
0.112	13.48
0.114	13.45
0.116	13.42
0.118	13.40
0.120	13.37
0.122	13.34
0.124	13.32
0.126	13.29
0.128	13.27
0.130	13.24
0.132	13.21
0.134	13.19
0.136	13.16
0.138	13.13
0.140	13.11
0.142	13.08
0.144	13.05
0.146	13.01
0.148	12.96
0.150	12.92
0.152	12.88
0.154	12.84
0.156	12.80
0.158	12.76
0.160	12.72
0.162	12.68
0.164	12.64
0.166	12.60
0.168	12.56
0.170	12.52
0.172	12.48
0.174	12.44
0.176	12.39
0.178	12.35
0.180	12.30
0.182	12.26
0.184	12.22

Table L.1: Explanation of various terms in the input file (*C4P.INP*)

TERM	EXPLANATION
NPOIN	Number of data points in confining pressure versus lateral strain curve
$f'_{co}$	Strength of column concrete
$E_c$	Secant modulus of elasticity of column concrete
POISSON	Initial Poisson's ratio of concrete
EPSILON-0	Strain at peak stress of column concrete (unconfined)
CP-ACTIVE	Magnitude of initial active confining pressure